Performance of glue-laminated beams from Malaysian Dark Red Meranti timber

Ong, Chee Beng

Award date:
2018

Awarding institution:
University of Bath

Performance of glue-laminated beams from Malaysian Dark Red Meranti timber

Chee Beng Ong

A thesis submitted for the degree of Doctor of Philosophy

University of Bath

Department of Architecture and Civil Engineering

March 2018

Abstract

In this study, Malaysian Dark Red Meranti (DRM) was used to manufacture glulam beams, following closely the requirements of BS EN 14080:2013 so as to emulate commercial production. Phenol resorcinol formaldehyde (PRF), commonly used in structural glulam production, was used in the fabrication of finger joints and laminations of the glulam beams. Factors influencing the mechanical properties of finger joints and bonding performance of laminations were investigated. Full size glulam beams were manufactured and tested in bending with partial and complete carbon fibre reinforced polymer (CFRP) reinforcement on the tension face and compared with the performance of unreinforced beams. A bench-scale fire test was proposed to describe the behaviour of DRM finger joints in tension under fire condition, in order to simulate the failure of finger joints on the tension side of a glulam beam in a standard fire test.

Overall, DRM finger joints exhibited better bending strength than Spruce finger joints which represented softwood used in European glulam. Wood density and end pressure were shown to affect the strength properties of the finger joints. Higher cramping pressure was needed to produce DRM laminations with higher shear strength. The glulam beam with CFRP reinforcement had a higher bending strength than the unreinforced glulam beams but partial reinforcement had an adverse effect on beam strength. In the bench-scale fire test, DRM finger-jointed specimens exhibited lower charring rate than Spruce. Furthermore, PRF finger-jointed specimens showed better fire performance than finger-jointed specimens bonded with polyurethane (PUR) adhesive.

In conclusion, it is hoped that results from this research will motivate engineers and architects in Malaysia to design and build structures from less-utilised local timber, specifically in the form of glulam, encouraging the timber industry in Malaysia to produce them commercially.

Acknowledgements

I am truly indebted to my supervisors, Professor Pete Walker, Dr Martin P. Ansell and Dr Chang Wen-Shao for their constant supports and guidance throughout my PhD. I am extremely grateful for their patience, motivation and invaluable ideas provided in the development of this thesis. Without them I would never have finished this study and unlikely to understand the significant of my works.

The financial support provided by the Public Service Department of Malaysia and Forest Research Institute Malaysia to this research is gratefully acknowledged.

I would also like to express my appreciations to the technical team of the Department of Architecture and Civil Engineering, Glen Stewart, Walter Guy, Miles Chambers, William Bazeley, David Surgenor and David Williams. Their advice and tireless efforts have continuously improved the experimental works and enlightened me in many technical aspects of the work.

Acknowledgement is given to Dr Daniël Brandon and Dr Magdalena Sterley for their supports and assistance during my work in SP Wood Building Technology, Sweden. Additional thanks are due to the COST Action FP1404 for the financial support during my research on fire tests.

I am thankful to my colleagues and friends in Malaysia and Bath for their encouragements and moral supports during the course of my PhD.

I am sincerely grateful to my dear parents, brothers and in-laws for their unwavering love and care that made me who I am today.

Finally, to my lovely wife, Thi Bee Kin, who sacrificed her time and work to be with me, I could never be able to repay your love, supports and hard work in the family. You are my life.

Contents

Abstract 1
Acknowledgements 3
List of figures 9
List of tables 15

Chapter 1 Introduction 17
1.1 Background 17
1.2 Research aims and objectives 24
1.3 Layout of thesis 25

Chapter 2 Literature review 27
2.1 Introduction 27
2.2 Glue-laminated timber 29
2.3 Finger joints 32
2.4 Lamination 34
2.5 Adhesives 37
2.6 Reinforced glulam 38
2.7 Fire performance 39
2.8 Summary 41
2.9 Research methodology based on the review of the literature 42

Chapter 3 Materials and test methods 45
3.1 Introduction 45
3.2 Materials 46
3.2.1 Timber 46
3.2.2 Adhesives 50
3.2.3 Carbon fibre reinforced polymer 51
3.3 Test methods 52
3.3.1 Four-point bending test 52
3.3.2 Tensile test parallel to grain 54
3.3.3 Compressive test parallel to grain 55
3.3.4 Density at the time of test 56
3.3.5 Moisture content by the oven dry method 57

3.3.6 Bench-scale fire tests 58
3.4 Assumptions 60
3.5 Summary 61

Chapter 4 Mechanical properties of finger joints 63
4.1 Introduction 63
4.2 Finger joints preparation 64
4.2.1 Test specimen preparation 64
4.2.2 Finger-jointing of laminations 71
4.2.3 Four-point bending test 75
4.2.4 Tensile test parallel to grain 78
4.2.5 Compressive test parallel to grain 80
4.2.6 Microscopic analysis 81
4.3 Results and discussion 83
4.3.1 Bending properties 83
4.3.2 Tensile strength parallel to grain 102
4.3.3 Compressive strength parallel to grain 113
4.3.4 Microscopic analysis of wood and bonding failures 118
4.4 Summary 121

Chapter 5 Bonding strength of beam laminations 125
5.1 Introduction 125
5.2 Test specimen preparation 126
5.2.1 Cramping jig preparation 126
5.2.2 Short beam preparation 129
5.2.3 Full size glulam beam preparation 132
5.2.4 Block shear specimen preparation 136
5.3 Block shear strength test 138
5.4 Results and discussion 141
5.4.1 Shear strength of glue lines parallel to grain 141
5.4.2 Beam with optimum cramping pressure, 0.80 N/mm^2 142
5.4.3 Beam with lower cramping pressure, 0.64 N/mm^2 144
5.4.4 Beam with higher cramping pressure, 0.96 N/mm^2 146
5.4.5 Full size glulam beams results 148

5.4.6 Average shear strength and wood failure percentage 150
5.4.7 Relationship between shear strength and wood failure of glue lines 152
5.4.8 Factors influencing the bonding performance of DRM specimens 155
5.5 Summary 158

Chapter 6 Full size glulam beam tests 161
6.1 Introduction 161
6.2 Materials and method 161
6.2.1 CFRP reinforcement preparation 162
6.2.2 Four-point bending test 164
6.2.3 Digital image correlation method 168
6.3 Results and discussion 171
6.3.1 Unreinforced glulam beam 171
6.3.2 Fully reinforced glulam beam 174
6.3.3 Reinforced finger joints glulam beam 178
6.3.4 Comparison of bending properties between unreinforced and reinforced glulam beams 182
6.3.5 Strain analysis 184
6.4 Summary 194

Chapter 7 Bench-scale fire tests 197
7.1 Introduction 197
7.2 Materials and method 198
7.2.1 Finger joints preparation 198
7.2.2 Bench-scale fire tests 199
7.3 Results and discussion 201
7.3.1 Fire performance of finger joints 202
7.3.2 Factors affecting the charring rates 204
7.3.3 Temperature profiles of DRM and Spruce specimens 206
7.3.4 Influence of density on the tensile strength of finger joints tested at ambient temperature 208
7.4 Summary 210

Chapter 8 Conclusions and future work 213
8.1 Conclusions 213
8.1.1 Mechanical properties of finger joints 213
8.1.2 Bonding strength of laminations 214
8.1.3 Full size glulam beam tests 215
8.1.4 Bench-scale fire tests 216
8.1.5 Major outcomes of the thesis 217
8.2 Recommendations for future work 217

References 221
Appendix A 239
List of publications 249

List of figures

Figure 1-1: Map of Malaysia 17
Figure 1-2: The first glulam mosque in Malaysia 19
Figure 1-3: Glue-laminated timber exhibition hall in Johor 20
Figure 2-1: Glulam arches in the waiting room of Stockholm Central Railway Station in Sweden 27
Figure 2-2: Leonardo da Vinci bridge in Norway 28
Figure 2-3: Richmond Olympic Oval in Canada 28
Figure 2-4: Stages of manufacturing glulam 30
Figure 2-5: Types of finger joint 32
Figure 2-6: Typical profile of finger joint 33
Figure 2-7: Efficient beam layup and minimum joints spacing 35
Figure 3-1: Dark Red Meranti timber 48
Figure 3-2: Four-point bending test configuration 53
Figure 3-3: Tensile test configuration 55
Figure 3-4: Specimen preparation for fire tests 58
Figure 3-5: Bench-scale fire test set-up 59
Figure 4-1: Finger cutter 65
Figure 4-2: Profile of the finger cutter 66
Figure 4-3: Spindle moulder for finger-cutting 67
Figure 4-4: Finger-cutting processes 68
Figure 4-5: Descriptions of the finger profile 69
Figure 4-6: Recommended end pressure for bonding finger joints as a function of finger length 70
Figure 4-7: Finger-jointing set-up 70
Figure 4-8: Arrangement of laminations and spacing of finger joints 72
Figure 4-9: Finger-jointing of laminations 73
Figure 4-10: Further finger-cutting (2 metre length) 74
Figure 4-11: Full length finger-jointed laminations 74
Figure 4-12: Four-point bending test set-up 75
Figure 4-13: Four-point bending test configuration 76
Figure 4-14: Bending test specimens 77
Figure 4-15: Tensile test parallel to grain set-up 80

Figure 4-16: Compressive test set-up 81
Figure 4-17: Edwards Sputter Coater S150B machine 82
Figure 4-18: JEOL JSM-6480LV Scanning Electron Microscope 83
Figure 4-19: Failures of solid DRM specimens in bending test 85
Figure 4-20: Failures of solid Spruce specimens in bending 86
Figure 4-21: Failure of DRM specimens bonded with PRF 88
Figure 4-22: Mixture of finger fractures and glue line failures 89
Figure 4-23: Mixture of failures at glue lines and along the slope of grain 89
Figure 4-24: DRM epoxy finger joints 90
Figure 4-25: Relationship between MOR and density of PRF and epoxy finger-jointed DRM specimens 91
Figure 4-26: PRF finger-jointed Spruce specimens 92
Figure 4-27: Bending strength as a function of density for PRF finger-jointed DRM and Spruce specimens 93
Figure 4-28: Finger joints failure of $FJ_{drm,prf,wv,R}$ specimens 94
Figure 4-29: Bending strength as a function of density for PRF finger-jointed (30 x 30 mm) and wider (30 x 60 mm) DRM specimens 94
Figure 4-30: Different orientations of finger joints in bending tests 96
Figure 4-31: Bending strength as a function of density for DRM specimens with different end pressures 98
Figure 4-32: Typical load-deflection curve for DRM finger-jointed specimens in bending 101
Figure 4-33: Bending stiffness as a function of density for solid and PRF finger-jointed DRM 101
Figure 4-34: $FJ_{T,prf,R}$ glue lines failure with attached pulled-out wood fibres ... 103
Figure 4-35: Wood crushing failure at gripped surface of $FJ_{T,prf,R}$ specimen ... 104
Figure 4-36: Wood and finger fractures of a $FJ_{T,\ epoxy,R}$ specimen 104
Figure 4-37: Mixture of glue lines and wood failures of a $FJ_{T,epoxy,R}$ specimen 105
Figure 4-38: Tensile strength as a function of density for DRM finger-jointed with PRF and epoxy 105
Figure 4-39: Failure of glue lines of $FJ_{T,prf,H}$ specimens 107
Figure 4-40: Mixture of glue lines and finger fractures of a $FJ_{T,prf,L}$ specimen . 107
Figure 4-41: Mixture of glue lines and wood failures of a $FJ_{T,prf,L}$ specimen 108

Figure 4-42: Tensile strength as a function of density for DRM finger-jointed with different end pressures 109
Figure 4-43: Combination of glue lines and wood failures of a $FJ15_{T,prf,R}$ specimen 110
Figure 4-44: Tensile strength as a function of density for DRM finger joints specimens with finger lengths of 10 and 15 mm 111
Figure 4-45: Relationship between moisture content and mechanical properties of wood 112
Figure 4-46: Compression failure of solid DRM specimens 114
Figure 4-47: Compression failure near knot of solid Spruce specimen 115
Figure 4-48: Wood compression failure near finger tips of finger-jointed DRM specimen 116
Figure 4-49: Compression failure near finger tips extending to the solid wood region 116
Figure 4-50: Compression wood failure near finger tips of Spruce specimen 118
Figure 4-51: Splitting of roots of Spruce specimen 118
Figure 4-52: DRM finger surface without adhesive at 10x magnification 119
Figure 4-53: Finger surface with wood resin at 270x magnification 119
Figure 4-54: Compressive failure at 50x magnification (compressive test) 120
Figure 4-55: Fractured finger joint surface with epoxy adhesive glue line at 27x magnification (tensile test) 120
Figure 4-56: Finger joint surface with PRF adhesive at 50x magnification (tensile test) 121
Figure 5-1: Calibration of the cramping jig 127
Figure 5-2: Cramping of the short beam 129
Figure 5-3: Glue squeeze-out 130
Figure 5-4: Block shear specimens 131
Figure 5-5: Locations of the block shear and density specimens 132
Figure 5-6: Positioning of finger joints in the beam layup 133
Figure 5-7: Full size glulam beam 135
Figure 5-8: Misaligned laminations 136
Figure 5-9: Block shear test specimen 137
Figure 5-10: Description of the block shear specimen 138
Figure 5-11: Shearing tool with block shear specimen 139

Figure 5-12: Block shear test set-up 140
Figure 5-13: Transparent grid for WFP measurement 141
Figure 5-14: Adequate wood failure for specimen bonded with optimum cramping pressure 143
Figure 5-15: Typical block shear failures for specimens bonded with lower cramping pressure 145
Figure 5-16: Typical block shear failures for specimens bonded with higher cramping pressure 147
Figure 5-17: Typical block shear failures for specimens gathered from the full size glulam beams 149
Figure 5-18: Shear strength of the individual glue lines and wood failure percentage of DRM specimens 153
Figure 5-19: Average shear strength and wood failure percentage of DRM specimens 154
Figure 5-20: Relationship between shear strength of glue lines and density of DRM specimens 156
Figure 5-21: Relationship between factor k_v and shear strength of glue lines of DRM specimens 157
Figure 5-22: Relationship between factor k_v and shear strength of glue lines . 158
Figure 6-1: Glulam beams externally bonded with CFRP sheet 162
Figure 6-2: Layout of Beam-FJ 163
Figure 6-3: Epoxy adhesive penetrating the CFRP sheet 164
Figure 6-4: Four-point bending test set-up 165
Figure 6-5: Location of strain gauges 167
Figure 6-6: TML PL-60-11 strain gauges and TML CN-E adhesive 167
Figure 6-7: Speckle pattern on the surface of glulam beams 169
Figure 6-8: DIC set-up in the bending test 170
Figure 6-9: Location of focused images 170
Figure 6-10: Failed unreinforced beam 172
Figure 6-11: Crack propagation of failed unreinforced beam 173
Figure 6-12: Load-deflection curve of unreinforced beam 174
Figure 6-13: Failed fully reinforced beam 175
Figure 6-14: Delamination of the CFRP sheet 176
Figure 6-15: Splitting in midsection of the beam 177

Figure 6-16: Load-deflection curve of fully reinforced beam 178
Figure 6-17: Load-deflection curve of reinforced finger joints beam 179
Figure 6-18: Crack initiation at the edge of CFRP sheet 179
Figure 6-19: Crack propagation along the outermost tension layer prior to ultimate failure of the beam 180
Figure 6-20: Failed reinforced finger joints beam 180
Figure 6-21: Crack initiation at the edge of the CFRP sheet 181
Figure 6-22: Load-deflection curves of unreinforced and reinforced beam 182
Figure 6-23: Load as a function of strain for unreinforced beam 185
Figure 6-24: Load as a function of strain for fully reinforced beam 186
Figure 6-25: Load as a function of strain for the beam with reinforced finger joints 187
Figure 6-26: Strain plotted versus depth for the unreinforced beam 188
Figure 6-27: Strain plotted versus depth for the fully reinforced beam 189
Figure 6-28: Strain plotted versus depth for the beam with reinforced finger joints 190
Figure 6-29: Strain ε_{xy} plots analysed by DIC method for the beam with reinforced finger joints 191
Figure 6-30: Strain ε_{xx} plots analysed by DIC method at the centre region of unreinforced beam with applied load 62 kN 192
Figure 6-31: Strain ε_{yy} plots analysed by DIC method at the centre region of the fully reinforced beam 193
Figure 6-32: Strain ε_{xx} plots at the center region of fully reinforced beam at applied load 62 kN 194
Figure 7-1: Finger-jointed specimen 199
Figure 7-2: Specimens with attached thermocouples 200
Figure 7-3: Typical failures of finger-jointed specimens 201
Figure 7-4: Residual tensile strength of finger-jointed specimens of DRM and Spruce as a function of density 203
Figure 7-5: Char rates as a function of density for finger-jointed specimens 204
Figure 7-6: Temperature profiles of Spruce and DRM specimens finger-jointed with PRF and PUR 207
Figure 7-7: Char depth as a function of time at a temperature of 300^{o}C 208
Figure 7-8: Typical tensile failures of specimens at ambient temperature 209

Figure 7-9: Tensile strength as a function of density for finger joints tested at ambient temperature..... 209

List of tables

Table 2-1: Timber strength grading machines 31
Table 2-2: Recommended finger geometries 33
Table 3-1: Service class and adhesive type classifications 50
Table 3-2: Mean results of coupon tensile tests 52
Table 3-3: Mechanical properties of Sikadur-330 52
Table 4-1: Bending test configurations and number of specimens 78
Table 4-2: Tensile test configurations and number of DRM specimens 79
Table 4-3: Compressive test configurations and number of specimens 81
Table 4-4: Average bending properties of finger joints and solid specimens 84
Table 4-5: Average tensile strength of DRM finger joints 102
Table 4-6: Average compressive strength parallel to grain 113
Table 5-1: Cramping pressures recommended by BS EN 14080:2013 126
Table 5-2: Cramping pressure with the resulting force and torque reading 128
Table 5-3: Block shear specimens 137
Table 5-4: Minimum requirements for WFP in relation to the shear strength 142
Table 5-5: Results of the individual block shear strength (optimum cramping pressure) 143
Table 5-6: Results of the individual block shear strength (lower cramping pressure) 144
Table 5-7: Results of the individual block shear strength (higher cramping pressure) 146
Table 5-8: Full size beams with optimal cramping pressure (0.80 N/mm^2) 148
Table 5-9: Average block shear strength and WFP of DRM specimens 151
Table 6-1: Glulam beam descriptions 162
Table 6-2: Bending properties of reinforced and unreinforced glulam beams 171
Table 7-1: Types of test configuration 199
Table 7-2: Fire performance of the finger-jointed specimens 202

Chapter 1 Introduction

1.1 Background

Malaysia is located in Southeast Asia and is divided into two regions, Peninsular Malaysia and East Malaysia (Sabah and Sarawak) (Figure 1-1).

Figure 1-1: Map of Malaysia (source: Google map)

In Malaysia, timber is currently the third largest export commodity after palm oil and rubber. Furthermore, Malaysia is one of the major tropical timber producers in the world with an export value of about RM 22 billion (~£4 billion - exchange rate of £1 to RM5.44) in the year 2016 (Malaysian Timber Industry Board, 2016). The export value would be increased with the introduction of value-added products such as structural timber products, specifically glue-laminated (glulam) timber, into the marketplace. This would increase the efficiency of timber utilization in the country and contribute positively to the Malaysian government's initiatives to improve sustainable forest management and increase usage of timber from fast-growing plantations. Ultimately, it will

contribute to the country's export target under the National Timber Industry Policy (NATIP) of up to RM53 billion (~£9.7 billion) by year 2020 (Zaini, 2010).

Malaysia is rich in both natural and plantation hardwood resources but the utilization of timber for structural applications is still lacking. Hence, the Malaysian government, together with local timber industries, has been actively promoting the use of timber in construction specifically by implementing glulam technology (Jumaat *et al.*, 2006).

In Malaysia structural glue-laminated was first investigated by researchers at the Forest Research Institute Malaysia (FRIM) in the 1960s and the first glulam footbridge was built in 1962 (Tan and Chu, 1990). In 1977, the first structural glulam mosque in Malaysia, known as Masjid Jamek (Figure 1-2) was built by FRIM and is located inside the institute's campus (How *et al.*, 2016). In the 1980s, FRIM, with the cooperation and assistance of the Japanese International Cooperation Agency (JICA) and the German Technical Cooperation (GTZ), trained research officers in glulam technology and provided machinery to establish the Glue-lamination Unit, or the present Wood Lamination Laboratory.

(a) Exterior view of the mosque

(b) Roof rafters made of glulam beams

Figure 1-2: The first glulam mosque in Malaysia

In recent years, there has been a concerted effort from the Malaysian government agencies and timber industry to promote glulam technology in buildings. The most recent example is the completion of commercial glue-laminated timber hall, the Malaysian Timber Industry Board (MTIB) Exhibition Centre (Figure 1-3), in Johor in 2011 (Smedley *et al.*, 2012) and the planned pedestrian glulam bridge spanning 47 metres in Putrajaya (Malaysian Timber Council, 2016). The glulam sections of the MTIB exhibition hall were manufactured by Woodsfield Glulam Manufacturing Sdn. Bhd., the first local glulam company in Malaysia. The glulam beams were made from Keruing (*Dipterocarpus* spp.), a local Malaysian species. The beams were connected by bonded-in steel rods using Rotafix thixotropic epoxy adhesive to produce the glulam arches as seen in Figure 1-3a (Smedley *et al*., 2012).

a) Main structure made of glulam beams

b) Exterior of the completed building

Figure 1-3: Glue-laminated timber exhibition hall in Johor (© Rotafix)

In addition, the Malaysian government has been promoting fast-growing plantation timber as an alternative to timber supply from natural forests. This fast-growing timber species with small log diameter makes it suitable for use in the production of large dimension glulam for structural applications where smaller pieces can be bonded to produce wider and thicker board, while defects can be removed and the shorter pieces finger-jointed to longer spans (Tan and Ong, 2007). To promote the establishment of plantations, the Compensatory Forestry Plantation Project was introduced in 1981 and some of the species being promoted include *Acacia mangium*, rubberwood (*Hevea brasiliensis*), teak (*Tectona grandis*), sentang (*Azadirachta excelsa*) and *Khaya ivorensis* (Krishnapillay and Varmola, 2002).

Despite the availability of timber resources together with the local government and industry support, technical information for the manufacture of glulam is still lacking. Further research on the quality and mechanical properties of the Malaysian hardwood glulam is required (Mohamad *et al.*, 2011, Wahab *et al*., 2016). The lack of expertise and technical information discourage local timber industries from venturing into the production of glulam for structural uses.

The resulting technical information gathered from this study will encourage engineers and architects to utilize the easily available local timber, especially from the plantation forest, as alternatives to building materials such as concrete and steel. Specifically, the aim of this study is to investigate the performance of glulam, as an engineered wood product, produced from Malaysian hardwood and to compare properties with those of glulam commonly made from European softwood species. Mechanical properties, such as bending strength, of both finger-jointed individual members and full size glulam beams will be investigated. The mechanical performance of the individual constituents of glulam is important because in a bending test, the strength of the glulam beam is governed by the weakest region, commonly at the finger joints of the outermost lamella experiencing the highest tensile stress (Serrano *et al.*, 2001).

The strength properties of finger-jointed products, especially for structural uses, are influenced by factors such as the finger profiles, jointing pressure, type of

adhesives, moisture content, density and species (Ayarkwa *et al.*, 2000; Bustos *et al.*, 2003a, 2003b, 2011; Jokerst, 1981; Knowles *et al.*, 2006; St-Pierre *et al.*, 2005; Vrazel and Sellers, 2004). Thus, it is important for manufacturers to follow the standard requirements when manufacturing structural finger joints. There are many established national standards (BS EN 14080:2013; ANSI A190.1-2012:2013; BS EN 15497:2014; JAS Notification No. 1152:2007) that govern the requirements for producing reliable finger joints for structural uses. These standards mostly cater for softwood species and may not be suitable for application to tropical hardwoods, especially the Malaysian species. Furthermore, the lack of published work describing the strength of Malaysian tropical hardwood finger joints discourages further research on its use for glulam production (Ahmad *et al.*, 2016; Hamid *et al.*, 2016). The findings of this research can be further used to improve the existing Malaysian Standard on glue-laminated timber (MS 758:2001), assisting local timber industries in the use of the abundance of local Malaysian hardwoods for structural purposes. At present, MS 758:2001 is based on the British (including European) and Australian Standards with amendments, following the requirements of Malaysian hardwoods.

In addition to finger joints, the strength of glulam beams can be further enhanced by reinforcing the outer layers with reinforcement materials. The reinforcement materials can replace layers of higher-grade laminations on the tension face of the beam, reducing the volume of wood required (Issa and Kmeid, 2005). This study aims to investigate the advantages of using carbon fibre reinforced polymer (CFRP) to reinforce glulam, specifically by increasing the bending properties of the beams.

Another significant factor, fire safety design, is an important consideration in the construction industry especially when using wood due to the misconception of the public that products made from wood are inferior in comparison to steel and concrete in term of combustibility. For this reason, the use of timber in buildings remains unpopular with the local construction industry in Malaysia. This PhD study investigates the fire performance of finger joints because of its importance for glulam as a building material. Specifically, a bench-scale fire test was

employed to investigate the fire performance of adhesives in finger joints. This bench-scale fire test was preferred instead of a full-scale method because the latter requires larger expensive facilities which are time-consuming and may not always produce adequate results related to the fire performance of the material (Craft *et al*., 2008; Klippel *et al*., 2014). Therefore, this study assesses the fire performance of the finger joints in tension using a bench-scale set-up.

The motivation for this study is to address the gaps in the technical knowledge pertaining the quality of glulam made from Malaysian hardwood, specifically Dark Red Meranti (DRM) species. The performance of the finger joints and lamination were investigated because of their importance in influencing the performance of a glulam beam. The experimental approach and subsequent tests were made based on the minimum production requirements stated in established standard testing methods. Standard processing and testing methods were needed to ensure repeatability, providing a comparison for future research on glulam produced from different species of Malaysian hardwood. The influence of finger geometry, end pressure, adhesive type and wood density on the strength of the structural finger joints were investigated. Subsequently, optimum finger joints and lamination configurations were used in the final production of structural size glulam beams. Comparing results gathered from testing finger-joints, laminations and glulam beams made from DRM with the more established Spruce species, pertinent new information was gathered to establish standard production requirements for Malaysian hardwood. In addition, carbon fibre reinforced polymer was used to reinforce the glulam beams to improve the performance of glulam in structural applications (Martin *et al.*, 2000). Ultimately, it is hoped that the success of this research will encourage the local timber industry, especially in Malaysia, to become actively involved in the use of local hardwood timber for the production of glulam and its application in structures.

1.2 Research aims and objectives

The aim of this thesis lies in the investigation of the strength properties of unreinforced and reinforced glulam beams and properties of the constituent material elements including finger joints and laminations. The bench-scale fire performance of finger joints is also evaluated. To achieve these aims, specific objectives are introduced:

1. To evaluate the mechanical properties of structural finger-jointed DRM specimens and compare to Spruce;

2. To investigate the factors affecting the strength properties of DRM finger joints such as density, end pressure, orientation of finger joints (vertical and horizontal joints), choice of adhesive and finger geometry;

3. To evaluate the bonding performance of the laminations in the DRM glulam beams and compare with the standard minimum requirements recommended by BS EN 14080:2013;

4. To investigate the factors influencing shear strength and mode of failure of the DRM glue lines such as wood density, cramping pressure and test set-up;

5. To evaluate the flexural properties and failure mode of unreinforced and CFRP reinforced full size DRM glulam beams in bending tests;

6. To analyse the strain distribution of DRM glulam beams during bending tests;

7. To evaluate the fire performance of finger joints using bench-scale fire test;

8. To investigate factors influencing the charring rates of the DRM finger joints in a bench-scale fire test.

1.3 Layout of thesis

Chapter 2 reviews the history, advances and recent developments in glulam technology. This chapter also describes the general requirements and processing stages involved in the manufacturing of glulam beams. The chapter summary emphasises the necessity for new work on the properties of glulam which determines the organization of the rest of the thesis. In Chapter 3, the preparation of materials and methodologies for the experimental work are explained.

Chapter 4 presents a detailed description of the results from bending, tensile and compressive tests of DRM finger-jointed specimens and comparison is made with the Spruce species. The factors influencing the mechanical properties of finger joints are discussed and the failure of joints observed using scanning electron microscope are explained in this chapter.

Chapter 5 discusses the influence of cramping pressure, wood density and size of specimens on the shear strength and wood failure percentage of the glue lines of DRM glulam beams. The results are compared to the minimum production requirements of the BS EN 14080:2013 standard and revised minimum requirements are proposed for DRM specimens.

Chapter 6 evaluates the bending performance of unreinforced and CFRP-reinforced DRM glulam beams. The failure behaviour of the beams during and after bending tests are discussed. The strain distribution during bending tests are analysed and compared for the unreinforced, fully reinforced and partially reinforced glulam beams.

The proposed bench-scale fire test is examined and discussed in Chapter 7. The fire performance of DRM finger joints is analysed and compared to the Spruce finger joints. The residual tensile strength of finger joints bonded with phenol resorcinol formaldehyde (PRF) adhesive is also compared to joints bonded with polyurethane (PUR) adhesive. The factors influencing the charring

rates such as the use of constant heat flux in contrast to the time-increasing heat flux and the smaller size of the finger-jointed specimens are discussed.

Chapter 8 presents the overall conclusions of the thesis and proposes the direction of possible future work. Finally, Appendix A reports the results of the finger joints tests conducted in Chapter 4.

Chapter 2 Literature review

2.1 Introduction

Glue-laminated timber is widely used in various structural and architectural applications because of its advantages as an engineered product that allows the construction of beams with large cross-sectional areas and wide spans in a variety of shapes. Glulam was first patented by Otto Hetzer in 1906 but some earlier structures were already using this technology such as the hall of King Edward College, England in 1860 (Lehringer and Gabriel, 2014; Riberholt, 2007), an auditorium in Basel, Switzerland in 1893 (Moody *et al*., 1999), arch sections of New Cross Music Hall in Nottingham, England in 1877, arches of the waiting room of Stockholm Central Railway Station, Sweden in 1925 (Figure 2-1) and arches of railway bridges in England and Scotland, built between 1835 to 1855 (Riberholt, 2007).

Figure 2-1: Glulam arches in the waiting room of Stockholm Central Railway Station in Sweden (Riberholt, 2007)

Glulam technology was also used to construct the Forest Products Laboratory service building in USDA Forest Service in 1935 (Wilson, 1939) and is still continuously being used in the construction sector such as the Hamar and Håkon Olympic Stadium in Lillehammer, Norway in 1994 (Farreyre and Journot, 2005), the roof structure of a tennis court in Croatia in 1997 (Haiman and Baljkas, 2000), the Oslo Leonardo da Vinci bridge, Norway in 2001 (Garbett, 2008) (Figure 2-2) and the 100 meters span main arches of Richmond Olympic Oval, Canada in 2008 (Canadian Wood Council, 2010) (Figure 2-3).

Figure 2-2: Leonardo da Vinci bridge in Norway (Garbett, 2008)

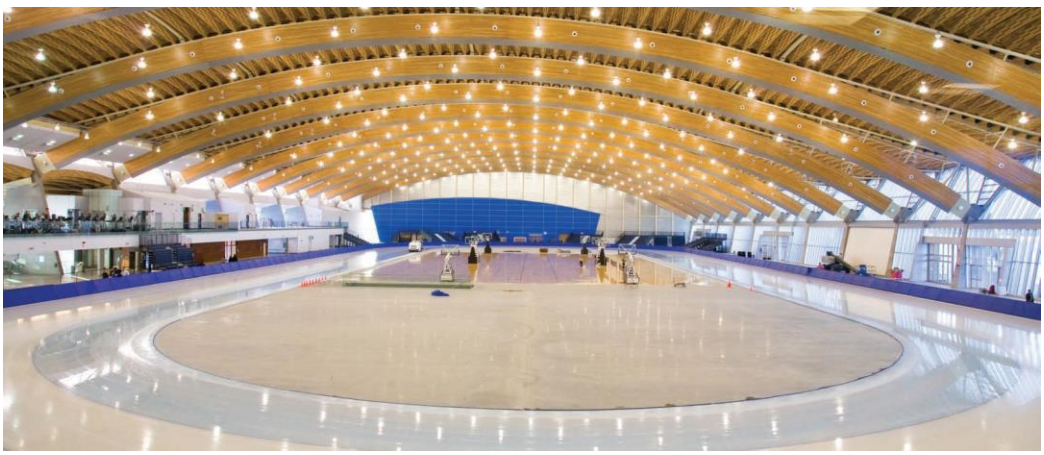

Figure 2-3: Richmond Olympic Oval in Canada (Canadian Wood Council, 2010)

Glulam can be manufactured to different shapes and sizes making it possible to produce wide-span beam that meet the aesthetic demands of the architects while maintaining the structural requirements of the engineers. In UK, a number of glulam manufacturers are able to produce bespoke glulam (Buckland Timber Ltd., Glulam Solutions Ltd., etc.) and the supply of standard lengths of structural glulam beams may be easily obtained from many glulam suppliers (Cowley Timber Ltd., AJ Laminated Beams Ltd., Lamisell Ltd., etc.).

2.2 Glue-laminated timber

Glulam beams consist of smaller pieces of solid wood which are finger-jointed and laminated to a desired larger dimension. In the production of glulam, there are various processing stages (Figure 2-4) and within them, there are requirements that the producer needs to meet. The first stage requires kiln-drying of sawn timber to a moisture content of 6 to 15% and between 11 to 18% if the pieces are treated with preservatives. In addition, the difference in moisture content between the pieces should not be more than 5% (Annex I.4.4 of BS EN 14080:2013), avoiding large moisture gradients that may affect the bonding later. The timber pieces are then planed and later strength graded visually and/or by machine as required in BS EN 14080:2013, the commonly used standard for glulam production in the United Kingdom and other European countries. There are many grading standards available in different regions of the world and the BS EN 14081 series provide general guidelines for both visual grading and machine grading in most European countries. The visual grading method identifies strength-reducing characteristics in planed sawn timber based on the detailed specifications in BS 4978:2007+A1:2011 for softwood, BS 5756:2007+A1:2011 for hardwood and BS EN 16737:2014 for tropical hardwood.

Machine grading classifies timber based on properties such as strength, stiffness or density. The various types of timber grading machine can be classified into bending, longitudinal or flexural resonant frequency (acoustic methods), x-ray (to measure density and knots) and ultrasonic wave speed

systems (Ridley-Ellis *et al*., 2016). The list of grading machines with their respective measuring methods is listed by Ridley-Ellis (2017) as summarized in Table 2-1.

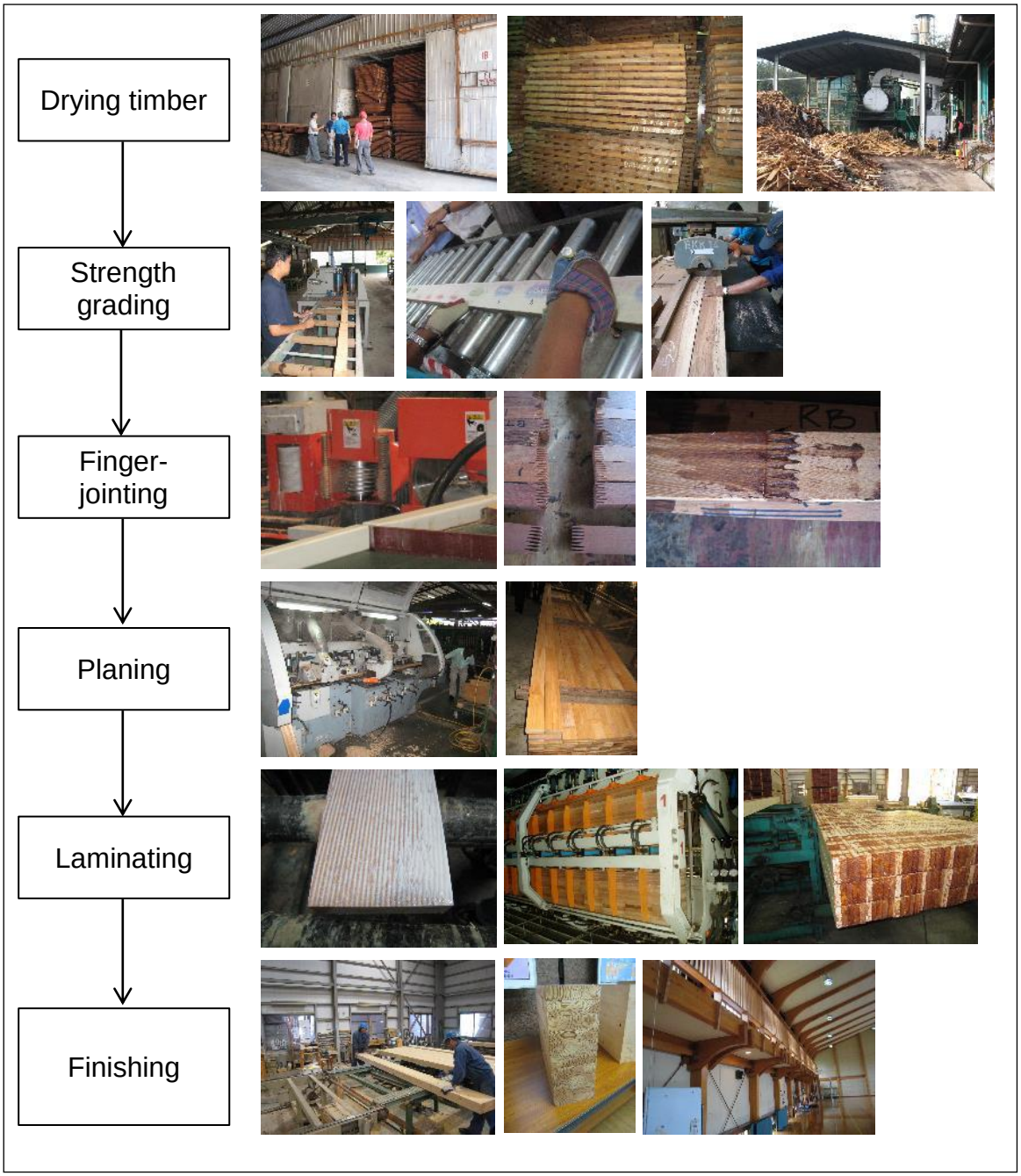

Figure 2-4: Stages of manufacturing glulam (Ong, 2015)

Table 2-1: Timber strength grading machines (Ridley-Ellis, 2017)

Machine	Type
Cook Bolinder	Mechanical bending
Computermatic Micromatic	Mechanical bending
Raute Timbergrader	Mechanical bending
EuroGreComat-702	X-ray
Goldeneye 702	X-ray
EuroGreComat-704	X-ray & mechanical bending
Dynagrade	Acoustic
Viscan	Acoustic
EuroGreComat-706	X-ray & acoustic
Goldeneye 706	X-ray & acoustic
MTG 960 (MTG with balance)	Acoustic
Precigrader	Acoustic
Grademaster (with optical scanner for knot measurements)	Acoustic
Escan FWM/FW	Acoustic
Triomatic	Acoustic
CRP	Mechanical bending
Xyloclass T	Acoustic
Noesys	Acoustic
MTG 920 (MTG without balance)	Acoustic
Viscan Plus	Acoustic
Xyloclass F	Acoustic
Viscan Compact	Acoustic
MTGbatch 962/966 (with balance)	Acoustic
MTGbatch 922/926 (without balance)	Acoustic
Rosegrade	Acoustic
EScan FM/F	Acoustic
E-CONTROL model AC	Acoustic
Rosgrade plus	Acoustic
Viscan portable (with balance)	Acoustic
Viscan portable (without balance)	Acoustic
WoodEye Strength Grader	Acoustic & laser tracheid effect
RS Strength Grader	Laser tracheid effect
LuxScan OptiStrength XE	X-ray & acoustic
LuxScan OptiStrength X	X-ray
STIG (strength timber grading machine for Slovenian Spruce)	Acoustic
USNR Lineal High Grader	X-ray & laser

Studies have been conducted to evaluate and compare the different types or combinations of commercial grading machine such as the Computermatic, Cook-Bolinder and Raute Timgrader (Benham *et al*., 2003); Metriguard's High Capacity Lumber Tester, Linear High Grader and WoodEye® (Baillères *et al*.,

2012); and MiCROTEC's machine, Brookhuis MTG and Metriguard (Barret *et al*., 2008; Bacher, 2008). The limitations of machine grading methods are the inability to measure the end of the timber pieces, approximately 800 mm for bending-type and 150 mm for radiation-type machine, which requires measurement using the visual override method (BS EN 14081-2:2010+A1:2012).

2.3 Finger joints

Graded timber is finger-jointed to produce continuous lengths as pre-determined by the producer of glulam. There are two types of finger joints which can be categorized based on the fingers orientation, either horizontal or vertical as shown in Figure 2-5.

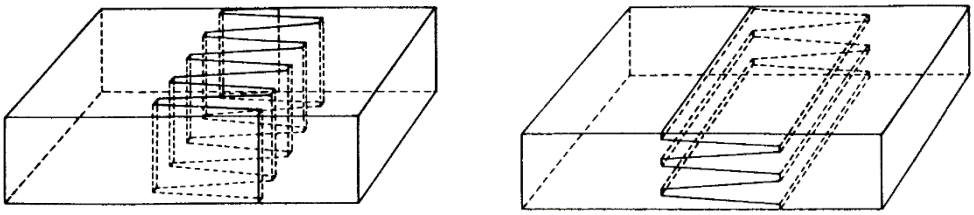

Vertical joint Horizontal joint

Figure 2-5: Types of finger joint (Jokerst, 1981)

The vertical joint is commonly used in the production of glulam due to the higher bending and tensile strength compared to the horizontal joint. Theoretically, in the finger-jointing process, the end pressures applied will tend to make the outer fingers spread out, resulting in lower joint strength with thicker glue lines at the face or edge. In comparison, the outer fingers of vertical joints which have a smaller bonding area, and thus smaller weak sections, perform better than the horizontal joints which have larger outer joint areas with weak sections (Jokerst, 1981).

The requirements for producing good finger joints for glulam are stated in BS EN 14080:2013. It is pertinent to avoid wane, edge damage, knots and distinct grain deviation within the joints. The knots should be located away from the

finger joints, with minimum distance of three times the knot diameter. The recommended finger geometries and cutter profiles are also given in BS EN 14080:2013 and BS EN 15497:2014 respectively. The descriptions for the finger joints profile are shown in Figure 2-6 and the recommended finger geometries are given in Table 2-2.

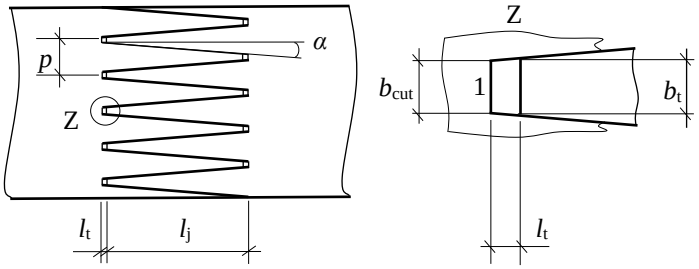

Key:
1 slot base
l_j finger length
p pitch
α finger angle
l_t tip gap
b_{cut} tip width of the cutter
b_t tip width

Figure 2-6: Typical profile of finger joint (BS EN 15497:2014)

Table 2-2: Recommended finger geometries (BS EN 14080:2013)

Finger length l_j (mm)	Pitch p (mm)	Tip width b_t (mm)	Reduction factor v
15	3,8	0,42	0,11
20	5,0	0,5	0,10
20	6,2	1,0	0,16
30	6,2	0,6	0,10

The standards recommend the finger angle, $\alpha \leq 7.1^{\circ}$. Finger length, l_j and reduction factor, v are as follows:

Finger length, $l_j \geq 4\ p\ (1 - 2\ v)$ (Eq. 2-1)

Reduction factor, $v = b_t/p$ (Eq. 2-2)

Furthermore, BS EN 15497:2014 requires the finger length, l_j to be more than or equal to 10 mm; the reduction factor, v to be less than or equal to 0.20; and the ratio between finger tip width, b_t to cutter width, b_{cut} to be $1.1 \leq b_t/b_{cut} \leq 1.2$. BS EN 14080:2013 specifies that the finger length, l_j should be more than 10 mm; and the reduction factor, v should be less than or equal to 0.18.

The geometries and different configurations of the finger joint profile play an important part in determining the strength of finger-jointed timber pieces (Tran *et al.*, 2014; Bustos *et al*., 2003a, Ayarkwa *et al*., 2000). The strength of finger joints will depend on the specification of different type of adhesives and cure temperature (Vrazel and Seller, 2004) as well as the curing time, end pressure and machining parameters (Bustos *et al*., 2003b, 2004 and 2011). Comparison made between solid timber and finger-jointed timber indicates that the strength of finger joints may vary based on the manufacturing process and may have a joint efficiency of up to 75% compared to solid wood if they are well-manufactured (Frihart and Hunt, 2010; Moody *et al*., 1999). The finger joint efficiency of some Malaysian timbers was also determined by Kok (2000); Tan and Hse (1998); Mansur *et al*. (1997). It was found that the modulus of elasticity (MOE) in bending of finger-jointed pieces was not significantly different to matched solid timbers while the bending and tensile strengths were substantially reduced.

2.4 Lamination

Cured finger-jointed timber is planed and then laminated, normally within 24 hours. This is to ensure the “freshness” of the surface is maintained and to minimize moisture uptake and dust accumulating on the surface of the timber. Typical glulam beam layup consists of laminations with the end joints scattered and the minimum spacing between the joints in adjacent laminations is 15 cm (JAS 1152:2007; ANSI A190.1-2012:2013). BS EN 14080:2013 does not specify the minimum spacing between joints, thus the requirements from JAS and ANSI standards were adopted in this study. This arrangement was intended to improve the bending performance of glulam beams compared to beams with

joints overlapping across the depth. For efficient use of timbers, the beam layup is arranged using different strength grade combinations where lower grade laminations are placed in the inner beam while the outer layers consist of better grades to resist higher stress (Figure 2-7). Falk *et al*. (1992) concluded that beams with an efficient distribution of laminations with different grades were comparable in bending strength to the beams made up of one single high-grade timber. In Malaysia, there were attempts to determine the bending MOE of the built up glulam beams using the MOE of individual lamellas with respect to the timber strength grade layup and placements of finger joints within the beams (Tan *et al*., 2002; Chai, 1994).

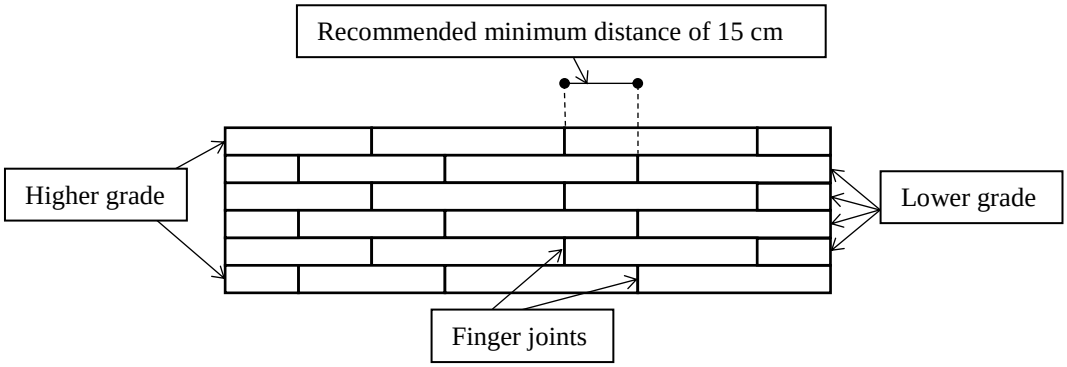

Figure 2-7: Efficient beam layup and minimum joints spacing (finger joint locations are not quite so regular in practice)

The bonding strength of the glue lines between laminations is one of the important factors in the evaluation of the performance of a glulam beam. The bonding performance of the glue lines can be determined using a block shear test as recommended in the production requirements of BS EN 14080:2013. Nevertheless, the evaluation of the shear strength and minimum requirements of the glue lines only apply to mainly softwoods listed in the standard and may not be applicable to other tropical hardwoods especially the Malaysian species. Furthermore, the lack of study related to the bonding performance of Malaysian hardwood for structural uses discourages the timber industry to make use of the local timber for the production of glulam beams (Wahab *et al*., 2016).

Factors affecting shear strength of the glue lines of a glulam beam such as using appropriate cramping pressure and proper application of suitable adhesive are crucial in producing good bond strength. BS EN 14080:2013 recommends a set of different cramping pressures according to the lamination thickness of the glulam beams. These cramping pressures may not be suitable for bonding Malaysian hardwood which has higher density compared to the softwood species. The large variation of density within a species also affects the gluability of the hardwood and an inadequate cramping pressure may resulted in lower bonding strength. Vick (1999) reported that high density wood needed higher cramping pressure to produce optimum contact between the wood surfaces and the adhesive. Frihart and Hunt (2010) stated that the bonding strength of the glue lines increases with density up to a range of 700 to 800 kg/m^3. In contrast, Hafizah *et al*. (2014) reported that the bonding strength of Malaysian hardwood, Kempas and Keruing, which were bonded with structural epoxy adhesive exhibited similar shear strength even though the density of Kempas specimens was higher than Keruing. They concluded that the bonding strength of the specimens was not influenced by density but depended on the mode of failure of the glue lines.

The shape and size of the specimens also influenced the bonding strength of the glue lines. The bonding strength of the glue lines can be evaluated using the block shear test method as recommended in BS EN 14080:2013. The standard introduces a modification factor to accommodate the effect of size on the shear strength of the specimens. This size effect refers to the condition where different shear strength results were obtained from specimens with different sheared area although the specimens may originated from the same block of beam. Gaspar *et al*. (2017) reported that this modification factor may not be suitable for specimens with shear strength above 15 N/mm^2 and may contribute to unsafe corrections.

2.5 Adhesives

Originally, the bonding of joints and lamination in the manufacturing of glulam was based on non-waterproof adhesive for products used in low humidity environments (Lehringer and Gabriel, 2014). The advancement of adhesives technology paved the way for improved glulam utilizing waterproof adhesives that are capable of withstanding harsh, wet and high humidity environments. BS EN 14080:2013 provides guidelines and relevant requirements for different adhesive types for different service classes. The standard recommended adhesive groups suitable for bonding of end joints and laminations such as the phenolic and aminoplastic adhesives (e.g. melamine formaldehyde (MF), melamine-urea formaldehyde (MUF), phenol resorcinol formaldehyde (PRF), urea-formaldehyde (UF)), moisture curing one-component polyurethane adhesives (PUR) and emulsion polymer isocyanate adhesives (EPI).

Further detailed descriptions of performance requirements for these load-bearing adhesives are stated in BS EN 301:2017, BS EN 15425:2017 and BS EN 16254:2013+A1:2016. Other related requirements include the assembly time under different conditions (BS EN 302-5:2013; BS EN 15416-4:2017), pressing time (BS EN 302-6:2013; BS EN 15416-5:2017) and working life (BS EN 302-7:2013) under referenced conditions. In general, the above specifications are given by the glue manufacturers for different type of adhesives. In the evaluation of the bonding performance, BS EN 14080:2013 provides methods and requirements needed to evaluate the glue lines of the finger joints and laminations in different climate conditions. Apart from the adhesive specifications, materials preparation also plays an important role in providing good bonding surfaces. Singh *et al*. (2002) concluded that poor bonding performances were the result of poor surfaces when planed with a blunt knife in comparison to a sharp knife. They observed microscopically the extent of damage to the cell walls in planing and its influence on glue bond strength. Özçifçi and Yapici (2008) also investigated the effect of using different machines such as a circular saw, band saw and thickness planer, on the bonding performance of different wood species. They concluded that machines

producing wood with higher surface roughness contribute to lower bonding strength.

Another factor influencing bonding performance is the occurrence of chemicals on wood surfaces including natural extractives and wood preservatives. These chemicals prevent proper wetting and penetration of adhesives, blocking full contact with wood. Over-drying also encourages the natural extractives to propagate to the wood surface, further contaminating the bonding process and reducing the resulting bonding strength (Frihart and Hunt, 2010). Alamsyah *et al*. (2008) studied the influence of *Acacia mangium*'s extractives on the curing of resorcinol formaldehyde adhesive and suggested improvement of bonding performance by extending the curing time and treating the wood surfaces with methanol to improve wettability. Gaspar *et al*. (2010) investigated the shear strength of glulam treated with copper azole and suggested that minimum possible preservative should be used in the glulam production because of its negative influence on the glue line's strength.

2.6 Reinforced glulam

Glulam beams are reinforced to increase their load-carrying capacity and also to reduce the number of laminations or materials used, thus lowering the production costs. Examples of reinforcement materials include steel (De Luca and Marano, 2012), bamboo (Echavarría *et al.,* 2012) and fibre reinforced polymers (FRP) such as carbon fibre reinforced polymer (CFRP), glass fibre reinforced polymer (GFRP) (Guan *et al.*, 2005; Micelli *et al.*, 2005) and basalt fibre reinforced polymer (BFRP) (Yeboah *et al.*, 2013). The reinforcements are normally located on the outer layers of the beam, in particular the tension face, where the stress is the highest.

The compatibility of FRP to wood composites is thought to be better than metal-wood composites and the FRP panels possess design tensile stresses of up to 70 times and tensile MOEs of up to 10 times greater than wood (Martin *et al*., 2000). In comparison, reinforced glulam beams tested in flexure show more

ductile behaviour than unreinforced beams that exhibit brittle behaviour (De Luca and Marano, 2012; Issa and Kmeid, 2005). The reinforcement will also increase the stiffness of the glulam beam when tested in bending (Alhayek and Svecova, 2012). The effect of the reinforcement is only significant if the stresses from the timber in a bending test are successfully transferred to the reinforcement material. Glišović *et al*. (2016) reported that glulam beams reinforced with CFRP plates in the tension region improved the ultimate load-carrying capacity and stiffness of the beam. They concluded that the reinforcement increases the compressive strain and reduces the tensile strain of the reinforced beams when compared to the unreinforced beams. They also indicated that the reinforcement was able to reduce the effect of natural defects in the beam.

Studies were also conducted on the reinforcement of selected Malaysian hardwood. Azlan *et al*. (2013) concluded that bending tests conducted on Kempas beams reinforced with CFRP showed an increase in bending strength compared to the unreinforced beams. A study by Hassan *et al*. (2015) reported a slight increase of load-carrying capacity of Yellow Meranti and Bintangor specimens in bending when reinforced with GFRP. Ahmad (2013) reinforced Yellow Meranti beams with CFRP plates and tested them under four-point bending tests. The author concluded that the reinforced beams showed ductile behaviour and the ductility improved with an increase in the ratio of CFRP surface area to the surface area of the timber to be reinforced.

2.7 Fire performance

The fire performance and structural behavior of glulam beams at elevated temperature are pertinent to the fire safety design and construction of buildings and bridges. Generally, glulam beams with larger cross-sectional dimension will have better flame retardancy due to the fact that charred surface layers may act as thermal insulator, preventing further damage to the inner sections (Frangi and Fontana, 2003; Martin and Tingley, 2000). Charring rate plays an important factor and is normally used in the calculation of fire resistance. Different timber

species have different charring rates. Yang *et al*. (2009) concluded that the increase in wood density showed a decrease in charring rate.

The behavior of finger joints in glulam beams was also widely investigated in relation to exposure to fire. Klippel *et al*. (2013) performed fire tests on finger-jointed timber boards and concluded that there is no significant difference between finger joints bonded with different adhesives. They also concluded that there is a negative linear relationship between fire resistance and the load applied in fire test.

The fire safety design of timber structures can be further improved by understanding the behaviour of timber when tested under fire conditions. In a standard fire resistance test such as in BS EN 1365-3:2000, glulam beams are tested in bending with the highest stress experienced by the outermost tension layer while exposed to severe fire conditions. The effective cross section of the glulam beam is reduced once the charred outmost layer loses its strength and this increases the deflection of the beam. The interface between the residual beam and the charred outermost layer will experience an increase in tensile stress and will further delaminate and fall from the beam. This condition is described as secondary failure and leads to a sudden increase of fire intensity on the unburnt inner wood when there is no charred outermost layer to act as thermal insulator. Consequently, this increases the charring rate of the uncharred layer. The difficulty in observing the behaviour of finger joints in secondary failure in a standard fire test has resulted in the lack of related published work. Thus, a simpler and less costly bench-scale fire test is proposed in this work to evaluate the fire performance of finger joints at secondary failure.

Bench-scale tests were introduced recently to evaluate the performance of glue lines in both finger joints and laminations at elevated temperature. Craft *et al*. (2008) proposed a new small-scale test method which is able to evaluate multiple finger-jointed specimens under tension with the use of an oven. The behaviour of finger joints at secondary failure was not described because the experiment uses lower temperature compared to the sudden exposure of high

temperature experienced by the finger joints during secondary failure. Klippel *et al*. (2014) reported moderate reduction in tensile strength of the finger joints when the testing temperature in the small-scale fire test was between 20 to 140^{o}C. They observed that wood failure was predominant when the temperature was increased to 220^{o}C and concluded that the wood itself was being tested instead of the adhesives. Further refinement to these bench-scale fire tests is needed and comparison of results between these tests and the full-scale fire tests is essential before they can be used to adequately describe the fire performance of a glulam beam.

2.8 Summary

This chapter reviewed previous studies on finger joints and laminations which are important components of the glulam beam. The production requirements when manufacturing finger joints and laminations were reviewed. The use of standardized methods, for both production and testing of finger joints, laminations and glulam beams, is essential to produce specimens that meet the minimum requirements for structural uses. The profile of the finger joints for the fabrication of finger-jointed specimens must meet minimum requirements, which are reached by the finger joints with shorter length investigated in this study. Factors such as the variation of density within a species, end cramping pressure, specimen configurations such as vertical and horizontal joints and size effect will affect the mechanical properties of the finger-jointed specimens. Better understanding of the factors affecting the behaviour of finger joints will help the glulam beam manufacturers to produce stronger finger joints using Malaysian wood species.

The factors influencing bonding performance of the glue lines in a glulam beam was also reviewed in this chapter. The findings of majority of the studies were based on softwood species and may not adequately or correctly describe the behaviour of specimens bonded using Malaysian hardwood for which there is scarce information. Thus, factors affecting shear strength of the glue lines of Malaysian glulam beams should be identified and adequately analysed to fill the

technical gap that discourages the use of Malaysian species for structural uses. Cramping pressure, density and size effect were some of the factors influencing the bonding performance of the Malaysian glulam beams and were investigated in this study.

2.9 Research methodology based on the review of the literature

The reinforcement of glulam beams improves the load-carrying capacity, stiffness and ductility of beams as mentioned in this chapter. This study further explores the behaviour of Malaysian glulam beams in bending where two different reinforcements were bonded to the test beams. A closer inspection of the mode of failure, crack initiation and propagation and the analysis of strain during the bending test yields a better understanding of the behaviour of the DRM glulam beam under deformation.

This chapter also reviewed published work on the behaviour of glulam beams when exposed to fire conditions. In general, charring rate is considered to be important in the evaluation of the fire performance of timber products. The focus of this study is to use a bench-scale fire test to imitate the testing conditions of the full-scale fire test. Information on the secondary failure of finger joints in fire is still lacking due to the difficulty of accessing and obtaining information pertaining to the condition of the finger joints in a glulam beam during a full-scale fire test. Thus, this study attempts to imitate the secondary failure of the glulam beam using a bench-scale fire test which is less costly and simpler to set up and has faster completion time compared to standard fire tests.

To produce reliable results relevant to the needs of the timber industry in Malaysia, it is important to produce specimens according to standard production requirements. For repeatability, the specimens should be tested using standard testing procedure so that future comparison can also be made when testing specimens made from other species available in Malaysia. Thus, the review of the minimum production requirements embodied in various standards will

ensure the production of quality glulam beams that are suitable for structural uses.

Chapter 3 Materials and test methods

3.1 Introduction

This chapter introduces the materials and test methods used throughout this study. The assumptions and reasons for employing these particular test methods are explained in relation to the research focus. The tests were conducted based on the standard production requirements and testing methods of the European Committee for Standardization (CEN). Malaysia is bestowed with a large number of timber species ranging from light hardwoods (density 400-720 kg/m^3) to heavy hardwoods (density 800-1120 kg/m^3) (Wong, 2002). Therefore, it is pertinent to use established standards to ensure repeatability and to allow comparison between the results of this study with the results of future research using different wood species.

In this study, the technical information derived from the rigorous testing of finger joints and laminations provides a foundation for the understanding of the performance of glulam beams produced from hardwood tropical timber. From the literature review presented in Chapter 2, the main focus areas of research relevant to the glulam industry in Malaysia were identified as below:

1. To evaluate the mechanical properties of the individual constituents of the glulam beams, namely the finger joints and laminations, made from Malaysian hardwood.
    a) What are the factors that influence the mechanical properties of the finger joints and laminations?
    b) What are the optimum configurations for producing reliable finger joints and laminations when manufacturing glulam beams?

2. To assess the bending properties of both unreinforced and reinforced glulam beams made from Malaysian hardwood.
    a) How do the CFRP reinforcements influence the bending properties of the glulam beams?

b) Can the existing standard production requirements and testing methods for softwood glulam be applied to Malaysian hardwood glulam?

The lack of relevant research relating to the performance of Malaysian hardwood in structural uses prompted the initiation of the first focus area. Full understanding of the performance of the finger joints and lamination are significant because the strength of glulam beam depends on the weakest individual constituents which most probably initiate the failure of the beam. The research questions in this focus area are discussed in detail in Chapters 4, 5 and 7. The second focus area investigates the influence of reinforcements on the bending properties of hardwood glulam beams produced in the study. The research questions will be discussed comprehensively in Chapter 6 and 8. Evidently, both focus areas will address the lack of technical information relating to the production of Malaysian hardwood glulam, paving the way for future research and encouraging the construction industry in Malaysia to specify glulam for large timber structures.

3.2 Materials

3.2.1 Timber

The focus of this study is to fill the technical gap in the utilisation of hardwood for glulam production, specifically using the Malaysian species Dark Red Meranti (*Shorea* spp.). Initial plans for using fast-growing Malaysian plantation timber, *Acacia mangium*, was eschewed because of the high transportation cost from Malaysia. As explained in Chapter 1, the supply of fast-growing timber in Malaysia is increasing due to decades of promotion and subsidy from the government to establish plantation forest and decreasing the dependence on timber from natural forests. In fact, the *Acacia mangium* trees planted in Malaysia are considered mature and ready to be harvested once they are 15 years old (Tan *et al.*, 2010). The average log diameter of 16 and 20 year-old *Acacia mangium* was reported to be 32.5 and 37.9 cm respectively, containing

a large number of knots because of its fast–growing nature (Lim *et al.*, 2011). In glulam technology, the limited width of this small diameter log can be glued together to produce wider and thicker boards, while the knots can be removed and the pieces can be subsequently finger-jointed, thus producing larger dimension and longer span glulam suitable for structural purposes. In addition, *Acacia mangium* is considered to be a light hardwood with a density of 467 to 675 kg/m^3 classified in the strength group SG5 or SG6 according to the Malaysian Standard MS 544:2001, based on its mechanical properties and density (Lim *et al.*, 2003). Khaidzir and Wahab (2011) reported that the average modulus of elasticity (MOE) and modulus of rupture (MOR) of 16 year-old *Acacia mangium* gathered from static bending tests were 10347 N/mm^2 and 96.6 N/mm^2 respectively, with average density of 608 kg/m^3 and moisture content of 19.9%.

Dark Red Meranti was used in this study because of its availability and similarity to *Acacia mangium* in terms of its density and mechanical properties compared to other species readily available in the UK. DRM is classified as a light hardwood with density range of 415 to 885 kg/m^3 and average MOE and MOR of 11200 N/mm^2 and 74 N/mm^2 respectively (Choo *et al.*, 1998; Wong, 2002). Similar to *Acacia mangium*, DRM is classified as SG5 in the strength grouping listed in MS 544:2001. Nevertheless, DRM is currently only used in non-structural products, extremely popular as general utility timber, furniture-making, joinery and is not utilised for structural uses in Malaysia.

The high density variation of DRM (*Shorea* spp.) is due to the fact that this genus consists of many species widely distributed in Malaysia. These species can be found in low-lying areas with dry soil (*Shorea platycarpa*) to high altitude areas up to 1100 m above sea levels with moister soil (*Shorea curtisii*). In an attempt to reduce material variability, the DRM was bought in one large batch from Sykes Timber with specified density of 530 to 630 kg/m^3 and with grade of ‘Selects and Better’. The timber was ordered as sawn to size with dimensions of 52 mm (depth) x 110 mm (width) x 1000 mm (length) and was already kiln-dried to approximately 12% before delivery. Inspection of the quality of the DRM timber batch (Figure 3-1) revealed few defects and consistency in density.

Figure 3-1: Dark Red Meranti timber

Norway Spruce (*Picea abies*) was used in the finger-jointing study to compare with the DRM. It is a popular commercial softwood available throughout Europe and is also cultivated in Russia and the Nordic countries. Spruce is also commonly used in the production of glulam beams in Europe (Falk and Hernandez, 1995) besides being used for joinery, flooring and construction purposes. The Spruce pieces were sourced from a local timber supplier Avon Plywood Ltd. The timber pieces were graded as C16 with density range of 410 to 580 kg/m^3 and kiln-dried to 12% moisture content.

'Selects and Better' grade is defined as one of the grade stresses for a batch of graded timber. The Malaysian Grading Rule (Malaysian Timber Industry Board, 2009) adopted three stress grades of timber, namely Select Structural, Standard Structural and Common Building grades. These grade stresses are derived from the basic stresses governed by visible defects such as knots, slope of grains, fissures etc. Select Structural, Standard Structural and Common Building grades correspond to the strength ratios of 80%, 63% and 50% of the basic stresses respectively. The strength ratio is defined as the ratio

of the strength of a piece of timber with defect to the same timber piece without the defect (Chu *et al*., 1997). 'Selects and Better' grade indicates the worst piece of the timber batch to be at least Select Structural grade. Both DRM and Spruce timber pieces were further visually sorted in the laboratory and the cross-sectional areas with major defects such as knots and splits were cut. The visually inspected timber is considered to be clear (defect-free) specimens because of the elimination of defects in the test pieces. These clear specimens are expected to have higher strength properties compared to timber pieces graded using machine grading because the machine graded pieces take into account the existing strength-reducing defects. Forest Research Institute Malaysia (FRIM) is currently researching a strength-grading machine suitable for grading Malaysian hardwood timber. The machine applies a predetermined load within the elastic limit to the timber piece and the resulting bending deflection is used to calculate bending stiffness. The bending stiffness is then used to predict bending strength of the test piece based on a close relationship between the two bending properties.

The timber pieces of DRM and Spruce were further processed into specimens and randomly selected for various test configurations. The preparation details of the specimens were described in Section 4.2.3 for four-point bending tests, Section 4.2.4 for tensile tests parallel to grain, Section 4.2.5 for compressive tests parallel to grain, Section 5.2.4 for block shear tests and Section 7.2.1 for bench-scale fire tests. The number of test pieces and dimensions were also described in the respective sections.

All density values in this study were adjusted to 12% reference moisture content according to BS EN 384:2016 standard. The mean and standard deviation of the adjusted density for DRM specimens were 582 and 82 kg/m^3 respectively, while for Spruce specimens, they were 500 and 60 kg/m^3. The compression strength parallel to grain and local modulus of elasticity were also adjusted to the reference moisture content according to BS EN 384:2016 but the bending strength of the test specimens were not adjusted to the size factor, k_h of the standard. The characteristic values of density (5th percentile) for both DRM and Spruce specimens were determined according to the BS EN 14358:2016

standard. The density values of the timber species were assumed to be normally distributed and the characteristic values were determined at a confidence level of 75%. The characteristic values of density for DRM and Spruce were 421 and 372 kg/m^3 respectively.

3.2.2 Adhesives

Phenol resorcinol formaldehyde (PRF) was used as the bonding medium for both the finger joints and laminations. Specifically, Casco Phenol Resorcinol Formaldehyde Adhesives System was used and consists of two-part systems, namely Resin 1711 and Hardener 2520. The resin and hardener are in liquid form and the mixing ratio by weight is 100 : 15 (resin : hardener). This PRF adhesive is well-established for structural uses and known to be able to withstand harsh weather conditions due to its high resistance to moisture, heat and chemical aging (Frihart and Hunt, 2010). In addition, the technical datasheet indicates that the adhesive fulfills the requirements of BS EN 301:2017, for glue types I and II and service classes 1, 2 and 3 making it suitable for the manufacture of glulam for exterior uses. The service classes correspond to the adhesive type and environmental conditions are shown in Table 3-1.

Table 3-1: Service class and adhesive type classifications (BS EN 301:2017)

Service Class	Adhesive type	Environmental conditions
1	I or II	Climatic conditions characterised by a moisture content in the materials corresponding to a temperature of 20°C and the relative humidity of the surrounding air only exceeding 65% for a few weeks per year.
2	I	Climatic conditions characterised by a moisture content in the materials corresponding to a temperature of 20°C and the relative humidity of the surrounding air only exceeding 85% for a few weeks per year.
3	I	Climatic conditions leading to higher moisture contents than in service class 2.

For comparison purposes, an epoxy adhesive, namely the Sircomin Wood Epoxy System, was also used as bonding medium in the finger-jointing process. Similar to PRF, the epoxy adhesive consists of a two-part system, the SR 5550 resin and SD 5503 hardener, both in liquid form, with mixing ratio by weight of 100 : 29 (resin : hardener). The adhesive is fully cured after 7 days at ambient temperature (as recommended in the technical datasheet). In general, epoxy adhesive is widely used as a bonding substance for repair and reinforcement of structural wood products. In addition, this Sircomin epoxy system is specially formulated for the use in the building of marine composites.

Throughout this study, cold pressing (pressing at room temperature) was used in both the finger-jointing and lamination processes. All the wood specimens were prepared and bonded within 24 hours of the planing process to ensure optimum bonding strength. The pot life used for the PRF mixture was kept to a minimum, and a maximum period of 70 minutes (in room temperature of 20°C) was adhered to before the adhesive starts to cure and increased in viscosity. Consistent glue squeeze-out was observed in the cramping process, indicating adequate glue spread applied to the surface of the specimen. Post curing of one day at room temperature was necessary before the specimens could be further processed. For full curing, the specimens were left for more than 7 days at room temperature before being subjected to further mechanical tests.

3.2.3 Carbon fibre reinforced polymer

Carbon fibre reinforced polymer (CFRP) was used to reinforce the DRM glulam beams. Specifically, Formax FCIM230 CFRP fabric was used together with a two-part thixotropic epoxy impregnation resin, Sikadur-330 as the bonding medium. The CFRP fabric was unidirectional and has a nominal thickness of 0.16 mm. This CFRP fabric was the same reinforcement material used in Tajaddini's (2015) dissertation. The average mechanical properties of the CFRP fabric are shown in Table 3-2.

Table 3-2: Mean results of coupon tensile tests (Tajaddini, 2015)

Thickness	Ultimate tensile strength (σ_f)	Tensile modulus (E_f)	Ultimate strain (ε_{fu})
0.16 mm	4.23 GPa	238 GPa	1.78%

The CFRP fabric was bonded by impregnation to the tension surface of the glulam beams using the commercial Sikadur-330 epoxy adhesive. The resin and hardener are in paste form with mixing ratio by weight of 4 : 1 (resin : hardener). The mechanical properties of Sikadur-330 resin are given by the manufacturer (see Table 3-3). For full curing, the specimens were left for more than 7 days at room temperature.

Table 3-3: Mechanical properties of Sikadur-330

Tensile strength	Tensile MOE	Elongation at break
30 N/mm^2	4500 N/mm^2	0.9%

3.3 Test methods

3.3.1 Four-point bending test

The finger-jointed specimens and the full size glulam beams were tested in bending throughout the study. Specifically, the four-point bending test used was based on the standard testing methods of BS EN 408:2010+A1:2012 for determining the modulus of rupture (MOR) and local modulus of elasticity (MOE) in bending. The configuration of this standard bending test followed the setup shown in Figure 3-2.

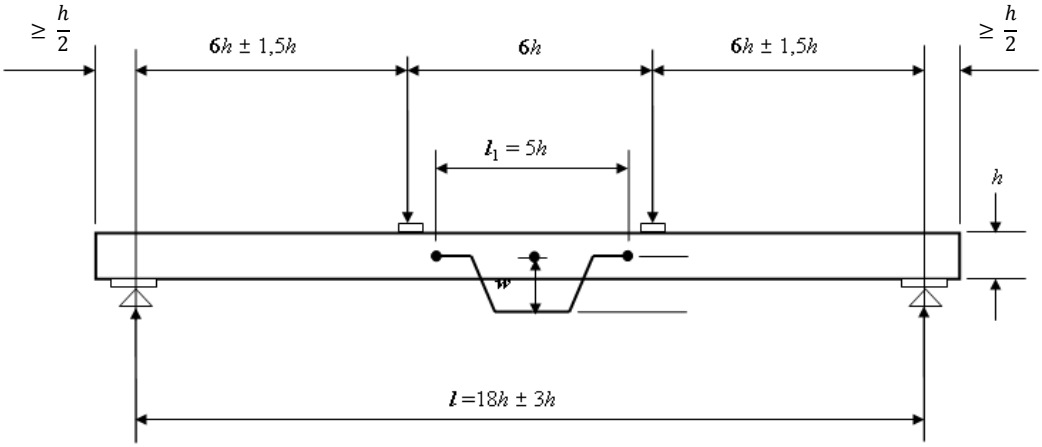

Key:

h depth of cross section, (mm)

l bending span, (mm)

l_1 gauge length for determination of MOE, (mm)

w deformation, (mm)

Figure 3-2: Four-point bending test configuration (BS EN 408:2010+A1:2012)

In this study, the specimens were simply supported and symmetrically loaded, with the length and bending span 19 and 18 times the depth respectively. The distance between the loading head and nearest support points was 1/3 of the bending span. A linear variable differential transformer (LVDT) transducer was attached to the centre of the gauge length (l_1) to measure the deformation (w) at the neutral axis for the determination of local MOE. Detailed descriptions of the positioning of the LVDT transducers are described in Sections 4.2.3 and 6.2.2 for the bending tests of finger-jointed specimens and glulam beams respectively. To minimize local indentation, steel plates with length shorter than half the depth of the specimen were inserted between the specimens and the loading points and supports. According to BS EN 384:2016, the worst defect in the specimen (for unjointed specimen) should be positioned in the middle of the bending span but timber (see Figure 3-1) from which test specimens were produced was selected to be defect free.

The expressions for calculating MOE and MOR follow BS EN 408:2010+A1:2012:

Local MOE in bending (N/mm^2), $E_{m,l} = \frac{a l_1^{\,2}(F_2 - F_1)}{16 I (w_2 - w_1)}$ (Eq. 3-1)

MOR in bending (N/mm^2), $f_m = \frac{3Fa}{bh^2}$ (Eq. 3-2)

Key:

$F_2 - F_1$	increment of load on the proportional limit of the load deformation curve, (N)
$w_2 - w_1$	increment of deformation corresponding to $F_2 - F_1$, (mm)
a	distance between the loading point and nearest support, (mm)
l_1	gauge length for determination of MOE, (mm)
I	second moment of area, (mm^4)
F	load, (N)
b	width of cross section, (mm)
h	depth of cross section, (mm)

MOE is known to provide good predictions of MOR of timber and its relationship is known to be highly positively correlated (Baillères *et al*., 2012). Non-destructive measurements of MOE include vibrational methods, ultrasonic methods and static methods such as the four-point bending test employed in this study. Stiffness values obtained from the four-point bending test are generally used as the standard reference stiffness to other non-destructive tests. Thus, it would be beneficial if good correlation between stiffness and strength were obtained for the DRM timber species.

3.3.2 Tensile test parallel to grain

BS EN 408:2010+A1:2012 was used to determine the tensile strength parallel to the grain of finger-jointed specimens. The specimens were prepared to the size of 10 x 42 x 300 mm. Both ends of the finger joints were gripped over a length of approximately 50 mm. The remaining test length clear of the grips was 200 mm, longer than nine times the depth of the specimen, with the position of the finger joints located in the middle (Figure 3-3). The loading speed was

adjusted to 0.4 mm/min so that the maximum load was reached within 3 to 7 minutes. The finger joints were positioned in the middle of the set-up and the specimen was properly aligned with the clamp, minimising bending when applying tensile load.

The tensile strength, $f_{t,0}$ was calculated based on the ratio of the maximum load, F_{max} to the cross-sectional area, *A* of the specimen (BS EN 408:2010+A1:2012):

Tensile strength parallel to grain, $f_{t,0} = \frac{F_{max}}{A}$ (Eq. 3-3)

Key:

F_{max} maximum load, (N)

A cross-sectional area, (mm^2)

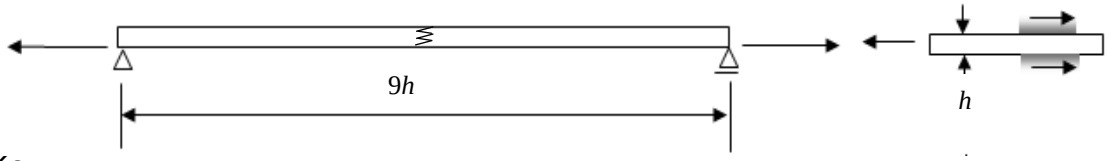

Key:

h depth of cross section, (mm)

Figure 3-3: Tensile test configuration (BS EN 408:2010+A1:2012)

3.3.3 Compressive test parallel to grain

Specimens were prepared to determine the compressive strength parallel to the grain following the requirements of BS EN 408:2010+A1:2012 with the finger joints located in the centre. The length of the specimens was 180 mm (six times the depth of the specimen) with cross-sectional dimension of 30 mm for both the depth and width of the specimens. The end surfaces were carefully cut so that they were flat and parallel to each other, thus, maintaining a compressive load without inducing bending in the specimens when tested. The loading speed applied was 0.5 mm/min so that maximum load was achieved within 3 to 7 minutes.

The compressive strength parallel to the grain was calculated as follows (BS EN 408:2010+A1:2012):

Compressive strength parallel to grain, $f_{c,0} = \frac{F_{max}}{A}$ (Eq. 3-4)

Key:

F_{max} maximum load, (N)

A cross-sectional area, (mm^2)

3.3.4 Density at the time of test

Density plays an important role in the investigation of the mechanical properties of the wood species. It is often used in the estimation of the bending properties of wood assuming the test piece has straight grain and is free from defects (Green *et al*., 1999). In this study, the density of the specimens at the time of the test was determined using a method from BS ISO 13061-2:2013. A test piece was cut from the tested specimen with length of 25 ± 5 mm along the grain and the cross section left as it was. The test piece was cut 150 mm from the end or nearest to the fracture location, avoiding any defects such as knots and wood resin. The test piece was cut and measured immediately after the test or was kept in a conditioning room at 20°C and relative humidity of 65% to avoid any further changes in moisture content if it was not possible to proceed with density determination at that time.

A digital caliper was used to measure the dimensions of the test piece with precision of 0.01 mm and a balance capable of measuring to the nearest 0.01 g was used to measure the mass.

The density of the test piece at the moisture content at the time of test was calculated using equation from BS ISO 13061-2:2013 as below:

$$\text{Density, } \rho_w = \frac{m_w}{a_w \times b_w \times l_w} = \frac{m_w}{V_w} \qquad \text{(Eq. 3-5)}$$

Key:

m_w	mass of test piece at moisture content *w,* (kg)
a_w, b_w, l_w	dimensions of the test piece at moisture content *w,* (m)
V_w	volume of the test piece at moisture content *w,* (m^3)

3.3.5 Moisture content by the oven dry method

Green timber pieces do have completely different physical and mechanical properties from drier pieces. For some wood species, with cross-sectional dimensions of 50 x 50 mm, the bending and compressive strength may increase to more than 50% and 100% from the green to air-dried condition respectively (Holtman, 1929). Furthermore, large variations in moisture content in a batch of timber meant for laminating, will have a negative influence on the bond quality. Moisture content variation will induce a considerable amount of swelling and shrinkage of the pieces when in service, which will cause stresses in the glue lines and ultimately cause delamination in severe cases. Thus, it is important to accurately measure the moisture content of timber pieces, especially when using them for the production of glulam for structural uses.

In this study, the same test piece used for density determination was also used to determine the moisture content of the specimen. The moisture content of the test piece was determined using the oven dry method following the standard requirements of BS EN 13183-1:2002. The test piece was weighed immediately after cutting from the specimen and dried in an oven at a temperature of 103 ± 2°C. The test piece was considered fully dried when successive weighing every two hours showed differences in mass of less than 0.1%. Typically, for test piece of this small dimension and density, the time needed for it to be fully dried was 24 hours.

The moisture content of the test piece was calculated using equation from BS EN 13183-1:2002 as follows:

Moisture content in percentage, $\omega = \frac{m_1 - m_0}{m_0} \times 100$ (Eq. 3-6)

Key:

m_1 mass of the test piece before drying, (g)

m_0 mass of the test piece after drying, (g)

3.3.6 Bench-scale fire tests

The preparation of specimens for the bench-scale fire tests is shown in Figure 3-4. Finger-jointed specimens were prepared from DRM and Spruce species. The ends of the specimens were reinforced with plywood and holes were made for anchoring purposes. These reinforcements were made to prevent failures at the gripping sections.

Figure 3-4: Specimen preparation for fire tests a) DRM without end reinforcement; b) Spruce with end reinforcement

Stone wool was used to protect both faces of the specimen against heat exposure, allowing the exposure of the specimen edge from one direction only. A load of 2.5 kN was introduced at the start of the test. This load was determined based on the load ratio of 8% (DRM) and 14% (Spruce) of the ultimate load of the reference finger-jointed specimens tested in tension at

ambient temperature. The 2.5 kN load was used for both species so that comparison can be made between the fire performance of the DRM and Spruce. Furthermore, the aim was to differentiate the time to failure of the adhesives by extending the time of the test when using smaller load values. A constant heat flux of 50 kW/m^2 was introduced at the start of the test. Prior to the tests, a heat flux gauge was used for calibration.

The specimen together with the protective stone wool was held together with a steel casing for ease of placing them directly under the cone heater (Figure 3-5). Additional stone wool was used to protect the outer region of the specimen near each end, thus exposing only the top edge of the specimen in the inner area of the casing where the finger joints were located. The reinforced ends of the specimen were clamped to steel tabs with a bolt passing through each hole (Figure 3-5b). One end was anchored to the wall and the other end was connected to dead weights using a simple pulley system (Figure. 3-5c).

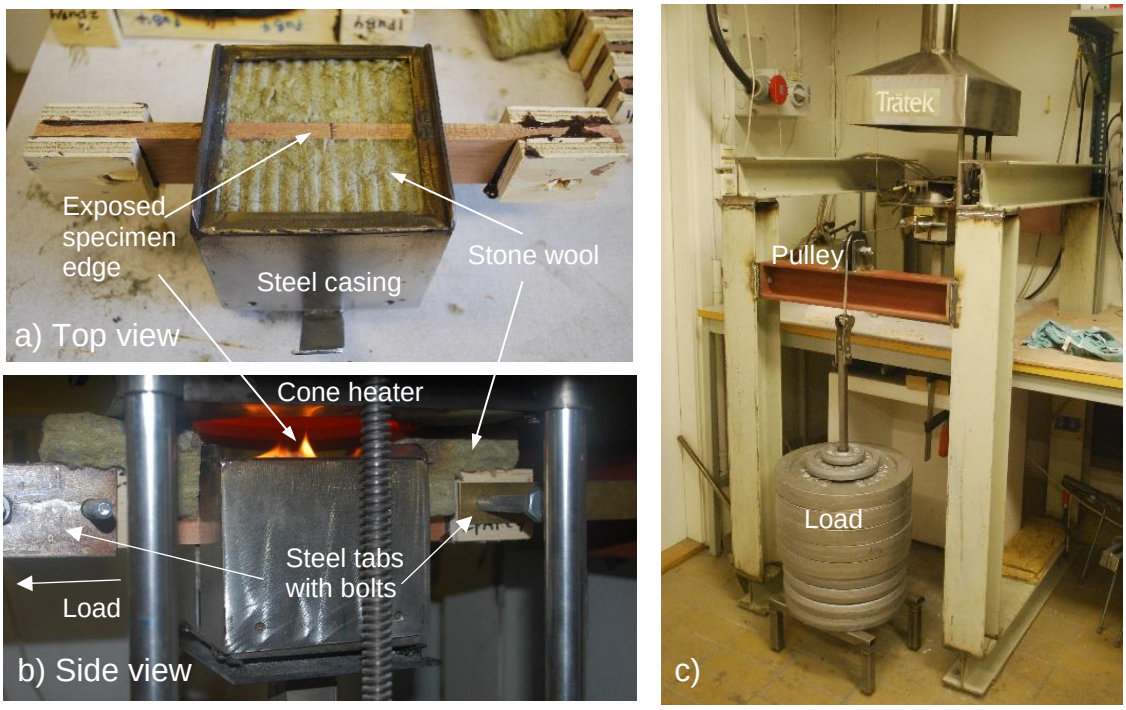

Figure 3-5: Bench-scale fire test set-up (a) specimen held within steel casing; (b) specimen under the cone heater; (c) general view with load applied

Prior to the start of the test, fibre glass wool was used to protect the specimen. The fibre glass wool was removed at the same time as the application of load

and the test began with the recording of time. It was pertinent to immediately start the fire test once the specimen was put under the cone heater because of the possibility that the specimen might start to heat up due to the elevated temperature in the surrounding region. The layout of this test attempts to imitate the conditions of secondary failure (further described in Chapter 7), where the finger joints were exposed to a sudden heat flux once the fibre glass wool was removed and the load was applied.

Immediately after the failure of the specimen, it was quickly removed and soaked in water to remove the remaining embers, preventing further charring once the test was completed. The charred area was brushed off and the residual depth was measured. The one dimensional charring rate (β) was calculated based on the ratio of the charred depth to the measured time to failure. The residual cross section was measured which includes an estimation of the rounded area of the charred line. The residual tensile strength was calculated based on the ratio of the applied load (2.5 kN) to the measured residual cross section after the fire test. The ignition time of the specimen and the time to reach failure for this bench-scale fire test was recorded.

3.4 Assumptions

The focus of this study was to examine the performance of the individual constituents of the glulam beams made from DRM and the bending properties of the beams reinforced with carbon fibre reinforced polymer (CFRP). Detailed descriptions of the experimental approach and the resulting strength performance are important to the glulam producers, especially in a country like Malaysia that has an abundant supply of resources from plantation forests. Given the limited resources in this study and the fact that the nature of glulam research covers wide range of detailed experimentation, the assumptions and limitations were given as below:

- The manufacturing of finger joints and glulam specimens followed closely the production requirements of BS EN 14080:2013 with some

modification when required because of the limited equipment and machinery in the laboratory compared to factory productions. This is important in order to produce results that closely represent the actual performance of the joints and beams produced under factory conditions.

- Evidently, the topic of this study has broad research areas that needs to be addressed. Comprehensive testing and manufacturing following standard production requirements are needed to evaluate the performance of any new wood species suitable for the production of the glulam beams. Given the limited resources and time, the scope of this study does not include the investigation of work such as the grading and lay-up of glulam beams, full-scale fire performance of glulam beams and the prediction of properties by modelling.

- Sampling of test specimens was limited to the batch purchased from the local timber merchant. Representation of the population of timber species could be improved by obtaining timber from different sources throughout the growth region.

- In this study, the timber pieces were sorted and strength-reducing defects were cut, resulting in clear specimens. In contrast, machine graded timber includes defects and specimens are tested to obtain mechanical properties at the worst defect as stated in BS EN 384:2016 standard.

3.5 Summary

The preparation of materials and establishment of methods are crucial to produce accurate and reliable results for future reference. The preparation of specimens and the corresponding tests follow the recommendations and requirements of international/national standards such as BS EN14080:2013, BS EN 408:2010+A1:2012, BS ISO 13061-2:2013, BS EN 13183-1:2012 and AITC

Test T103:2007. This would enables researchers to compare results with less uncertainties of errors that arises from using non-standardized tests.

Chapter 4 Mechanical properties of finger joints

4.1 Introduction

The structural performance of Dark Red Meranti finger joints is presented in this chapter. The aim is to evaluate the mechanical properties of DRM finger joints in bending, tension and compression and to investigate the suitability of using DRM containing structural finger joints for the manufacture of glue-laminated timber. Factors affecting the mechanical properties of DRM finger joints are discussed and comparison made with Spruce structural finger joints.

In Malaysia, local timber is mainly used non-structurally in the production of furniture components. The technical information related to structural finger joints is inadequate, thus further research is needed when using Malaysian hardwood (Ahmad *et al*., 2016). The technical gap includes information pertaining to the processing and fabrication of structural finger joints utilising hardwood species. The domination of softwood species as construction materials, specifically in glulam, has also contributed to the lack of research on hardwood timber (Aicher *et al*., 2001).

This study involves the planning and setting up of a finger-jointing facility in the laboratory. Arrangement of the set-up was made so as to produce structural finger joints with quality equivalent to commercial production. Structural finger-jointed specimens were produced according to the production requirements of the BS EN 14080:2013 standard. The performance of finger joints was evaluated using standard mechanical tests embodied in BS EN 408:2010+A1:2012 including four-point bending, tensile and compressive tests, which are commonly used in testing of structural timber products. The findings in this chapter are important for the manufacture of glulam in view of the fact that strong finger joints are pivotal to producing strong glulam beams which is a key aim of this study.

4.2 Finger joints preparation

Dark Red Meranti timber was used in the fabrication of the finger-jointed specimens and the finger joints were evaluated to determine their mechanical properties. The finger joints were bonded using different jointing pressures according to the standard production requirements of BS EN 14080:2013. The optimum set-up of the finger-jointing process was then used to produce 5 metre length laminations, consisted of multiple finger joints, to be used in the fabrication of glulam beams.

4.2.1 Test specimen preparation

The objective of this section was to describe in detail the preparation of finger-jointed specimens for mechanical testing. DRM test pieces with nominal dimensions 40 mm (thickness) x 105 mm (width) x 500 mm (length) were used in the fabrication of the finger joints. A finger cutter knife was purchased from Leitz Tooling, UK, a company specialized in manufacturing cutters to produce structural joints. The finger cutter knife consisted of individually brazed cutting edges attached to a main steel body, to reduce risk of breakage (Figure 4-1). The cutting edges were made of high-speed steel (HSS) with finger length and pitch of 10 and 3.8 mm respectively. It was specifically fabricated to be used with a spindle moulder operated with a sliding table, clamping jig and manual feed. The configurations of the finger cutter followed safety regulation according to the German Accident Prevention Regulation (VBG 7j § 75) as indicated in the manufacturer's specification sheet. The profile of the finger cutter is shown in Figure 4-2.

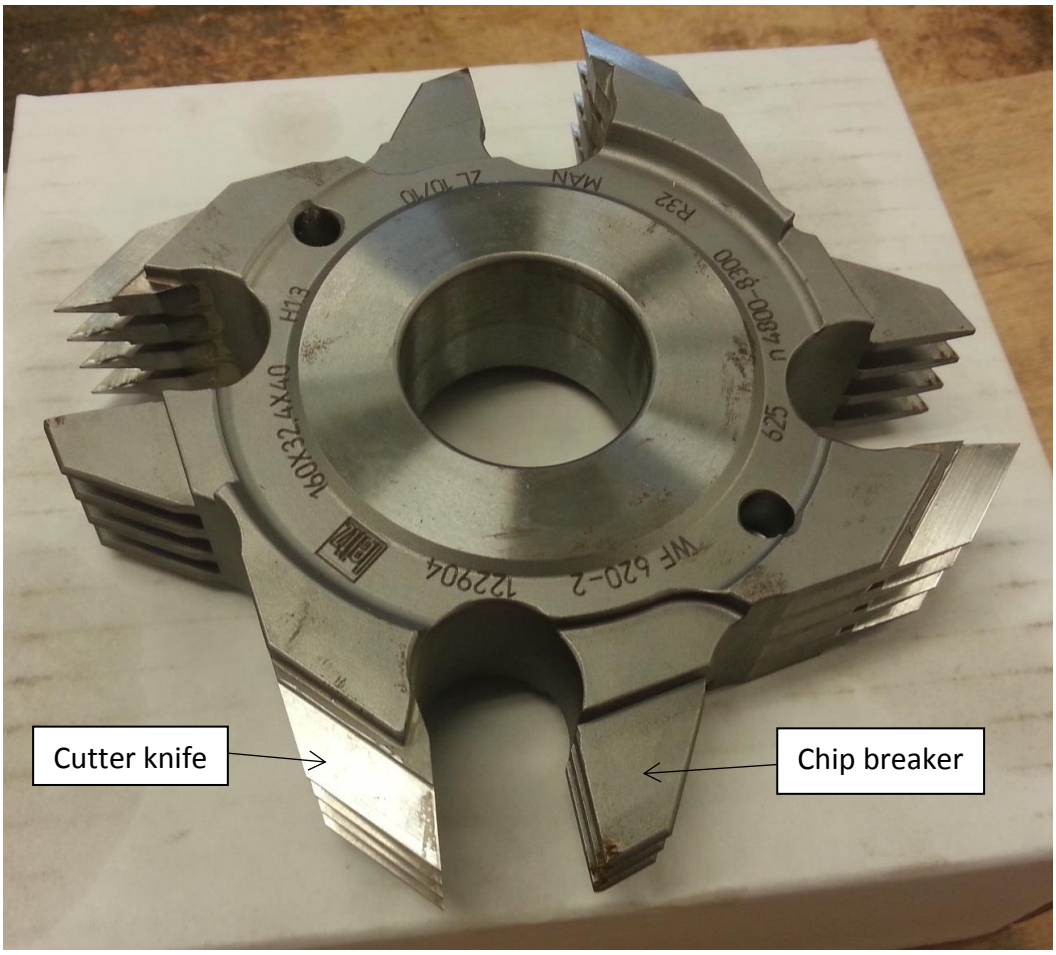

a)

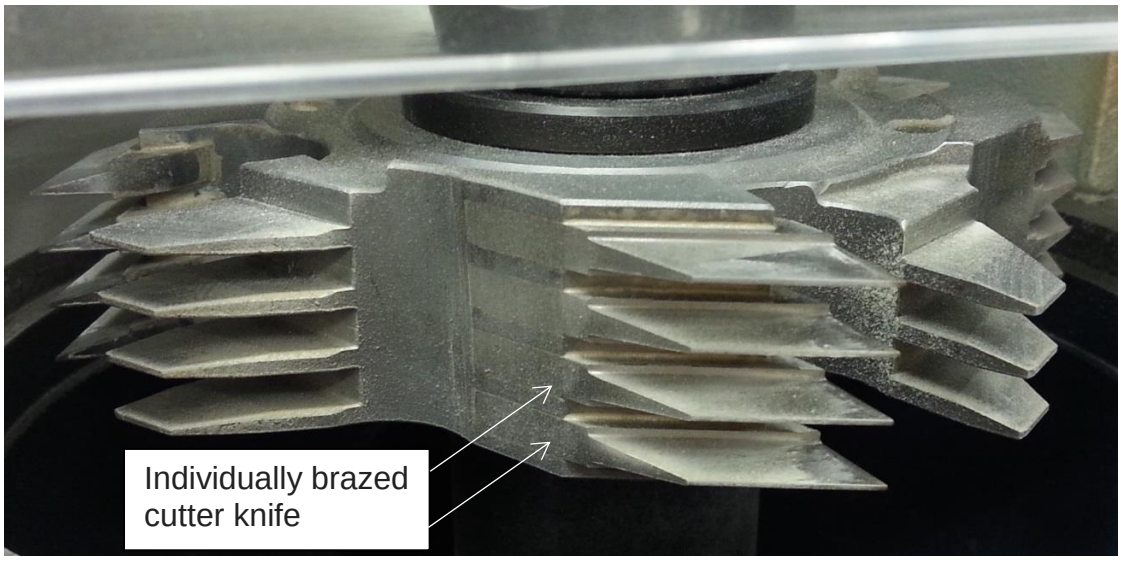

b)

Figure 4-1: Finger cutter a) top view; b) side view

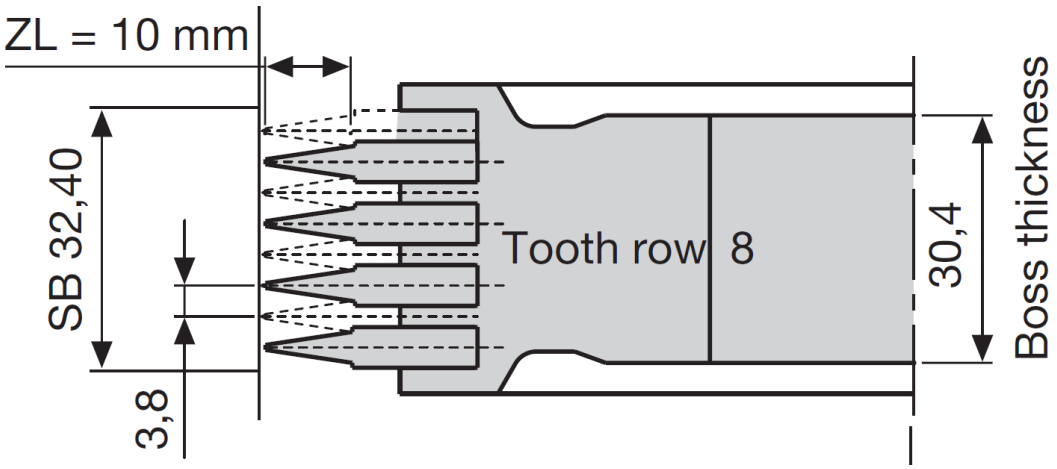

Key:

ZL	finger length
SB	cutting width

Figure 4-2: Profile of the finger cutter (© Leitz Tooling) (dimensions in mm)

An industrial spindle moulder was purchased to be used together with the finger cutter (Figure 4-3). The spindle moulder was mounted on a heavy steel chassis to minimise vibration that could affect the cutting precision of the finger joints. The spindle could be adjusted to a maximum height of 130 mm and had three speed variations of 5500, 7500 and 10000 rpm. The speed of 7500 rpm was used in the cutting process because the allowable maximum speed for the finger cutter knife was 8000 rpm.

Figure 4-3: Spindle moulder for finger-cutting

The fingers were cut in phases because of the limits in the cutting width (32.4 mm) of the cutter (Figure 4-4). The spindle height was increased by 32.4 ± 0.02 mm after each cut to cover the whole width (105 mm) of the timber piece. The resulting finger cuts from the cutter produced finger length of 10 mm. The tip width and pitch of the finger joints were approximately 0.8 and 3.8 mm respectively (Figure 4-5).

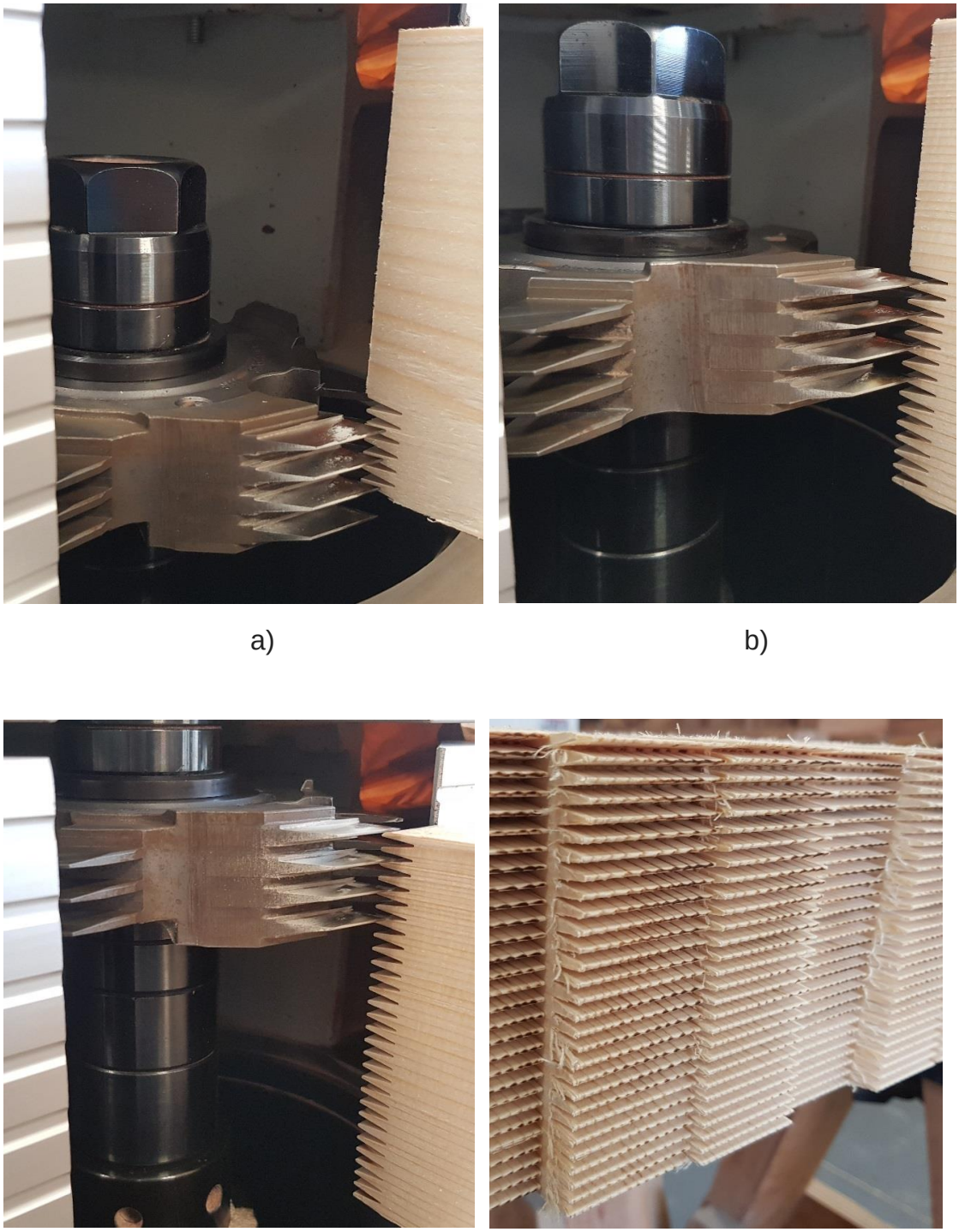

a) b)

c) d)

Figure 4-4: Finger-cutting processes a) first cut; b) spindle height increased; c) cutting extended entire specimen’s width; d) finished finger cuts

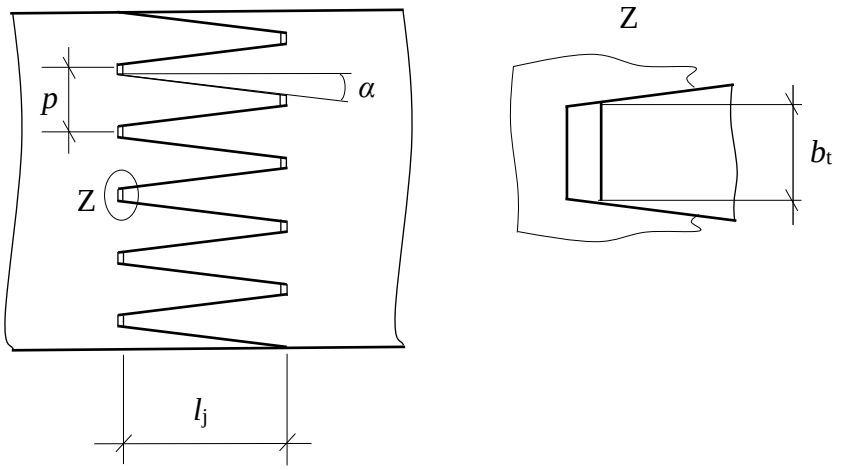

Key: l_j finger length 10 mm

p pitch 3.8 mm

α finger angle 6.3°

b_t tip width 0.8 mm

Figure 4-5: Descriptions of the finger profile

Phenol resorcinol formaldehyde and epoxy adhesives were used to bond the finger joints. Detailed descriptions of the adhesives were given in Chapter 3. Prior to application of adhesive, sawdust was removed from the surface of the finger cuts. The finger cuts were then bonded within six hours after the cutting process as recommended in BS EN 14080:2013. Adhesive was applied to both pairs of finger cuts to be joined, making sure that the adhesive spread more than 75% of the finger length. The amount of adhesive applied was deemed adequate when glue squeeze-out was observed in the cramping process.

The end pressure used in this study was 12.5 N/mm^2, following recommendation from the standard BS EN 14080:2013 (Figure 4-6) for finger length of 10 mm. Full cramping pressure was applied and maintained for 10 seconds to achieve an interlocking condition between the timber pieces before being released for further curing. The finger-jointing facility was set up using metal jigs and fittings, a hydraulic jack and a load cell for monitoring of end pressure. The set-up was fixed to the strong floor (Figure 4-7) in the Structures Laboratory of the Department of Architecture and Civil Engineering, University of Bath.

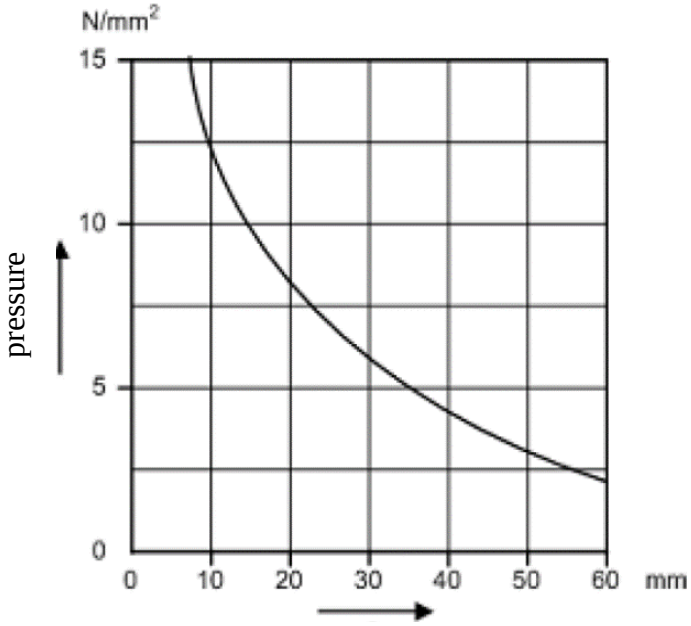

Figure 4-6: Recommended end pressure for bonding finger joints as a function of finger length (BS EN 14080:2013)

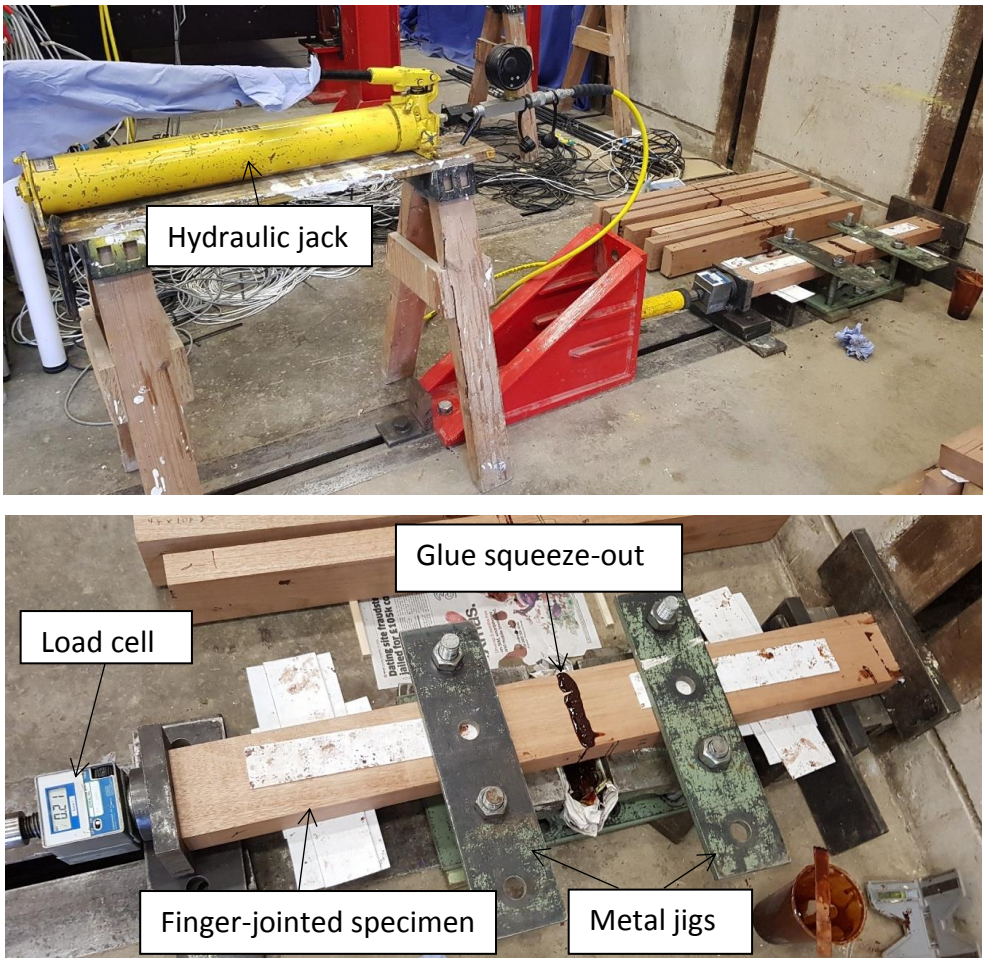

Figure 4-7: Finger-jointing set-up

Specimens finger-jointed with PRF adhesive were left to cure at ambient temperature for 1 day while finger joints bonded using epoxy were cured for more than 7 days as indicated in the technical datasheet. For comparison, finger-jointed PRF specimens were also prepared using lower (10.0 N/mm^2) and higher (15.0 N/mm^2) end pressures, approximately ± 20% from the recommended end pressure (12.5 N/mm^2). After curing, the specimens were planed to remove excess glue residues. The final dimensions of finger-jointed pieces were 38 mm (thickness) x 100 mm (width). Further processing was made to produce finger-jointed specimens of different sizes, following the requirements of standard tests. At least ten finger-jointed and solid specimens were prepared for each different test configuration.

4.2.2 Finger-jointing of laminations

Solid DRM pieces were finger-jointed to produce 5 metre length laminations for the fabrication of full size glulam beams. Prior to finger-jointing, these pieces were planed and ripped to obtain a flat board with the surfaces and edges parallel to each other respectively. A perfectly squared board made the finger-cutting process easier because the flat surfaces were easier to clamp, which was crucial for the production of straight finger-jointed pieces. This was important since a long lamination consisted of multiple finger joints and one distorted finger-jointed piece would make the whole piece unusable in the manufacturing of glulam beam.

Planed DRM test pieces with nominal dimensions of 40 mm (thickness) x 105 mm (width) x 1000 mm (length) were finger-jointed to produce the laminations of glulam beams. A total of five pieces were used to produce each lamination with length of 5 metres (Lamination A). To avoid overlapping of finger joints between the adjacent laminations, six pieces of DRM were finger-jointed to produce laminations of 6 metres in length (Lamination B). These laminations were cross-cut approximately 500 mm at both ends to obtain the final length of 5 metres. Initial arrangement to assess the layup of the beams was then made,

alternating Laminations A and B to avoid overlapping of the finger joints (Figure 4-8).

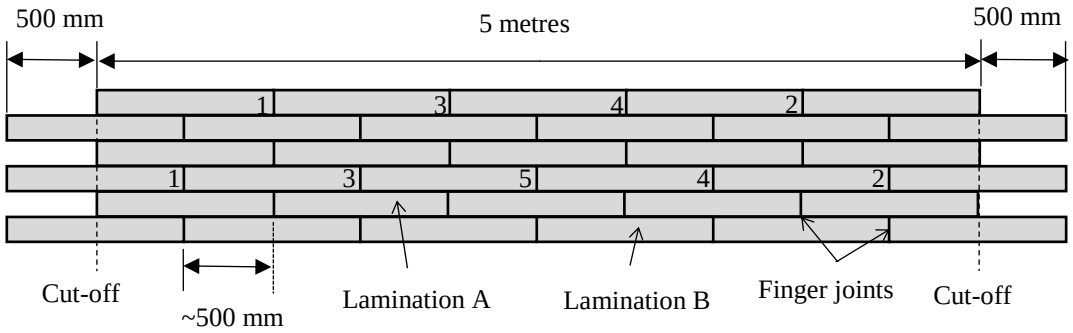

Key:

1 to 5 finger-jointing sequence (within a lamination)

Figure 4-8: Arrangement of laminations and spacing of finger joints

The cutting of fingers is described in the Section 4.2.1. PRF adhesive was used to bond all the finger joints and an end pressure of 12.5 N/mm^2 was used as recommended by BS EN 14080:2013. Although there were multiple finger joints in one lamination, only one joint could be completed at a time because of the need to have flat surfaces at both ends of the piece when cramping (Figure 4-9). After curing, further finger-cuts were made at the end of each piece (Figure 4-10) and they were then finger-jointed. These processes were repeated for the full length of the laminations (Figure 4-11). The laminations were planed to 35 mm (thickness) x 100 mm (width) and laminated to produce full size glulam beams as described in Chapter 5.

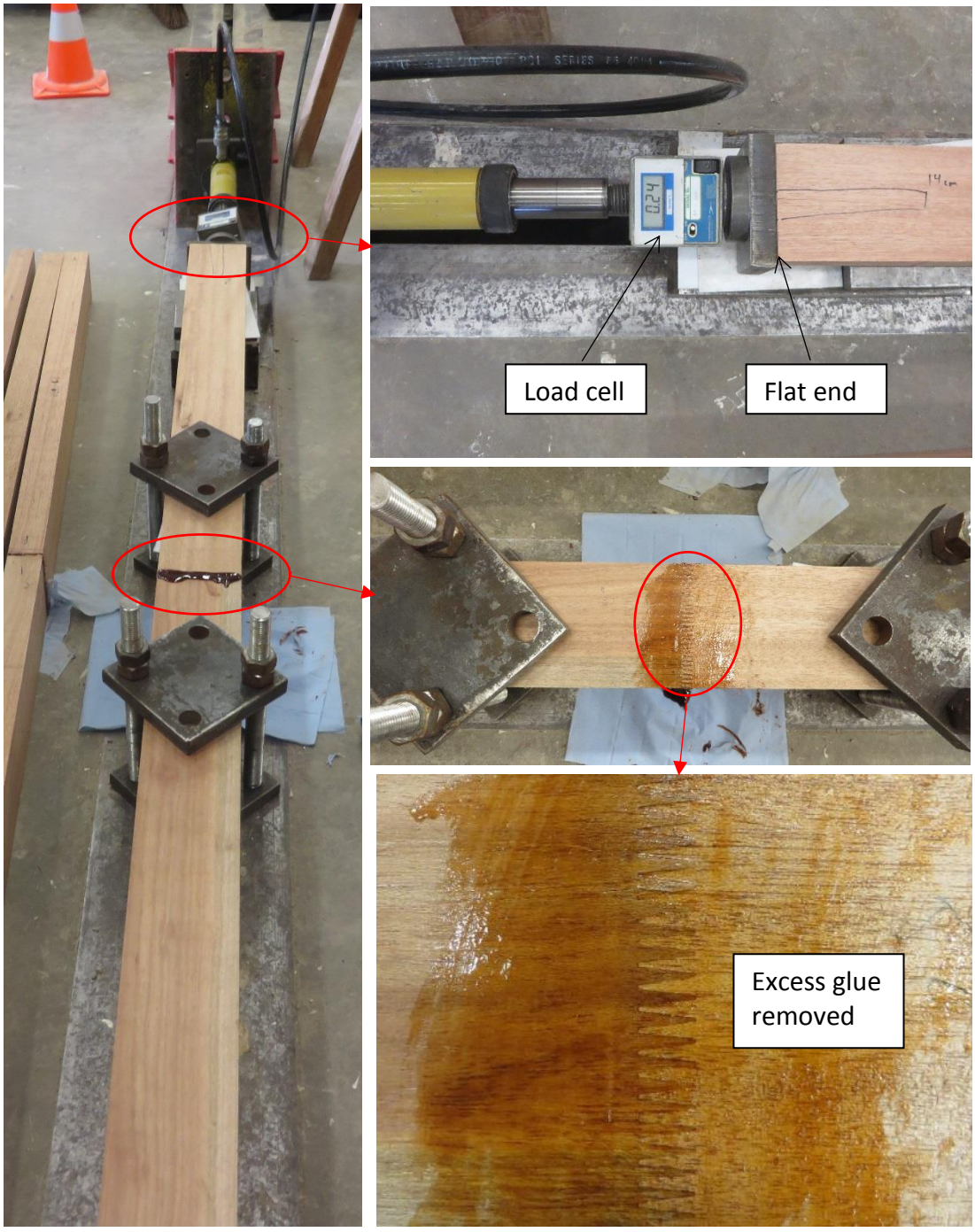

Figure 4-9: Finger-jointing of laminations

Figure 4-10: Further finger-cutting (2 metre length)

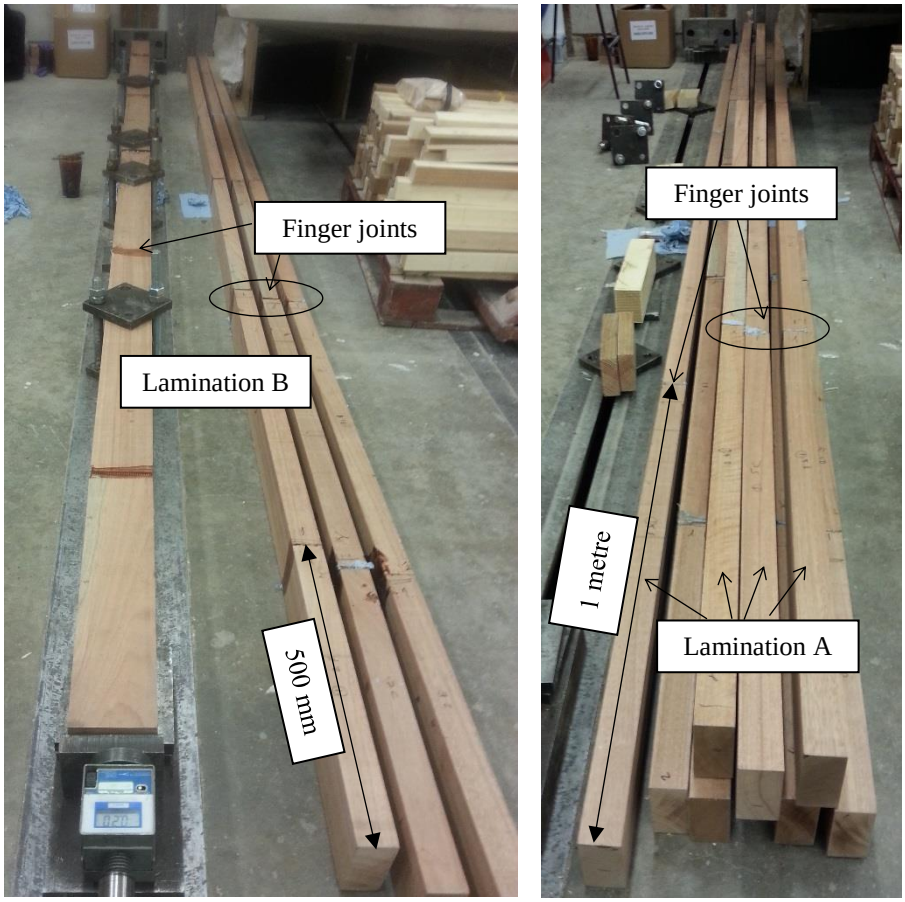

Figure 4-11: Full length finger-jointed laminations

4.2.3 Four-point bending test

Four-point bending tests were conducted to determine the modulus of rupture and local modulus of elasticity based on the requirements and conditions of BS EN 408:2010+A1:2012 as described in Chapter 3. Nominal dimensions of DRM specimens were approximately 30 mm (depth) x 30 mm (width) x 600 mm (length) with finger joints located in the middle (Figure 4-12). The bending and loading span were 540 mm and 180 mm respectively (Figure 4-13). Similar sized solid DRM and Spruce as well as PRF finger-jointed Spruce specimens were also prepared.

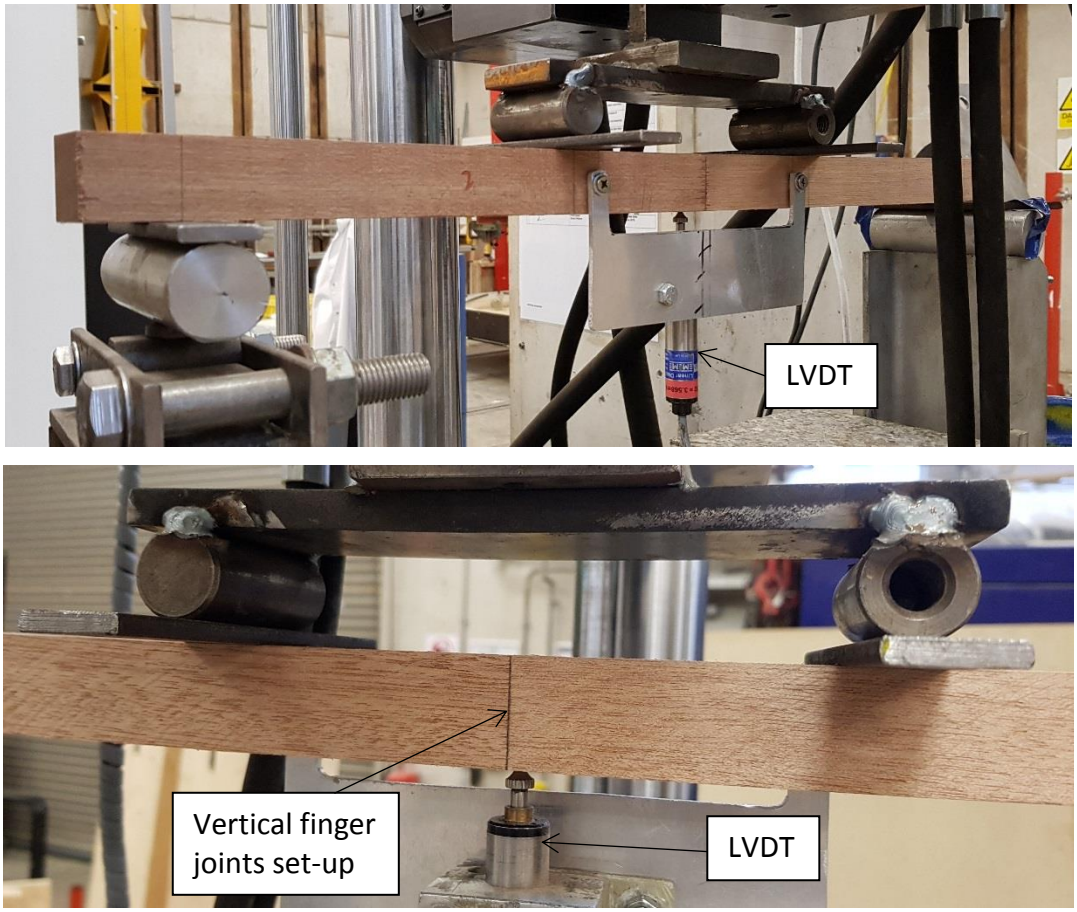

Figure 4-12: Four-point bending test set-up

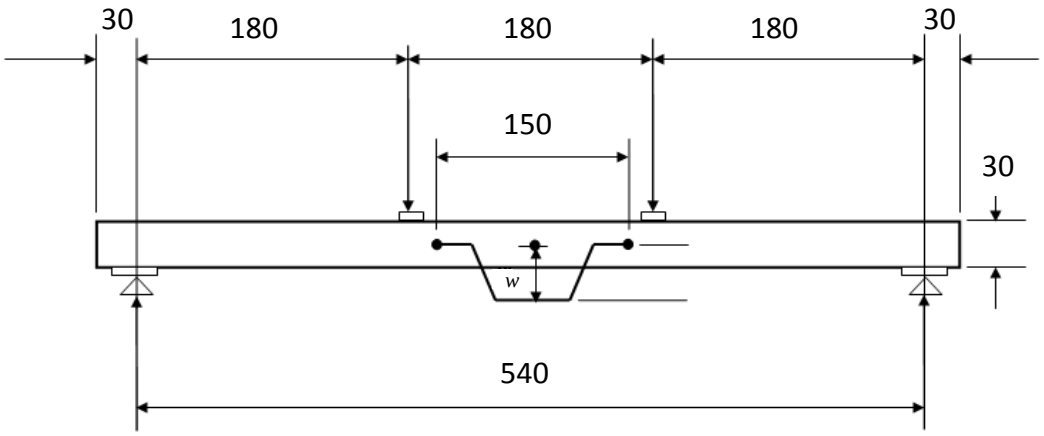

Key:

w deformation, (mm)

Figure 4-13: Four-point bending test configuration (dimensions in mm)

Additional DRM specimens were finger-jointed using different end pressures, 10.0 N/mm^2 (low pressure) and 15.0 N/mm^2 (high pressure) for these tests. These pressures were approximately ± 20% different from the recommended cramping pressure (12.5 N/mm^2) and were introduced to determine the suitable range of pressures to produce DRM finger joints. The bending tests also include finger-jointed DRM specimens with horizontal joints and specimens with increased width and dimensions of 30 x 60 x 600 mm (Figure 4-14). The detailed description of vertical and horizontal finger joints was explained in Chapter 2. The number of specimens for different test configurations is shown in Table 4-1.

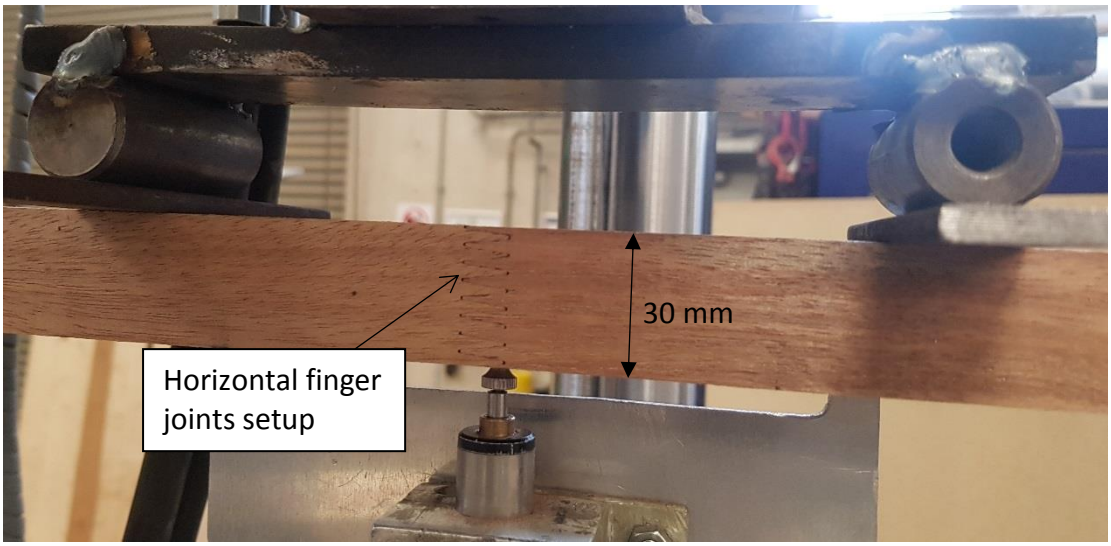

a)

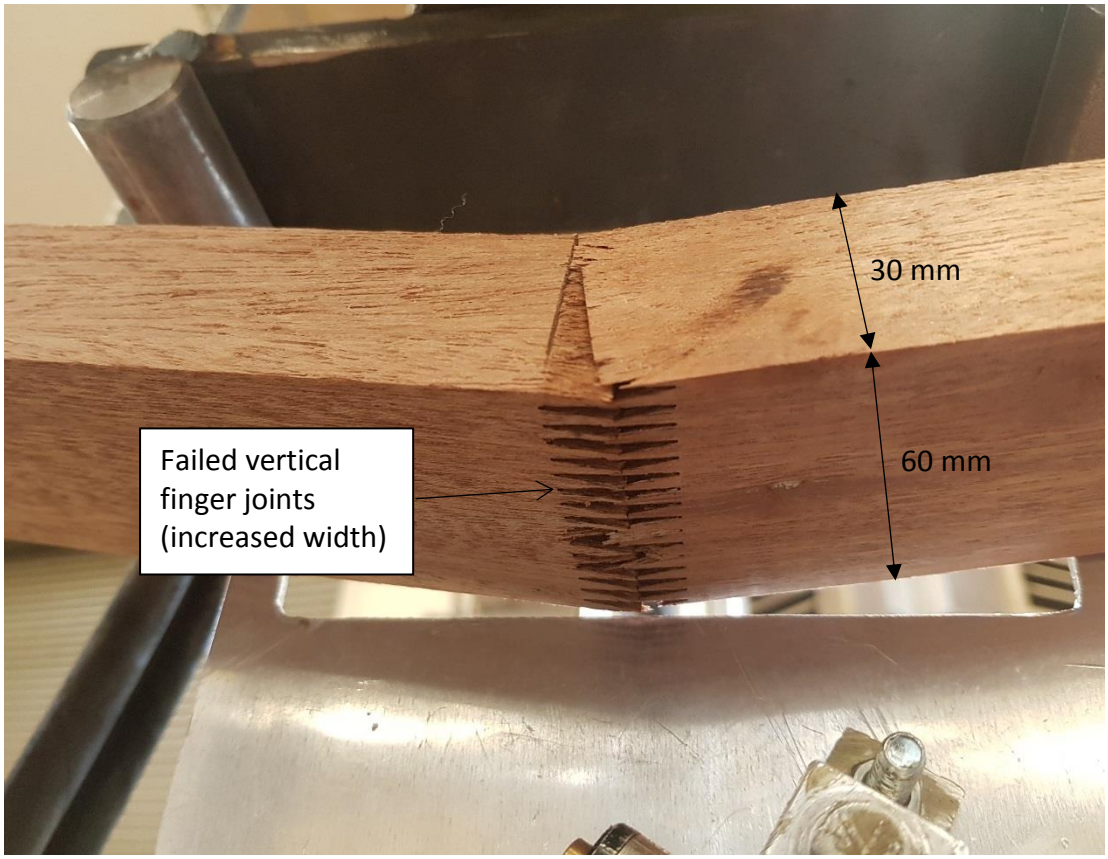

b)

Figure 4-14: Bending test specimens a) side view of horizontal finger joints; b) bottom view of failed vertical finger joints

Table 4-1: Bending test configurations and number of specimens

No.	Descriptions	Species	End pressure (N/mm^2)	Adhesive	No. of specimens
1	Solid	DRM	-	-	10
2	Vertical finger joints	DRM	12.5	PRF	10
3	Horizontal finger joints	DRM	12.5	PRF	10
4	Vertical finger joints	DRM	10.0	PRF	12
5	Vertical finger joints	DRM	15.0	PRF	12
6	Wider vertical finger joints	DRM	12.5	PRF	10
7	Vertical finger joints	DRM	12.5	Epoxy	12
8	Solid	Spruce	-	-	12
9	Vertical finger joints	Spruce	12.5	PRF	13

For determination of local MOE, deformation (w) was measured using a 5 mm linear variable differential transformer (LVDT) gauge with a precision of 0.001 mm. The LVDT was placed at the centre of the loading span and its gauge length was 150 mm (see Figure 4-13). Only one LVDT was used in the bending test, which deviated from the recommended standard method in BS EN408:2010+A1:2012 (see Figure 4-12). The LVDT was positioned at the bottom of the specimen to avoid attaching additional plate at the neutral axis where the finger joint is located. This prevents the need for pasting or drilling close to or on the joints in order to attach the plate, which might affect the bending performance of the specimen. To minimise local indentation, 15 mm length steel plates were inserted between the specimens and loading point or supports. The loading speed was set to 3.0 mm/min for finger joints and 4.0 mm/min for solid specimens and the maximum load was reached within 3 to 7 minutes. The loading speed for solid specimens was higher since they were expected to have higher maximum load and need longer time to fail compared to the finger-jointed specimens. The bending results presented in this chapter include the values of local MOE and the corresponding MOR of the specimens.

4.2.4 Tensile test parallel to grain

DRM finger-jointed specimens with nominal dimensions of 10 mm (depth) x 42 mm (width) x 300 mm (length) were prepared and tested. Additional finger-

jointed DRM specimens were prepared using different end pressures and specimens finger-jointed with epoxy adhesive were also tested. PRF finger-jointed DRM specimens with finger length of 15 mm were also prepared. These specimens were produced at SP Wood Building Technology, Sweden which has the facility to produce 15 mm length finger joints. The specimens were also used as reference for tensile tests under fire condition as described in Chapter 7. The number of test specimens according to the different test configurations is given in Table 4-2. A detailed description of the tensile test parallel to grain was given in Chapter 3 and the actual test set-up is shown in Figure 4-15.

Table 4-2: Tensile test configurations and number of DRM specimens

No.	Descriptions	End pressure (N/mm^2)	Adhesive	No. of specimens
1	Finger joints with recommended pressure	12.5	PRF	10
2	Finger joints with recommended pressure	12.5	Epoxy	10
3	Finger joints with lower pressure	10.0	PRF	10
4	Finger joints with higher pressure	15.0	PRF	10
5	Finger joints with recommended pressure (finger length 15 mm)	12.5	PRF	10

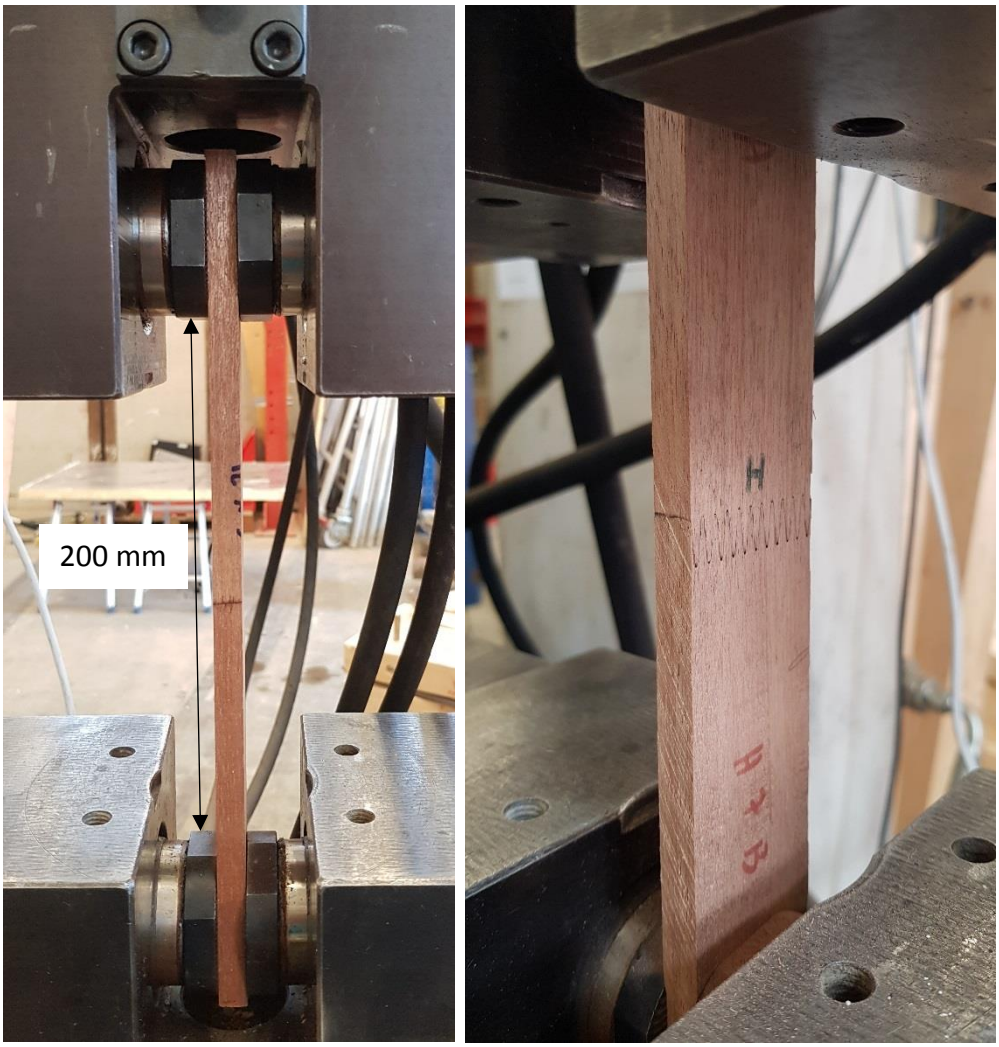

Figure 4-15: Tensile test parallel to grain set-up

4.2.5 Compressive test parallel to grain

DRM test specimens (solid and finger-jointed with PRF) with dimensions of 30 mm (depth) x 30 mm (width) x 180 mm (length) were prepared for compressive testing. The end surfaces of the specimens were carefully cut to ensure they were parallel to each other. Additional DRM finger joints were also prepared using epoxy adhesive. Solid and finger-jointed (with PRF) Spruce specimens were prepared for comparative tests. The test configurations and number of specimens are shown in Table 4-3. A detailed description of the compressive test was given in Chapter 3. Figure 4-16 shows the actual compressive test set-up.

Table 4-3: Compressive test configurations and number of specimens

No.	Descriptions	Species	End pressure (N/mm^2)	Adhesive	No. of specimens
1	Solid	DRM	-	-	12
2	Vertical finger joints	DRM	12.5	PRF	12
3	Vertical finger joints	DRM	12.5	Epoxy	13
4	Solid	Spruce	-	-	11
5	Vertical finger joints	Spruce	12.5	PRF	10

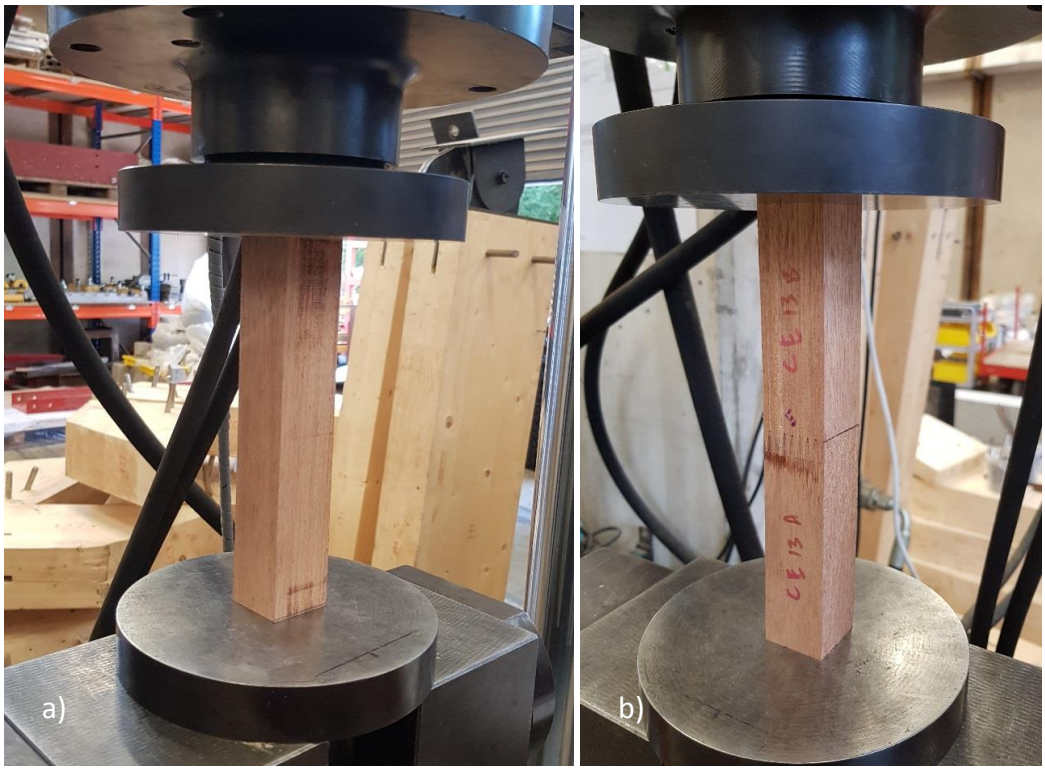

Figure 4-16: Compressive test set-up a) solid; b) finger-jointed specimen

4.2.6 Microscopic analysis

A scanning electron microscope (SEM) was used to observe the modes of failure of the tested specimens. Specimens examined following mechanical tests were further cut to a smaller size. The specimens were cut to a consistent length so that they had the same height when mounted on the specimen stub in order to facilitate focusing of the specimen's surface. Careful clean handling was needed during preparation so that the surface intended for scanning was not damaged or contaminated. The specimens were further dried overnight in a vacuum vessel to ascertain complete dryness of the scanned surface. They

were then sputter-coated with a thin layer of gold using a sputter coater machine, Edwards Sputter Coater S150B (Figure 4-17).

Figure 4-17: Edwards Sputter Coater S150B machine

The specimens were mounted on the specimen stub using electrically conductive double-sided tape to prevent electrostatic charge from accumulating at the surface of the specimens, increasing signal detection and minimising noise when examined in the microscope. The specimens were observed using a JEOL JSM-6480LV SEM (Figure 4-18) and the microstructural images were captured and saved.

Figure 4-18: JEOL JSM-6480LV Scanning Electron Microscope

4.3 Results and discussion

The performance of finger-jointed DRM specimens, evaluated using standard mechanical tests in BS EN 408:2010+A1:2012, are presented and discussed in this section. The finger joints were evaluated using four-point bending, tensile and compressive tests. Additional Spruce specimens were tested for comparison.

4.3.1 Bending properties

Table 4-4 shows average modulus of rupture, local modulus of elasticity, moisture content and density results for solid and finger-jointed specimens bonded with PRF and epoxy. Individual test results for the specimens are given in Appendix A. The results are discussed below.

Table 4-4: Average bending properties of finger joints and solid specimens

Descriptions	Species	Adhesive	Joint configuration	End pressure (N/mm^2)	MOR (N/mm^2)		MOE (N/mm^2)		Moisture Content (%)	Density (kg/m^3)
					Mean	SD	Mean	SD		
$Solid_{drm}$	DRM	-	-	-	93.1	8.03	15900	1450	11.5	565
$Solid_{spruce}$	Spruce	-	-	-	81.8	16.2	17000	3860	12.4	495
$FJ_{drm,prf,v,R}$	DRM	PRF	Vertical	12.5	71.9	6.50	15500	2270	12.1	599
$FJ_{drm,epoxy,v,R}$	DRM	Epoxy	Vertical	12.5	54.0	10.6	14800	3300	12.2	470
$FJ_{spruce,prf,v,R}$	Spruce	PRF	Vertical	12.5	52.9	9.31	16100	2700	12.4	505
$FJ_{drm,prf,wv,R}$	DRM	PRF	Wide vertical	12.5	69.6	8.02	15000	2240	12.3	601
$FJ_{drm,prf,h,R}$	DRM	PRF	Horizontal	12.5	67.8	11.9	13900	1250	12.1	606
$FJ_{drm,prf,v,L}$	DRM	PRF	Vertical	10.0	59.4	6.46	17000	2930	12.5	584
$FJ_{drm,prf,v,H}$	DRM	PRF	Vertical	15.0	65.4	9.09	20400	2070	12.7	656

Key:

FJ	finger-jointed specimens
v	vertical finger joints
h	horizontal finger joints
wv	vertical finger-jointed specimens with increased width (30 x 60 mm)
R	recommended end pressure (12.5 N/mm^2)
L	lower end pressure (10.0 N/mm^2)
H	higher end pressure (15.0 N/mm^2)

4.3.1.1 Solid test specimens

In four-point bending test, all the DRM solid specimens ($Solid_{drm}$) showed failures on the tension face (Figure 4-19). Spruce solid specimens ($Solid_{spruce}$) also failed on the tension face with some failures occurring near knots (Figure 4-20).

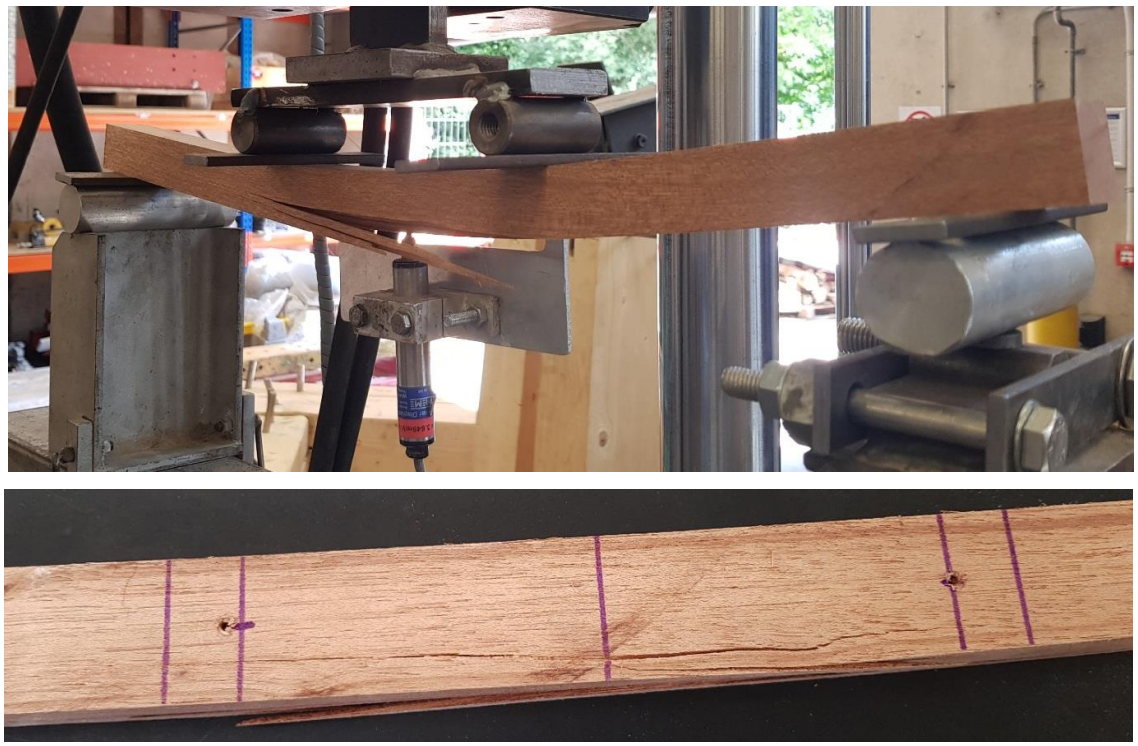

a)

b)

Figure 4-19: Failures of solid DRM specimens in bending test a) tension region; b) along slope of grain

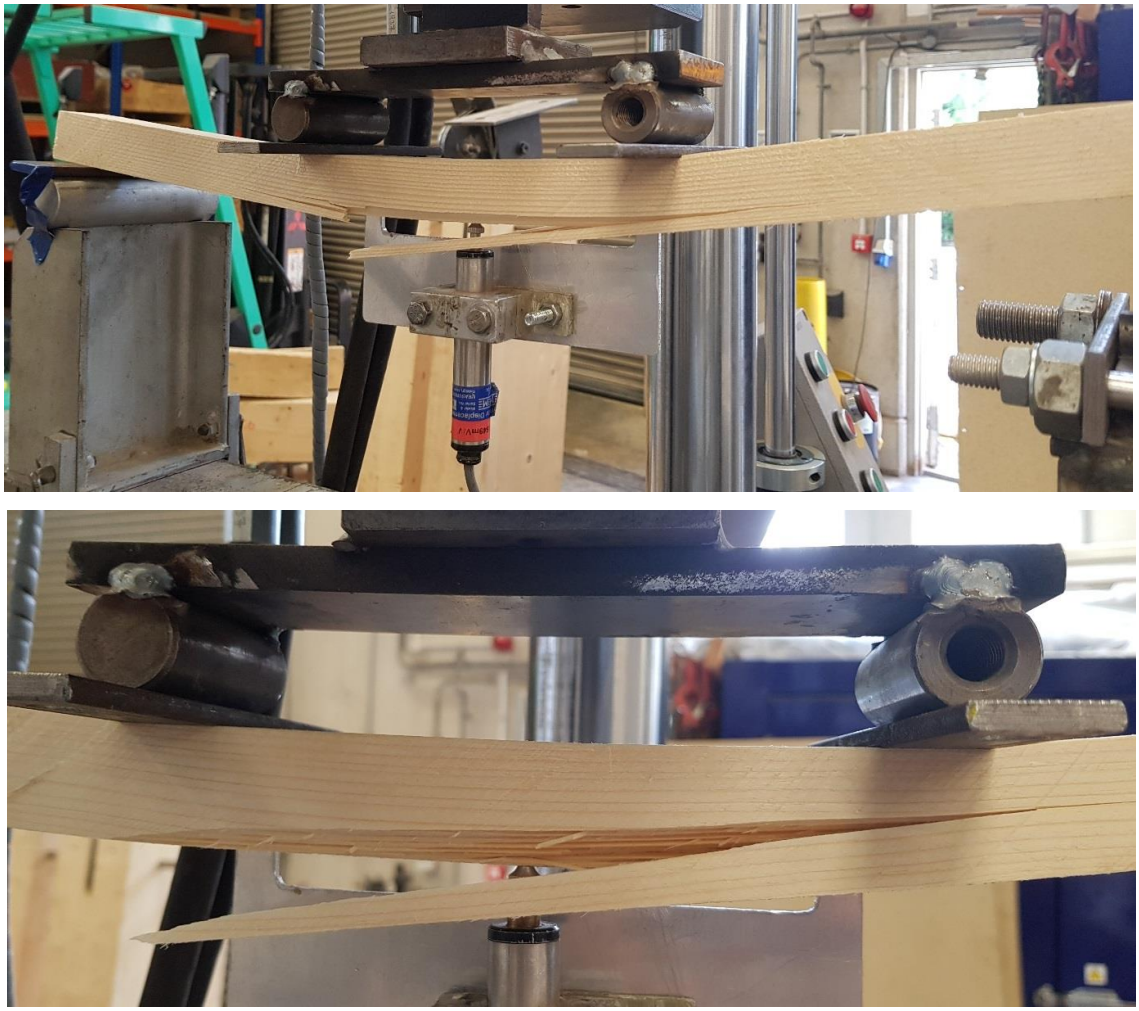

a)

b)

Figure 4-20: Failures of solid Spruce specimens in bending a) tension region; b) near knot

Comparing the average bending properties of solid test specimens (see Table 4-4), $Solid_{drm}$ possessed an average MOR 12% higher than $Solid_{spruce}$. Individual test results for $Solid_{drm}$ and $Solid_{spruce}$ are given in Tables A-1 and A-2 respectively in Appendix A. A one-way ANOVA test (analysis of variance) was used to examine whether there was a significant difference between the

bending properties of $Solid_{drm}$ and $Solid_{spruce}$ specimens. The results indicate no significant differences at 95% confidence level between MOR values of these solid specimens. This is expected since the density of $Solid_{drm}$ (493 to 651 kg/m^3) is similar to $Solid_{spruce}$ (428 to 597 kg/m^3) specimens. Dinwoodie (1981) stated that density is commonly used to estimate the strength properties of timber and its relationship is known to be highly positively correlated.

4.3.1.2 Test specimens with vertical finger joints

Bending strength results of DRM and Spruce specimens with vertical finger joints using the recommended end pressure of 12.5 N/mm^2 are discussed in this section. DRM finger joints bonded with PRF ($FJ_{drm,prf,v,R}$) showed failures mainly at the glue lines where pulled-out wood fibres can be seen attached to the adhesive (Figure 4-21). A mixture of finger fractures was also observed in some of the specimens (Figure 4-22). One of the specimens showed failure along the slope of grain (Figure 4-23). These observations indicate good bonding performance of finger joints because the failures occurred within the wood and not because of a weak adhesive bond.

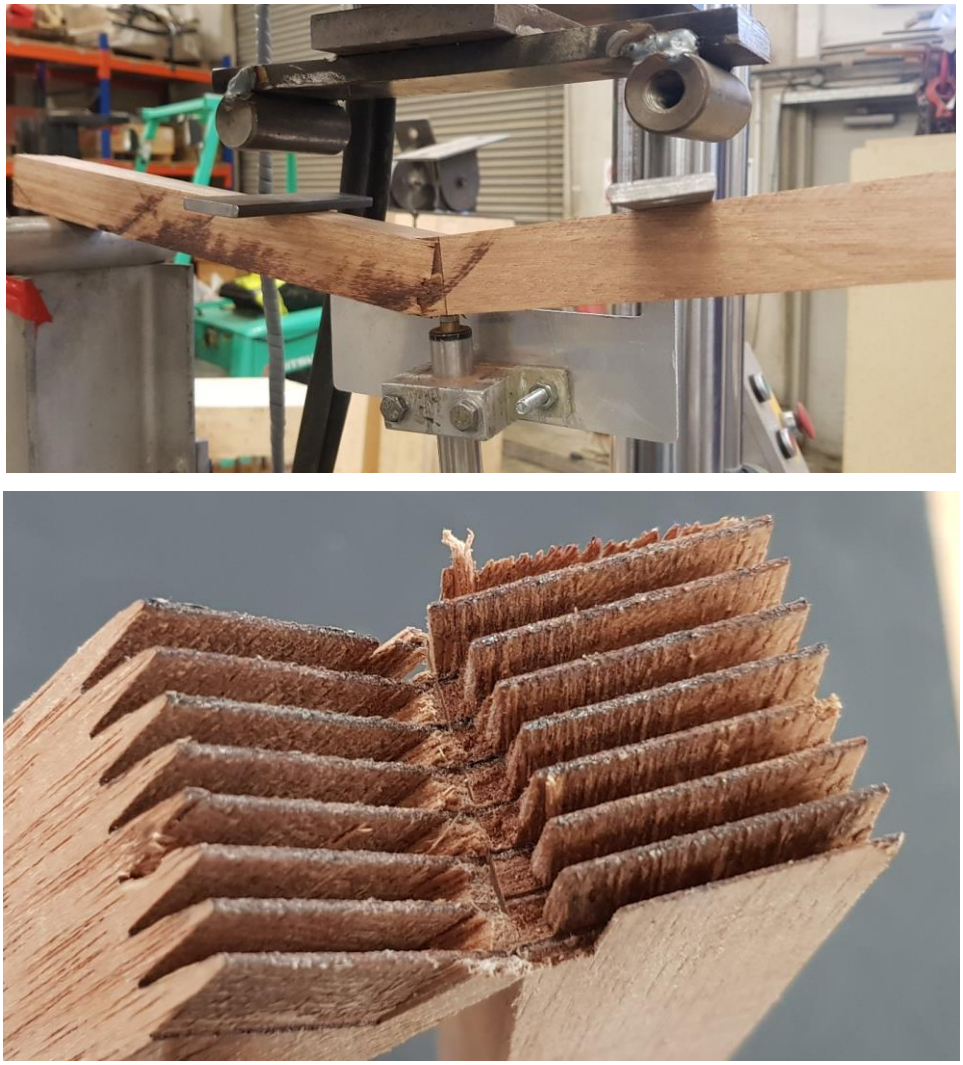

Figure 4-21: Failure of DRM specimens bonded with PRF

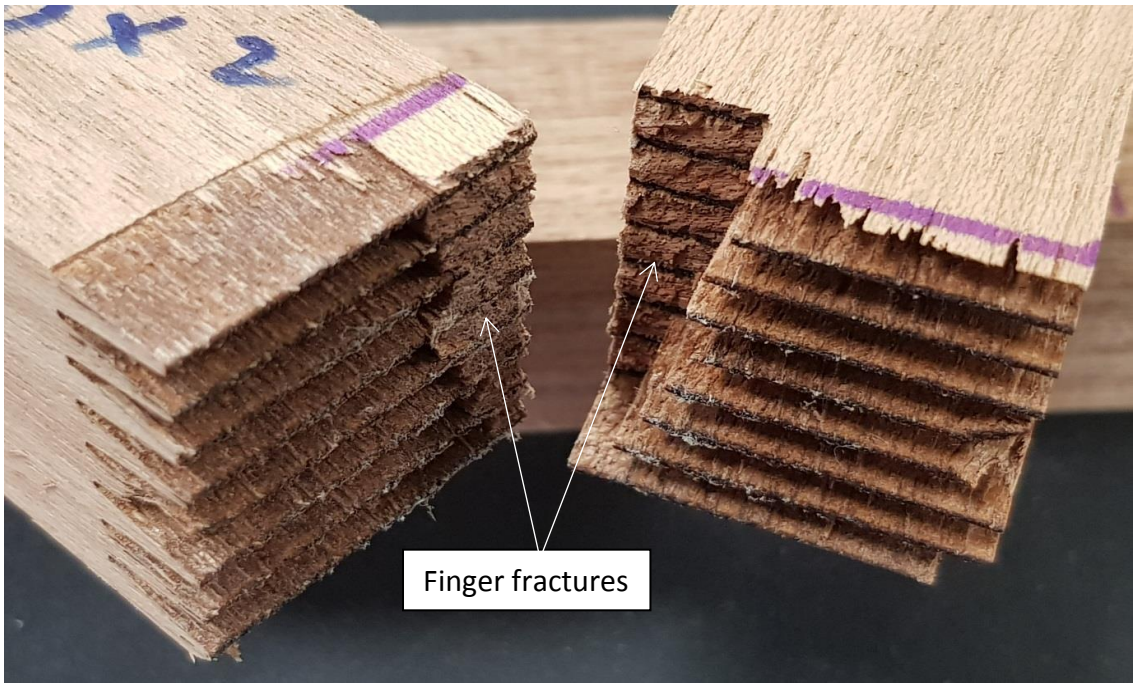

Figure 4-22: Mixture of finger fractures and glue line failures

Figure 4-23: Mixture of failures at glue lines and along the slope of grain

DRM finger joints bonded with epoxy ($FJ_{drm,epoxy,v,R}$) exhibited a mixture of finger fractures and failure at glue lines with pulled-out wood fibres attached to the adhesive (Figure 4-24). The average MOR values (see Table 4-4) for $FJ_{drm,prf,v,R}$ (71.9 N/mm^2) were approximately 25% higher than $FJ_{drm,epoxy,v,R}$ (54.0 N/mm^2) specimens. The individual test results for $FJ_{drm,prf,v,R}$ and $FJ_{drm,epoxy,v,R}$ specimens are given in Tables A-3 and A-4 respectively in Appendix A.

a)

b)

Figure 4-24: DRM epoxy finger joints a) mixture of finger fractures, glue line and wood failures; b) finger and wood fractures

ANOVA test results showed a statistically significance difference at the 95% confidence level between the MOR values of $FJ_{drm,prf,v,R}$ and $FJ_{drm,epoxy,v,R}$. Density variation of $FJ_{drm,prf,v,R}$ and $FJ_{drm,epoxy,v,R}$ may contributes to the differences in MOR values. As explained earlier, a higher wood density generally indicates a higher bending strength. In this section, good bonding performance of the finger joints is depicted by a high proportion of wood failures and finger fractures. Thus, the bending strengths of PRF and epoxy finger joints are dictated by the density variation of DRM and are not influenced by the different bonding medium in this study. Comparison of MOE values using ANOVA test showed no significant difference between $FJ_{drm,prf,v,R}$ and $FJ_{drm,epoxy,v,R}$ specimens. It is to be expected that DRM specimens finger-jointed with PRF and epoxy show similar bending strength but there is a broad trend for higher density specimens to exhibit higher MOR values (Figure 4-25). Thus, density influenced the bending strength of finger-jointed specimens when the adhesive interfaces were strongly bonded (Vrazel and Sellers, 2004).

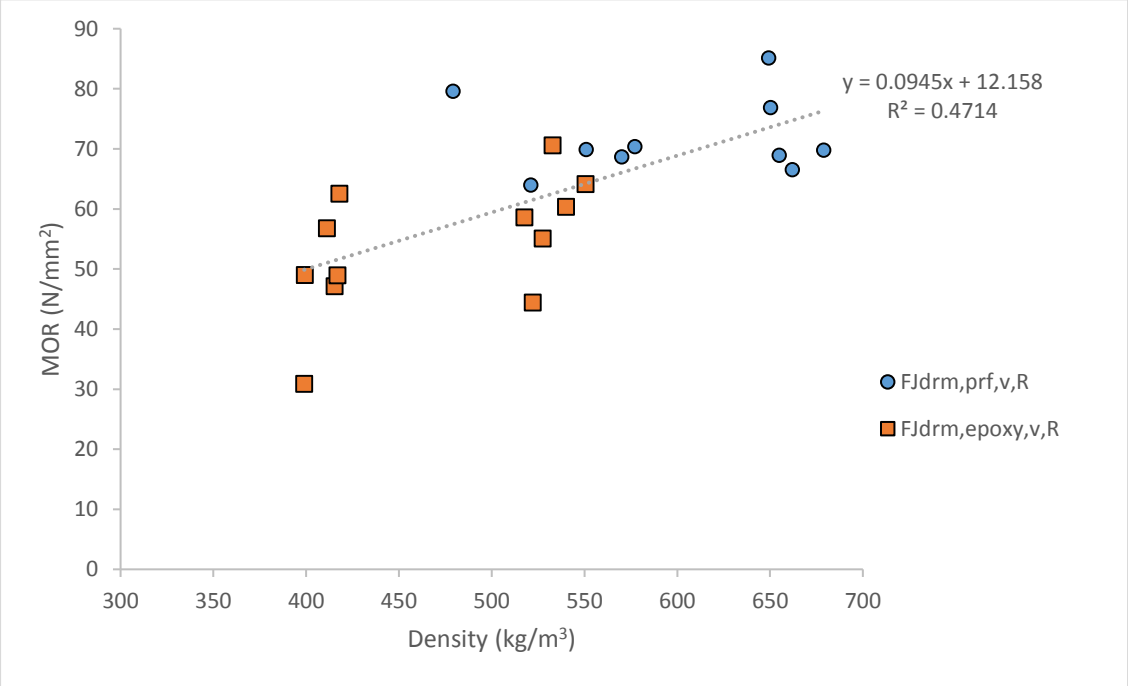

Figure 4-25: Relationship between MOR and density of PRF and epoxy finger-jointed DRM specimens

Spruce specimens bonded with PRF ($FJ_{spruce,prf,v,R}$) exhibited finger fractures, wood and glue lines failures (Figure 4-26). The average MOR value for DRM finger-jointed with PRF ($FJ_{drm,prf,v,R}$) (71.9 N/mm^2) is 26% higher than Spruce

specimens (52.9 N/mm^2). Individual results of $FJ_{spruce,prf,v,R}$ are given in Table A-5 in Appendix A. ANOVA test results indicated a significant difference at 95% confidence level between MOR values of $FJ_{spruce,prf,v,R}$ and $FJ_{drm,prf,v,R}$. It can be concluded that DRM finger joints perform better than Spruce in four-point bending tests in this study (Figure 4-27) although the bending properties of solid DRM specimens were similar to solid Spruce specimens as mentioned in the previous section.

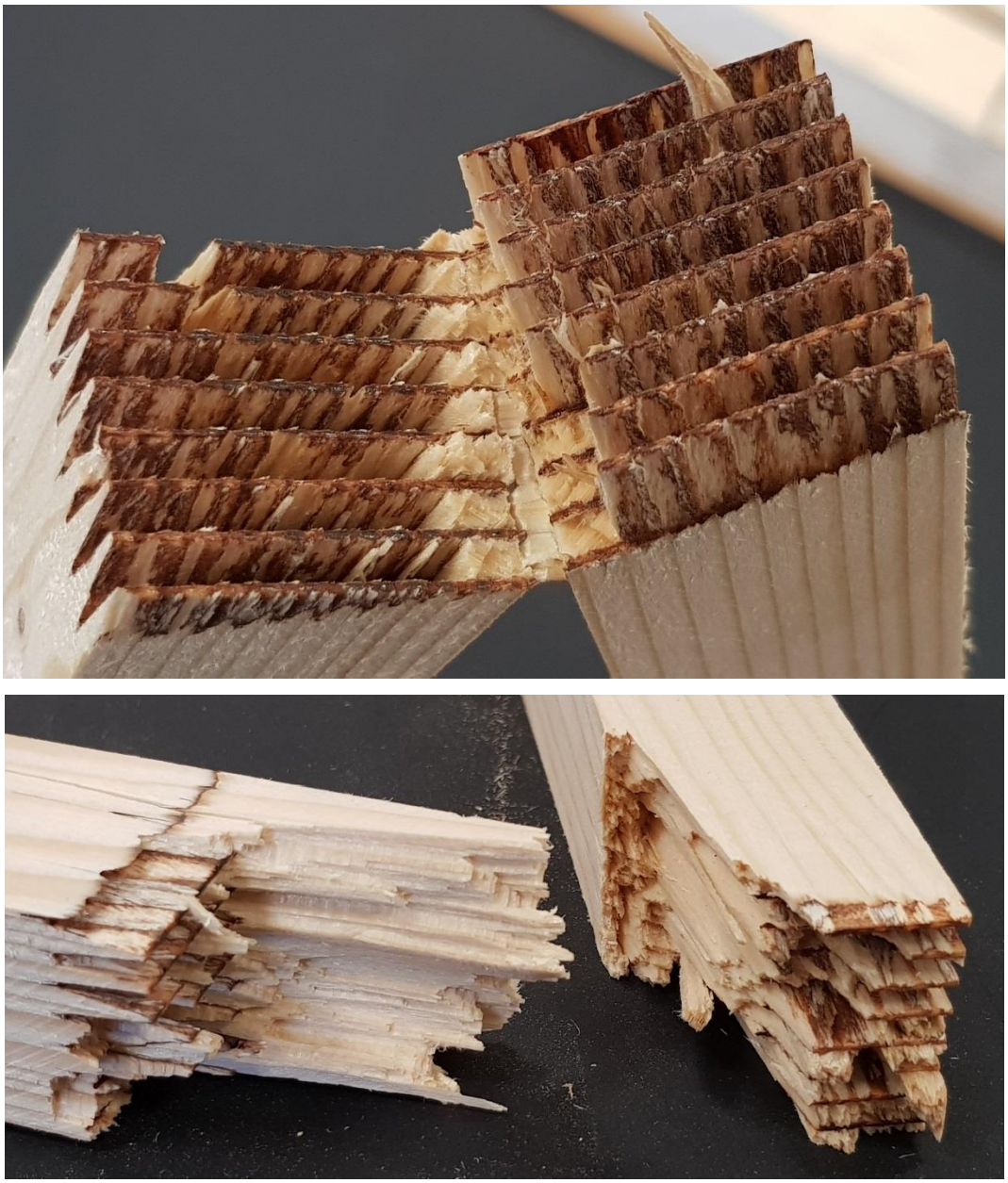

Figure 4-26: PRF finger-jointed Spruce specimens

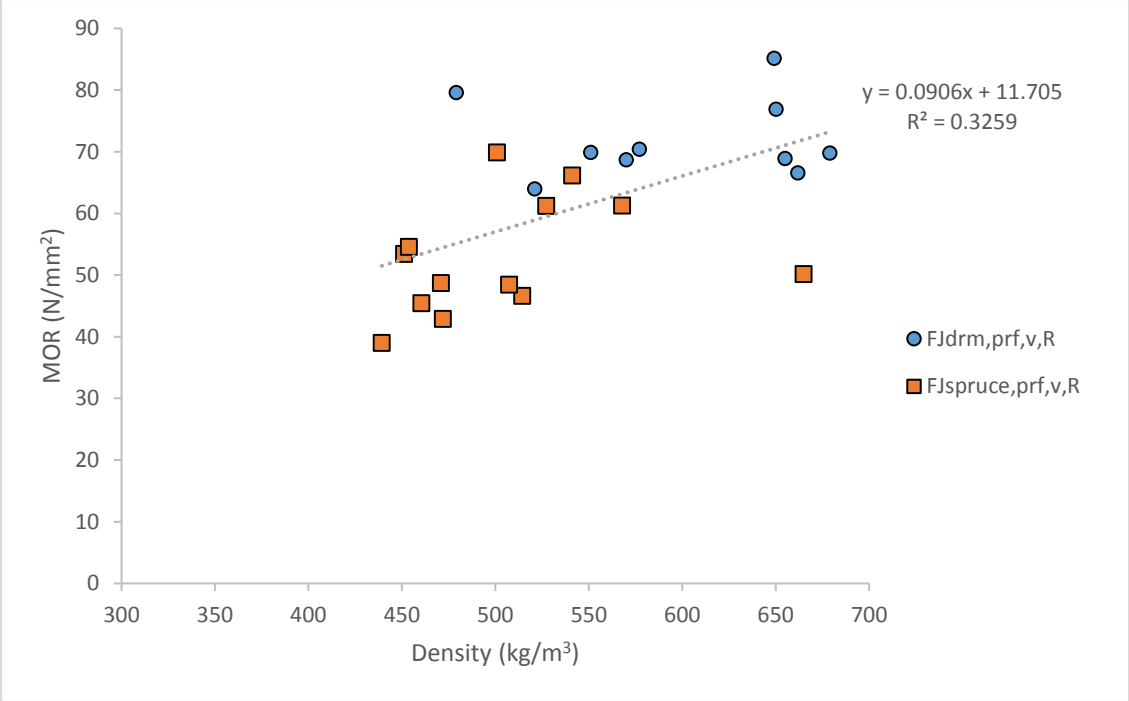

Figure 4-27: Bending strength as a function of density for PRF finger-jointed DRM and Spruce specimens

4.3.1.3 DRM specimens with increased width

Finger-jointed DRM specimens with dimensions of 30 x 60 mm ($FJ_{drm,prf,wv,R}$) were tested to determine if increases in width influenced the bending test results. The finger joint failure of $FJ_{drm,prf,wv,R}$ is shown in Figure 4-28. Most of the failures occurred along the glue lines with some finger fractures. From Table 4-4 it can be seen that DRM finger-jointed specimens showed similar average MOR values $FJ_{drm,prf,v,R}$ (71.9 N/mm^2) to the wider $FJ_{drm,prf,wv,R}$ (69.6 N/mm^2) specimens. ANOVA test results revealed no significant differences at the 95% confidence level between these MOR values. ANOVA results also indicated no significance differences between the MOE values of these two groups. Individual test results for $FJ_{drm,prf,wv,R}$ are shown in Table A-6 in Appendix A. The distribution of MOR values for both groups of specimens were shown in Figure 4-29.

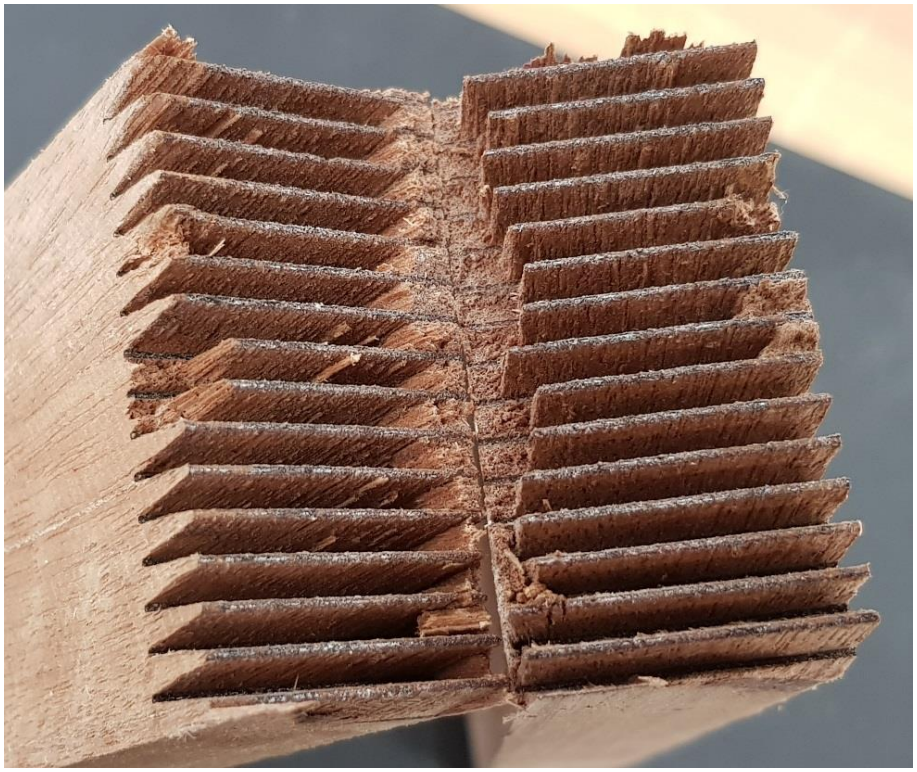

Figure 4-28: Finger joints failure of $FJ_{drm,prf,wv,R}$ specimens

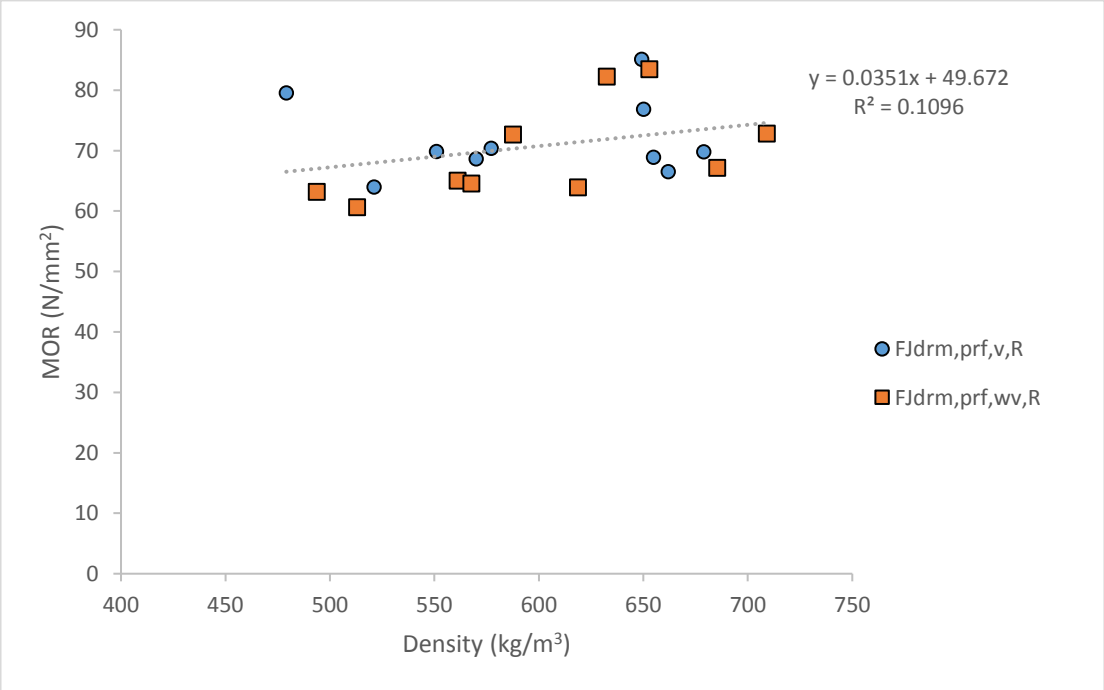

Figure 4-29: Bending strength as a function of density for PRF finger-jointed (30 x 30 mm) and wider (30 x 60 mm) DRM specimens

It can be concluded that the width of test pieces does not influence MOR and MOE results in four-point bending. These results agree with the findings of Madsen (1992) who observed that changes in width did not significantly affect the bending strength of specimens. He concluded that variations in specimen length (length effect) and load configurations substantially influenced the bending properties of timber. In this study the length and bending span of specimens were held constant, thus a length effect was not an influencing factor in the bending strength results of DRM specimens.

4.3.1.4 DRM specimens with horizontal finger joints

Comparison was made between the bending strength of vertical and horizontal finger-jointed specimens bonded with PRF adhesive. The average MOR of horizontal finger-jointed specimens, $FJ_{drm,prf,h,R}$ (67.8 N/mm^2) was slightly lower than vertical finger-jointed specimens, $FJ_{drm,prf,v,R}$ (71.9 N/mm^2). The individual bending results for $FJ_{drm,prf,h,R}$ specimens are shown in Table A-7 in Appendix A. ANOVA tests indicate no significant difference between the individual MOR of $FJ_{drm,prf,h,R}$ and $FJ_{drm,prf,v,R}$ specimens. This is expected since the cross sections of both $FJ_{drm,prf,v,R}$ and $FJ_{drm,prf,h,R}$ specimens are similar.

In reality, vertical joints are commonly used in the production of glulam beams. Vertical joints possess higher bending and tensile strengths compared to horizontal joints as discussed in Chapter 2. In this study, the horizontal finger joints have similar bonding area as the vertical finger joints since both have the same cross-sectional dimensions (30 x 30 mm). The only difference between the specimens is the orientation of finger joints in the bending tests as shown in Figure 4-30. The similar bonding area of the $FJ_{drm,prf,v,R}$ and $FJ_{drm,prf,h,R}$ specimens resulted in similar bending strength when tested in four-point bending. Significant difference is expected if the width of the specimen is increased so that the effective bonding area of the finger joints is significantly different (see Figure 2-5).

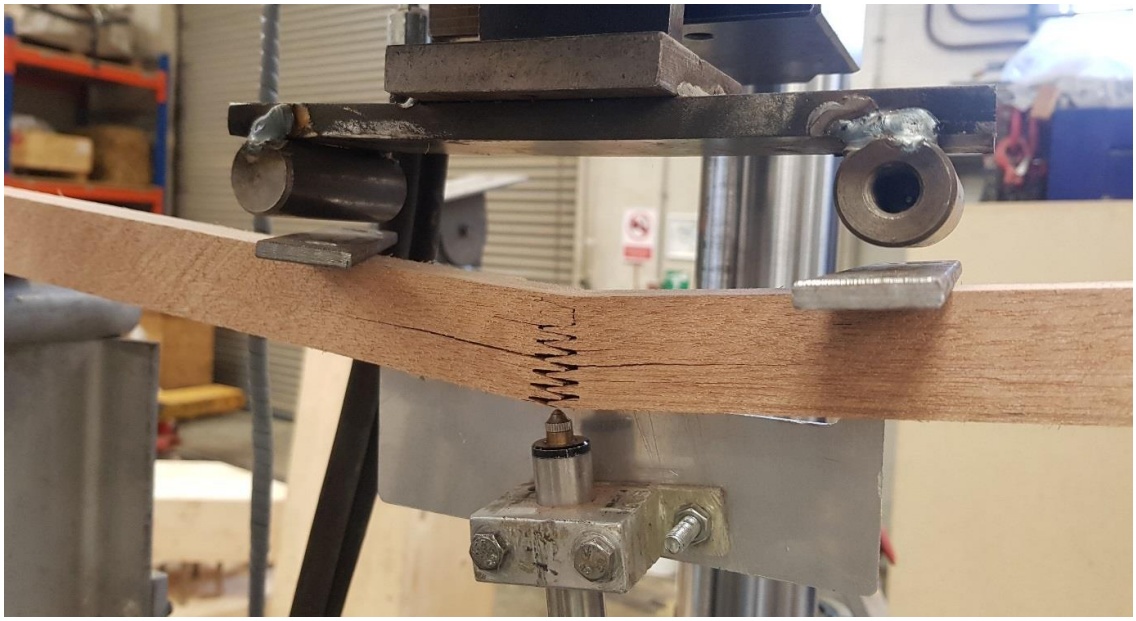

a)

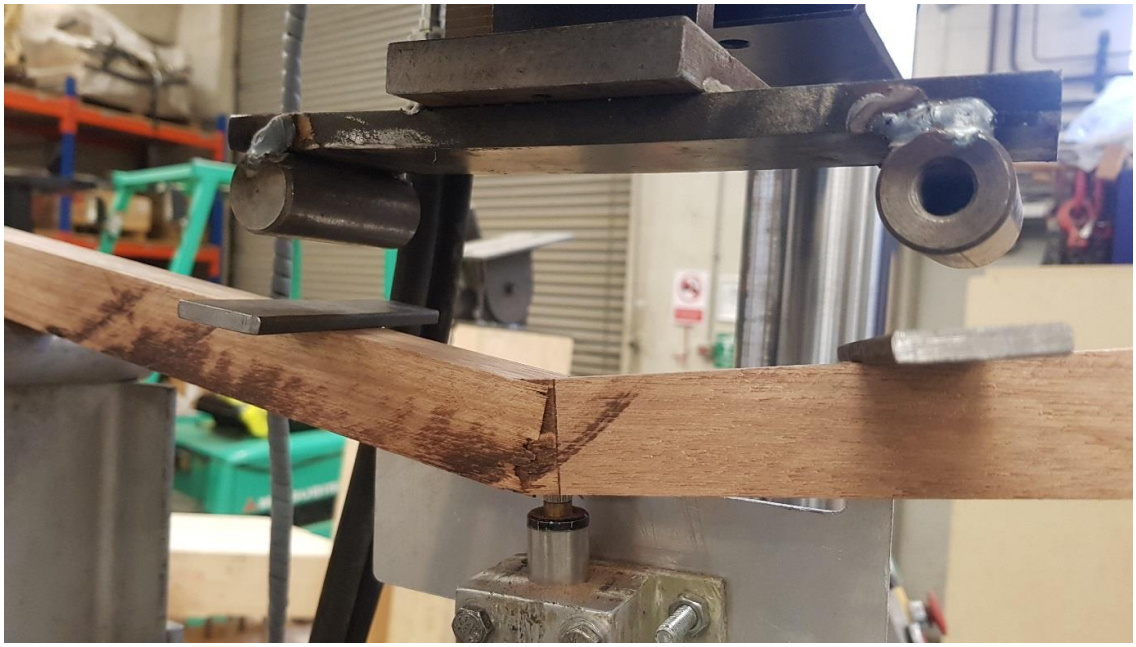

b)

Figure 4-30: Different orientations of finger joints in bending tests a) horizontal joint; b) vertical joint

4.3.1.5 Effect of different end pressure on bending strength of DRM finger joints

Finger-jointed PRF specimens were prepared using different end pressures to investigate its effect on the bending strength of DRM finger joints. Additional finger-jointed specimens were prepared using a lower pressure 10.0 N/mm^2 ($FJ_{drm,prf,v,L}$) and a higher pressure 15.0 N/mm^2 ($FJ_{drm,prf,v,H}$). The resulting bending strengths of these finger-jointed specimens were compared to specimens finger-jointed using an end pressure of 12.5 N/mm^2 as recommended by BS EN 14080:2013. From Table 4-4 the average MOR of $FJ_{drm,prf,v,L}$ specimens (59.4 N/mm^2) is lower than $FJ_{drm,prf,v,R}$ specimens (71.9 N/mm^2). ANOVA test results showed a statistically significant differences at the 95% confidence level between the MOR values of $FJ_{drm,prf,v,L}$ and $FJ_{drm,prf,v,R}$.

Comparing the MOR of $FJ_{drm,prf,v,R}$ and $FJ_{drm,prf,v,H}$ specimens, ANOVA test results indicated no significant differences between these two group of specimens. The individual MOR values of $FJ_{drm,prf,v,L}$ and $FJ_{drm,prf,v,H}$ are given in Tables A-8 and A-9 in Appendix A. The distribution of MOR values for specimens with different end pressures is shown in Figure 4-31.

It can be concluded that the lower end pressure 10.0 N/mm^2 is not suitable for the production of structural finger joints using DRM species. Higher end pressures of 12.5 and 15.0 N/mm^2 produced stronger joints. As discussed in the earlier section, the recommended end pressure for joints with finger length of 10.0 mm is 12.5 N/mm^2 (see Figure 4-6) as recommended by BS EN14080:2013. However, the standard indicates that the recommendation covers mostly softwood species and a few European hardwood species. Thus, findings in this study suggest that the recommended pressure of 12.5 N/mm^2 is suitable for finger-jointing tropical Malaysian hardwood, specifically for DRM species. Furthermore, end pressures in the range 12.5 to 15.0 N/mm^2 are capable of producing strong finger joints. This is pertinent since DRM species exhibit large variations in density and denser wood may requires higher end pressure to produce adequately bonded structural finger joints.

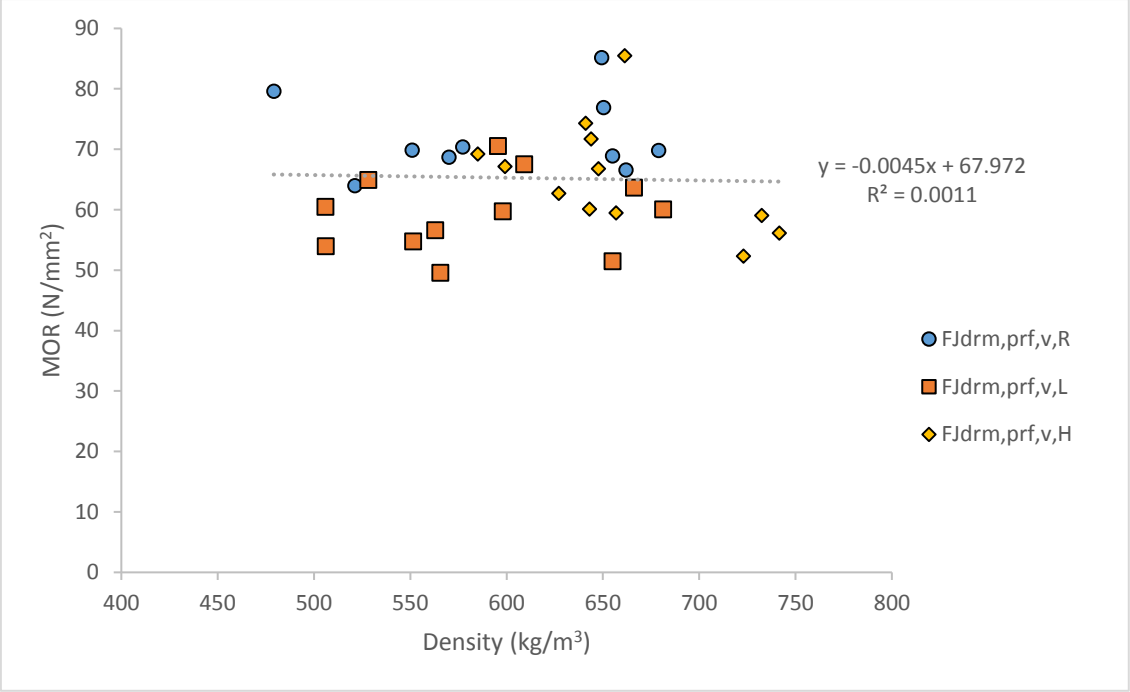

Key:

R recommended end pressure, 12.5 N/mm^2

L lower end pressure, 10.0 N/mm^2

H higher end pressure 15.0 N/mm^2

Figure 4-31: Bending strength as a function of density for DRM specimens with different end pressures

The variation of density makes it difficult to estimate end pressure in the finger-jointing of Malaysian hardwood. Optimum pressure is needed to produce strong finger joints that have uniform glue spread along the surface of the joints. Low end pressure results in inadequate force to produce interlocking connection and results in stress concentrations in the thick adhesive layer due to shrinking when the adhesive starts to cure (Bustos *et al*., 2003b). Excessive end pressure results in starved joints because of excessive glue squeeze-out. In most cases, excessive pressure can also damage the wood cell and split the roots of fingers (Jokerst, 1981; Bustos *et al*., 2004). Bustos *et al*. (2011) indicated that the effect of end pressure on short finger joints is more significant than joints with longer finger length. They discovered that lower end pressure induced air bubbles inside the glue lines of their specimens and significantly reduced the finger joint performance. Increasing end pressure reduced the gap between finger tips and

roots, thus increasing contact area between the two joining surfaces and improving the strength of finger joints.

4.3.1.6 Joint efficiency

Joint efficiency of finger joints is calculated based on the ratio of the individual MOR of a finger-jointed specimen to the average MOR of solid specimens. In this study, solid specimens showed higher bending strengths than finger-jointed DRM specimens as expected. The joint efficiency of $FJ_{drm,prf,v,R}$ specimens ranged from 69% to 92% with an average value of 77% while values for finger-jointed Spruce specimens, $FJ_{spruce,prf,v,R}$ ranged between 48% and 85% with an average value of 65%. Although there was no statistical difference between MOR values for solid DRM and Spruce specimens (see Section 4.3.1.1), finger-jointed DRM specimens were superior in strength to finger-jointed Spruce specimens.

The joint efficiency of DRM finger joints in this study is comparable to the findings of other research. Ahmad *et al*. (1997) tested Meranti finger joints with various finger lengths. They produced finger joints with average MOR of 35.00, 41.07 and 48.73 N/mm^2 and joint efficiency of 55%, 65% and 77% for finger length of 11, 12 and 13 mm respectively. Comparing results in this study, DRM finger-jointed specimens with finger length of 10 mm possessed average MOR of 71.9 N/mm^2, more than 32% higher than the values published by Ahmad *et al*. (1997). There were differences in their test method such as the span to depth ratio of 12 compared to 18 in this study, which is recommended by BS EN 408:2010+A1:2012. Their end pressure was 7.0 N/mm^2, because of increased finger length, which was much lower than the recommended 12.5 N/mm^2 in this study. The different test configurations, lower end pressure and different finger profiles may have resulted in a low bending strength compared to the MOR results in this study.

Ong and Ting (2011) managed to produce PRF finger-jointed *Acacia mangium* specimens with average joint efficiency of 59% and 85% for 16-year-old and 20-

year-old trees with average density 598 and 680 kg/m^3 respectively. The length of the finger in their study was 12 mm and the span to depth ratio of their test specimens was 24. Ahmad *et al*. (2016) tested finger joints of selected Malaysian timber species with finger lengths of 15 and 25 mm. One of their test species, White Meranti with an average density of 783 kg/m^3 had a joint efficiency of 55 and 66% for finger length of 15 and 25 mm respectively.

Comparing the results of this research with the studies mentioned above, it can be concluded that DRM finger joints with finger length of 10 mm are capable of producing joint efficiencies comparable to other hardwood species with longer finger lengths. Importantly, standard production requirements and testing methods need to be established for tropical hardwood species. This will ensure that finger-jointed products made from tropical hardwood species can be consistently produced and uniformly tested to meet the requirements for structural uses especially in the production of glulam beams.

4.3.1.7 Bending stiffness of finger joints

The average MOE of DRM finger joints ($FJ_{drm,prf,v,R}$) specimens is 15500 N/mm^2 which is similar to the MOE of solid DRM ($Solid_{drm}$) specimens, 15900 N/mm^2, as shown in Table 4-4. The individual MOE values for $FJ_{drm,prf,v,R}$ and $Solid_{drm}$ are given in Table A-3 and Table A-1 respectively in Appendix A. ANOVA tests indicate that there is no significant difference between these MOE values. This is true since the MOE values depends on the initial slope of the load-deflection curve in bending, which is in the elastic region (Figure 4-32). From this result, it can be concluded that the bending stiffness of DRM species in this study is not significantly affected by the finger-jointing process. Figure 4-33 shows the distribution of MOE values for both $Solid_{drm}$ and $FJ_{drm,prf,v,R}$ specimens.

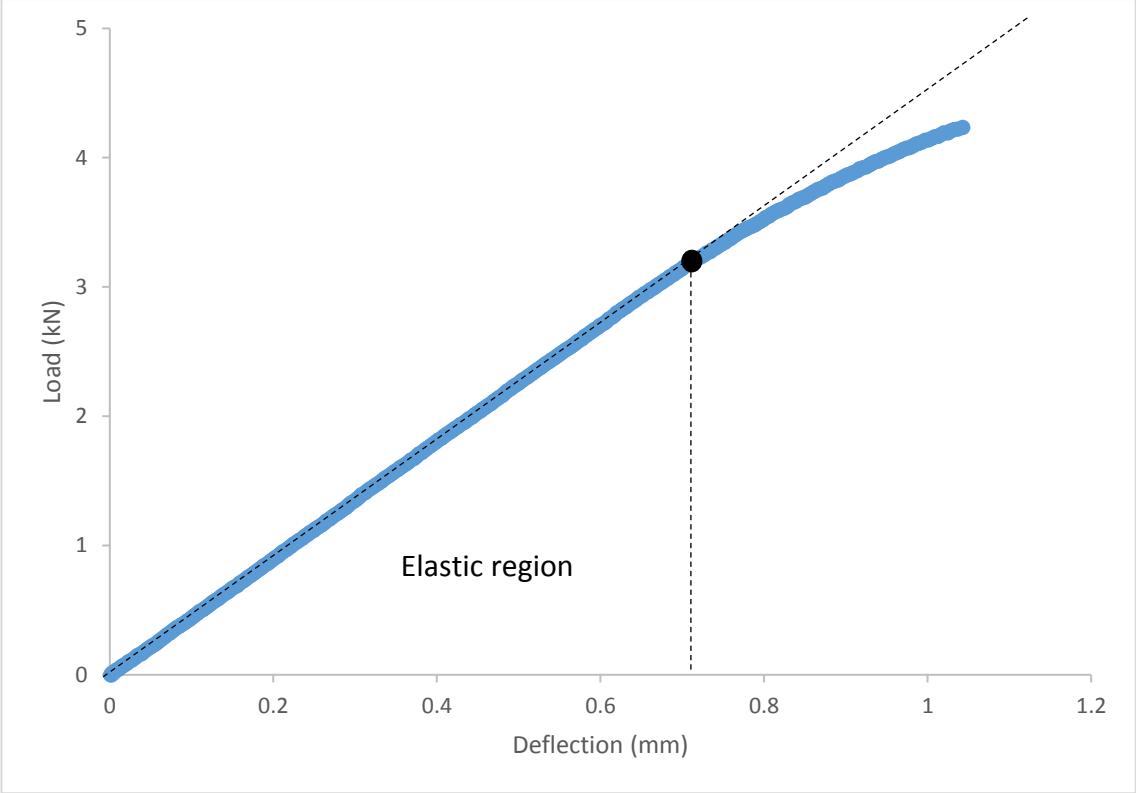

Figure 4-32: Typical load-deflection curve for DRM finger-jointed specimens in bending

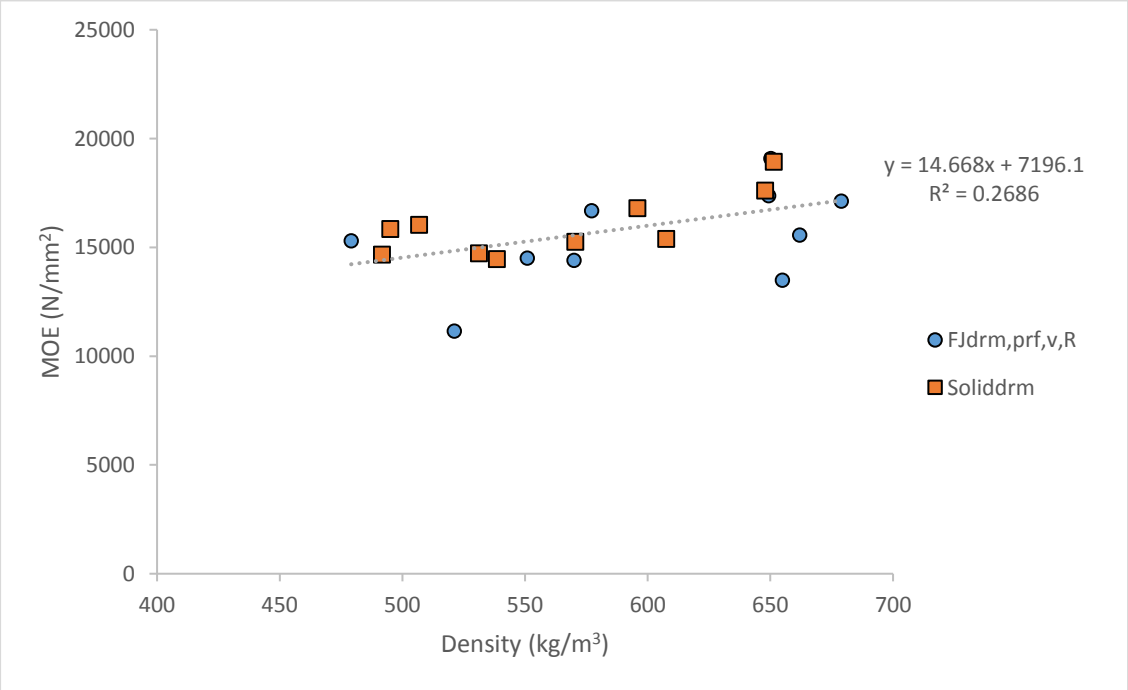

Figure 4-33: Bending stiffness as a function of density for solid and PRF finger-jointed DRM

4.3.2 Tensile strength parallel to grain

Tensile strength results for DRM specimens with vertical finger joints are discussed in this section. Table 4-5 summarises the average tensile strength of DRM finger-jointed specimens with their respective moisture content and density. Additional finger-jointed specimens with finger length of 15 mm, $FJ15_{T,prf,R}$, were fabricated at SP Wood Building Technology, Sweden because of the availability of a 15 mm finger cutter. Due to transportation and prolonged storage of the DRM pieces, the moisture content of the 15 mm finger-jointed specimens increased to a moisture content slightly higher than the 10 mm finger-jointed specimens.

Table 4-5: Average tensile strength of DRM finger joints
(10 specimens for each test configuration)

Descriptions	Adhesive	End pressure (N/mm^2)	Tensile strength (N/mm^2)		Moisture Content (%)	Density (kg/m^3)
			Mean	SD		
$FJ_{T,prf,R}$	PRF	12.5	49.9	7.16	12.0	651
$FJ_{T,epoxy,R}$	Epoxy	12.5	44.3	13.5	11.7	545
$FJ_{T,prf,L}$	PRF	10.0	39.3	21.8	11.8	538
$FJ_{T,prf,H}$	PRF	15.0	52.2	8.85	12.1	642
$FJ15_{T,prf,R}$	PRF	12.5	72.8	7.77	14.1	631

Key:

T	tensile strength parallel to grain
FJ	finger-jointed specimens (finger length 10 mm)
FJ15	finger-jointed specimens (finger length 15 mm)
R	recommended pressure (12.5 N/mm^2)
L	lower pressure (10.0 N/mm^2)
H	higher pressure (15.0 N/mm^2)

It was difficult to determine the tensile strength parallel to grain for solid wood due to the high ultimate force required for failure and high stress concentrations at the grips. In this study, solid specimens were tested but all failed due to crushing of wood at the grips. Thus, these tensile strength values are not

reported because they are not representative of actual tensile strength of solid DRM specimens. The values were expected to be higher than the finger-jointed specimens.

4.3.2.1 Tensile strength of DRM specimens finger-jointed with PRF and epoxy adhesives

The average tensile strength of DRM finger joints bonded with PRF ($FJ_{T,prf,R}$) was 11% higher than for specimens bonded with epoxy adhesive ($FJ_{T,epoxy,R}$). Individual tensile strength results of $FJ_{T,prf,R}$ and $FJ_{T,epoxy,R}$ are given in Tables A-10 and A-11 in Appendix A. The failures of $FJ_{T,prf,R}$ specimens are shown in Figure 4-34. All the $FJ_{T,prf,R}$ specimens failed along the glue lines with pulled-out wood fibres attached to the surfaces except for two specimens which failed at the grips (Figure 4-35). For $FJ_{T,epoxy,R}$ specimens, the mode of failure consisted of failure at glue lines, failure in the grips, a mixture of wood and finger fractures (Figure 4-36) and a combination of wood and glue line failures (Figure 4-37).

Figure 4-34: $FJ_{T,prf,R}$ glue lines failure with attached pulled-out wood fibres

Figure 4-35: Wood crushing failure at gripped surface of $FJ_{T,prf,R}$ specimen

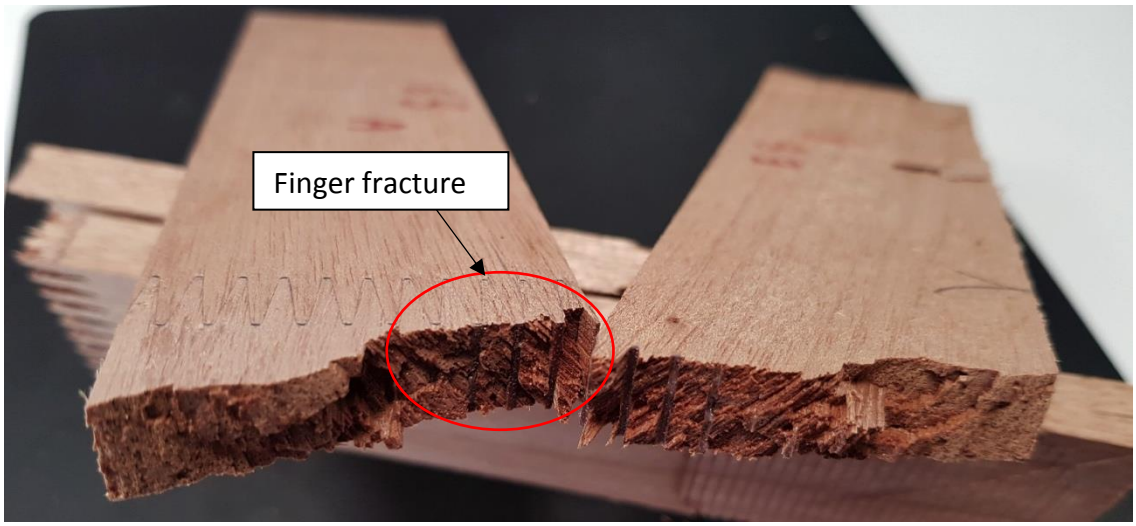

Figure 4-36: Wood and finger fractures of a $FJ_{T,epoxy,R}$ specimen

Figure 4-37: Mixture of glue lines and wood failures of a $FJ_{T,epoxy,R}$ specimen

From the results in Tables A-10 and A-11 in Appendix A, the tensile strength of $FJ_{T,prf,R}$ specimens showed less variability ranging from 35.9 to 57.1 N/mm^2 compared to $FJ_{T,epoxy,R}$ specimens which ranged from 27.9 to 63.7 N/mm^2. The low tensile strength of several $FJ_{T,epoxy,R}$ was a result of fracture in the wood and slipping at grips, so it is not representative of the actual performance of the finger joints. ANOVA tests indicated statistically no significant difference at 95% confidence level between the tensile strength of $FJ_{T,prf,R}$ and $FJ_{T,epoxy,R}$ specimens. The distribution of tensile strengths for $FJ_{T,prf,R}$ and $FJ_{T,epoxy,R}$ specimens is shown in Figure 4-38.

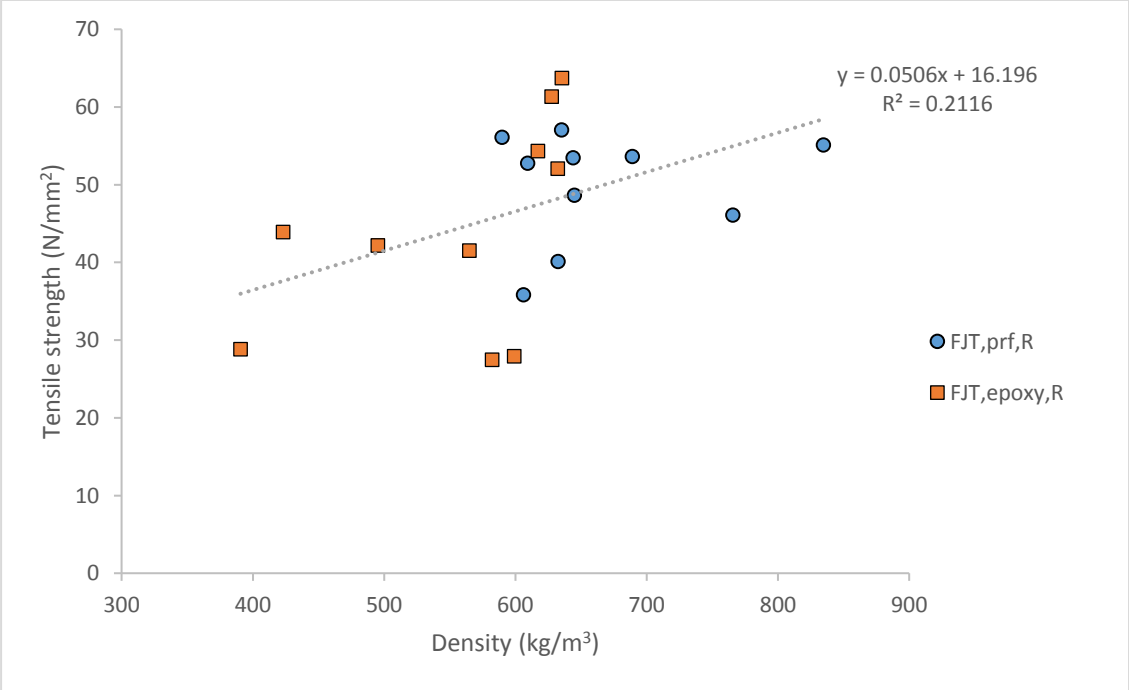

Figure 4-38: Tensile strength as a function of density for DRM finger-jointed with PRF and epoxy

It can be concluded that there are no significant differences in tensile strength between DRM specimens finger-jointed with PRF and epoxy adhesives in this study. Similar to the results of bending tests in the previous section, the tensile strength of DRM finger joints was not influenced by different bonding media. Increasing the number of test specimens and excluding results that are not related to failures in the finger joints region may further clarify the results of this study.

4.3.2.2 Effect of end pressure on tensile strength of DRM finger joints

The tensile strength results for DRM specimens finger-jointed with different end pressures are discussed in this section. Additional DRM specimens were finger-jointed using lower end pressure 10.0 N/mm^2 ($FJ_{T,prf,L}$) and higher end pressure 15.0 N/mm^2 ($FJ_{T,prf,H}$). The tensile strength results were compared to DRM specimens finger-jointed with end pressure of 12.5 N/mm^2 as recommended by BS EN 14080:2013. The individual tensile strength results for $FJ_{T,prf,L}$ and $FJ_{T,prf,H}$ specimens are given in Tables A-12 and A-13 respectively. All $FJ_{T,prf,H}$ specimens failed at glue lines with pulled-out wood fibres attached to the surfaces (Figure 4-39). $FJ_{T,prf,L}$ specimens exhibited glue line failure, failure at the grips, a mixture of glue line failure and finger fractures (Figure 4-40) and a mixture of wood and glue line failures (Figure 4-41).

Figure 4-39: Failure of glue lines of $FJ_{T,prf,H}$ specimen

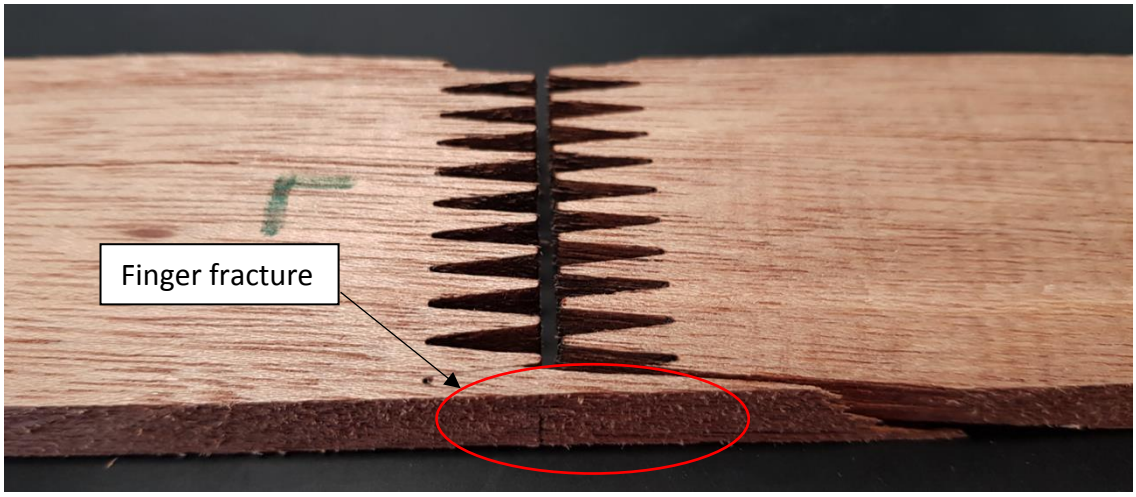

Figure 4-40: Mixture of glue lines and finger fractures of a $FJ_{T,prf,L}$ specimen

Figure 4-41: Mixture of glue lines and wood failures of a $FJ_{T,prf,L}$ specimen

The average tensile strength of $FJ_{T,prf,R}$ (49.9 N/mm^2) is 21% higher than $FJ_{T,prf,L}$ (39.3 N/mm^2) specimens (see Table 4-5). ANOVA test results showed statistically significant differences between the individual tensile strength of $FJ_{T,prf,R}$ and $FJ_{T,prf,L}$. In contrast, the tensile strength of $FJ_{T,prf,H}$ was not significantly different from $FJ_{T,prf,R}$ specimens when analysed by the ANOVA test. It can be concluded that the lower end pressure of 10.0 N/mm^2 was not able to produce optimum tensile strength for structural finger-jointed DRM specimens. The recommended end pressure of 12.5 N/mm^2 and the higher value of 15.0 N/mm^2 produced stronger structural DRM finger joints. Similar to the results from the bending strength tests, the lower end pressure of 10.0 N/mm^2 is not suitable for producing structural DRM finger joints with adequate tensile strength. Figure 4-42 shows the distribution of tensile strengths of DRM specimens finger-jointed with different end pressures.

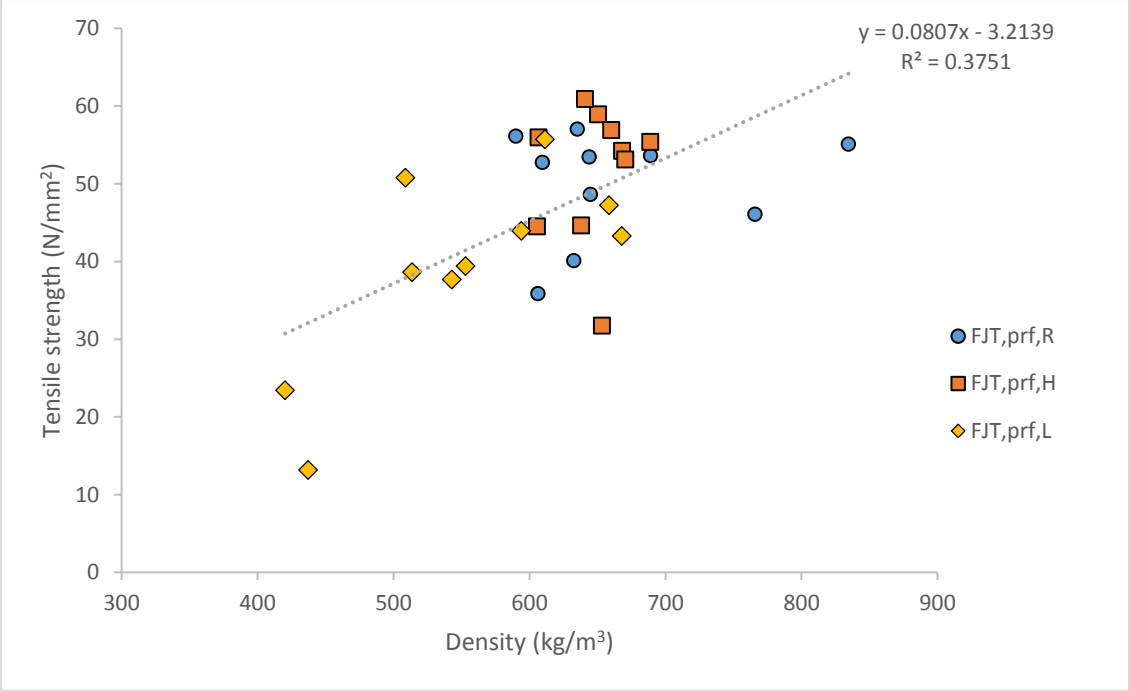

Key:

R recommended end pressure, 12.5 N/mm^2

H higher end pressure 15.0 N/mm^2

L lower end pressure, 10.0 N/mm^2

Figure 4-42: Tensile strength as a function of density for DRM finger-jointed with different end pressures

Ayarkwa *et al*. (2000) studied the influence of end pressure on tensile properties of finger joints produced from tropical African hardwood. They indicated that the tensile strength of finger joints increased with increase of end pressure up to an optimum value, which can be different for wood species of different density. In this study, it can be concluded that end pressures ranging from 12.5 to 15.0 N/mm^2 are suitable for finger-jointing DRM species and capable of producing optimum tensile strength. Further tests using end pressure higher than 15.0 N/mm^2 may provide an even wider range of suitable end pressures. This will be advantageous to manufacturers finger-jointing DRM for structural uses because of the variation in density of this species. Care must be taken to avoid using excessive pressure such that an optimum end pressure is achieved when the finger joint assembly is adequately tight without splitting the roots of the fingers (Jokerst, 1981; Ayarkwa *et al*., 2000).

4.3.2.3 Comparison of DRM specimens with different finger length

Tensile strength results for DRM specimens, $FJ15_{T,prf,R}$ with finger length of 15 mm were compared to $FJ_{T,prf,R}$ specimens with finger length of 10 mm in this section. The average tensile strength of $FJ15_{T,prf,R}$ (72.8 N/mm^2) was 31% higher than $FJ_{T,prf,R}$ (49.9 N/mm^2) as shown in Table 4-5. The results for the individual tensile strengths of $FJ15_{T,prf,R}$ are given in Table A-14 in Appendix A. All $FJ15_{T,prf,R}$ specimens failed at glue lines with variation in wood splits (Figure 4-43). ANOVA tests indicated a significant difference between the tensile strength of $FJ_{T,prf,R}$ and $FJ15_{T,prf,R}$ specimens. Figure 4-44 shows the tensile strength distribution of $FJ_{T,prf,R}$ and $FJ15_{T,prf,R}$ specimens.

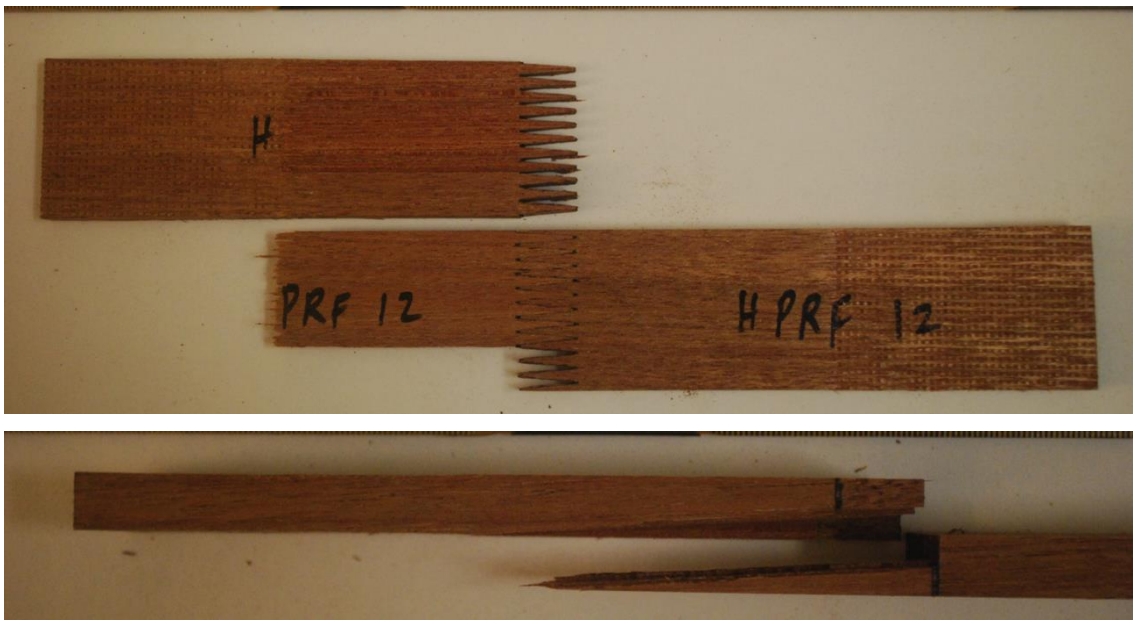

Figure 4-43: Combination of glue lines and wood failures of a $FJ15_{T,prf,R}$ specimen

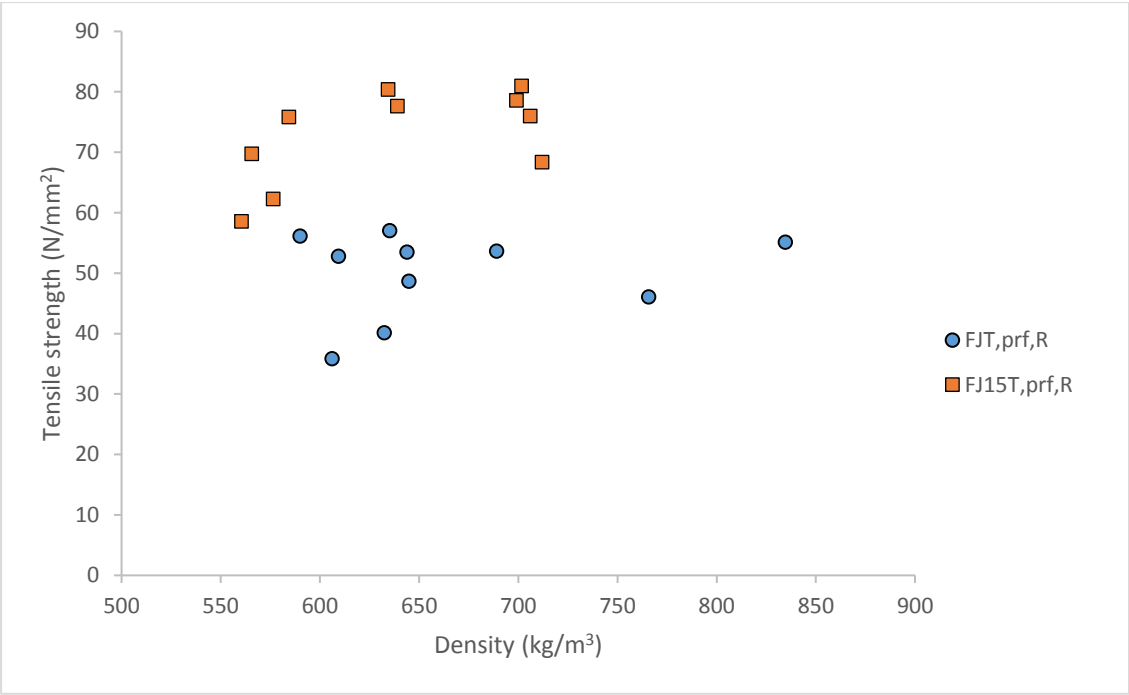

Figure 4-44: Tensile strength as a function of density for DRM finger joints specimens with finger lengths of 10 and 15 mm

As explained in the earlier Section 4.3.2, the average moisture content of $FJ15_{T,prf,R}$ specimens (14.1%) was higher than $FJ_{T,prf,R}$ specimens (12.0%) as shown in Table 4-5. Green *et al*. (1999) indicated that an increase in the mechanical properties of wood is related to a decrease of moisture content resulting from the drying process (Figure 4-45). In the graph, it can be seen that the effect is less significant for tensile strength parallel to grain. Thus, it can be safely assumed that the higher moisture content of $FJ15_{T,prf,R}$ specimens does not influence significantly the tensile properties of the DRM finger joints.

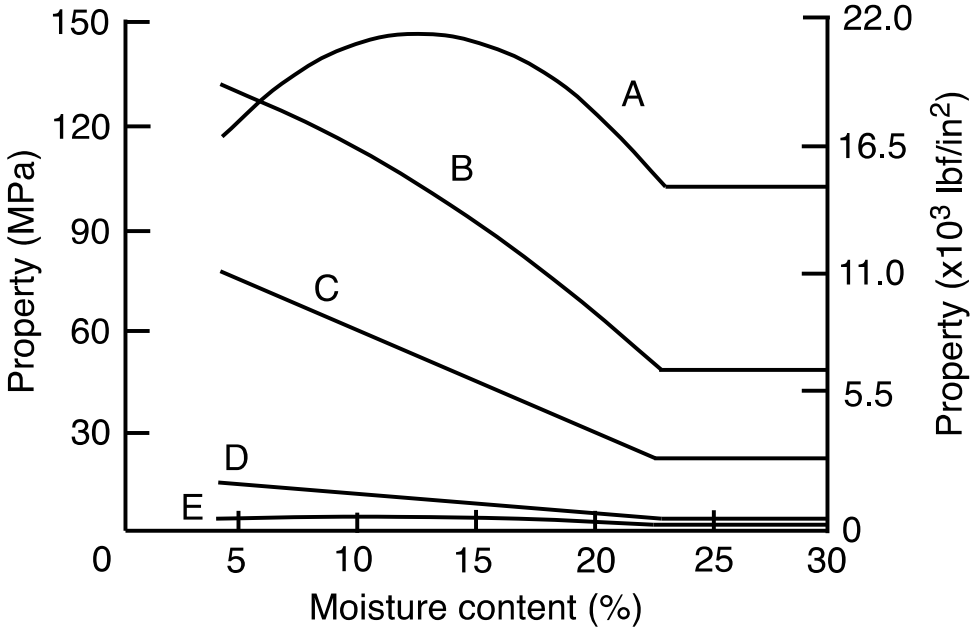

Key:

A tension parallel to grain

B bending

C compression parallel to grain

D compression perpendicular to grain

E tension perpendicular to grain

Figure 4-45: Relationship between moisture content and mechanical properties of wood (Green *et al*.,1999)

Finger joints with longer finger length are generally known to have better strength properties than shorter finger joints because of the larger bonding area of the longer finger joints (Barboutis, 2007; Hamid *et al*., 2016). The strength of finger joints is also influenced by factors such as the ratio of finger length to pitch, finger geometry, orientation of finger joints, species and density of the wood (Jokerst, 1981; Ahmad *et al*., 1997; Ayarkwa *et al*., 2000; Özçifçi and Yapıcı, 2007; Habipi and Ajdinaj, 2015). In this study, the finger joints were consistently prepared according to requirements for the production of structural finger joints for glulam embodied in BS EN 14080:2013. Factors, including the ratio of finger length to pitch, finger geometry and orientation of finger joints, met the requirements of the standard. Any changes to these parameters would affect the tensile strength of DRM finger joints in this study. Thus, it is important

to consistently produce finger-jointed specimens according to the standard requirements so that comparison can be made to future finger-jointed specimens produced from different hardwood species.

4.3.3 Compressive strength parallel to grain

The compressive strength results of DRM and Spruce specimens are discussed in this section. All specimens were finger-jointed using the recommended end pressure of 12.5 N/mm^2. The average compressive strength results of solid and finger-jointed DRM and Spruce specimens are shown in Table 4-6. Results for individual compressive strength of the specimens are given in Tables A-15 to A-19 in Appendix A.

Table 4-6: Average compressive strength parallel to grain

Descriptions	Adhesive	Compressive strength (N/mm^2)		Moisture Content (%)	Density (kg/m^3)
		Mean	SD		
$Solid_{C,drm}$	-	54.2	4.24	12.0	592
$Solid_{C,spruce}$	-	45.9	6.24	12.2	502
$FJ_{C,drm,prf}$	PRF	51.9	5.30	11.8	621
$FJ_{C,drm,epoxy}$	Epoxy	54.6	3.69	12.3	629
$FJ_{C,spruce,prf}$	PRF	40.5	5.30	12.1	500

Key:

C compressive strength parallel to grain

FJ finger-jointed specimens

4.3.3.1 Compressive strength of solid DRM and Spruce specimens

The solid DRM ($Solid_{C,drm}$) specimens exhibited compression failure (creases) near the edges and inner region of the specimens (Figure 4-46). The solid Spruce ($Solid_{C,spruce}$) specimens also showed similar compression failure in addition to some failure around knots (Figure 4-47). The average compressive

strength of $Solid_{C,drm}$ was 16% higher than $Solid_{C,spruce}$ specimens. The results for individual compressive strengths of $Solid_{C,drm}$ and $Solid_{C,spruce}$ are given in Tables A-15 and A-16. ANOVA test results showed statistically significant differences between the compressive strength of $Solid_{C,drm}$ and $Solid_{C,spruce}$ specimens. It can be concluded that solid DRM specimens possessed higher compressive strengths compared to Spruce in this study. Compression failure near knots in some of the Spruce specimens contributed to the lower compressive strengths in this study in comparison to the knot-free solid DRM specimens.

Figure 4-46: Compression failure of solid DRM specimens

Figure 4-47: Compression failure near knot of solid Spruce specimen

4.3.3.2 Compressive strength of finger-jointed specimens

DRM specimens finger-jointed with PRF ($FJ_{C,drm,prf}$) contained failures mostly at the finger tips of the joints (Figure 4-48) with several pieces showing failures extending to the solid wood region away from the joints (Figure 4-49). The results of individual compressive strengths of $FJ_{C,drm,prf}$ are given in Table A-17 in Appendix A. Comparing the compressive strength of $FJ_{C,drm,prf}$ and $Solid_{C,drm}$, ANOVA analysis indicated statistically no significant differences at 95% confidence level between these values.

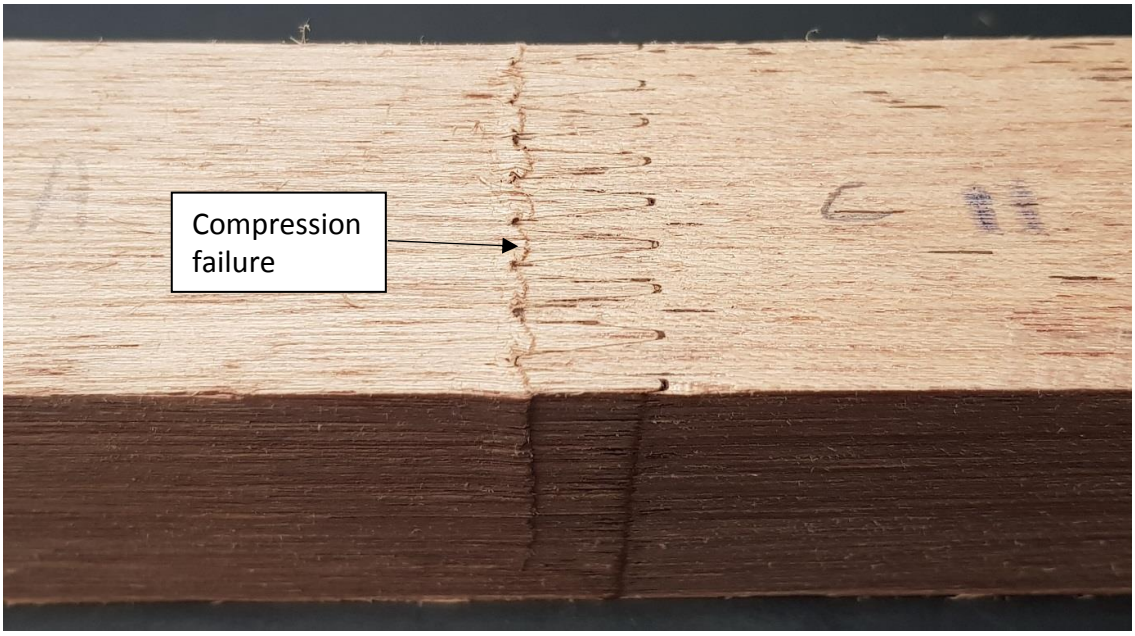

Figure 4-48: Wood compression failure near finger tips of finger-jointed DRM specimen

Figure 4-49: Compression failure near finger tips extending to the solid wood region

Comparing epoxy finger-jointed DRM specimens ($FJ_{C,drm,epoxy}$) with $FJ_{C,drm,prf}$, the average compressive strength of $FJ_{C,drm,epoxy}$ (54.6 N/mm^2) was not much higher than $FJ_{C,drm,prf}$ specimens (51.9 N/mm^2). The individual test results of $FJ_{C,drm,epoxy}$ are given in Table A-18. ANOVA test results indicated no significant differences between the compressive strength of $Solid_{C,drm}$, $FJ_{C,drm,prf}$ and $FJ_{C,drm,epoxy}$. It can be concluded that solid DRM specimens have similar compressive strengths to finger-jointed PRF and epoxy DRM specimens. The

shorter finger length and well-fitted finger tips were able to transfer efficiently the compressive load and the stress concentrations at the finger joints are defect-closing rather than crack-opening as they would be in tension.

From Table 4-6, the average compressive strength of PRF finger-jointed Spruce ($FJ_{C,spruce,prf}$) specimens (40.5 N/mm^2) is 29% lower than $FJ_{C,drm,prf}$ specimens (51.9 N/mm^2). The individual test results for $FJ_{C,spruce,prf}$ are given in Table A-19. From ANOVA test results, there is a significant difference between $FJ_{C,drm,prf}$ and $FJ_{C,spruce,prf}$ specimens, thus indicating finger-jointed DRM specimens have higher compressive strength than Spruce. All the $FJ_{C,spruce,prf}$ specimens showed failure near finger tips. Interestingly, one of the Spruce specimens did not show failure near a knot although it is located near to the finger joints (Figure 4-50). This indicates that the finger joints of Spruce specimens in this study may in some cases be weaker than natural defects. Closer inspection revealed splitting of roots in some of the $FJ_{C,spruce,prf}$ specimens (Figure 4-51). This condition was evident in the finger-jointed Spruce specimens but not visible in DRM specimens. Although the end pressure of 12.5 N/mm^2 was used in finger-jointing of Spruce specimens, as recommended in BS EN14080:2013, the splitting of finger roots indicated that the pressure may be excessive. Nevertheless, wider finger tips may also contribute to splitting of finger roots but it was not evident in DRM specimens which used the same finger cutter in the preparation of finger joints. Kishan Kumar *et al*. (2010) studied the effect of finger tip area on the compressive strength parallel to grain of finger-jointed specimens. They concluded that better compressive strength of finger joints could be produced by reducing the tip area in relation to the total area of the joints.

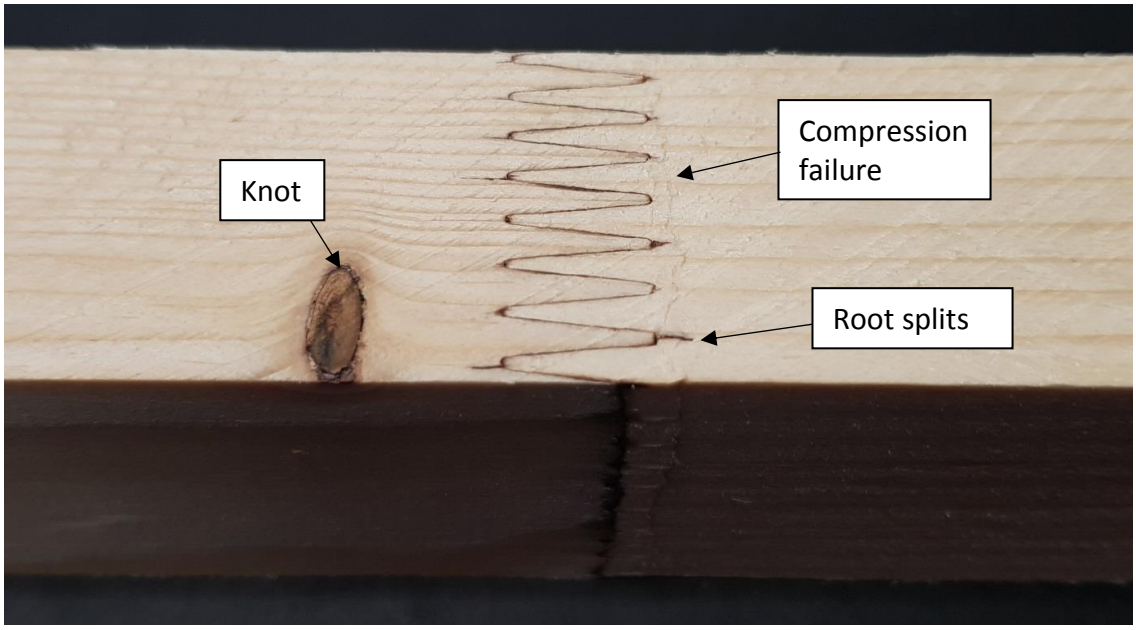

Figure 4-50: Compression wood failure near finger tips of Spruce specimen

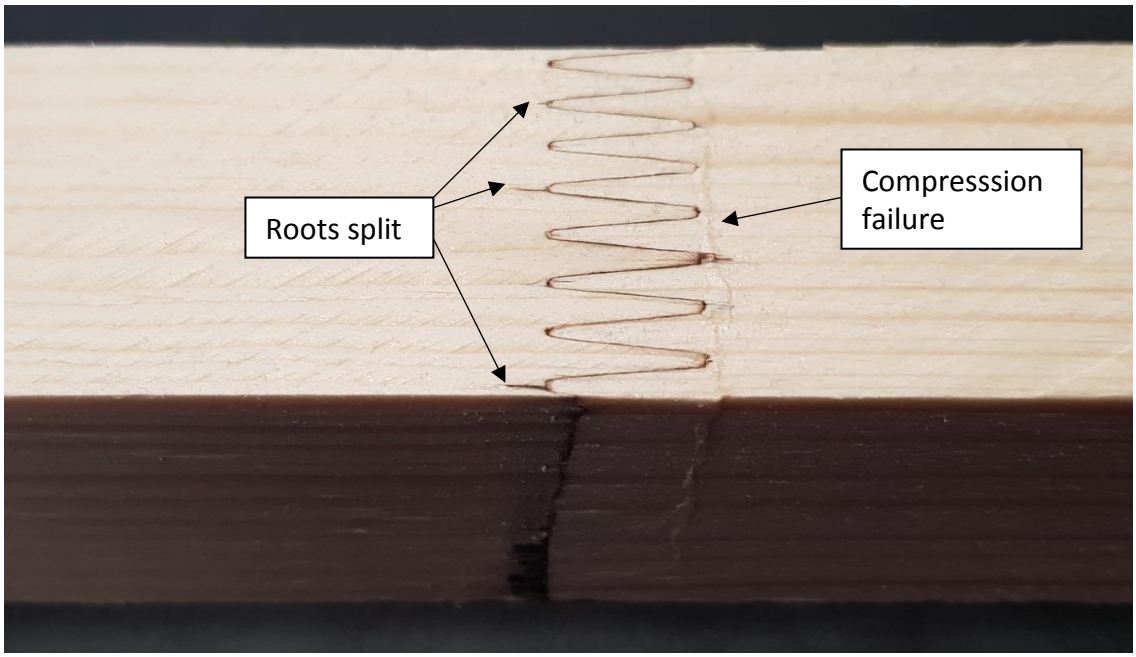

Figure 4-51: Splitting of roots of Spruce specimen

4.3.4 Microscopic analysis of wood and bonding failures

The failure of DRM finger-jointed specimens tested in tension and compression were observed in the scanning electron microscope (SEM). For comparison purposes, the profile of the unbonded finger joints was also examined. Figure 4-52 shows the surface conditions of unjointed finger profile at 10x magnification.

At 10x magnification, the unbonded finger profile shows a smooth surface. Interestingly, wood resin from the specimens in the shape of oval can be seen in the scanning electron microscope (Figure 4-53).

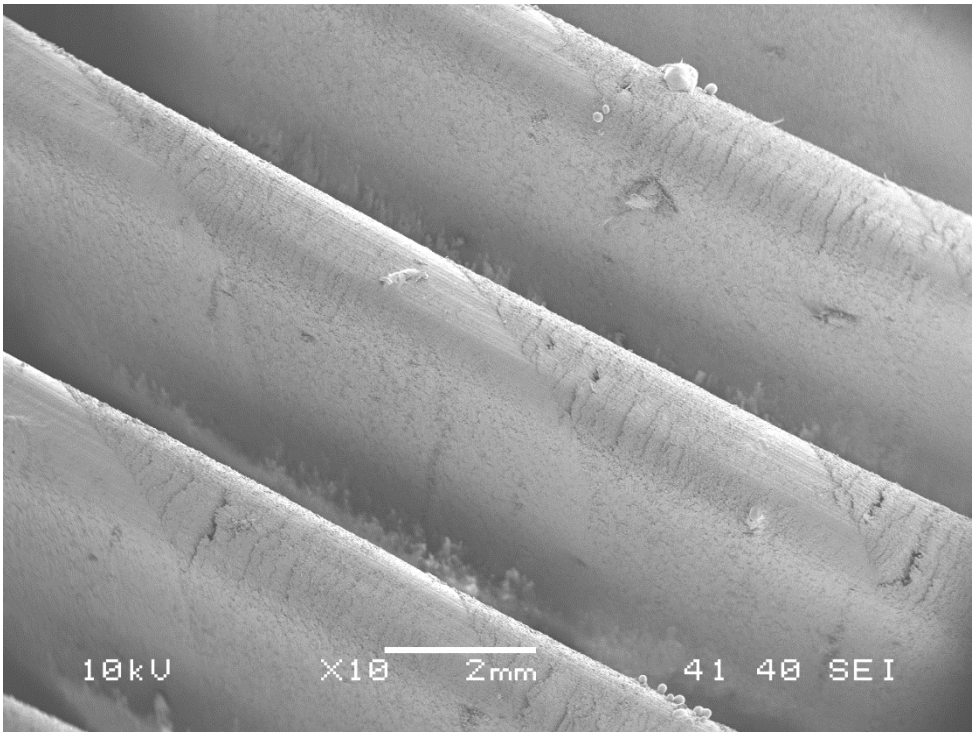

Figure 4-52: DRM finger surface without adhesive at 10x magnification

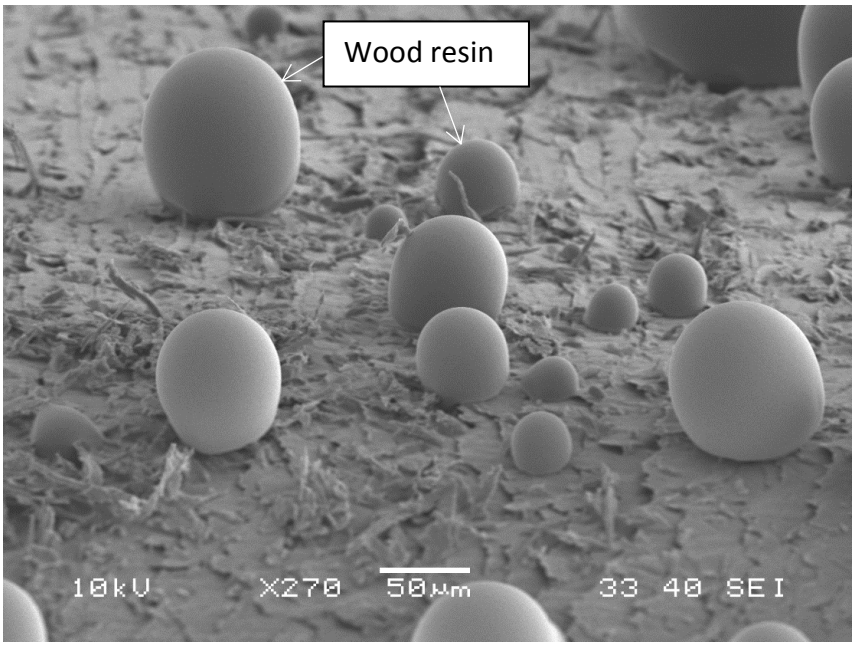

Figure 4-53: Finger surface with wood resin at 270x magnification

Figure 4-54 images the compressive failure of specimens at 50x magnification while Figure 4-55 presents the fracture surface of finger-jointed specimens following a tensile test. The image shows fracture of wood fibres (right) and the base surface of the finger joints that is covered with adhesive (left). Visually, this specimen shows failures with few broken fingers and pulled-out wood fibres at glue lines.

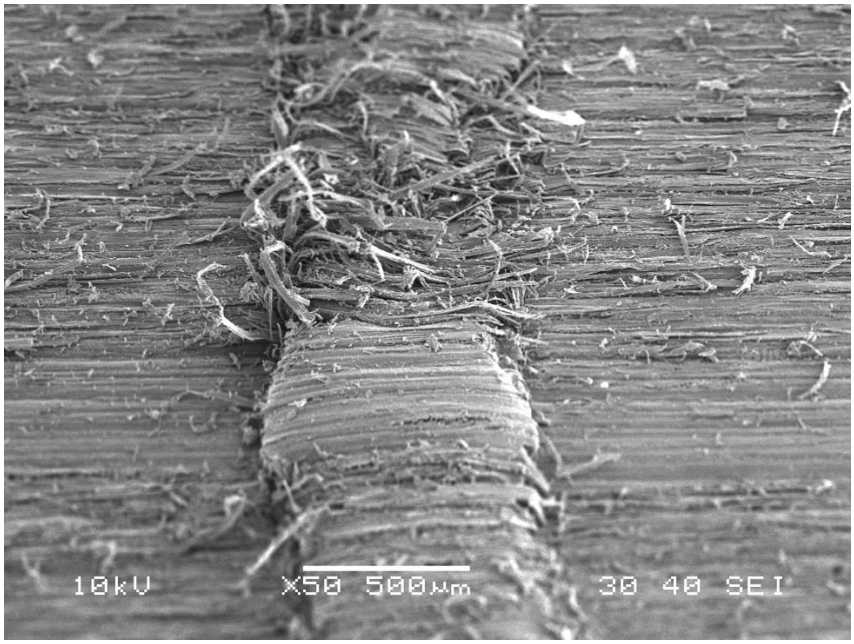

Figure 4-54: Compressive failure at 50x magnification (compressive test)

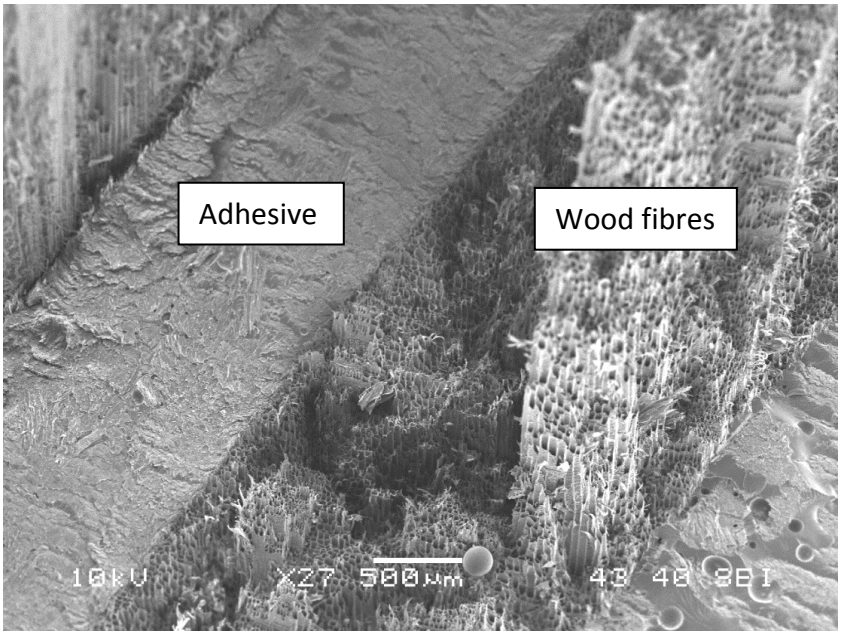

Figure 4-55: Fractured finger joint surface with epoxy adhesive glue line at 27x magnification (tensile test)

Figure 4-56 shows the tensile fracture surface at the side of the finger (right) and the surface of finger tip (left) that is covered with PRF adhesive. The image shows that failure occurs in the wood and not at glue lines which indicates a strong finger joint bond.

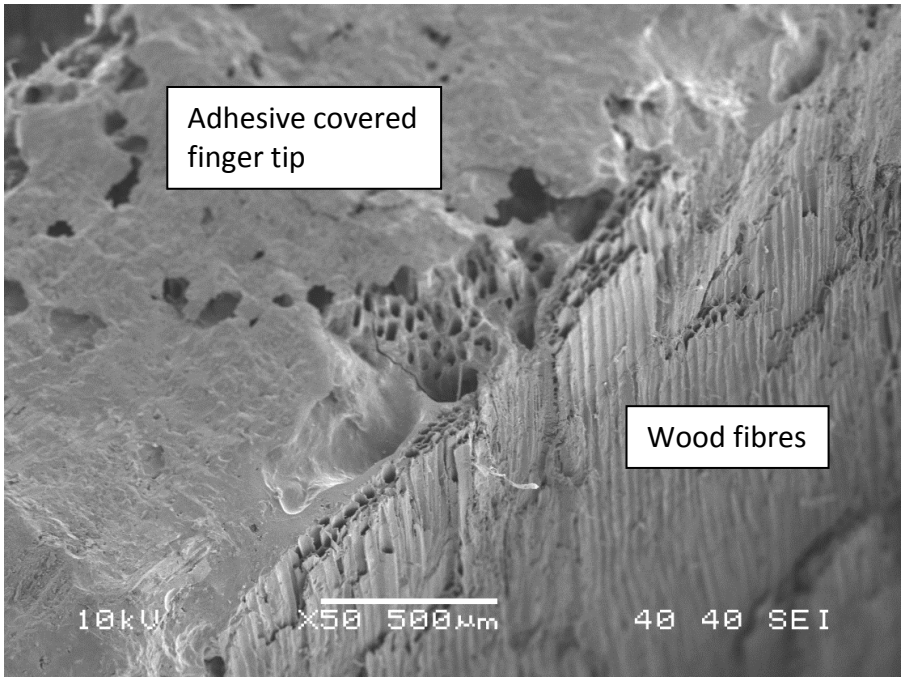

Figure 4-56: Finger joint surface with PRF adhesive at 50x magnification (tensile test)

4.4 Summary

The objective of this chapter was to investigate the performance of Malaysian Dark Red Meranti finger joints and their suitability to be used as structural finger joints in the production of glulam beams.

In four-point bending tests, DRM finger joints achieved average joint efficiency of 77% and showed better bending strength performance compared to Spruce finger joints. The DRM specimens finger-jointed with PRF and epoxy exhibited failures at the glue lines with a mixture of pulled-out wood fibres and finger fractures, indicating good bonding performance of the joints. The findings of the bending tests can be summarised as follows:

- The bending strength of finger-jointed DRM specimens was not affected by changes in the width of test pieces with cross-sectional dimensions of 30 x 30 mm and 30 x 60 mm.

- The bending strength of vertical DRM finger joints showed no significant differences to the bending strength of horizontal finger joints if both test pieces had the same bonding area, as shown in this study.

- The application of a low end pressure of 10.0 N/mm^2 produced weaker DRM finger joints when compared to specimens produced with higher end pressures of 12.5 and 15.0 N/mm^2. Thus, end pressure affects the bending strength of finger joints. DRM species required higher end pressure to obtain adequate bonding which resulted in stronger finger joints.

- The bending stiffness of DRM pieces was not affected by finger-jointing. There were no significant differences in the MOE values of solid and finger-jointed DRM specimens.

In tensile tests, DRM finger joints were well bonded with most failures consisting of a mixture of glue line failures with pulled-out wood fibres, wood and finger fractures. The findings can be summarised as below:

- The tensile strength of DRM finger joints bonded with PRF showed no significant differences from epoxy bonded finger joints.

- Low end pressure of 10.0 N/mm^2 was not able to produce structural DRM finger joints with tensile strength comparable to finger-jointed specimens produced with end pressures of 12.5 and 15.0 N/mm^2.

- DRM finger-jointed specimens with a finger length of 15 mm showed higher tensile strength compared to specimens with a shorter 10 mm finger length.

In compressive tests, both solid and finger-jointed DRM specimens showed higher compressive strength parallel to grain than Spruce specimens. The findings of this test are summarised below:

- The compressive strength of solid DRM specimens showed no significance differences from finger-jointed specimens.

- DRM specimens finger-jointed with PRF showed similar compressive strength to epoxy specimens.

- An end pressure of 12.5 N/mm^2, as recommended by BS EN 14080:2013, was suitable for finger-jointing DRM specimens but was not recommended for Spruce species. The splitting of roots in the finger-jointed Spruce specimens indicates the end pressure of 12.5 N/mm^2 is excessive for the softwood species.

Closer inspection of the finger joints failure was conducted using SEM. The magnified image of the surface of failed tensile specimens evidently showed failures occurred in wood, as in the fracture of wood fibres, indicating strong bonding performance of DRM finger joints (see Figure 4-55). The failure modes imaged in the SEM indicated that the finger tip does not have strong adhesive bond as seen with the adhesive-rich zones depicted in Figure 4-56. Nevertheless, the surface area of the finger tip was relatively small compared to the overall surface area of the glued finger joints. In this study, the strength of finger joints in tension was dictated by the bonded surface area of the finger slope and not by surface area of the finger tip. The tensile strength of the finger joints would be affected if the surface area of the finger tip was relatively large compared to the overall bonded surface area of the finger joints (Rao *et al*., 2012).

The results presented in this chapter show that DRM finger-jointed specimens exhibited strength properties higher than Spruce finger-jointed specimens. The properties of the wood influenced the strength of finger joints, where higher density DRM specimens were stronger than lower density specimens of the

same species. The higher end pressures of 12.5 and 15.0 N/mm^2 produced stronger finger-jointed DRM specimens compared to the end pressure of 10.0 N/mm^2. The finger-jointing of DRM for structural uses is feasible when adequate pressure is used, resulting in an average joint efficiency of 77%. Due to the importance of finger joints in the fabrication of glulam, understanding their mechanical properties in bending, tension and compression is critical for the production of beams that meet the standard minimum quality requirements.

Chapter 5 Bonding strength of beam laminations

5.1 Introduction

This chapter presents the findings of the shear strength tests conducted on the glue lines of the Dark Red Meranti species. The aim is to evaluate the bonding performance of DRM species and to assess its suitability in the manufacture of glulam beams. The effect of different cramping pressures and other factors affecting the bonding strength of the glue lines are also discussed. The findings of this study contribute to the technical knowledge gap pertaining to the quality of glulam made from Malaysian hardwood and encourages glulam producers to utilise DRM species.

The fabrication of the glulam specimens was completed under laboratory conditions while following closely the production requirements in BS EN 14080:2013, so as to replicate glulam production in a factory environment. Prior to the bonding of the laminations for full size glulam beams, shorter pieces of DRM were bonded using different cramping pressures of 0.64, 0.80 and 0.96 N/mm^2. The objective in producing these short beams was to evaluate the effect of different cramping pressures on the bonding strength of the glue lines in glulam beams, specifically using DRM species. Generally, the strongest bond lines are often produced using an optimum cramping pressure which has different values for wood of different density.

High density wood requires higher cramping pressure because its thicker cell walls and smaller lumens are harder to compress to produce close contact between its surface and the adhesive (Vick, 1999). However, excessive pressure incurs over-penetration and excessive glue squeeze-out that results in starving of the glue lines, producing weaker joints (Frihart and Hunt, 2010). There is a positive relationship between the strength of glue lines and wood density up to the range of 700 to 800 kg/m^3 at a typical moisture content of 12% (Frihart and Hunt, 2010).

The recommended cramping pressures for the production of glulam beams are given in Table 5-1. In this study, the lamination thickness for the glulam beams was 35 mm. The higher limit of 0.80 N/mm^2 was used as the optimum cramping pressure because the DRM hardwood has a higher density compared to typical softwood species. In addition, cramping pressures of 0.64 and 0.96 N/mm^2 (± 20% of 0.80 N/mm^2) were used to bond shorter pieces of DRM to produce beams similar in cross section to the full size glulam beams. The objective was to evaluate the effect of different cramping pressures on the shear strength of the glue lines in the DRM glulam beams.

Table 5-1: Cramping pressures recommended by BS EN 14080:2013

Lamination thickness t_l (mm)	$t_l \leq 35$	$35 < t_l \leq 45$	$45 < t_l \leq 85$
Cramping pressure (N/mm^2)	0.6 to 0.8	0.8 for grooved laminations 1.0 for laminations without grooves	0.8 to 1.0

5.2 Test specimen preparation

The preparation of the block shear specimens is described in this section. The DRM laminations were bonded to produce three short beams using different cramping pressures and three full size glulam beams using the optimum cramping pressure.

5.2.1 Cramping jig preparation

Prior to the lamination process, the cramping jig was calibrated to measure the corresponding force and torque on the bolts, ensuring uniform pressure was established. This procedure followed closely the calibration of the cramping system stated in the standard AITC Test T103:2007. A torque wrench, load cell, bolts and nuts, metal plates and blocks were assembled for this calibration. The arrangement of the cramping jig is shown in Figure 5-1. The cramping jig was

anchored to a strong floor using a pair of bolts and the load cell was positioned in the middle. Adequate metal blocks and plates were used as spacers to match the full length of the bolts. The washers and nuts were used in the tightening of the bolts. They were also lubricated to ease tightening later.

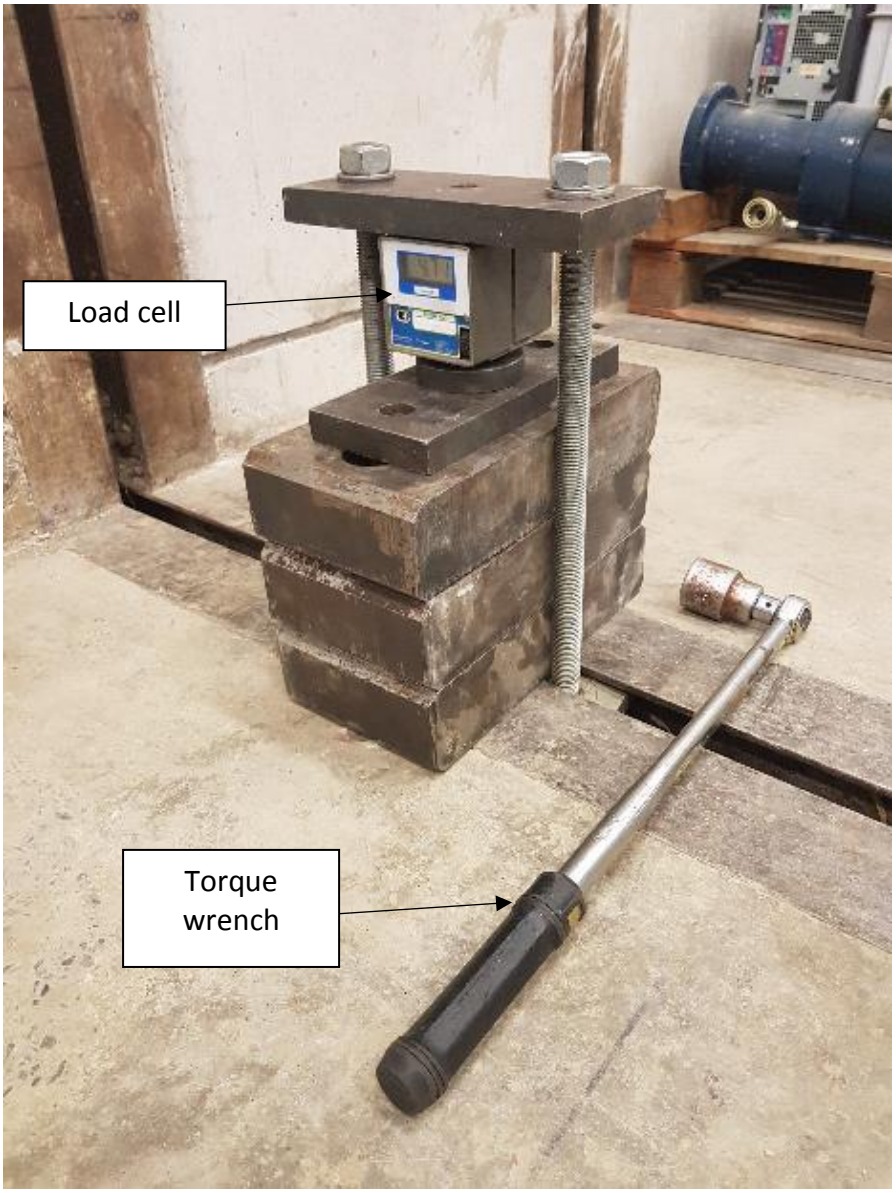

Figure 5-1: Calibration of the cramping jig

The cramping pressure was calculated using the equation below (AITC Test T103:2007):

Cramping pressure, $P = \frac{F}{l_{space} \times b}$ (Eq. 5-1)

Key:

F measured force applied to the pair of bolts, (N)

l_{space} spacing between bolts of the adjacent cramping jig*, (mm)

b nominal width of laminations, (mm)

**In the laminating of the full size glulam beam, five identical cramping jigs were used and the spacing between the bolts of the adjacent jig was 1 metre (see Figure 5-7 in section 5.2.3).*

As explained in Section 5.1, cramping pressures of 0.64, 0.80 and 0.96 N/mm^2 were used in this study. Using Eq. 5-1, the resulting force values correspond to the cramping pressures with l_{space} and b of 1 metre and 100 mm respectively are given in Table 5-2.

Table 5-2: Cramping pressure with the resulting force and torque reading

Cramping pressure (N/mm^2)	Resulting force (kN)	Torque reading (Nm) (each bolt)
0.64	64	140
0.80	80	160
0.96	96	180

The bolts were tightened evenly using a torque wrench. They were tightened with an increment of 5 Nm torque. The torque readings were recorded (column 3) when the load cell showed the approximate values of force (column 2) as listed in Table 5-2. Eventually, the recorded torque readings were used in the bonding of the glulam beams.

5.2.2 Short beam preparation

The aim of this study was to evaluate the influence of different cramping pressures on the bonding performance of the glue lines. As discussed in Section 5.1, the cramping pressures of 0.64, 0.80 and 0.96 N/mm^2 were used. Six DRM pieces with nominal dimensions 35 mm (thickness) x 100 mm (width) x 500 mm (length) without any finger joints were used in the bonding of the beam. The common structural adhesive, phenol resorcinol formaldehyde was used as the bonding medium. This PRF adhesive was also used in the bonding of the laminations to produce full size glulam beams. The cramping jig was prepared as described in the previous section. The metal spacers were replaced with wider and longer pieces of wood measuring 40 x 150 x 1000 mm to overlay the entire DRM pieces (Figure 5-2). Three pieces were used as the top spacers and one piece was used at the base of the DRM laminations.

Figure 5-2: Cramping of the short beam

The bonding of the laminations was done on the same day as the planing of the DRM pieces. This was to ensure the wood surfaces remained fresh, with little contaminant and less moisture accumulation. The PRF adhesive and its hardener were prepared according to the mixing ratio by weight 100 : 15 (resin : hardener) and thoroughly mixed. Then, the mixture was spread adequately and evenly onto the surface of each side of the laminations (double spreading) using a hand roller. The laminations were then positioned in the middle of the jig and the bolts were tightened evenly using the torque wrench. The tightening was stopped once it reached the specified torque related to the cramping pressure in Table 5-2. In general, the amount of glue is considered sufficient and evenly spread if glue squeeze out is observed along the edge of the glue lines after applying pressure (Figure 5-3). The assembly time was less than 40 minutes at room temperature as recommended by the adhesive specification. The beam was left for more than 24 hours before the cramping pressure was released. It was then put aside for post curing for more than 24 hours to reach full bonding strength before being subject to further processing. Three beams were produced with cramping pressures of 0.64, 0.80 and 0.96 N/mm^2.

Figure 5-3: Glue squeeze-out

After post curing, the beams were further processed to produce specimens for the block shear tests (Figure 5-4). The specimens were cut from the full cross section of the beams to include all the glue lines. Three block shear specimens were cut from each beam. One specimen was cut from the middle and two specimens were gathered from each side of the beam, approximately 100 mm from the end (Figure 5-5). All the three specimens were cut at the middle of the width of the beam. A total of nine specimens were gathered from the three beams, each cramped with different pressures.

Figure 5-4: Block shear specimens

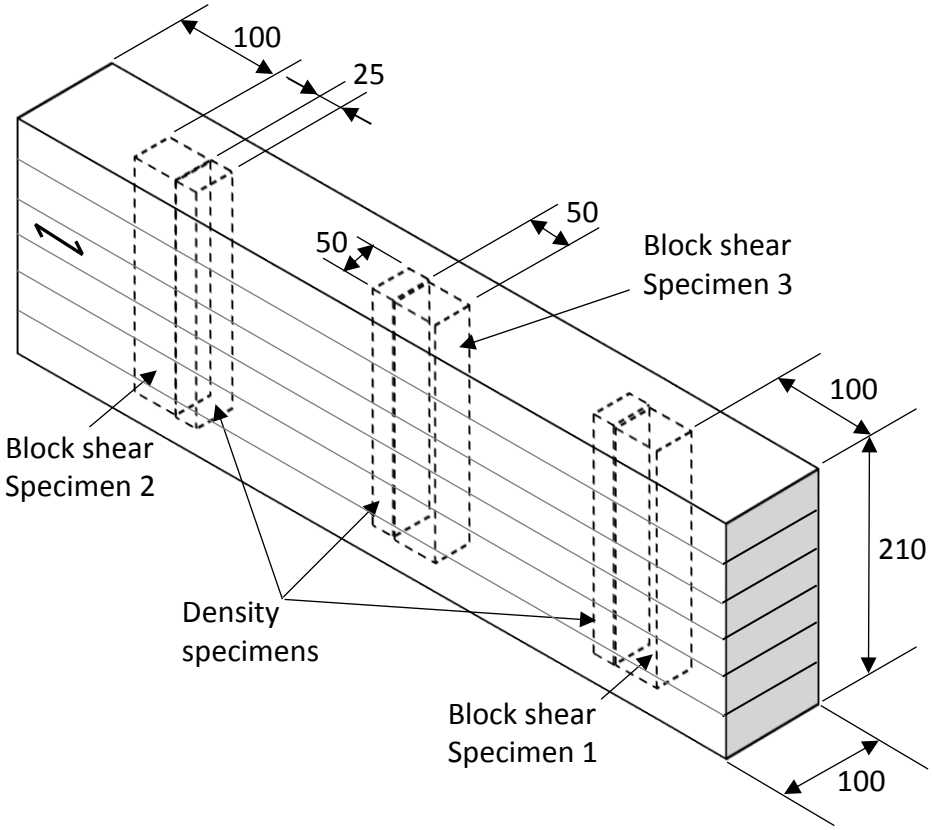

Key:

direction of grain

Figure 5-5: Locations of the block shear and density specimens (dimensions in mm)

5.2.3 Full size glulam beam preparation

Solid DRM pieces of 1 metre in length were finger-jointed to produce laminations of 5 metres in length. A total of six laminations was used to produce a full size glulam beam. Prior to the bonding process, an initial arrangement of the laminations was made to assess the layup of the beams. This was to avoid overlapping of finger joints between the adjacent laminations. A minimum distance of 15 cm between the finger joints was specified as recommended by JAS Notification No. 1152:2007 and ANSI A190.1-2012:2013 (Figure 5-6). The laminations were processed to the nominal cross section of 35 x 100 mm and were bonded within 24 hours to ensure the freshness of the surface.

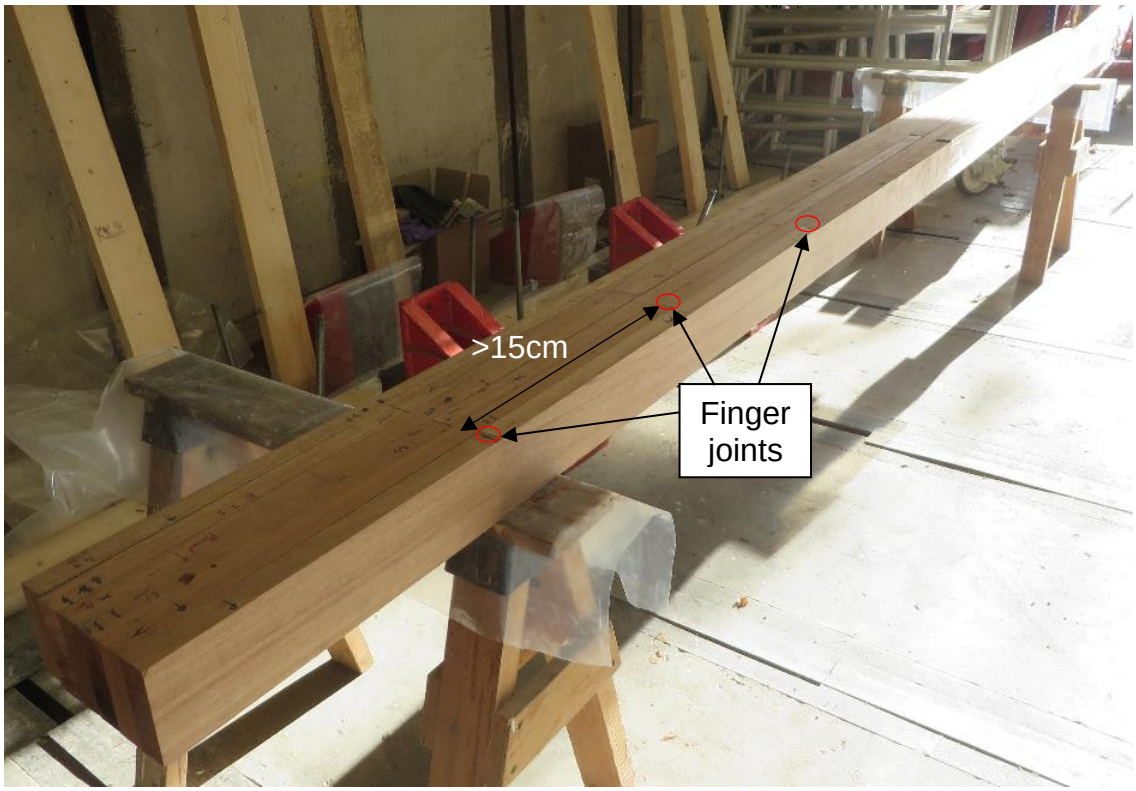

Figure 5-6: Positioning of finger joints in the beam layup

The cramping system consisted of five jigs, positioned at a distance of 1 metre from each other, over the length of the laminations (Figure 5-7). The PRF was used as the bonding medium and was spread evenly onto both side of the surface using a hand roller. After applying the adhesive, the laminations were positioned centrally on the cramping jigs. Wood spacers with cross sections of 40 x 150 mm were used. One layer of spacer was laid at the bottom and three layers at the top of the beam, overlaying the entire length of the laminations. The bolts were then tightened evenly, applying the optimum cramping pressure of 0.80 N/mm^2. The tightening of the bolts started from the jig in the middle of the layout (Jig 1) and proceeded alternately to the left and right of the cramping system, until the end of the beam was reached. The tightening of the bolts was stopped once it reached the torque relating to the cramping pressure of 0.80 N/mm^2 as listed in Table 5-2. Retightening was carried out 30 minutes after the initial cramping. Glue squeeze out was observed along the edge of the glue lines, over the full length of the laminations. The assembly time was less than 40 minutes at room temperature and the beam was left for more than 24 hours before the cramping pressure was released. Post curing of more than 24 hours

was completed before processing was continued. In this study, three full size glulam beams were produced with nominal dimensions of 210 mm (depth) x 95 mm (width) x 5000 mm (length).

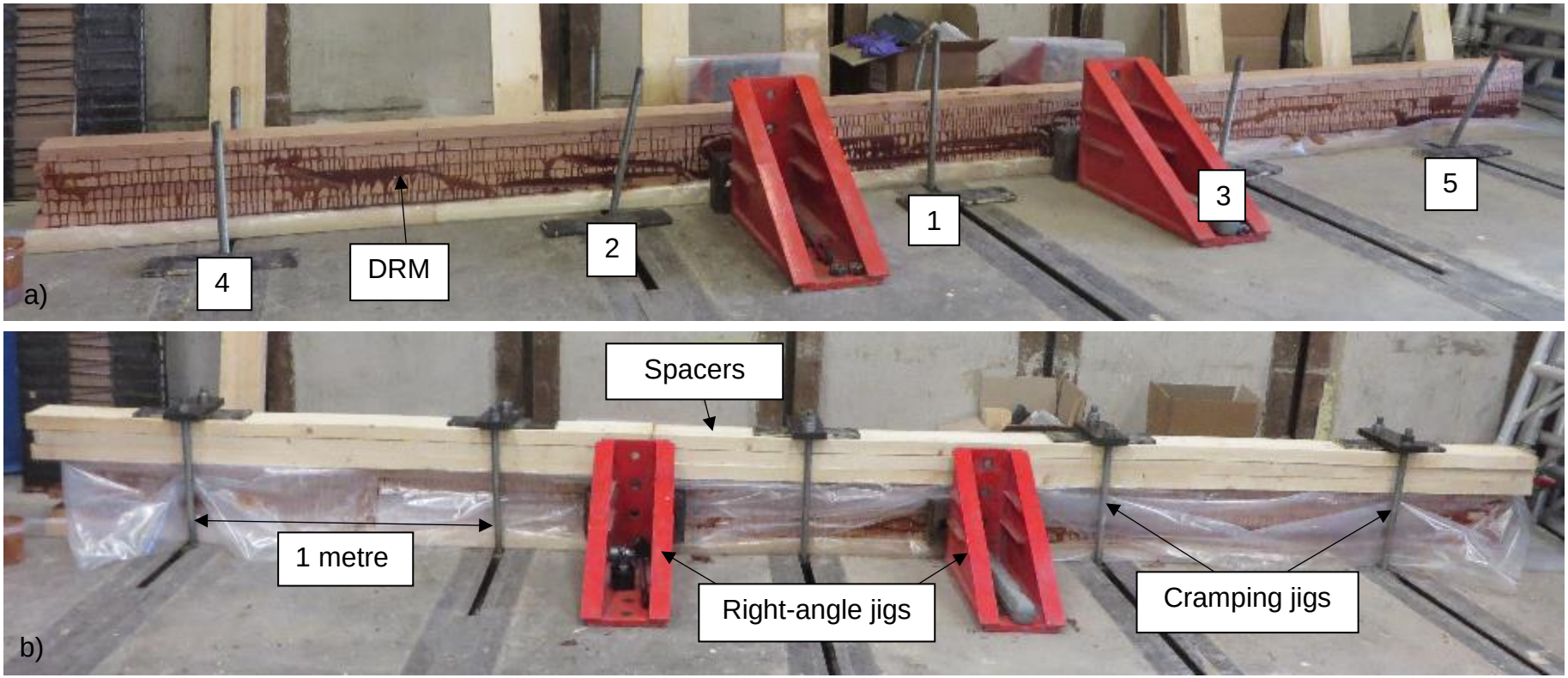

Key:

1 to 5	cramping sequence
right-angle jigs	ensure good beam alignment

Figure 5-7: Full size glulam beam a) before cramping; b) after applying pressure

After the post curing period, the beams were planed to remove the misalignment of the width sections (Figure 5-8) and to remove the glue residues. Approximately 400 mm from the end of the beam was cut off and the final length of the full size glulam beam was 4.2 metres. The end blocks from each glulam beam were further processed to produce block shear specimens. A total of three block shear specimens were gathered from the three glulam beams.

Figure 5-8: Misaligned laminations

5.2.4 Block shear specimen preparation

The number of block shear specimens produced from the glulam beams is shown in Table 5-3. Each specimen was cut from the full cross-section of the beam and consisted of 5 glue lines (Figure 5-9). Attention was given to ensuring that the loaded surfaces of the specimens were perpendicular to the glue line. An offset cut of 5 mm in depth was made in the glue line on the end grain of the specimen (Figure 5-10). The width of the offset was approximately 1 mm. The

offset cut, which was not specified in BS EN 14080:2013, was adopted from JAS Notification No.1152:2007 because of the difficulty in positioning the shearing tool accurately on the glue line of the specimen. The sheared area was 40 x 50 mm and the lamination thickness was 35 mm. All the specimens were kept in a conditioning room at a temperature of 20°C and relative humidity of 65% for at least 7 days until constant weight was reached prior to testing.

Table 5-3: Block shear specimens

Beam descriptions (cramping pressure)	No. of specimens
Short beam (0.64 N/mm^2)	3
Short beam (0.80 N/mm^2)	3
Short beam (0.96 N/mm^2)	3
Full size beam (0.80 N/mm^2)	3

Key:

1 to 5 glue line number

⟷ direction of grain

Figure 5-9: Block shear test specimen

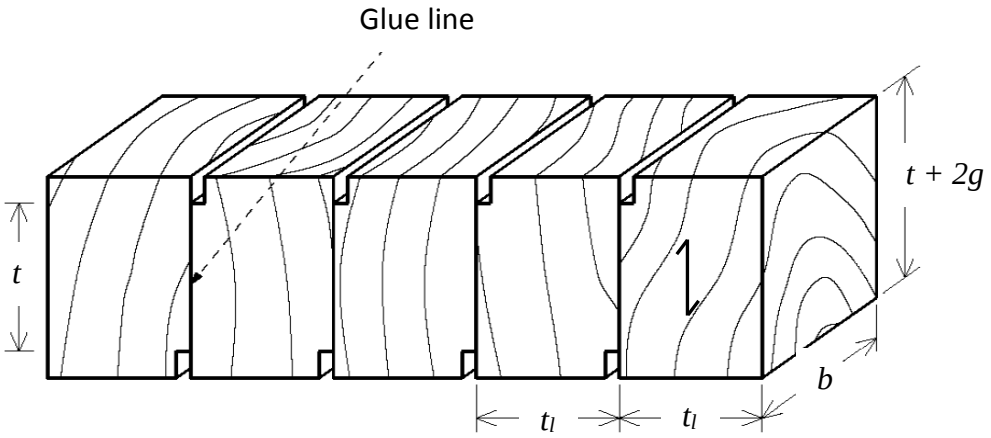

Key:

t	thickness 40 mm
b	width 50 mm
t_l	lamination thickness 35 mm
g	offset cut 5 mm
⟷	direction of grain

Figure 5-10: Description of the block shear specimen
(JAS Notification No.1152:2007)

5.3 Block shear strength test

The bonding strength of the glue lines was evaluated using the block shear testing method as stated in Annex D of BS EN 14080:2013. The test setup was prepared as shown in Figure 5-11. The block shear specimen was loaded at the surfaces of the end grain and a self-aligning cylindrical bearing was used to ensure the loading was uniform. Importantly, the end grain surfaces were carefully cut so that they were parallel to each other.

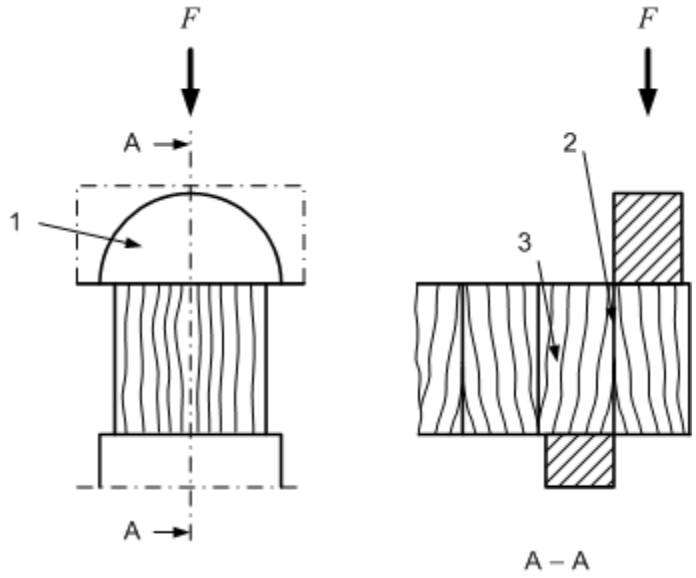

Key:

1 cylindrical bearing

2 sheared plane

3 test bar to be clamped

F ramp load

a)

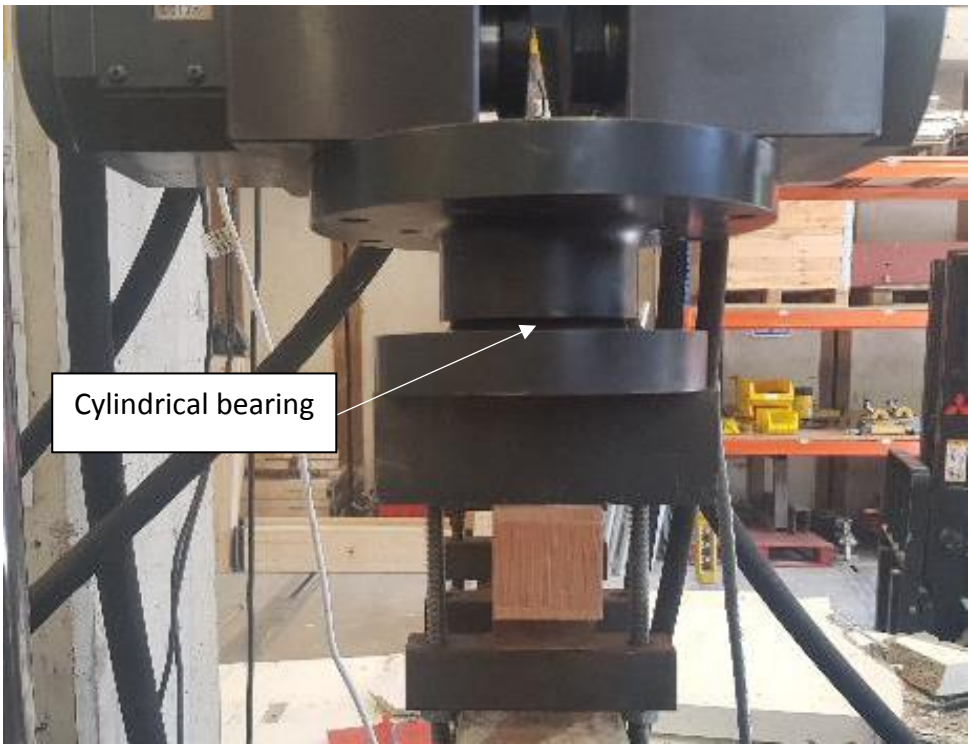

b)

Figure 5-11: Shearing tool with block shear specimen a) diagram from BS EN 14080:2013; b) actual test setup

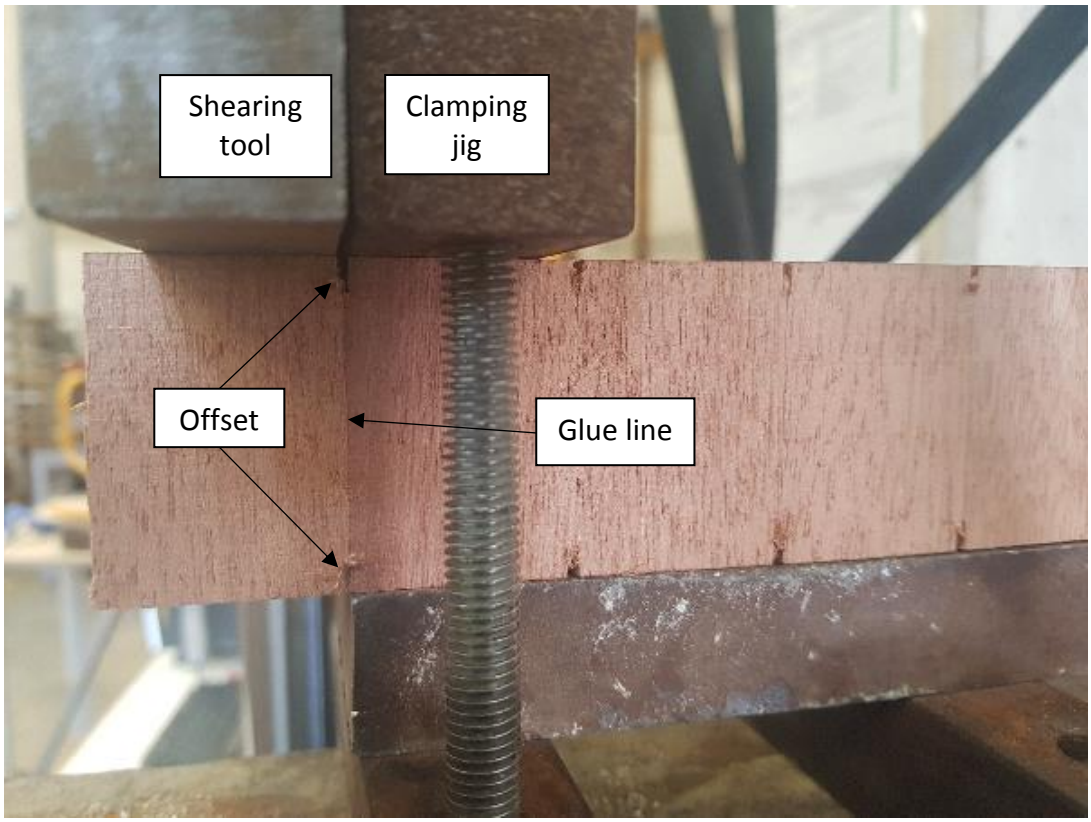

Figure 5-12: Block shear test setup

The shear strength of the glue line was calculated based on the equation below (BS EN 14080:2013):

Shear strength (N/mm^2), $f_v = k_v \frac{F_u}{A}$ (Eq. 5-2)

Key:

F_u ultimate load, (N)

A sheared area, (mm^2)

$A = b \times t$

b width, (mm)

t thickness, (mm)

k_v factor that modifies the shear strength for test pieces where the thickness in the grain direction of the sheared area is less than 50 mm

$k_v = 0.78 + 0.0044\, t$

The wood failure percentage (WFP) of the sheared area was measured after the tests. The WFP refers to the presence of the wood fibres instead of the adhesive residue. It was measured with the use of a transparent grid consisted of squares measuring 5 x 5 mm (Figure 5-13) and was estimated to the nearest percentage divisible by five.

Figure 5-13: Transparent grid for WFP measurement

5.4 Results and discussion

The results of the shear strength of glue lines in the DRM glulam beams, evaluated using block shear tests, are presented and discussed in this section.

5.4.1 Shear strength of glue lines parallel to grain

The minimum requirements for the wood failure percentage (WFP) in relation to the shear strength, as recommended by BS EN 14080:2013, are given in Table

5-4. These values are used to evaluate the performance of the glue lines in a glulam beam, generally for species listed in the standard which comprises mostly softwood. In this study, the bonding performance of the DRM hardwood is studied, to evaluate its suitability for the production of glulam beams.

Table 5-4: Minimum requirements for WFP in relation to the shear strength (BS EN 14080:2013)

	Average			Individual values		
Shear strength f_v[a] (N/mm^2)	6	8	$f_v \geq 11$	$4 \leq f_v < 6$	6	$f_v \geq 10$
Minimum WFP[b] (%)	90	72	45	100	74	20
[a] For values in between linear interpolation shall be used [b] For average values the minimum WFP shall be: $144 – (9 f_v)$ For the individual values the minimum WFP for the shear strength $f_v \geq 6.0$ N/mm^2 shall be $153.3 – (13.3 f_v)$						

The results of the shear strength of the individual glue lines and measured WFP of the DRM laminations are given in Tables 5-5 to 5-8 below. The minimum requirements of the individual WFP values listed in the tables were calculated according to the suggested linear interpolation equation of $153.3 – (13.3 f_v)$, as given in Table 5-4, for the shear strength $f_v \geq 6.0$ N/mm^2.

5.4.2 Beam with optimum cramping pressure, 0.80 N/mm²

Table 5-5 shows the individual shear strength results of specimens gathered from the short beam bonded using cramping pressure of 0.80 N/mm^2 as recommended in Table 5-1, for lamination thickness of 35 mm. The specimens showed good WFP (Figure 5-14) and met the minimum requirements of the BS EN 14080:2013.

Table 5-5: Results of the individual block shear strength (optimum cramping pressure)

Specimen no.	Glue line no.	Shear strength (N/mm^2)	Wood failure (%)	
			Individual	Minimum requirement*
O1	1	8.61	100	33
	2	8.11	100	40
	3	7.55	100	48
	4	6.80	100	58
	5	6.92	100	57
O2	1	7.18	100	53
	2	7.07	100	55
	3	7.32	100	51
	4	7.08	100	55
	5	6.23	95	67
O3	1	7.90	100	44
	2	6.71	100	60
	3	7.33	100	51
	4	6.00	100	70
	5	5.64	100	100
	Average	7.10	99.7	

*All specimens met minimum requirement

Figure 5-14: Adequate wood failure for specimen bonded with optimum cramping pressure

5.4.3 Beam with lower cramping pressure, 0.64 N/mm^2

Table 5-6 shows the results of the shear strength and WFP of the block shear specimens prepared using cramping pressure of 0.64 N/mm^2 (20% lower than the optimum pressure 0.80 N/mm^2). Four glue lines from specimens L1 and L2 did not meet the minimum WFP requirement. The typical block shear failures for these specimens are shown in Figure 5-15. Specimen L3 was cut from the middle of the beam while specimens L1 and L2 were cut 100 mm from the end of the beam (see Figure 5-5). The use of lower pressure as well as the inadequate pressure at the end sections of the beam resulted in both specimens L1 and L2 experienced insufficient cramping pressure. This explains the low WFP of some of the glue lines in the specimens. Specimen L3, gathered from the middle section of the beam, passed the minimum WFP requirement. From these results, it can be concluded that the glue lines of the DRM beams are not able to produce consistent adequate WFP when bonded using the low cramping pressure of 0.64 N/mm^2.

Table 5-6: Results of the individual block shear strength (lower cramping pressure)

Specimen no.	Glue line no.	Shear strength (N/mm^2)	Wood failure (%)		Requirement remark
			Individual	Minimum requirement	
L1	1	7.15	20	53	Not met
	2	6.94	90	57	Met
	3	7.20	100	53	Met
	4	6.88	100	57	Met
	5	6.71	100	60	Met
L2	1	7.08	20	54	Not met
	2	6.18	65	66	Not met
	3	7.02	100	55	Met
	4	6.54	100	62	Met
	5	4.93	20	100	Not met
L3	1	7.82	85	43	Met
	2	7.37	85	50	Met
	3	7.48	100	48	Met
	4	7.54	100	47	Met
	5	7.37	100	50	Met
Average		6.95	79.0		

a) Specimen L1, glue line 1

b) Specimen L3, glue line 4

Figure 5-15: Typical block shear failures for specimens bonded with lower cramping pressure a) insufficient WFP; b) adequate WFP

Comparison of these shear strength values with the results of specimens gathered from the beam cramped with optimum pressure indicates no significant differences at 95% confidence level when tested using a one-way analysis of variance (ANOVA). On the contrary, the ANOVA test indicates significant differences between the WFP values of specimens produced using

lower and optimum cramping pressures. It can be concluded that the use of lower cramping pressure in the bonding produces adequate shear strength of the glue lines but reveals inadequate WFP compared to using the suggested optimum cramping pressure.

5.4.4 Beam with higher cramping pressure, 0.96 N/mm^2

The results of the individual shear strength and WFP for the glue lines bonded using higher cramping pressure 0.96 N/mm^2 are shown in Table 5-7. The measured WFP showed adequate wood failure for all the individual glue lines, meeting the minimum requirement of the standard. This indicates good bonding performance of the individual glue lines when pressed with higher cramping pressure. The typical block shear failures of these specimens are shown in Figure 5-16.

Table 5-7: Results of the individual block shear strength (higher cramping pressure)

Specimen no.	Glue line no.	Shear strength (N/mm^2)	Wood failure (%)	
			Individual	Minimum requirement*
H1	1	7.07	100	54
	2	6.67	95	60
	3	6.02	75	69
	4	5.73	100	100
	5	7.18	100	53
H2	1	5.63	100	100
	2	8.07	95	40
	3	6.44	100	63
	4	6.51	100	62
	5	6.94	100	56
H3	1	7.78	90	45
	2	7.81	80	44
	3	5.34	100	100
	4	6.73	95	59
	5	6.92	100	56
	Average	6.72	95.3	

*All specimens met minimum requirement

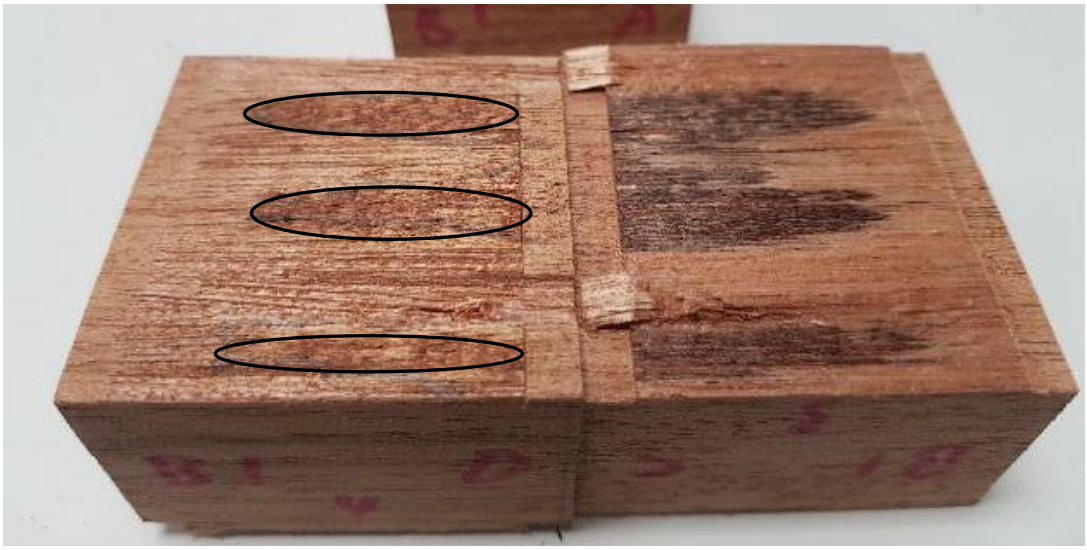

a) Specimen H1, glue line 3 (circled areas depict glue failure)

b) Specimen H3, glue line 2

Figure 5-16: Typical block shear failures for specimens bonded with higher cramping pressure

ANOVA test indicates no significant differences at 95% confidence level in the shear strength values for specimens prepared with higher pressure and the specimens from optimum pressure. Further comparison of WFP results using

ANOVA test showed statistically significant differences between the specimens from the two different cramping pressures. Nevertheless, the specimens prepared using higher cramping pressure still meet the minimum requirement of WFP.

5.4.5 Full size glulam beams results

Following the testing of the short beams, the cramping pressure, 0.80 N/mm^2 gave satisfactory results and met the minimum requirement as set by BS EN 14080:2013. Thus, this 0.80 N/mm^2 cramping pressure was used in the bonding of the full size glulam beams. The shear strength and WFP of the block shear specimens taken from the full size glulam beams are shown in Table 5-8.

Table 5-8: Full size beams with optimal cramping pressure (0.80 N/mm^2)

Specimen no.	Glue line no.	Shear strength (N/mm^2)	Wood failure (%)	
			Individual	Minimum requirement*
Beam 1	1	6.98	100	56
	2	7.76	100	45
	3	7.18	100	53
	4	6.48	100	63
	5	5.85	100	100
Beam 2	1	7.46	100	50
	2	7.10	100	55
	3	7.69	100	47
	4	8.14	100	41
	5	7.54	100	49
Beam 3	1	6.44	100	64
	2	7.96	85	42
	3	7.20	100	53
	4	7.02	100	55
	5	6.94	100	57
	Average	7.18	99.0	

*All specimens met minimum requirement

The high WFP shown in the table indicates good bonding performance of the laminations in the full size glulam beams. ANOVA test conducted showed no significance differences at 95% confidence level in the shear strength values between the specimens prepared from the full size glulam beams and the

specimens prepared using different cramping pressures. ANOVA test results showed no significant differences between the WFP values gathered from the specimens of the full size glulam beams and specimens from the beam cramped with optimum pressure. These results indicate that the cramping setup (one jig) of the short beams is consistent with the setup of the full size glulam beams which consisted of four jigs along the length. The typical block shear failures of the specimens are shown in Figure 5-17.

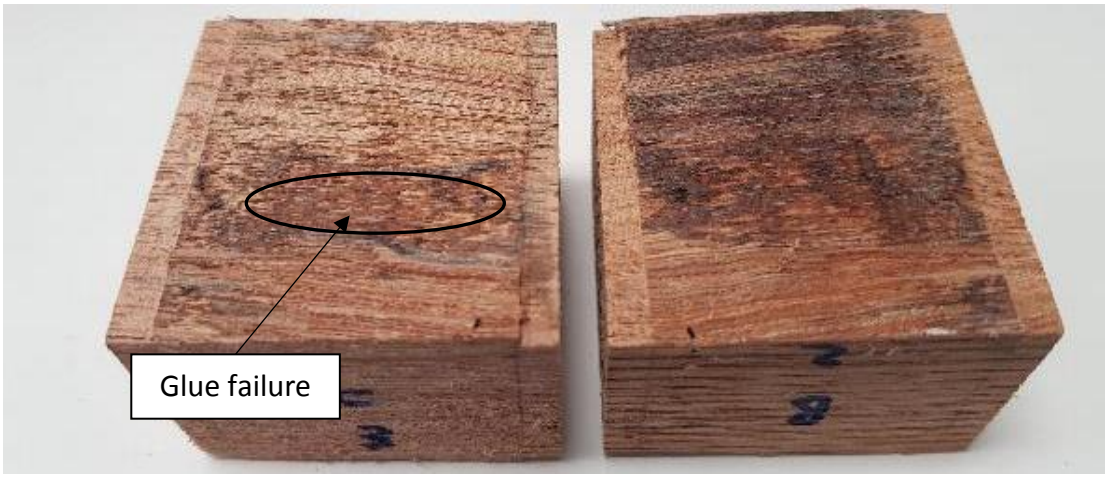

a) Specimen Beam 3, glue line 2

b) Specimen Beam 2, glue line 4

Figure 5-17: Typical block shear failures for specimens gathered from the full size glulam beams

5.4.6 Average shear strength and wood failure percentage

The average shear strength and WFP of the specimens are shown in Table 5-9. These results are evaluated according to the requirement of BS EN 14080:2013. The minimum requirement of the average WFP values were calculated according to the linear interpolation equation, 144 – (9 f_v), as given in Table 5-4.

The average WFP of the specimens fulfilled the minimum requirement of the standard, indicating good bond performance except for specimen L2. The low average WFP of specimen L2 is expected because of the low WFP of its individual glue lines (see Table 5-6). From both the individual and average results, it can be concluded that the low cramping pressure of 0.64 N/mm^2 is not suitable for the bonding of DRM glulam beams.

In addition, the higher cramping pressure of 0.96 N/mm^2 is able to produce good bonding performance, meeting the minimum shear strength and WFP requirements. Although the pressure 0.64 N/mm^2 is within the range of the recommended cramping pressure stated in BS EN 14080:2013 (Table 5-1) but the specimens produced inadequate WFP. Understandably, the range of recommended cramping pressure covers only for glulam products produced from the species listed in the standard. Thus, the recommended values may not be applicable to other tropical hardwood species, such as DRM as shown in this study.

Table 5-9: Average block shear strength and WFP of DRM specimens

Cramping pressure (N/mm^2)	Specimen no.	No. of glue lines	Density (kg/m^3)		Moisture content (%)		Shear strength (N/mm^2)		Wood failure (%)		Requirement remark
			Average	SD	Average	SD	Average	SD	Average	Minimum requirement*	
0.80 (optimal)	O1	5	622	89	12.1	0.4	7.60	0.77	100	76	Met
	O2	5	623	94	12.4	0.4	6.98	0.43	99	81	Met
	O3	5	590	59	12.0	0.4	6.71	0.93	100	84	Met
						Average	7.10		99.7		
0.64 (low)	L1	5	599	91	13.2	0.3	6.97	0.20	82	81	Met
	L2	5	605	92	13.4	0.3	6.35	0.87	61	87	Not met
	L3	5	605	97	13.2	0.2	7.51	0.18	94	76	Met
						Average	6.95		79.0		
0.96 (high)	H1	5	557	68	12.8	0.2	6.53	0.64	94	85	Met
	H2	5	560	67	12.9	0.3	6.72	0.89	99	84	Met
	H3	5	558	61	12.9	0.3	6.92	1.01	93	82	Met
						Average	6.72		95.3		
0.80 (beams)	Beam 1	5	640	31	12.2	0.5	6.85	0.72	100	82	Met
	Beam 2	5	648	83	12.3	0.4	7.59	0.38	100	76	Met
	Beam 3	5	605	51	11.7	0.2	7.11	0.55	97	80	Met
						Average	7.18		99.0		

*Values interpolated based on 144 – (9 f_v) for the average shear strength values

5.4.7 Relationship between shear strength and wood failure of glue lines

It is generally known that high percentages of wood failure are preferred when determining the bonding performance of the glue lines. Test results with high WFP indicate that the adhesive bond is stronger than the strength of the wood. This is important since the load design values are based on the known strength values of the wood and should not be dictated by weaker bond lines.

Figure 5-18 depicts the relationship between the shear strength and WFP of all the individual glue lines of the tested DRM specimens. There is no correlation observed between the shear strength and WFP. In the graph, the solid line represents the minimum requirement of the WFP as stated in BS EN 14080:2013 (Table 5-4). It can be seen that almost all the results meet the minimum requirements except for some glue lines produced with low cramping pressure (specimen L). By excluding specimen L from the graph, the results achieve the minimum requirements of the standard, indicating good bonding performance of DRM, when using adequate cramping pressure in the production of the glulam beams. In addition, revised minimum requirements are proposed based on the findings in this study as depicted by the dashed line in the graph. A limit of 70% WFP was proposed taking into consideration the lowest WFP values of 75% (specimen H1, glue line 3) while excluding the few WFP values of specimen L that did not meet the minimum requirements of BS EN 14080:2013. The revised minimum requirements are proposed to reflect the findings of this study which shown lower shear strength and high wood failure of the DRM specimens. Nevertheless, the proposed minimum requirements need to be further improved by increasing the number of specimens because of the high density variation within the DRM species. The average density of DRM block shear specimens in this study ranged from 558 to 648 kg/m^3 (see Table 5-9) compared to the values of 415 to 885 kg/m^3 published by Wong (2002). Thus, further testing is needed to validate the proposed minimum requirement by using DRM with densities with lower and higher values.

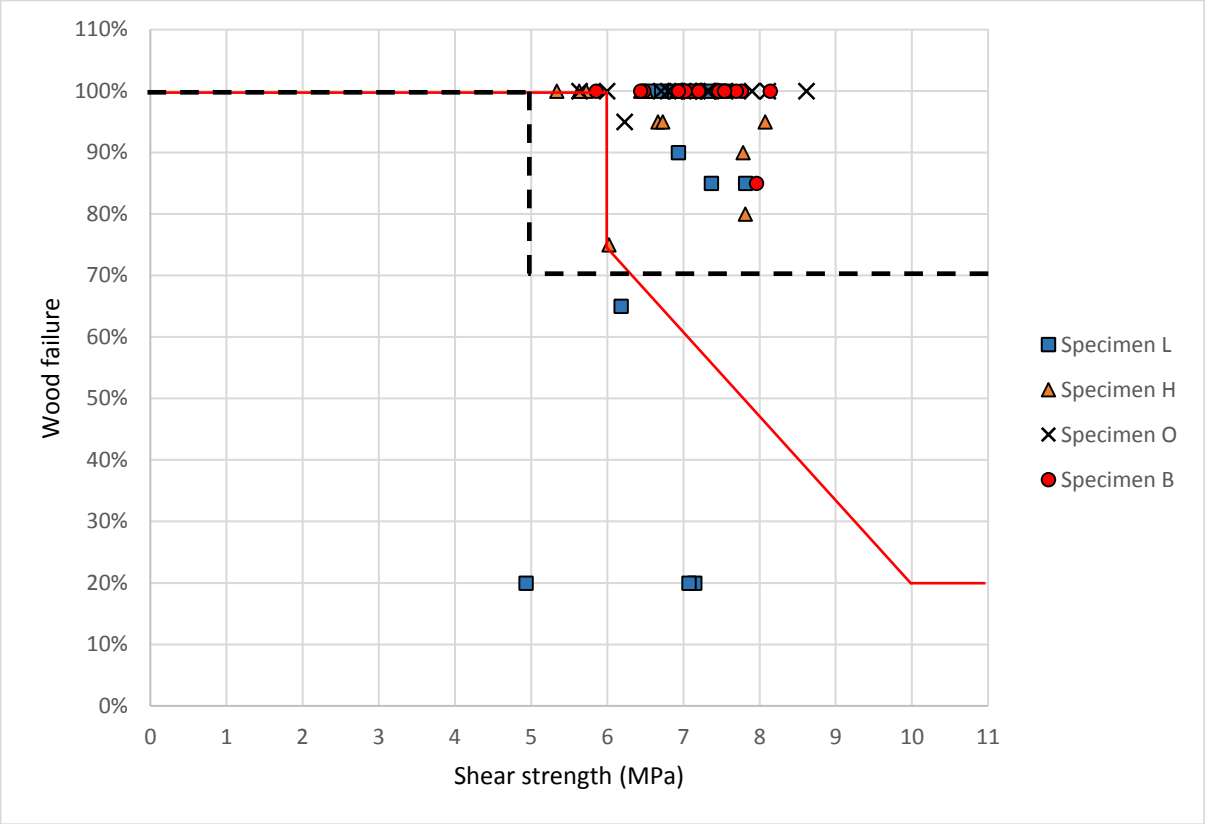

Key:

———	minimum WFP individual requirement (BS EN 14080:2013)
- - - - - - - -	proposed minimum WFP requirement
Specimen L	low cramping pressure (0.64 N/mm^2)
Specimen H	high cramping pressure (0.96 N/mm^2)
Specimen O	optimum cramping pressure (0.80 N/mm^2)
Specimen B	full size beams with optimum cramping pressure (0.80 N/mm^2)

Figure 5-18: Shear strength of the individual glue lines and wood failure percentage of DRM specimens

The relationship between the average shear strength and wood failure percentage is shown in Figure 5-19. There is also no correlation observed between the values of shear strength and WFP. Similar to the results in the previous section, average shear strength results of one of the specimens (specimen L2) is lower than the minimum requirement of BS EN 14080:2013, as depicted by the solid line. A revised minimum requirement for these average

values is depicted by the dashed line. Due to the limited samples, the proposed minimum requirements are rather stringent with WFP of 80% for shear strength above 6.0 N/mm^2, as shown in the graph. This limit was chosen after taking into consideration the lowest average WFP of 82% (specimen L1) while excluding the average WFP values (61%) of specimen L2 which did not meet the minimum requirements of BS EN 14080:2013. This limit applies to the current batch of DRM specimens in this study and can be further improved by increasing the number of DRM specimens gathered from a wider density distribution.

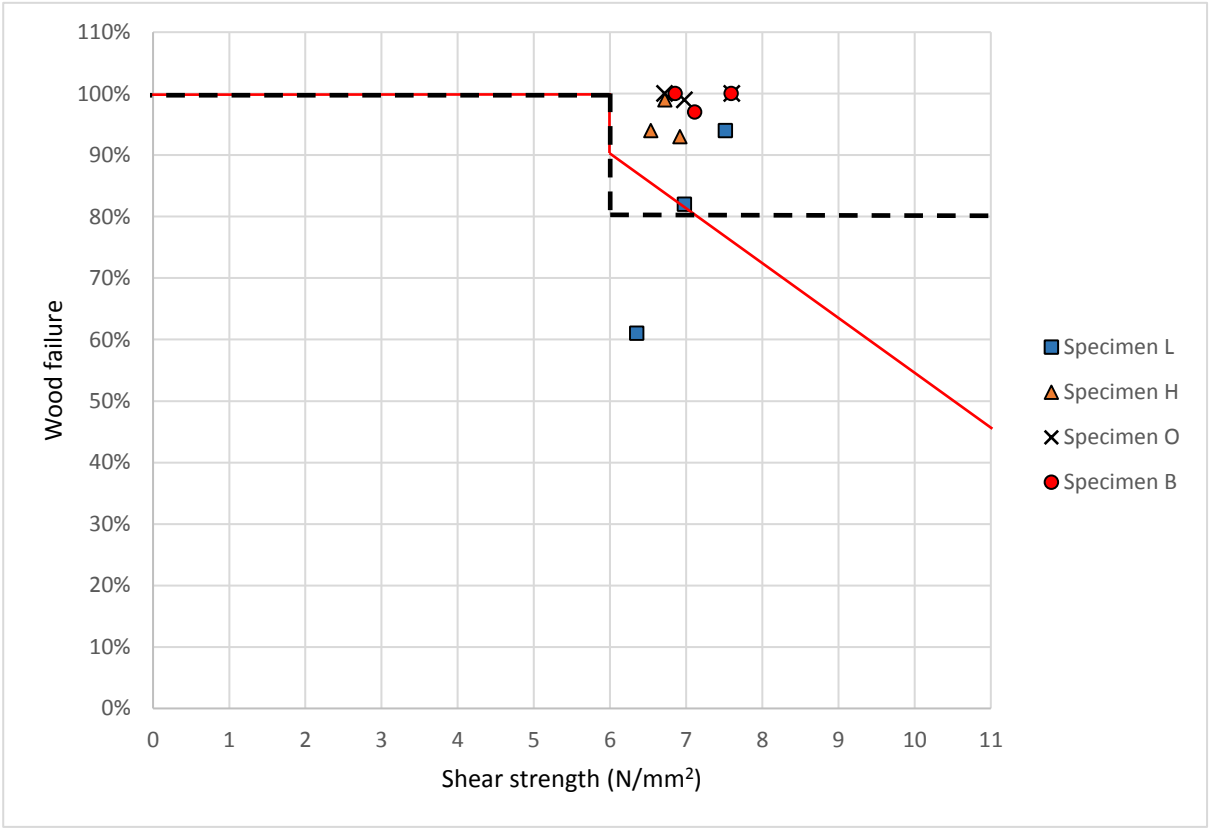

Key:

minimum WFP average requirement (BS EN 14080:2013)

proposed minimum WFP requirement

Figure 5-19: Average shear strength and wood failure percentage of DRM specimens

5.4.8 Factors influencing the bonding performance of DRM specimens

As discussed in the previous sections, cramping pressure affects the bonding performance of the DRM specimens. In this study, the specimens produced using low cramping pressure of 0.64 N/mm^2 failed to meet the minimum requirement of the standard. In addition, there are several other factors that affect the bonding performance of the DRM specimens.

5.4.8.1 Density

For the determination of density, additional pieces were cut from the glulam beams, adjacent to each block shear specimen. Since each glue line of the block shear specimens is sandwiched by two timber blocks (Figure 5-10), the density specimens were cut along the glue lines to separate them. The lower density values between the pair of timber blocks were used to correlate with the shear strength of the glue lines. It is generally known that the shear strength of wood increases with density (Hernández and Almeida, 2003), thus the less dense wood is the weakest link and is likely to fail at a lower stress in the block shear test due to its lower strength.

The density of the DRM specimens in these block shear tests ranged from 487 to 777 kg/m^3. Figure 5-20 shows the trend between shear strength of the glue lines and density of the specimens. The results gathered from the specimens bonded using low cramping pressure were excluded from the graph to minimize this effect on the shear strength values. The trend in the graph agrees with the findings of other studies (Frihart and Hunt, 2010; Selbo, 1975), indicating that there is a trend of increasing glue lines strength with the increase of wood density. Furthermore, Frihart and Hunt (2010) stated that this positive relationship is accurate for wood densities of up to 700 to 800 kg/m^3 (for moisture content 12%) and it is difficult to obtain a consistent high shear strength and high WFP for density above this range. Glue lines produced using wood with higher density often showed higher bond strength but lower percentage of wood failure compared to the lower density species. In this

regard, increasing the number of specimens in the block shear tests and the inclusion of DRM with higher wood density will improve the correlation in Figure 5-20. These will also improve the proposed minimum requirement in Figure 5-18 and lower the stringent WFP.

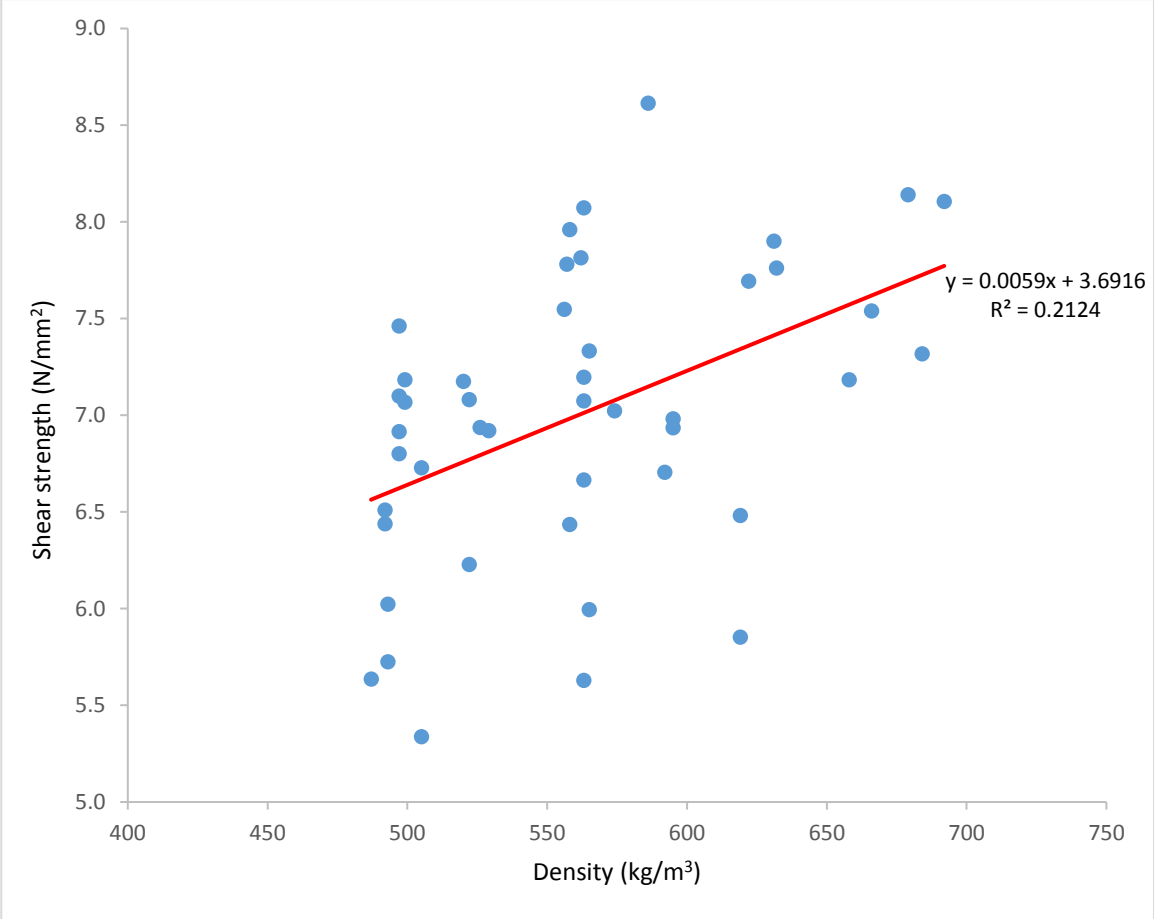

Figure 5-20: Relationship between shear strength of glue lines and density of DRM specimens

5.4.8.2 Size effect of test specimens

The evaluation of shear strength of glue lines is influenced by the size of the specimens in the block shear tests (Gaspar *et al.*, 2017). Thus, for consistency in the standard block shear tests, BS EN 14080:2013 recommended a nominal sheared area of between 40 to 50 mm for both width and thickness of the block shear specimens. In this regard, a factor k_v was introduced to the calculation of the shear strength (see Eq. 5-2) for specimens with thickness of less than

50 mm. In this study, the relationship between factor k_v and shear strength of the DRM specimens is shown in Figure 5-21.

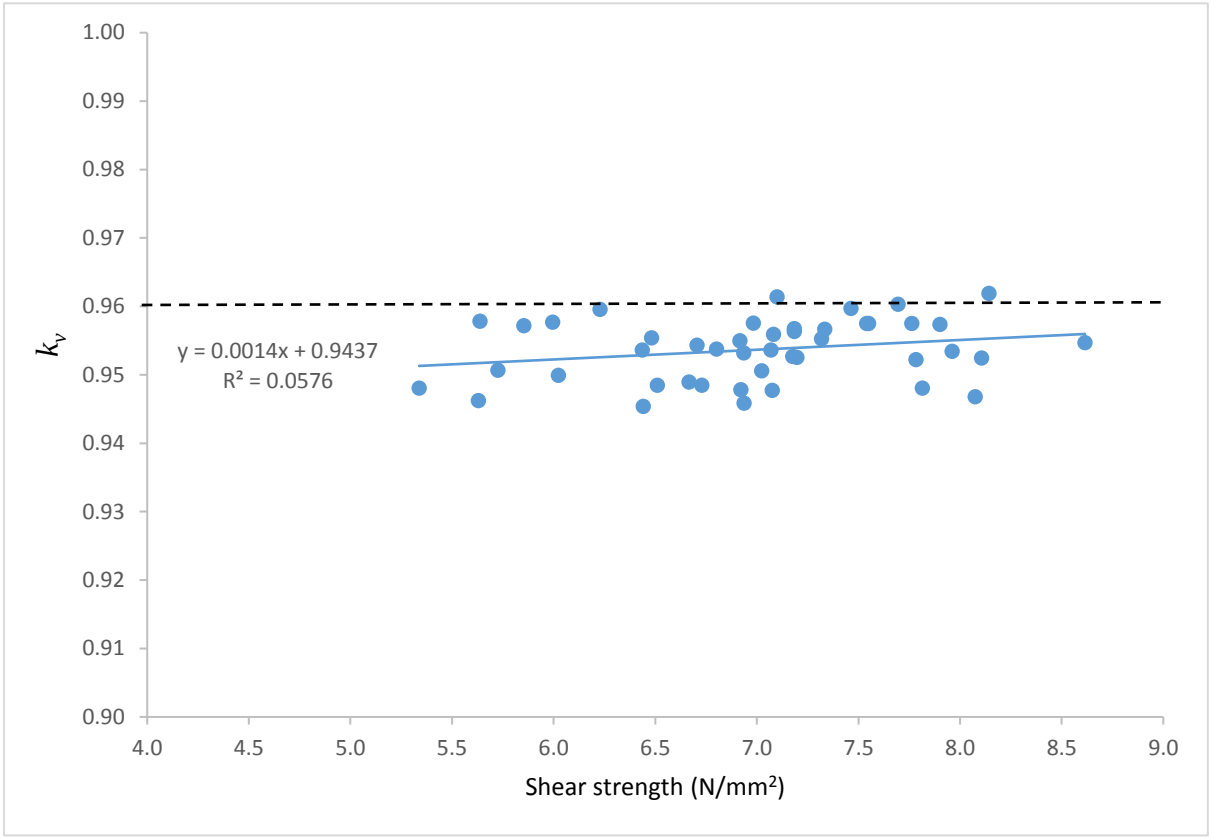

Figure 5-21: Relationship between factor k_v and shear strength of glue lines of DRM specimens

From the graph, the dashed line depicts the factor k_v of 0.96, for block shear specimens having sheared area of nominal dimensions 50 mm (width) x 40 mm (thickness). Most of the DRM specimens in this study have measured sheared area smaller than the nominal size, thus the majority of the k_v values were less than 0.96. The findings of Gaspar *et al.* (2017) indicate an increase of shear strength with the decreasing k_v values (Figure 5-22). When comparing their results (dashed lines) with the modification factors suggested by BS EN 14080:2013 (solid lines), they concluded that the modification of the shear strength using k_v values may lead to unsafe corrections for specimens with stronger glue lines above 15.0 N/mm^2.

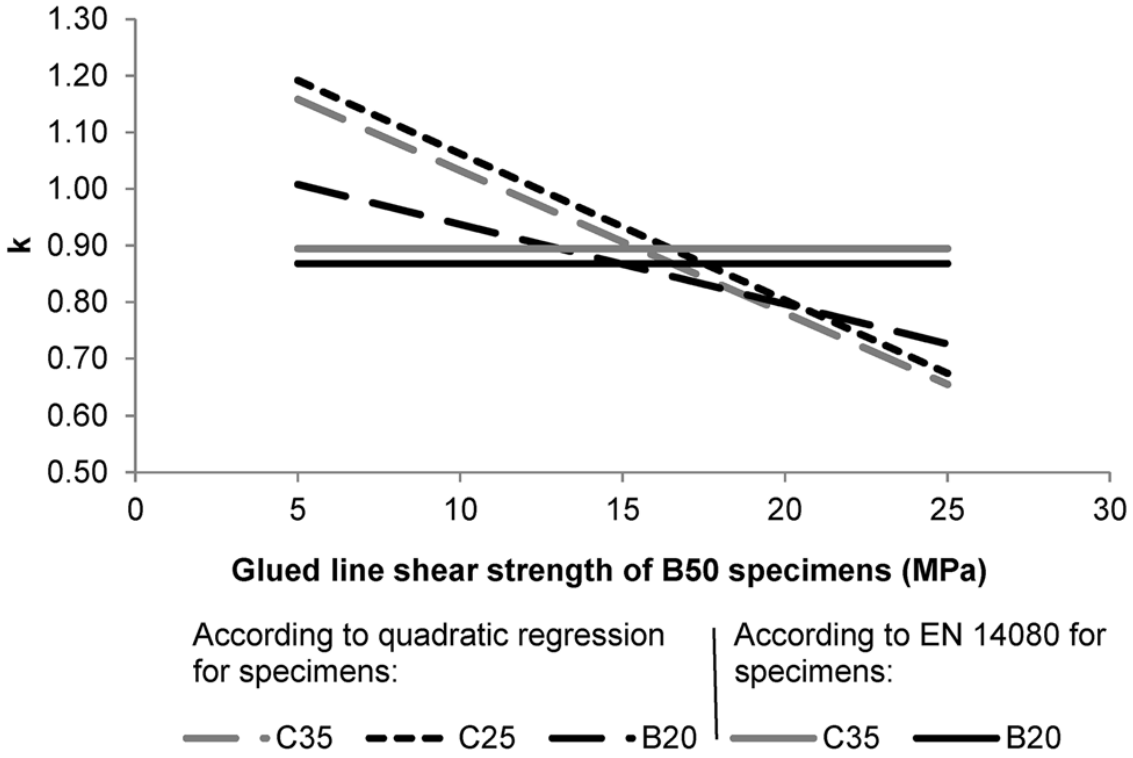

Key:

C35, C25, B20, B50 specimen name

Figure 5-22: Relationship between factor k_v and shear strength of glue lines (Gaspar *et al.*, 2017)

Further improvement to the relationship in the graph (Figure 5-21) can be made by increasing the number of DRM specimens and using different sizes of test specimens to produce wider range of k_v and strength values. It can be concluded that the effect of size on the block shear strength of the DRM specimens may not be definitive in this study because of the small distribution range of DRM in terms of density and size variation of the test specimens.

5.5 Summary

The results in this study showed the influence of different cramping pressures on the bonding performance of the DRM specimens. Specifically, the lower cramping pressure of 0.64 N/mm^2 test specimens did not meet the minimum wood failure requirement recommended by BS EN 14080:2013 for both the

individual and average glue lines results. Higher cramping pressures of 0.80 and 0.96 N/mm^2 showed good bonding performance and are suitable for the production of DRM glulam beams. ANOVA results indicated no significant differences at 95% confidence level between the shear strength of test specimens produced with different cramping pressures. On the contrary, the wood failure percentages showed statistically significant differences between the samples produced with the different cramping pressures. It can be concluded that although all the DRM specimens produce adequate shear strength, the percentage of wood failure indicates the quality of the bonding.

Revised minimum requirements are proposed for the DRM specimens because of the lower shear strength and higher wood failure results as shown in the graphs in Figures 5-18 and 5-19. Nevertheless, these revised minimum requirements can be improved by increasing the number of specimens and including higher variation in the density of DRM specimens. It can be concluded that a revision is needed to adjust the minimum requirement to better suit the DRM species, as the recommended requirements cover only limited species, as listed in the BS EN 14080:2013. Another study by Aicher and Ohnesorge (2011) also concluded that the minimum requirements of the block shear strength in the standard may not be applicable to their test specimens produced from beech glulam.

The block shear strength of the DRM specimens ranged from 4.93 to 8.61 N/mm^2 with the average results of each glulam beams ranged from 6.35 to 7.60 N/mm^2. These shear strength results are lower than the published DRM wood shear strength of between 8.0 to 8.7 N/mm^2 (Chu *et al.*, 1997; Malaysian Timber Council, 2018). This is expected since the DRM test specimens in this study have density in the range 487 to 777 kg/m^3, which do not entirely represent the density range of 415 to 885 kg/m^3 of this species. Increasing the number of specimens from different sources will improve the results so that they will adequately describe the overall bonding performance of the DRM species. Furthermore, the offset cut on the test specimens (see Figure 5-10) may resulted in crack initiation in the wood and reduces the shear stress.

Other than the block shear strength tests, another important test method in evaluating the bonding performance of the glue lines is the delamination test (BS EN 14080:2013). In this test, the integrity of the glue lines is tested according to the service classes in which the glulam beams are intended to be used. Generally, both the block shear and delamination tests are significant in the evaluation of the bonding strength of glue lines in glulam beam production. There are other factors influencing the bonding performance of glue lines not included in the scope of this study. Some of them are the effect of physical properties of the timber, wood processing and bonding parameters (Ohnesorge *et al.*, 2010; Knorz *et al.*, 2014), the influence of preservative treatment (Kilmer *et al.*, 1998) and the variation in the block shear test methods (Steiger *et al*., 2010).

The bonding performance of glulam beams can also be further investigated by comparing the shear behaviour of structural adhesives with the shear strength of wood. The shear behaviour of the structural adhesives can best be evaluated using the Thick Adherend Shear Test (TAST) method (BS ISO 11003-2:2001). This method is capable of producing pure shear stress by using thicker adhesive layer to increase the stiffness of the bonding medium and minimizing undesired stresses (Roseley, 2013).

Chapter 6 Full size glulam beam tests

6.1 Introduction

The mechanical properties of components of DRM glulam beam such as the finger joints and laminations were discussed in Chapter 4 (finger joints) and Chapter 5 (beam laminations). The results were used to inform the fabrication of full size glulam beams for testing in this chapter. The beams were reinforced by bonding CFRP sheet onto the surface of the outermost tension layer. The flexural behaviour and failure modes of both unreinforced and reinforced beams were observed. The stiffness, ductility, ultimate load capacity and strain profiles of the beams were also measured. Strain gauges and digital image correlation methods were used to observe displacement of the beams in bending. Comparisons were made between (a) unreinforced, (b) partially reinforced beams at finger joints and (c) fully reinforced beams using results from four-point bending tests. The aim of this chapter was to evaluate the flexural properties of Malaysian DRM glulam beams manufactured in accordance to the production requirements in BS EN14080:2013.

6.2 Materials and method

The fabrication of finger joints and gluing of laminations to produce the DRM glulam beams were described in the previous chapters. This section will describe in detail the preparation of CFRP reinforced beams and testing of the full size glulam beams. A four-point bending test was used to evaluate the bending properties of the glulam beams according to the BS EN 408:2010+A1:2012 standard.

6.2.1 CFRP reinforcement preparation

A total of three DRM glulam beams with nominal dimensions of 210 mm (depth) x 95 mm (width) x 4200 mm (length) was produced in this study (Table 6-1). Carbon fibre reinforced polymer sheets were used to reinforce the surface of the outermost tension layer of two of the glulam beams. Beam-R was reinforced over the entire length of the tension surface and Beam-FJ was reinforced at the finger joints of the tension layer (Figure 6-1).

Table 6-1: Glulam beam descriptions

Specimen	Descriptions
Beam-U	Unreinforced
Beam-R	Full length reinforcement
Beam-FJ	Reinforcement at finger joints

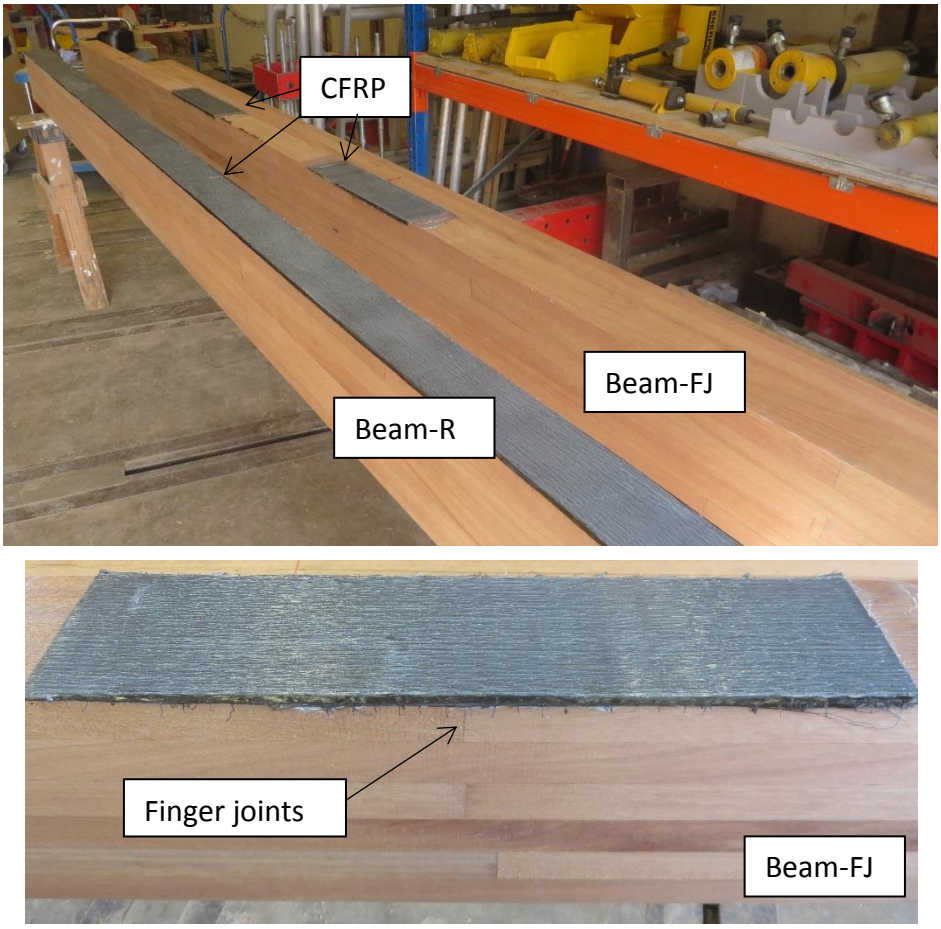

Figure 6-1: Glulam beams externally bonded with CFRP sheet

Reinforcements were made at the finger joints because the locations were expected to experience the highest concentrated stresses in the bending test and the joints together with other defects such as knots and splits were generally the weakest component in the glulam beam. The layout of the finger joints reinforced glulam beam is illustrated in Figure 6-2. The bonding medium used was Sikadur-330 impregnating epoxy adhesive. The technical specifications of the CFRP sheet and Sikadur-330 were given in Section 3.2.3 in Chapter 3.

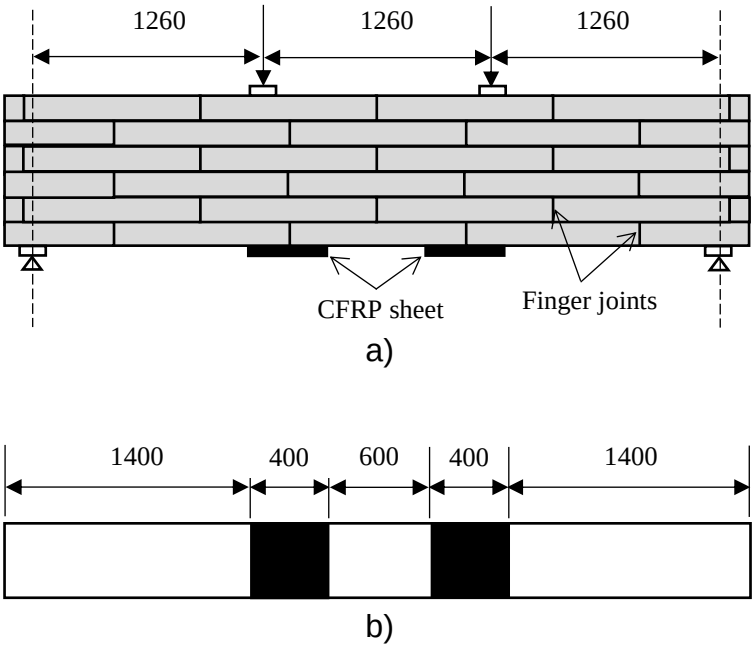

Figure 6-2: Layout of Beam-FJ a) side view; b) bottom view
(dimensions in mm; figures not drawn to scale)

As shown in Figure 6-1, the beams were externally bonded with CFRP sheet on the surface of the outermost tension layer. Prior to the bonding process, the surfaces of the beams were sanded and wood dust was removed. The CFRP sheet was bonded within 24 hours after the sanding to ensure freshness of the surface. Epoxy adhesive (Sikadur-330) was applied to the surface of the beam to be reinforced. The CFRP sheet was laid parallel to the grain and carefully pressed into the adhesive with a roller along the grain while avoid creasing the CFRP sheet. Adequate bonding was demonstrated when the epoxy adhesive penetrated the CFRP sheet and could be seen squeezing out through the fibre strands of the CFRP (Figure 6-3).

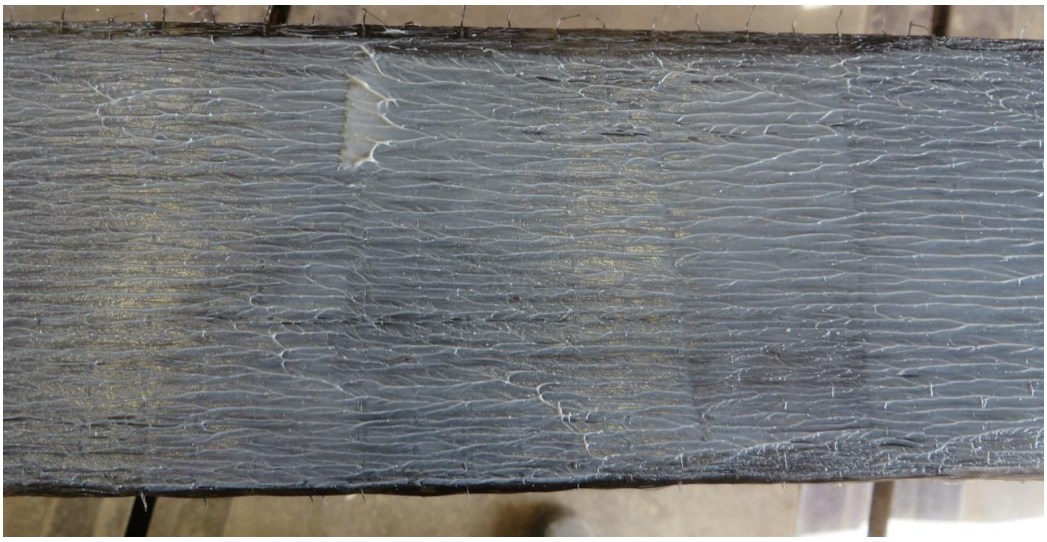

Figure 6-3: Epoxy adhesive penetrating the CFRP sheet

An additional layer of CFRP sheet was immediately applied to the wet surface of the first layer and the laminating process was repeated. Prior to the bonding of the second layer, additional epoxy adhesive was added to the surface of the first layer. The whole laminating process took less than 60 minutes, as recommended by the technical specification of Sikadur-330. No cramping was needed in the curing process and the bonding was left to cure at ambient temperature for more than 7 days.

6.2.2 Four-point bending test

The four-point bending test according to the standard BS EN 408:2010+A1:2012 was used to determine the bending properties of unreinforced and reinforced glulam beams. The determination of modulus of rupture and modulus of elasticity were described in Chapter 3. The set-up of the test is shown in Figure 6-4. The nominal dimensions of the glulam beams were 210 mm (depth) x 95 mm (width) x 4200 mm (length). The bending and loading span were 3780 and 1260 mm respectively. Load cells were placed under each hydraulic jack to record the load applied to the beam. The reinforced beams were positioned with the CFRP sheet located at the bottom.

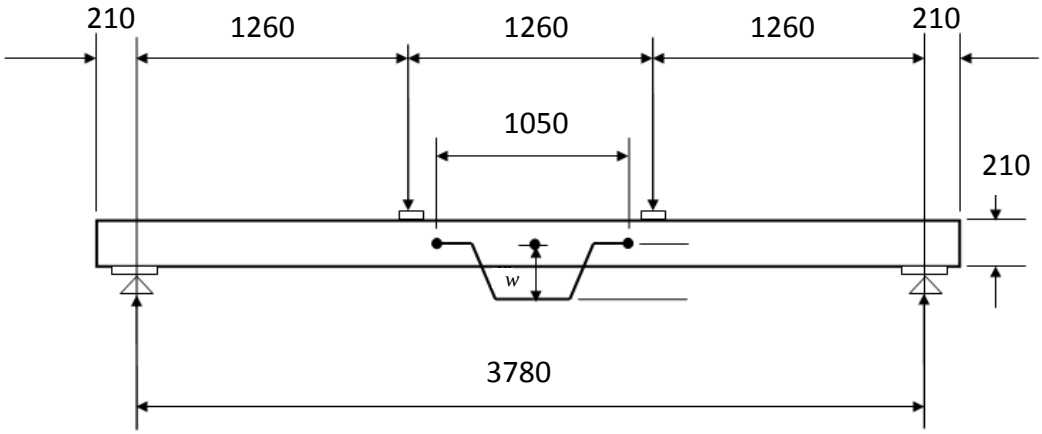

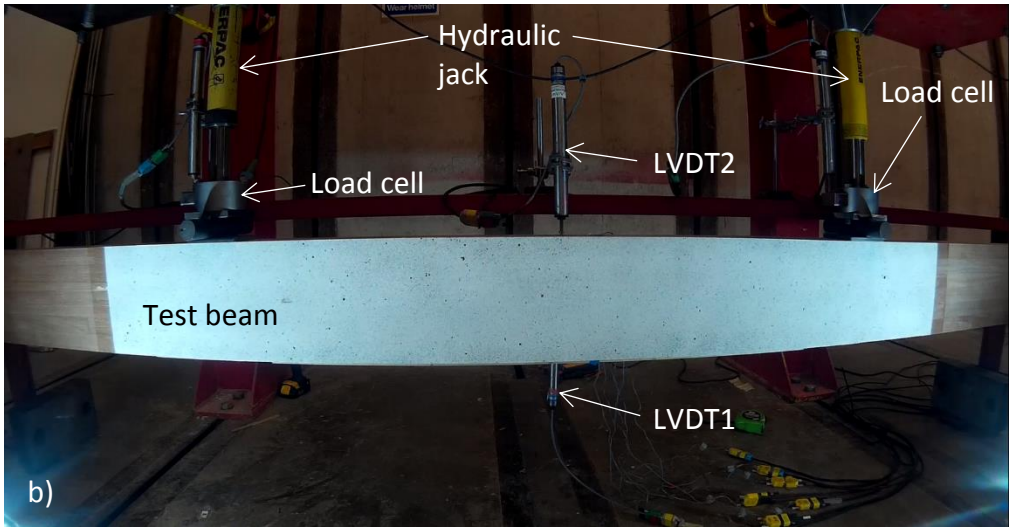

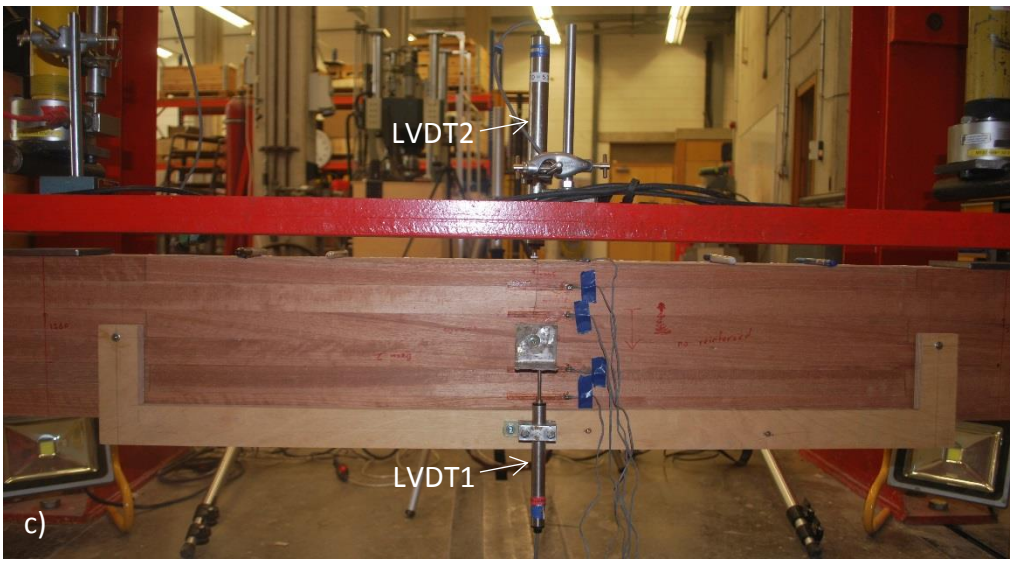

Figure 6-4: Four-point bending test set-up (dimensions in mm) a) test diagram; b) actual test setup; c) location of LVDTs

Linear variable differential transformer LVDT1 was positioned in the middle of the bending span to measure the beam's deformation (w). Only one LVDT was used in the measurement of local deflection because the opposite surface of the beam was used for measuring deformation with the digital image correlation method which is described in the next section. The gauge length of LVDT1 was 1050 mm and the resulting deflection was used to determine the local modulus of elasticity ($E_{m,l}$). The $E_{m,l}$ was calculated using Equation 3-1 in Chapter 3. An additional LVDT2 was located at the centre of the span and positioned at the top of the beam (compression edge) according to the standard BS EN 408:2010+A1:2012. The resulting deflection gathered from LVDT2 was used to calculate the global modulus of elasticity ($E_{m,g}$). The $E_{m,g}$ was determined using the equation below (BS EN 408:2010+A1:2012). The global MOE in bending was not corrected for shear because a good estimate of the shear modulus (G) was not available since the shear displacement was not measured in this study.

Global MOE in bending, $$E_{m,g} = \frac{3al^2 - 4a^3}{2bh^3\left(2\frac{w_2 - w_1}{F_2 - F_1} - \frac{6a}{5Gbh}\right)}$$ (Eq. 6-1)

Key:

$F_2 - F_1$	increment of load on the proportional limit of the load deformation curve, (N)
$w_2 - w_1$	increment of deformation corresponding to $F_2 - F_1$, (mm)
a	distance between the loading point and nearest support, (mm)
l	loading span (mm)
b	width of cross section, (mm)
h	depth of cross section, (mm)
G	shear modulus

Six strain gauges were used to measure the strain of the beams when tested in bending. Two strain gauges were attached on the surfaces of the outermost layer of the beam, S1 at the top surface and S6 at the bottom surface. The remaining strain gauges (S2 to S5) were positioned across the depth of the beams (Figure 6-5). The type of strain gauge used for the beams was TML PL-60-11, single-element wire strain gauge with resistance of 120 Ω and gauge length of 60 mm (Figure 6-6). This strain gauge was suitable for measuring

wood strain. The gauges were glued to the wood surface using single component cyanoacrylate adhesive, TML CN-E. All the strain gauges and other measuring instrumentation such as the LVDTs and load cells, were connected to a data logger.

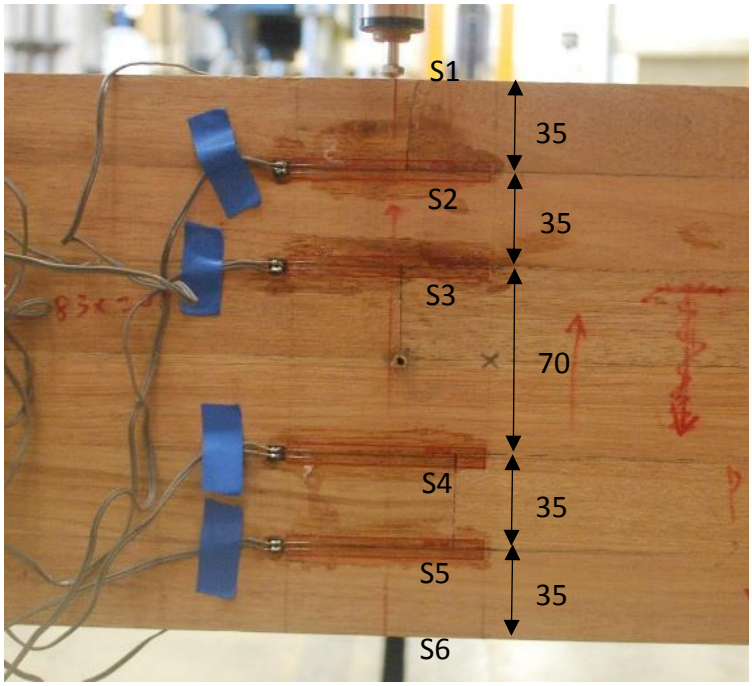

Figure 6-5: Location of strain gauges (dimensions in mm)

Figure 6-6: TML PL-60-11 strain gauges and TML CN-E adhesive

6.2.3 Digital image correlation method

The digital image correlation (DIC) method is commonly used to measure strain distribution in bamboo and wood-based materials in various studies (Archila *et al*., 2014; Pop *et al*., 2013, Jeong *et al*., 2009; Zink *et al*., 1995). DIC method was introduced to measure strain by correlating a sequence of images during loading with the first reference image taken without applying any load. Speckle patterns were sprayed onto the surface of the material so that strong contrast and sharp focus could be obtained. The deformation was measured when there were changes in the displacement of pattern on the specimen surface. One of the benefits of using DIC method was the ability to exclude the influence of external factors such as clamp slippage which causes over-estimation of strain in a tensile test (Jeong *et al*., 2009).

In this study, the DIC method was used to measure the strain distribution of the glulam beams during bending test. The surface of the glulam beams was painted white and later sprayed with black paint to generate a speckle pattern (Figure 6-7). The pattern was created in the middle region approximately 2 metres along the side of the glulam beams.

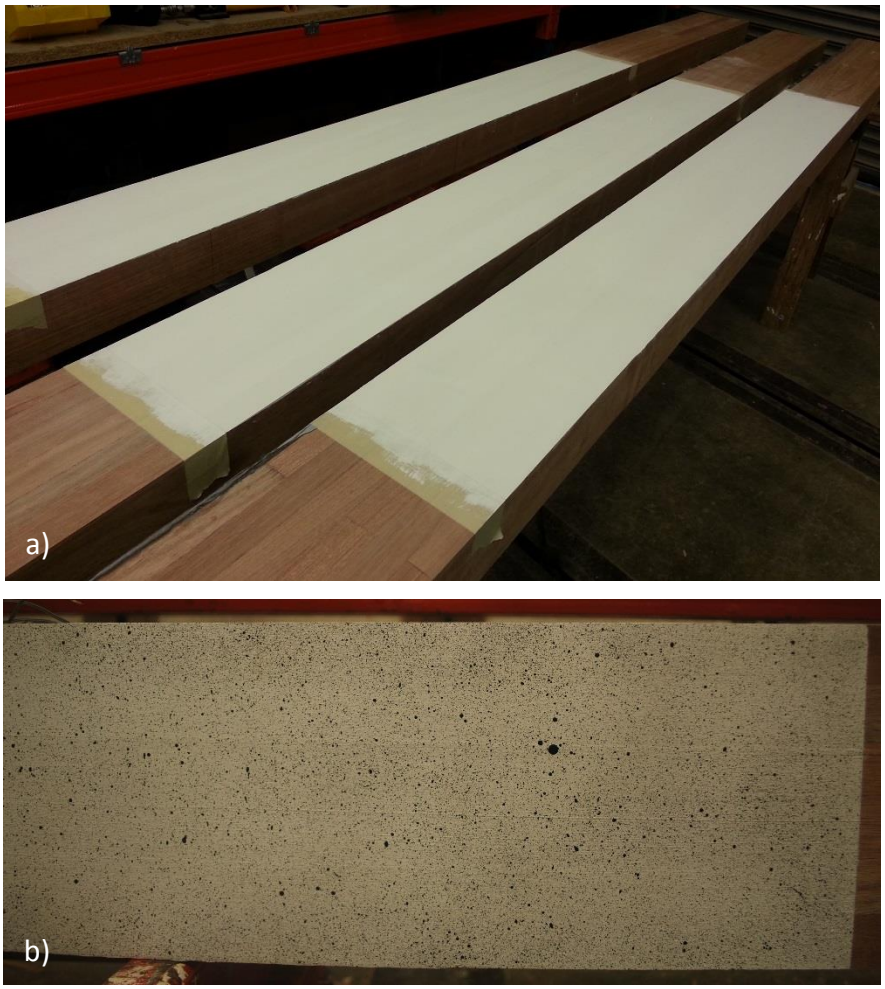

Figure 6-7: Speckle pattern on the surface of glulam beams
a) white background; b) with black specks

The DIC set-up is shown in Figure 6-8. Three high-resolution digital DSLR cameras were used to capture images for the DIC analysis. Each camera focused on a region (left, centre and right) approximately 600 mm along the surface of the beam with speckle pattern (Figure 6-9). The surface was adequately illuminated with two strong floodlights in order to produce images with sharp focus. All three cameras were connected and controlled by a data acquisition software in the computer. The shutter of each camera was controlled with one single click, thus avoiding further physical adjustment that might affect the consistency of producing highly focused images.

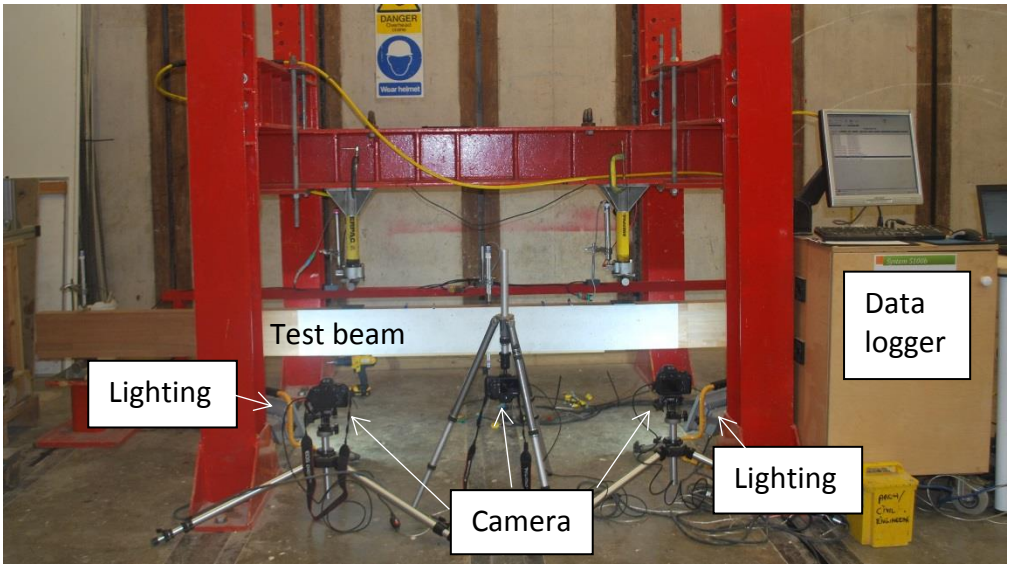

Figure 6-8: DIC set-up in the bending test

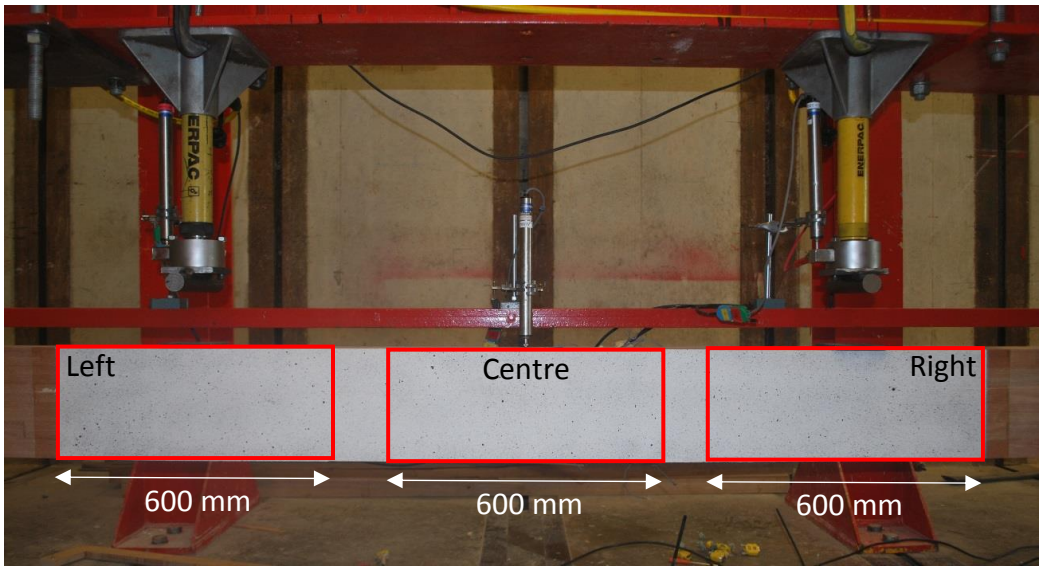

Figure 6-9: Location of focused images

The first image was taken when there was no load applied and the subsequent images were taken after each load increment of 2 kN. All the images were stored sequentially in the computer and they were identified according to the load applied. The first image (without load) was used as reference to the subsequent images (with increment of load), in the calculation of strain of the timber in bending. The strain distribution was analysed by the DIC software, MatchID, developed by Lava and Debruyne. While using the MatchID application, the Approximated Normalised Sum of Squares was used for the

correlation process because of the good results reported in a previous study by Lava *et al*. (2009). The subset and step size were 21 and 10 respectively, ensuring accurate results while minimising processing time of the DIC analysis.

6.3 Results and discussion

The bending properties of the reinforced and unreinforced glulam beams, evaluated using standard mechanical tests in BS EN 408:2010+a1:2012 are presented and discussed in this section. The modes of failure and the influence of CFRP on the bending properties of the glulam beams are also discussed in detail. The overall four-point bending test results are presented in Table 6-2. Further discussion of the results was presented in the later sections.

Table 6-2: Bending properties of reinforced and unreinforced glulam beams

Specimen	Descriptions	Max load (kN)	MOR (N/mm^2)	Local MOE (N/mm^2)	Global MOE (N/mm^2)
Beam-U	Unreinforced	64.7	61.3	17200	14900
Beam-R	Fully reinforced	70.3	70.8	16900	15800
Beam-FJ	Finger joints reinforced	39.5	41.6	15600	13400

6.3.1 Unreinforced glulam beam

This unreinforced beam (Beam-U) was used as the reference specimen for comparison with the reinforced glulam beams (Beam-R and Beam-FJ). Beam-U in the four-point bending test showed failure on the tension face. The beam failed predominantly at the finger joints which are the weakest links in the beam (Figure 6-10). The failure initiated from the central finger joint at the outermost tension layer and cracks propagated upward along the wood to the internal finger joints across the beam (Figure 6-11). The cracks also propagated toward

the supports along the longitudinal axis of the beam. Some of the cracks occurred near glue lines 1 and 3 as shown in Figure 6-11. Closer inspection found pulled-out wood fibres attached to the surfaces of the glue lines. The majority of the cracking occurred in the wood indicating strong bond performance between the laminations. Fine compression creases were visible on the upper layers of the beam.

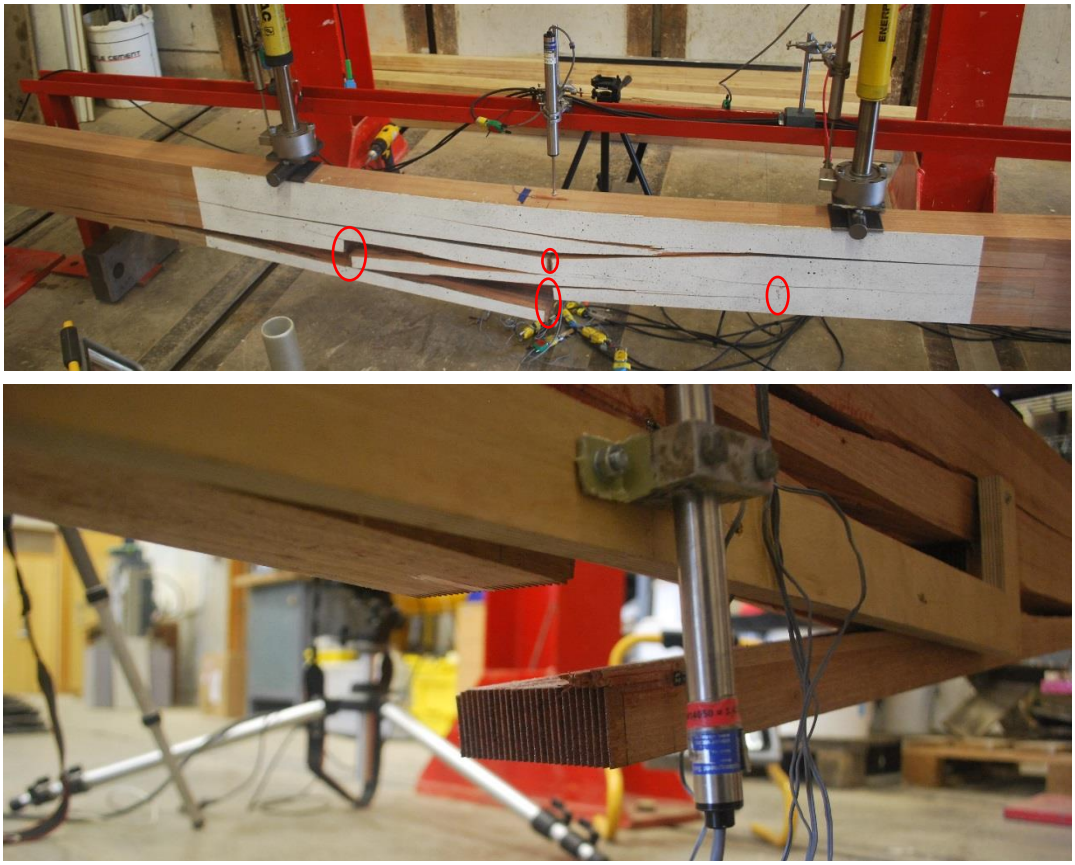

Figure 6-10: Failed unreinforced beam (failed finger joints in red circles)

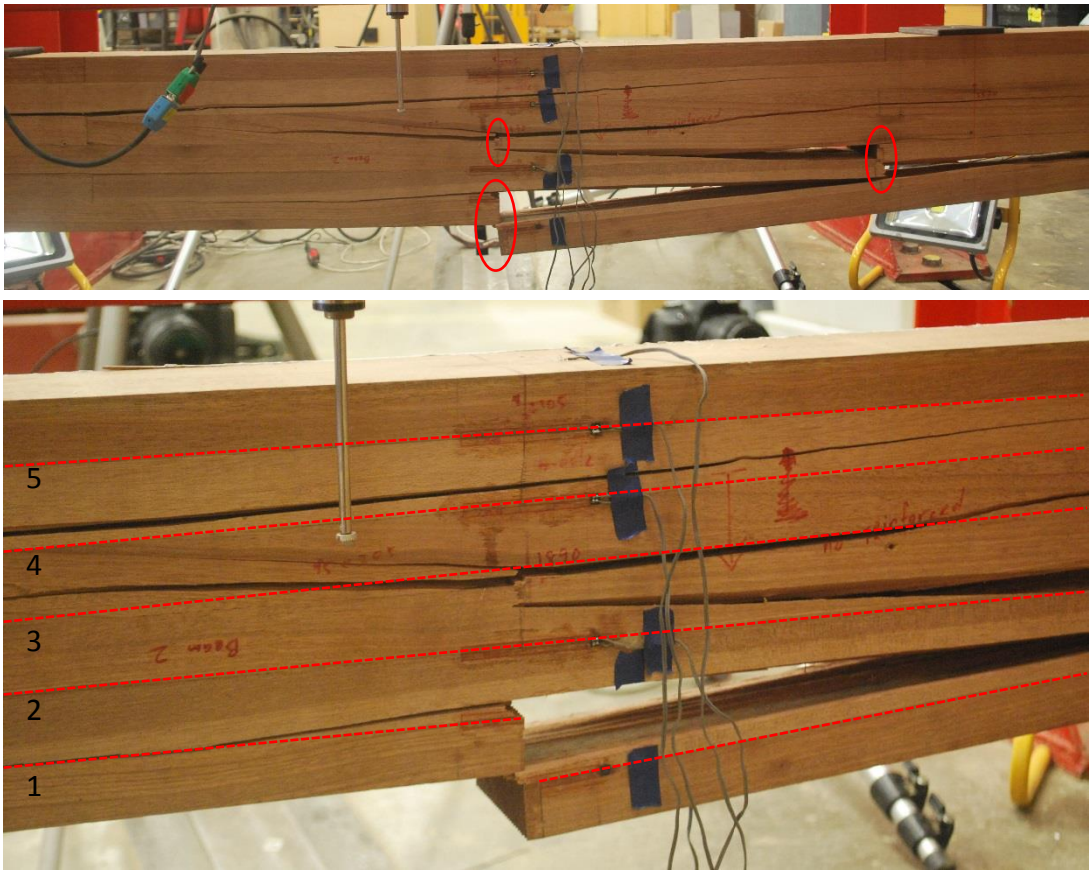

Figure 6-11: Crack propagation of failed unreinforced beam (failed finger joints in red circles; dashed lines with numbers represent glue lines)

The failure of the unreinforced beam occurred at an applied load of 64.7 kN and the load-deflection curve is presented in Figure 6-12. The beam showed brittle failure because no crack or any signs of failure were observed prior to the sudden catastrophic failure in the bending test. The failure behaviour of the beam was depicted by the load-deflection curve which showed small nonlinearity near the end of the curve.

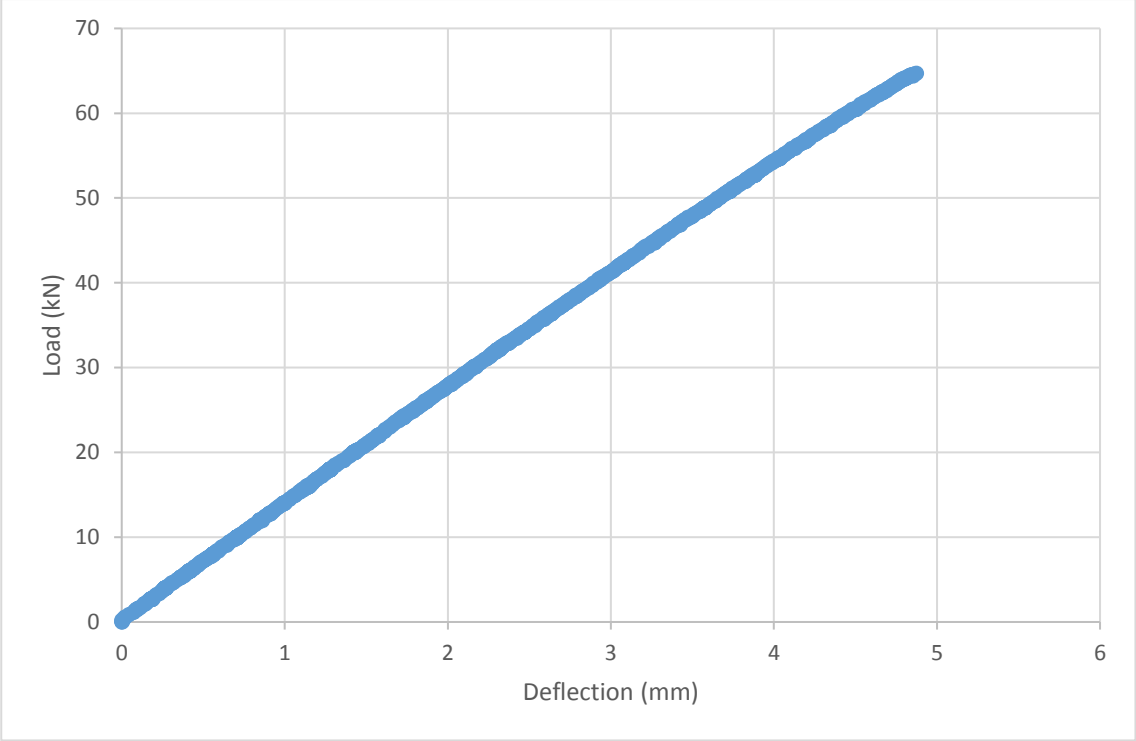

Figure 6-12: Load-deflection curve of unreinforced beam

6.3.2 Fully reinforced glulam beam

CFRP sheet was used to reinforce the whole length of the outermost tension surface of the glulam beam. No anchoring of the CFRP sheet was made on the surface of the beam. The beam failed on the tension face and exhibited failures predominantly at finger joints (Figure 6-13), similar to the unreinforced beam. In post-failure observations, the first crack appeared to originate from the failure of the finger joint at the outermost tension layer of the beam. The cracks propagated upward to the higher finger joints and also longitudinally toward the supports. The double-layered CFRP sheet also debonded from the glulam (Figure 6-14). The crack propagated at mid-depth towards the end of the beam which completely split the beam (Figure 6-15). The crack path comprised a mixture of glue line failure with pull-out of wood fibres and splitting of wood, indicating good bond performance between laminations. Fine compression creases were seen on the compression region of the beam.

Figure 6-13: Failed fully reinforced beam (failed finger joints in red circles)

Figure 6-14: Delamination of the CFRP sheet

Figure 6-15: Splitting in midsection of the beam

The ultimate load of the fully reinforced beam is 70.3 kN and the load-deflection curve is shown in Figure 6-16. The graph is linear-elastic initially and exhibits significant nonlinearity after the applied load of 60 kN. This nonlinear behaviour indicates improved ductility of CFRP reinforced beam compared to the unreinforced beam.

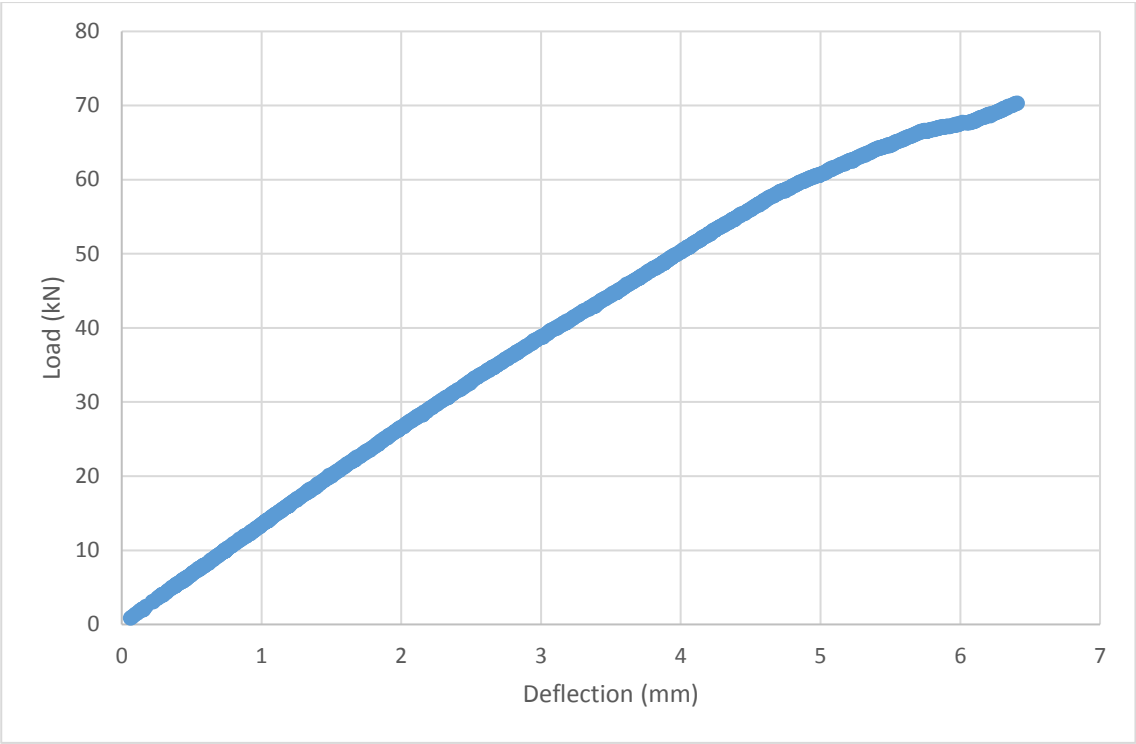

Figure 6-16: Load-deflection curve of fully reinforced beam

6.3.3 Reinforced finger joints glulam beam

Beam-FJ was reinforced with CFRP sheets at the finger joints of the outermost tension layer because the joints, which are the weakest link of the beam, were expected to fail earlier than the fully reinforced Beam-R. The load-deflection curve of the beam is shown in Figure 6-17. From the graph, crack initiation occurred approximately at 22 kN applied load. Localized wood failure was seen occurring at the edge of the CFRP reinforcement during the bending test (Figure 6-18). The failure was caused by stress concentration at the edge of the CFRP sheet. Further loading caused crack propagation along the glue line in the longitudinal direction of the beam (Figure 6-19).

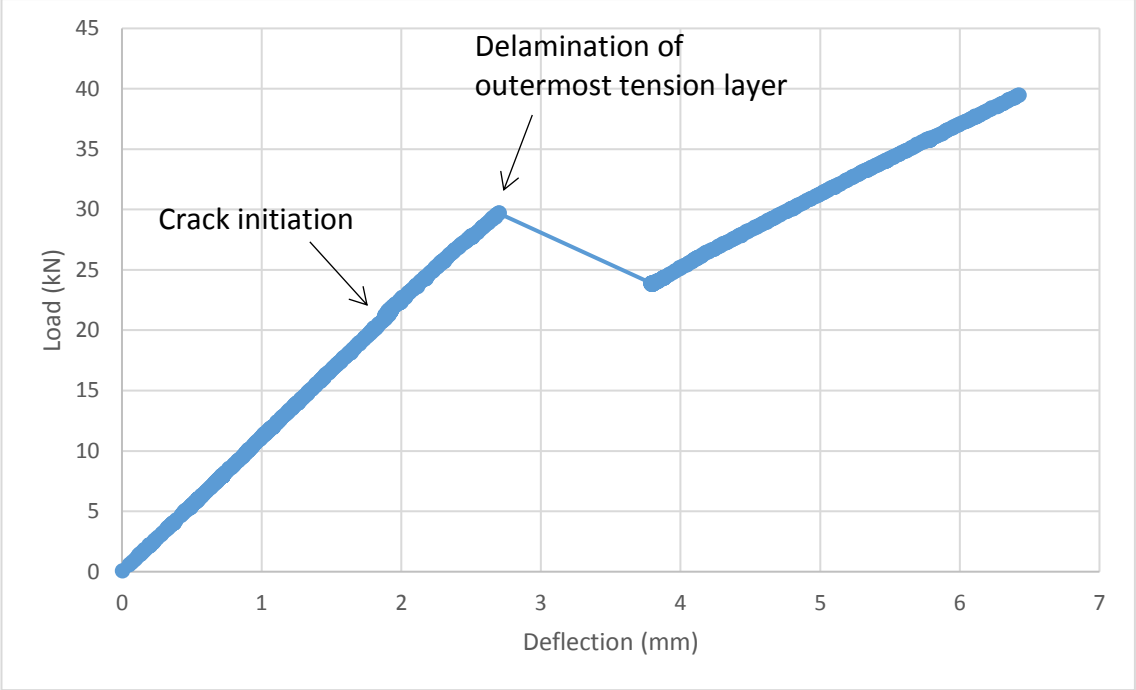

Figure 6-17: Load-deflection curve of reinforced finger joints beam

Figure 6-18: Crack initiation (circled red) at the edge of CFRP sheet

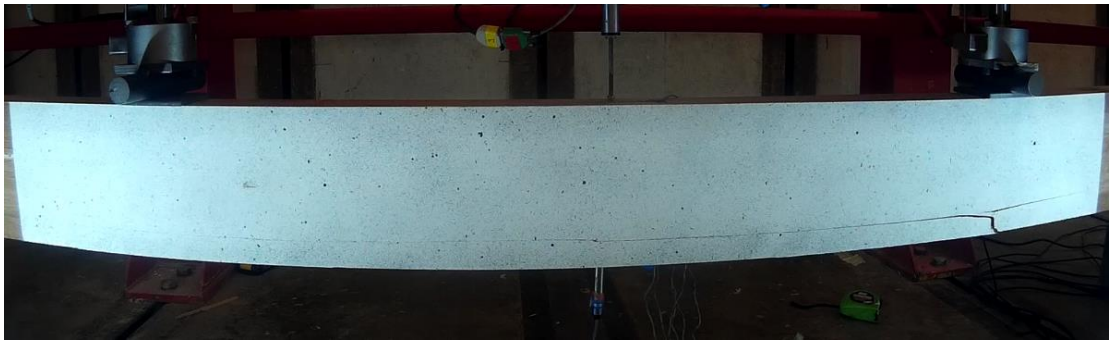

Figure 6-19: Crack propagation along the outermost tension layer prior to ultimate failure of the beam

The ultimate failure of the beam occurred at an applied load of 39.5 kN with catastrophic failure on the tension face at the end of the test. No evidence of compression failure was observed in the compression region of the beam. The failure of the beam is shown in Figure 6-20. The load-deflection curve showed no significant nonlinearity near the end of the test, indicating brittle fracture in the bending test.

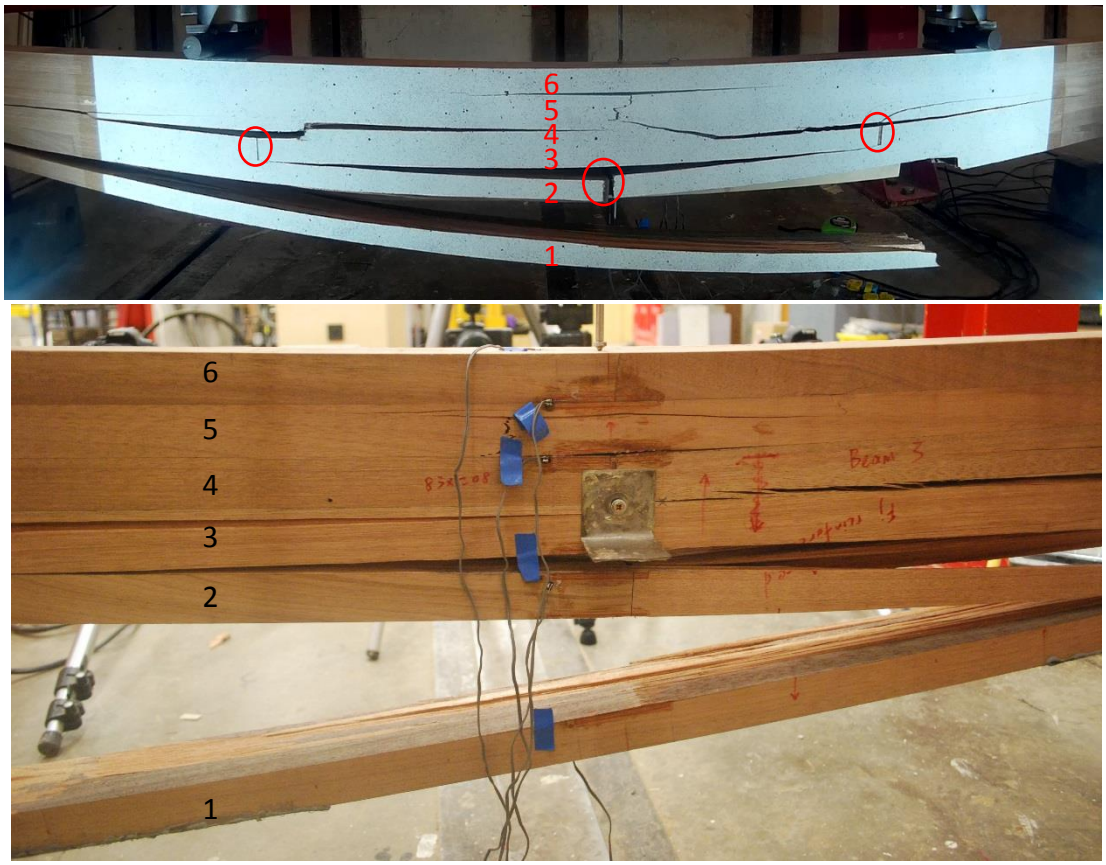

Figure 6-20: Failed reinforced finger joints beam
(failed finger joints in red circles; 1 to 6 represent laminations)

In the post-failure examination, closer inspection of the beam failure showed crack initiation from the edge of the CFRP sheet (Figure 6-21). The crack propagated along the glue line, separating the outermost tension layer. The finger joints in lamination 1 which was reinforced with the CFRP sheets showed no fracture but subsequent laminations 2 and 3 failed at finger joints. The cracks propagated upward from these failed finger joints with a mixture of failed glue lines and wood. Further inspection of the failed glue lines showed pull-out of wood fibres indicating good bonding performance between the laminations.

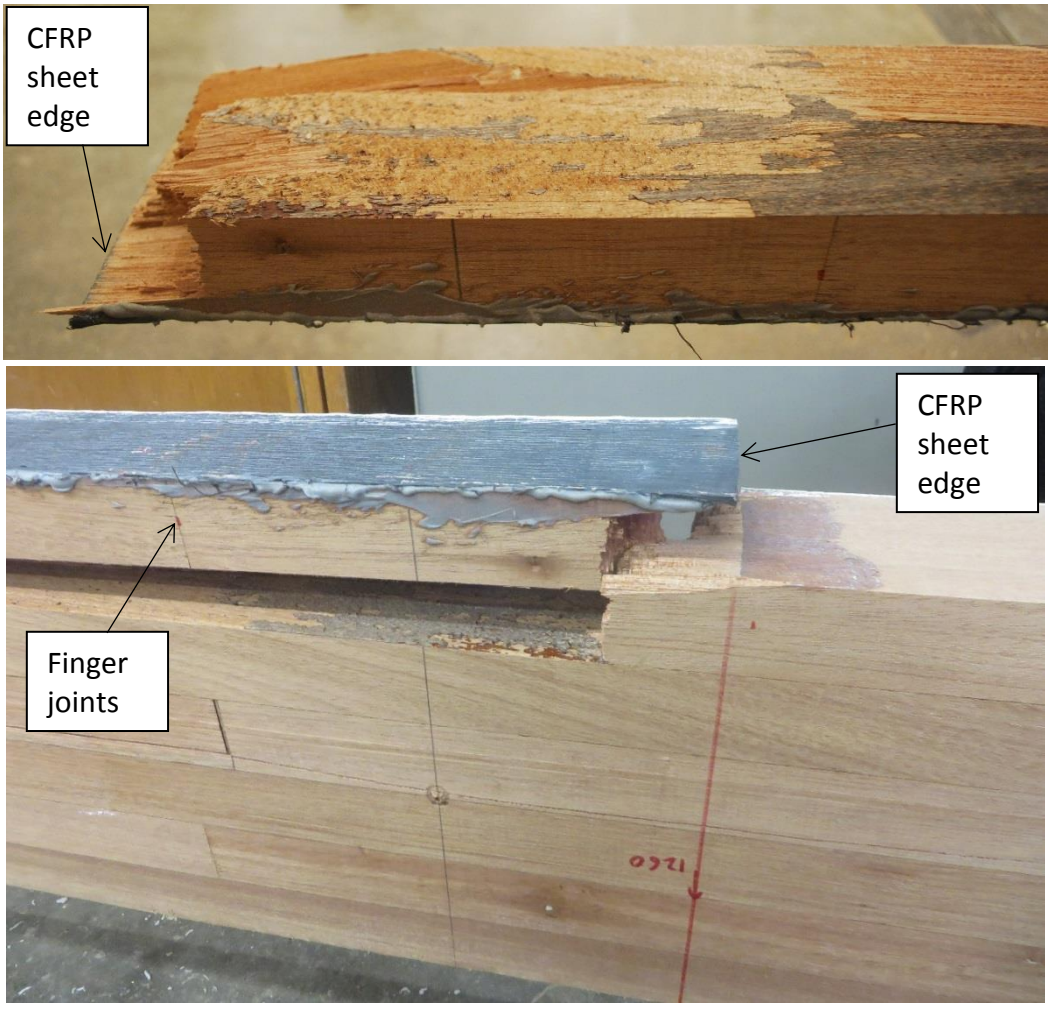

Figure 6-21: Crack initiation at the edge of the CFRP sheet

6.3.4 Comparison of bending properties between unreinforced and reinforced glulam beams

From the results in Table 6-2, the bending strength of fully reinforced beam, Beam-R (70.8 N/mm^2) was 13% and 41% higher in bending strength (MOR) than the unreinforced beam, Beam-U (61.3 N/mm^2) and reinforced finger joints beam, Beam-FJ (41.6 N/mm^2) respectively. Beam-U possessed a 32% higher MOR than Beam-FJ. The reinforcement at the finger joints of Beam-FJ was designed to reduce the utilisation of expensive CFRP sheet. Nevertheless, Beam-FJ exhibited the lowest MOR due to premature cracking caused by the stress concentration at the edge of CFRP sheet. The load-deflection curve for all the beams is shown in Figure 6-22.

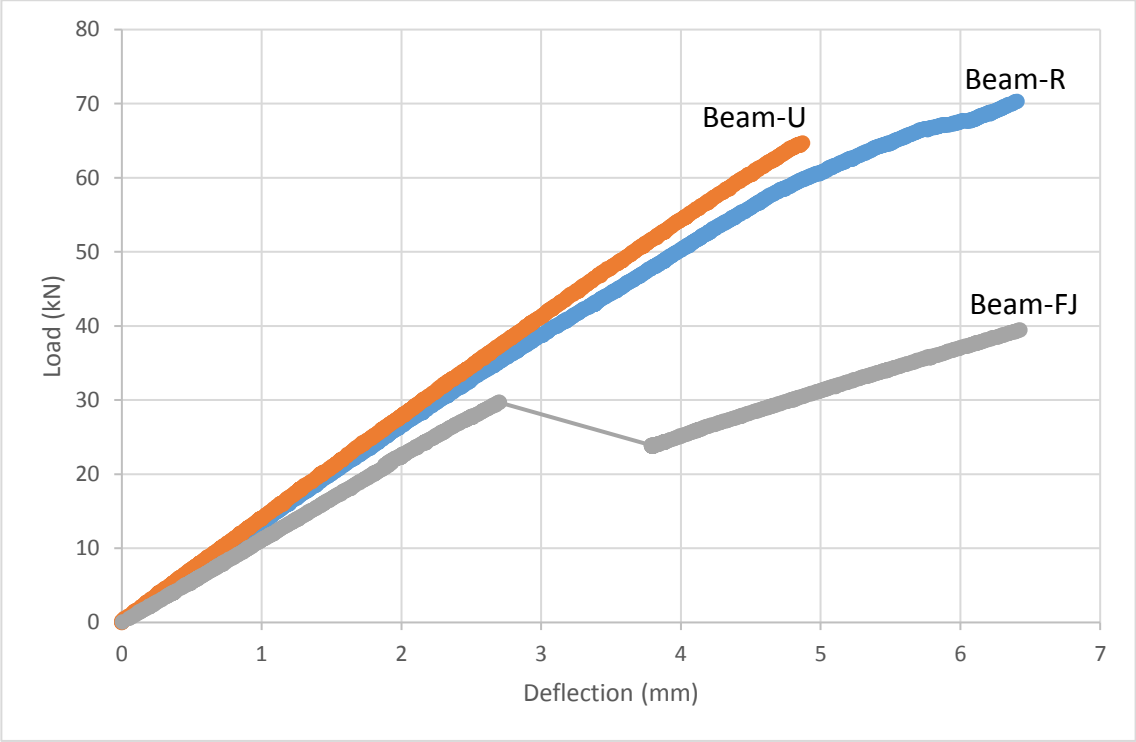

Key: Beam-U Unreinforced beam
Beam-R Fully reinforced beam
Beam-FJ Finger joints reinforced beam

Figure 6-22: Load-deflection curves of unreinforced and reinforced beam

As discussed in the earlier section, Beam-U and Beam-FJ did not exhibit any significant nonlinearity in the load-deflection curve in Figure 6-22 and the beams

failed catastrophically at the ultimate load, indicating brittle fracture in the bending tests. Beam-R showed nonlinearity in the load-deflection curve and higher load carrying capacity compared to the unreinforced beam. Beam-FJ showed low load-carrying capacity because of the early crack initiation at the edge of the CFRP sheet due to stress concentration which resulted in the delamination of the outermost tension layer.

The configuration of the CFRP reinforcement played a significant role in the four-point bending tests in this study. As shown in the results, partial reinforcement at the finger joints created stress concentrations at the edge of the CFRP sheets which initiated cracking at the outermost tension layer of the beam. This in turn increases the tensile stress between the outermost tension layer and the subsequent lamination and resulted in delamination along the glue line. The separation of the outermost tension layer reduces the effective cross-section of the beam and increases the beam's deflection while reducing the load-carrying capacity of the beam. Thus, the beam with reinforced finger joints possessed the lowest bending strength when compared to the fully reinforced DRM beam and the unreinforced beam.

The local modulus of elasticity ($E_{m,l}$) did not show any trend between the tested beams. Beam-U showed slightly higher $E_{m,l}$ (17200 N/mm^2) when compared to Beam-R (16900 N/mm^2) and Beam-FJ (15600 N/mm^2). Alhayek and Svecova (2012) indicated that the effect of reinforcement on the stiffness of beam was more significant at smaller span to depth ratios (6 to 8.5). They indicated that beams with larger span to depth ratio will not achieve a significant increase in stiffness when tested in bending. The DRM glulam beams in this study had a span to depth ratio of 18, thus might not be expected to show any significant increase in the $E_{m,l}$ when reinforced with CFRP sheet.

The global moduli of elasticity ($E_{m,g}$) of the beams, as shown in Table 6-2, were lower than $E_{m,l}$. The determination of $E_{m,g}$ was underestimated because it did not include the shear deformation which was not evaluated in this study. The ratio between $E_{m,l}$ and $E_{m,g}$ was 1.15, 1.07 and 1.16 for Beam-U, Beam-R and Beam-FJ respectively. These ratios were higher compared to the results gathered

from bending tests of European softwood by Boström (1999) which varied from 1.03 to 1.09. Boström also reviewed results from other studies and concluded that the ratio between $E_{m,l}$ and $E_{m,g}$ can vary from 0.7 to 1.3 for softwood species. The variation in the ratio was influenced by the configuration of the bending tests, size and position of defects in the tested beams and dimensions of the beams. A further study would benefit from increasing the number of specimens to accurately determine the ratio of $E_{m,l}$ and $E_{m,g}$ of tropical hardwood species in bending tests.

6.3.5 Strain analysis

Strain was measured across the depth of the beam (see Figure 6-5) using strain gauges as described in Section 6.2.2. The strains were measured in relation to the applied load at both compression and tension regions of the beam. The strain profiles of the unreinforced beam are shown in Figure 6-23. The locations of the strain were identified as S1 to S3 for strain gauges in the compression region and S4 to S6 for strain gauges in the tension region. The compressive strains are shown as negative values and the tensile strains as positive values. In the graph, the distribution of the strain profiles is linear and the compressive strains are almost identical to the tensile strains.

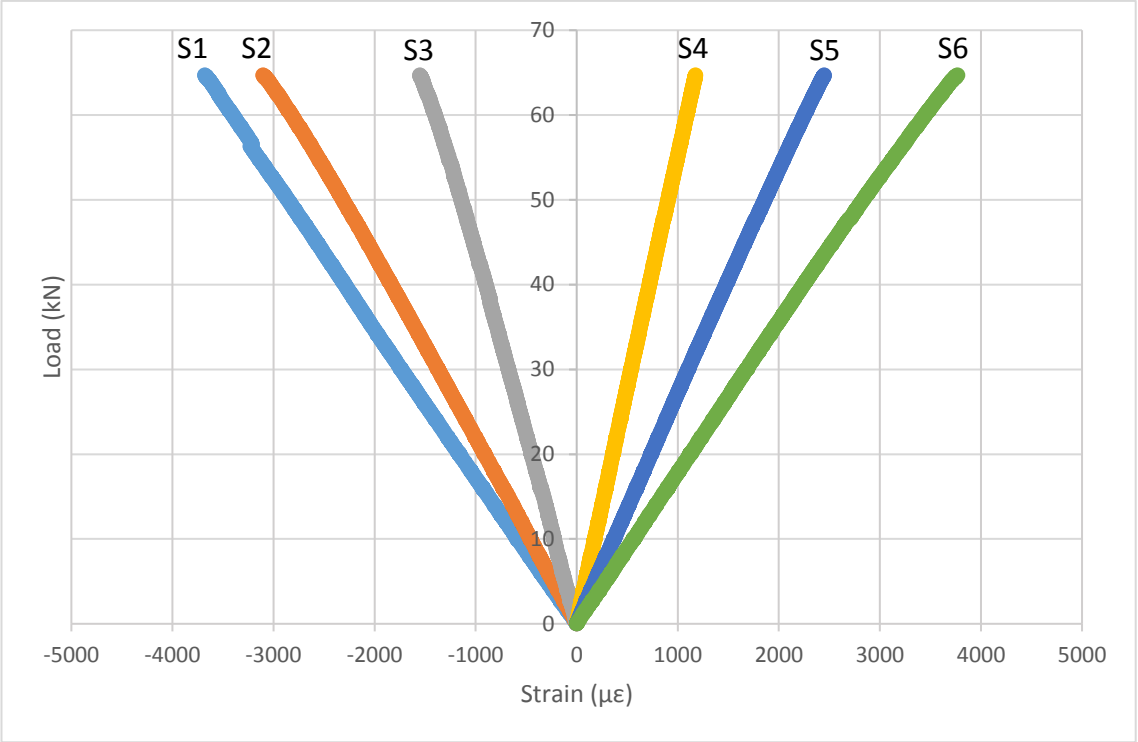

Key: S1 to S6 Strain gauges

Figure 6-23: Load as a function of strain for unreinforced beam

The load-strain curve for the fully reinforced beam is shown in Figure 6-24. The distribution of the strain profiles in the compression region (S1, S2 and S3) remained linear up to applied load 55 kN. Exceeding this load, the strain gauges showed higher strain with S1 which is attached to the surface of the outermost compression region showed erroneous data indicating failure of the strain gauge due to compression wrinkling. The strain results for the strain gauges in the tension region showed nonlinearity above an applied load 60 kN. Similar to the load-deflection curve in Figure 6-16, the nonlinearity indicated ductile behaviour of the CFRP reinforced beam. Compared to the strain profiles of unreinforced beam in Figure 6-23, the strain profiles of fully reinforced beam showed that higher compressive strains were attained. The compressive strain profiles also showed higher values than the tensile strain profiles in the fully reinforced beam indicating a shifting of the neutral axis toward the tension region. The high modulus carbon fibre reduces the strains in the wood bonded to the CFRP hence increasing the compressive strains.

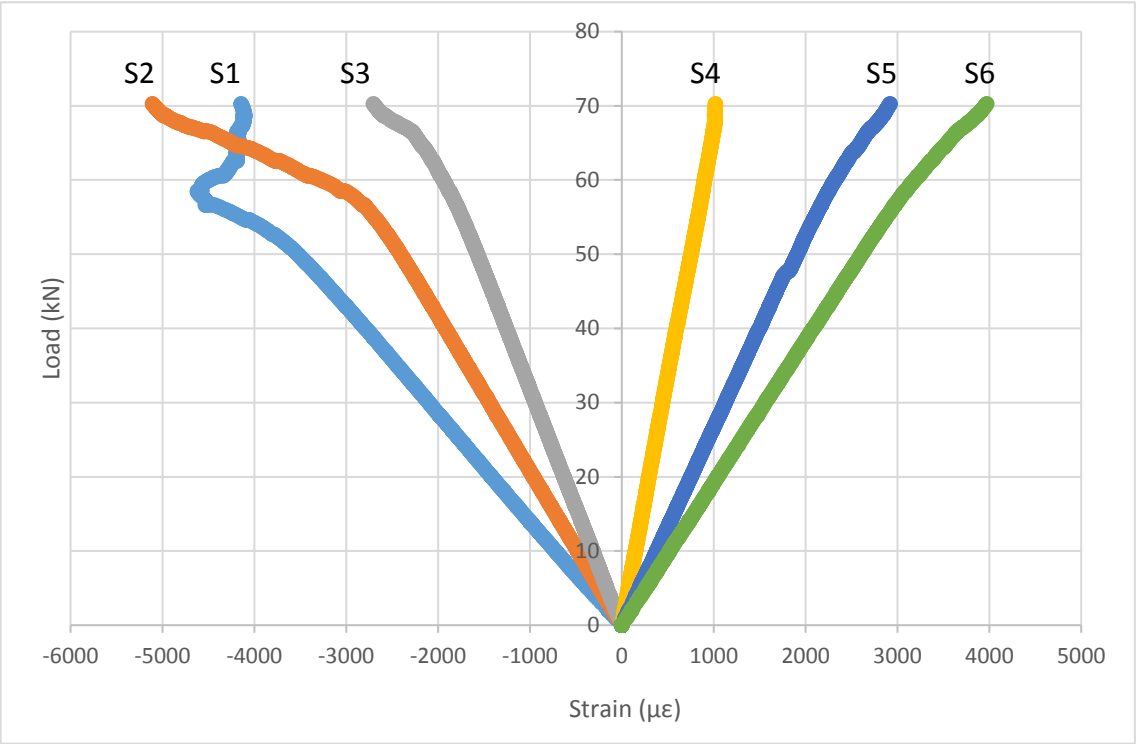

Figure 6-24: Load as a function of strain for fully reinforced beam

The strain profiles of finger joints reinforced beam are presented in Figure 6-25 and splitting failure of the outermost tension layer is evident at an applied load of 30 kN, which correspond to the drop in load in the load-strain curve. Strain gauge S4 in the tension region exhibited failure and was unable to measure strain after an applied load 27 kN while S3 showed erroneous data, indicating a faulty gauge after applying a load of approximately 10 kN. The measurement of the strain comes to a halt once the applied load reached 40 kN where the reinforced finger joints failed catastrophically in flexure on the tension face.

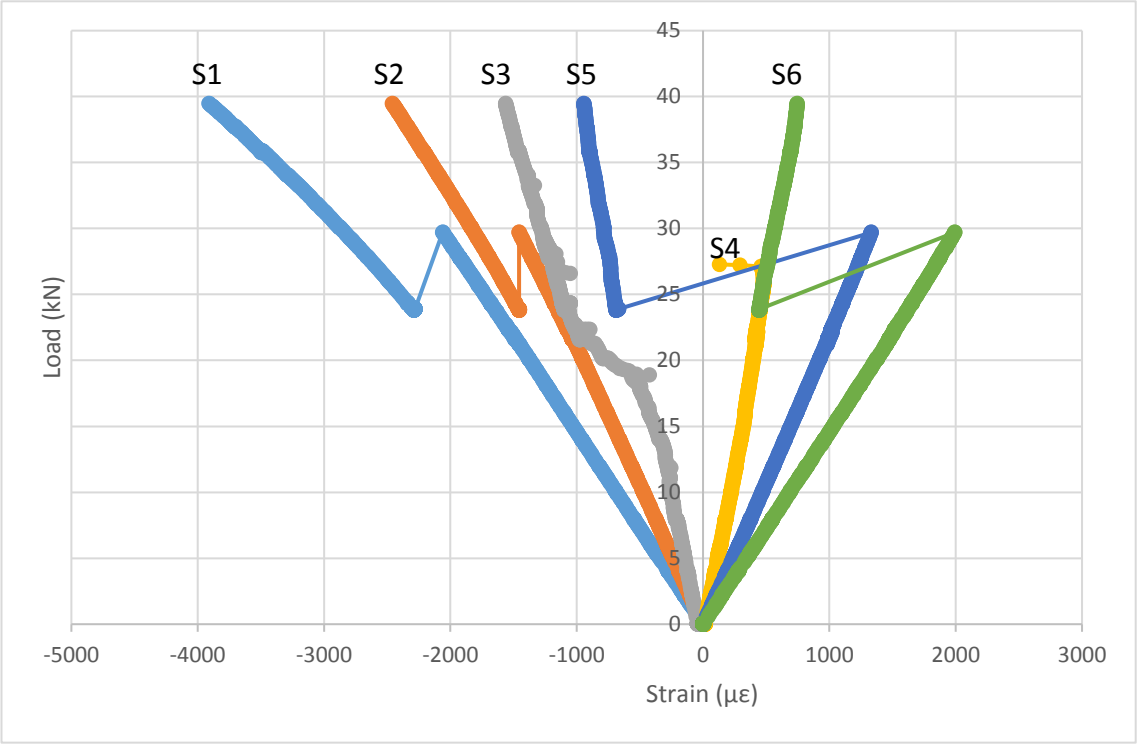

Figure 6-25: Load as a function of strain for the beam with reinforced finger joints

Figures 6-26 to 6-28 show the distribution of strain profiles at different depths in the beams. The locations of the strain gauges were shown in Figure 6-5 with the gauge positions measured from the middle of the beam. Strain gauges S1, S2 and S3 were positioned at the compression region at approximately +105 (top surface), +70 and +35 mm from the midsection of the beam's depth. In the tension region, strain gauges S4, S5 and S6 were located at -35, -70 and -105 (bottom surface) mm from the midsection of the beam's depth.

Figure 6-26 shows the strain profiles across the depth of the unreinforced beam. All the strain profiles intersected at a depth of approximately -5 mm, indicating slight movement of the position of neutral axis of the unreinforced beam toward the tension region. The insignificant changes of the position of the neutral axis with the increase of applied load indicates no plasticization in the compression region (Glišović *et al*., 2016).

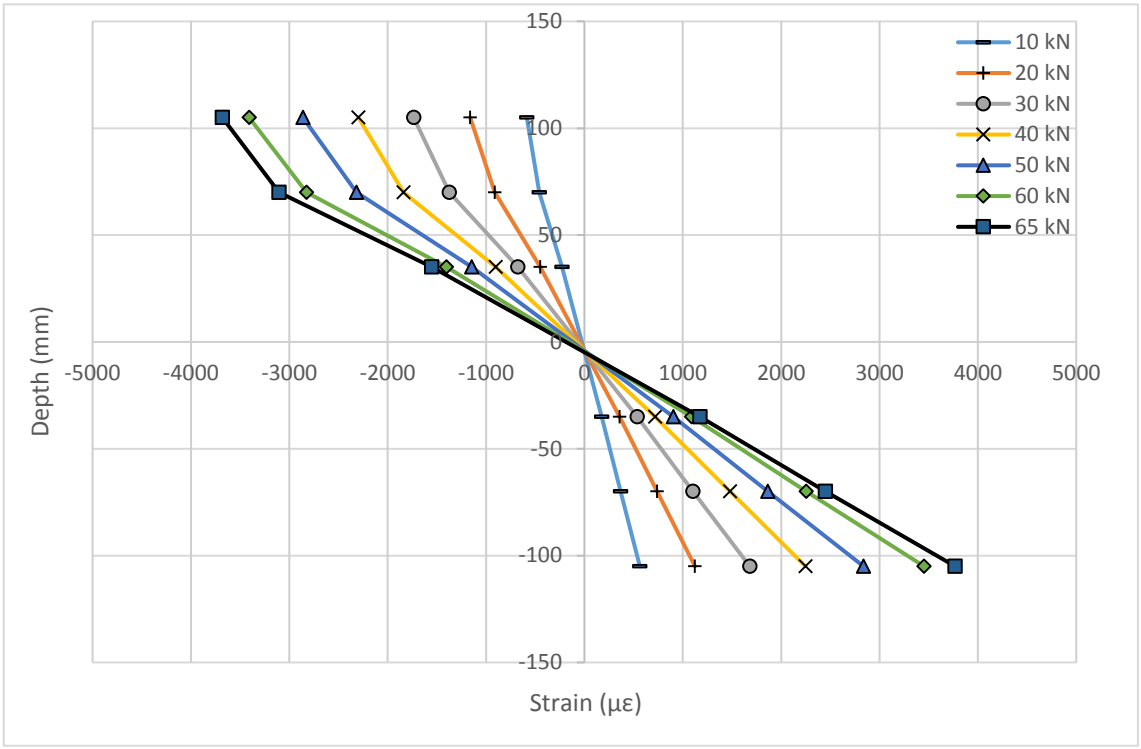

Figure 6-26: Strain plotted versus depth for the unreinforced beam

The strain profiles across the beam's depth for the fully reinforced beam presented in Figure 6-27 indicate that the neutral axis is located approximately 10 mm from the midsection of the beam. In comparison to the unreinforced beam, the CFRP sheet caused shifting of the neutral axis of the fully reinforced beam. Furthermore, the fully reinforced beam showed higher compressive strain and lower tensile strain when compared to the unreinforced beam. These findings were similar to the findings of Glišović *et al*. (2016) and De Luca and Marano (2012) indicating successful transfer of stresses from the timber to the reinforcement material in the tension region of the beam.

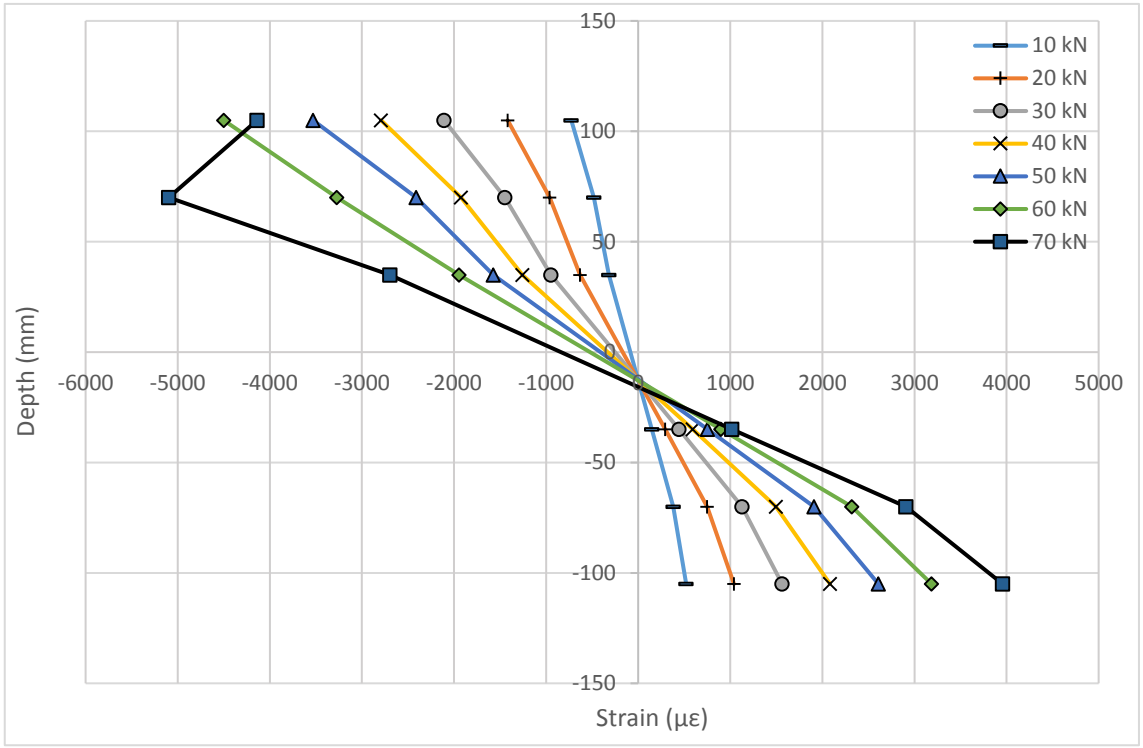

Figure 6-27: Strain plotted versus depth for the fully reinforced beam

The distribution of strain across the depth of the beam with reinforced finger joints is shown in Figure 6-28. The strain-depth curve reveals that the position of the neutral axis changes with each increment of applied load. The neutral axis is located near to the beam's midsection when the applied load is smaller than 15 kN. In this stage, the beam with reinforced finger joints exhibited similar strain profiles to the unreinforced beam because the effect of the CFRP sheet was not significant at the lower applied load. Further increase in applied load shifted the neutral axis downwards, indicating the transfer of load from the timber to the CFRP reinforcement. Nevertheless, the stress concentration at the edge of the CFRP sheet caused crack initiation and resulted in premature failure of the beam due to delamination of the outermost tension laminations as discussed in Sections 6.3.3 and 6.3.4. The strain gauges showed erroneous strain measurement after an applied load 30 kN, thus were not included in the graph.

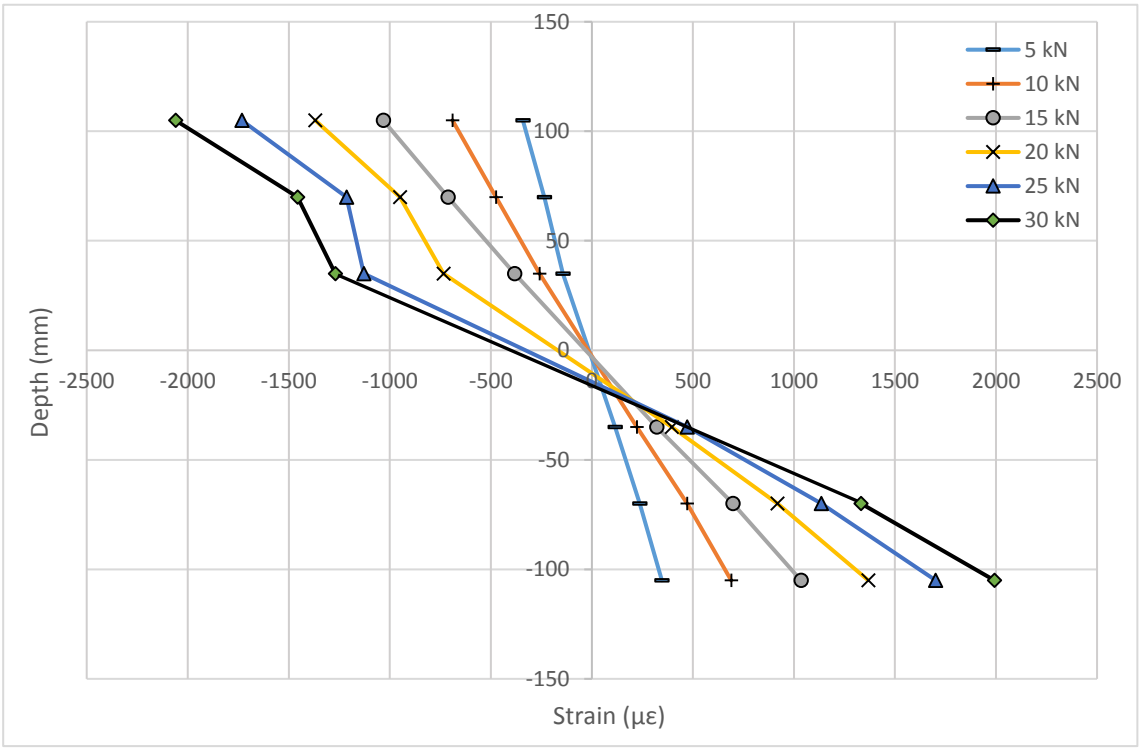

Figure 6-28: Strain plotted versus depth for the beam with reinforced finger joints

The strain plots calculated by the digital image correlation method are shown in Figures 6-29 to 6-32. The results from the DIC analysis provide further understanding of the bending performance of both reinforced and unreinforced DRM glulam beam in this study. As explained in Section 6.2.3, the DIC analysis focused on the critical region (see Figure 6-9) where crack initiation and beam failure were expected to take place and not the full length of the beam.

The strain ε_{xy} plots calculated by the DIC method were used to observe the crack initiation and propagation of the unreinforced beam. Figure 6-29 shows the strain ε_{xy} plots at applied loads of 0, 22 and 30 kN. The set of figures in each row represented the DIC focus area (left, centre and right). The scale bar indicates the strain values at different points. Strain values not in the range of the minimum and maximum of the scale bar (considered as off-scale) were displayed in grey.

In Figure 6-29b, crack initiation can be seen in the focus area on the right of the beam when applied at a load of 22 kN. This corresponds well with the results

gathered from the load-deflection curve (see Figure 6-17) in Section 6.3.3 which indicated the occurrence of wood failure where the edge of the CFRP sheet was located. Further loading showed crack propagation across the longitudinal direction of the beam as shown in Figure 6-29c, delaminating the outermost tension layer of the beam.

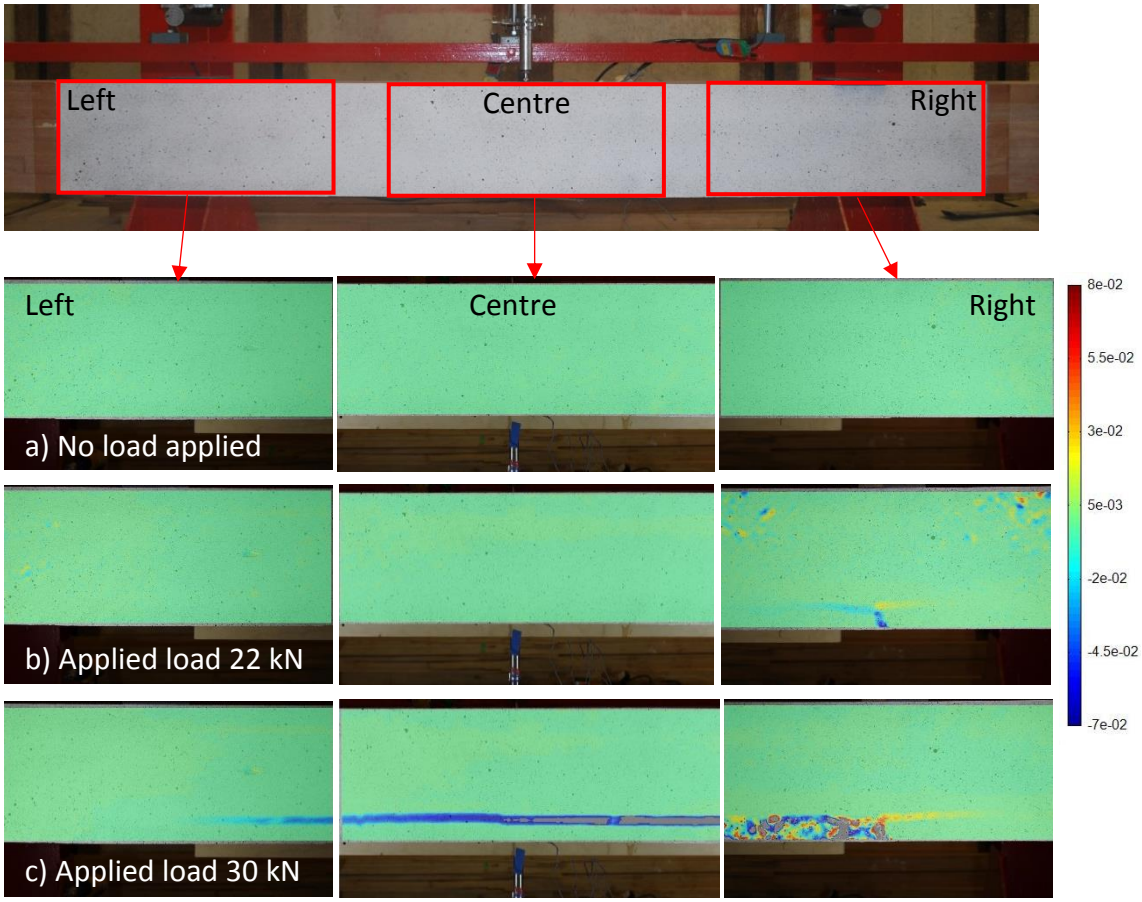

Figure 6-29: Strain ε_{xy} plots analysed by DIC method for the beam with reinforced finger joints

Figure 6-30 shows the results of component strain ε_{xx} which is the normal strain along the longitudinal axis of the beam. The figure showed the strains in the centre region of the unreinforced beam with applied load of 62 kN. As discussed in Section 6.3.1, the unreinforced beam showed brittle fracture. The finger joints at the outermost tension layer, as seen in Figure 6-30, indicated higher strain prior to the catastrophic failure at an applied load 64.7 kN.

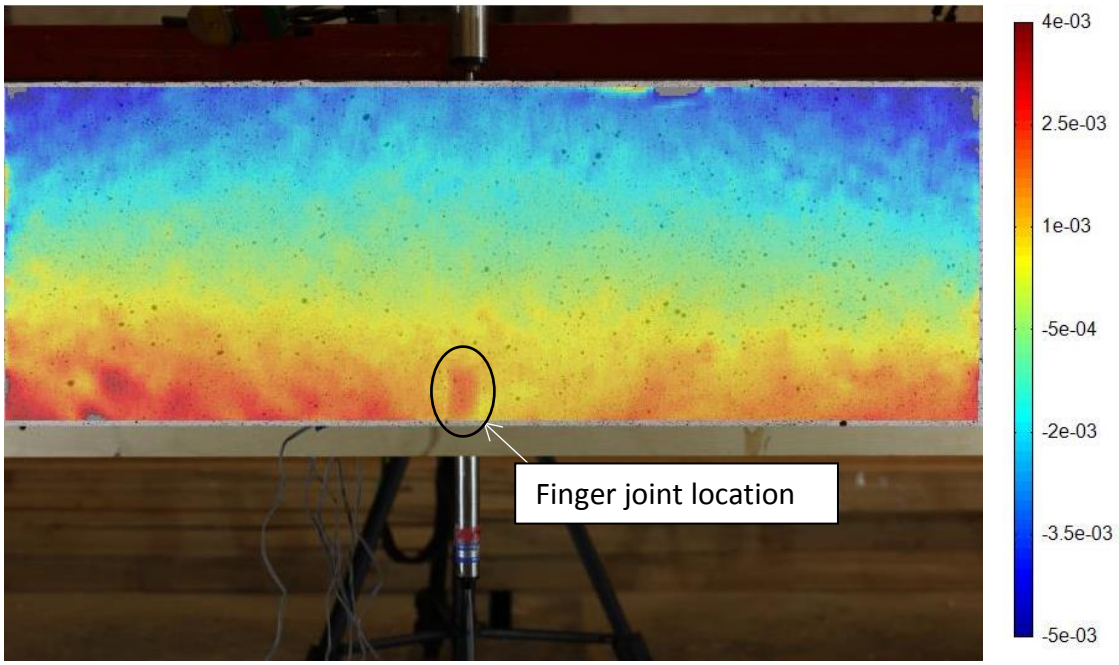

Figure 6-30: Strain ε_{xx} plots analysed by DIC method at the centre region of unreinforced beam with applied load 62 kN

Figure 6-31 shows the results of component strain ε_{yy} which is the normal strain along the y-axis of the fully reinforced beam. The results focused on the centre region of the beam. From Figures 6-31b and 6-31c, the bottom region of the beam showed uneven strain near the glue line, which is the interface between the wood and CFRP sheet. The bottom region showed compressive strain while spots of tensile strain were also observed (grey indicates off-scale values). Overall, the upper region of the beam experienced positive ε_{yy} (tensile strain) while negative ε_{yy} (compressive strain) was observed at the bottom region near to the CFRP sheet. This is expected because in the bending test, the bottom laminations were pushed towards the rigid CFRP sheet thus experiencing compressive strain along the y-axis.

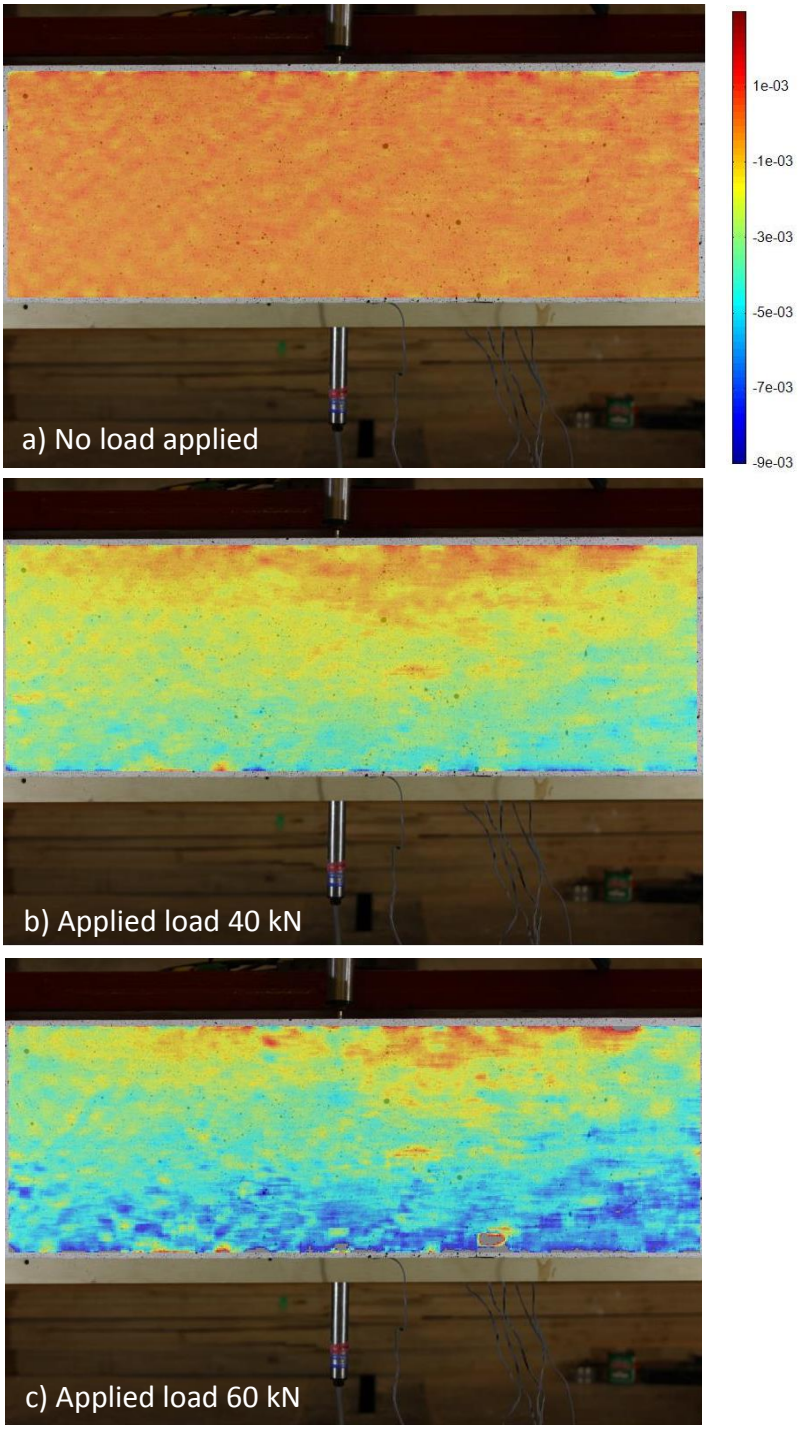

Figure 6-31: Strain ε_{yy} plots analysed by DIC method at the centre region of the fully reinforced beam

The component strain ε_{xx} was plotted in Figure 6-32 for the fully reinforced beam along the longitudinal axis. As expected, the top region of the beam experienced compressive strain and the bottom region tensile strain. The finger joints in the centre of the beam showed higher tensile strain indicated by the

grey area (off-scale values). The strain ε_{xx} plots of the fully reinforced beam, showed higher compressive strain than the unreinforced beam (see Figure 6-30) because of the effect of CFRP reinforcement. Furthermore, the tensile strain at the bottom region of the fully reinforced beam also showed lower strain than the unreinforced beam at the same applied load 62 kN. These results agree with the findings of Glišović *et al*. (2016) who concluded that beams reinforced with CFRP in the tension region, reduced the strains in the timber, which showed increment of compressive strain and reduction of tensile strain compared to unreinforced beams.

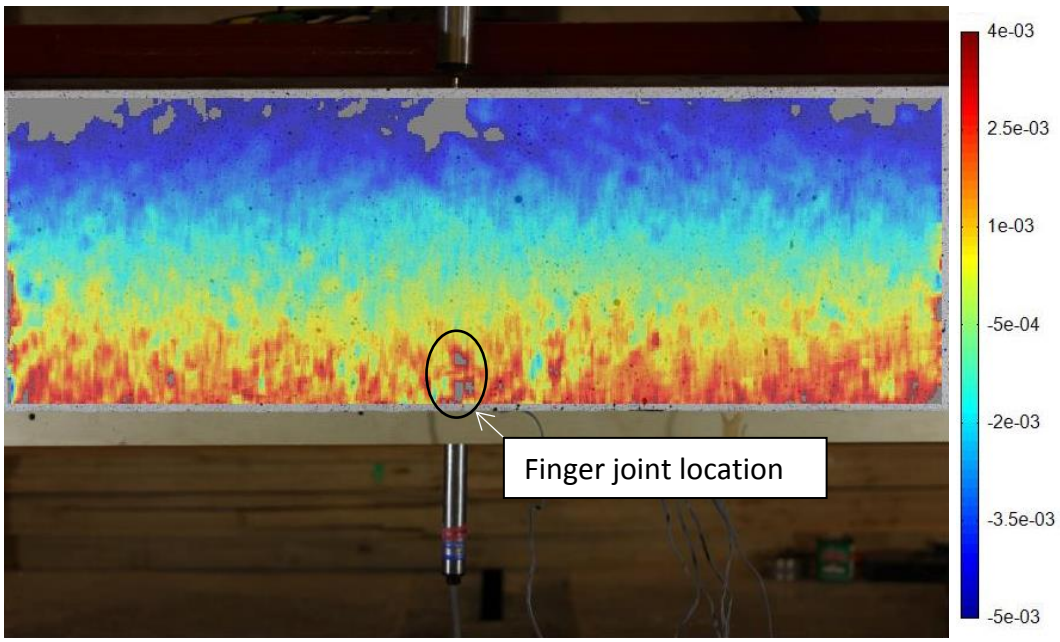

Figure 6-32: Strain ε_{xx} plots at the centre region of fully reinforced beam at applied load 62 kN

6.4 Summary

The results in this chapter showed the influence of CFRP reinforcement on the bending properties of Malaysian Dark Red Meranti glulam beams. The fully reinforced glulam beam, Beam-R showed higher bending strength compared to the unreinforced beam, Beam-U. The beam with partial reinforcement at the finger joints region, Beam-FJ showed the lowest bending strength. Beam-FJ experienced stress concentration at the edge of the CFRP sheet, resulting in

early crack initiation which delaminated the outermost tension layer of the beam. The reduced effective cross-section due to delamination resulted in the reduction of the load-carrying capacity of the beam. Beam-U showed sudden catastrophic tension failure in the bending test indicating brittle failure of the beam. CFRP reinforcement in Beam-R exhibited more ductile behaviour compared to Beam-U.

The failure of the beams was predominantly at the finger joints which was the weakest link in the DRM glulam beam in this study. Beam-U and Beam-R suffered failures initiated at the finger joints of the outermost tension layer unlike Beam-FJ which started to crack at the edge of the CFRP sheet. All the beams showed crack propagation from the outermost tension layer upward to the finger joints in the subsequent laminations and also toward the location of the supports. The strain distribution observed using strain gauges and DIC analysis showed the shifting of the neutral axis of the reinforced beam toward the tension region. Increased of compressive strains and reduction of tensile strains were observed in the reinforced beam compared to the unreinforced beam.

The results in this study showed no significant differences in local modulus of elasticity between the reinforced and unreinforced beams. The interface between the CFRP reinforcement and timber showed no delamination during the bending tests. Post-failure observation showed debonding between the first and second layer of the CFRP and no debonding on the interface between the wood and CFRP sheet of the fully reinforced beam (see Figure 6-14). It can be concluded that the load from the beam was effectively transferred to the CFRP reinforcement.

Chapter 7 Bench-scale fire tests

7.1 Introduction

This chapter investigates the secondary failure of finger joints in DRM glulam beams using a bench-scale fire test. In a standard fire resistance test (BS EN 1365-3:2000), the failure of bond lines in the full size glulam beam resulted in the delamination of the outermost tension layers. This incident was described as a secondary failure which resulted in the exposure of subsequent uncharred inner layers to a severe fire condition. The high cost of testing glulam beams in full-scale standard fire tests has resulted in a lack of published work describing the occurrence of secondary failure. Furthermore, full-scale standard fire tests for glulam beams are time-consuming and may not adequately describe the performance of the beams in a fire situation (Craft *et al*., 2008; Klippel *et al*., 2014). Thus, in this chapter, a simple bench-scale fire test is proposed to investigate the secondary failure of finger joints when tested under conditions similar to the standard fire test.

In a standard fire test, the finger joints at the outermost tension layer of a glulam beam tested in bending experienced tensile stress and will most likely to fail first. Thus a tensile test was used to simulate the behaviour of finger joints in a fire test. A study was conducted by Frangi *et al*. (2012) to evaluate the performance of finger joints at elevated temperature using both tensile and bending tests. They indicated that the tensile tests adequately described the influence of different types of adhesive on the performance of the finger joints when tested at elevated temperature compared to the bending tests. They also concluded that there was no significant correlation between bending strength and the type of adhesive used in their tests.

In general, it is commonly known that the charring rate of wood is used to describe the fire performance of timber structures. Wood properties such as moisture content, density, chemical composition and permeability are known to influence the charring rate of the wood. Furthermore, test conditions such as

direction of burning, thermal exposure and size effect of the test specimens will also affect the charring rate of wood (Friquin, 2011; Cachim and Franssen, 2009).

In this chapter, factors influencing the charring rate such as density, size effect and constant heat flux exposure are discussed using a bench-scale fire test. The aim of this study is to determine the fire performance of DRM finger joints in tension when exposed to a constant heat flux using the bench-scale fire test set-up. The objective is to imitate the behaviour of the finger joints when exposed to sudden high temperature following the secondary failure of the glulam beam in a standard fire test.

7.2 Materials and method

7.2.1 Finger joints preparation

Dark Red Meranti specimens with average density and moisture content of 659 ± 99 kg/m^3 and 14% respectively were used in this study. The DRM was described in detail in Chapter 3. For comparison, additional finger joints were prepared using Spruce with average density and moisture content of 462 ± 92 kg/m^3 and 12% respectively. All the specimens were kept in a conditioning room with temperature of 20°C and relative humidity of 65% prior to the finger-jointing process.

The finger joints were fabricated at SP Wood Building Technology, Sweden because of the availability of a facility to produce 15 mm length finger joints. DRM pieces with cross-section of 51 x 99 mm and with little or no defects were used in the fabrication of the finger-jointed specimens. A manual feed finger cutter was used to cut the profiles of the fingers. The length and pitch of the finger joints were 15 and 3.8 mm respectively which satisfied the requirements of the BS EN 14080:2013 standard. Phenol resorcinol formaldehyde adhesive was used as bonding medium of the finger joints. Additional finger joints were produced using polyurethane (PUR) adhesive for comparison. After bonding of

the finger joints, the specimens were left to cure for two weeks. The finger-jointed specimens were then processed to dimensions of 10 x 42 x 300 mm as shown in Figure 7-1. The number of finger-jointed specimens is listed in Table 7-1 for different types of test condition. To minimise fluctuation in moisture content, the finger-jointed specimens were kept in the conditioning room before being tested.

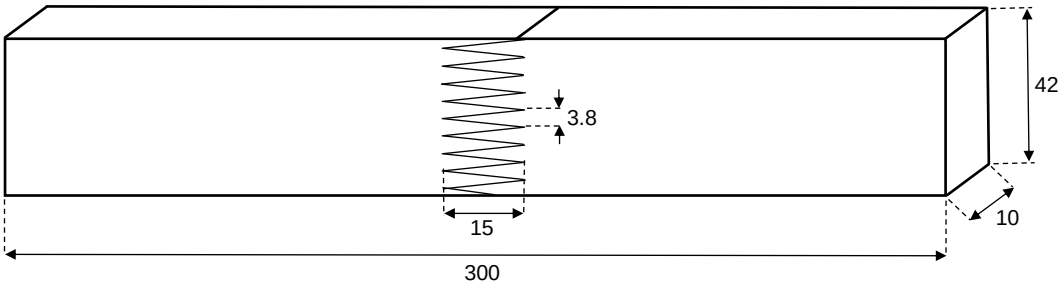

Figure 7-1: Finger-jointed specimen (dimensions in mm)

Table 7-1: Types of test configuration

Test conditions	Species	Adhesives	Quantity
Tensile test in fire	DRM	PRF PUR	10 10
	Spruce	PRF PUR	10 10
Tensile test at ambient temperature	DRM	PRF PUR	10 10
	Spruce	PRF PUR	10 10
Specimens with thermocouples	DRM	PRF PUR	1 1
	Spruce	PRF PUR	1 1
		Total	84

7.2.2 Bench-scale fire tests

The bench-scale fire test set-up was described in detail in Chapter 3. A constant heat flux of 50 kW/m^2 was used in this study. A previous study by Brandon *et al*. (2015) showed that tests exposed with 50 kW/m^2 incident radiant heat flux resulted in a charring depth of approximately 40 mm in one hour. This is similar

to the expected charring depth in a standard fire resistance tests. The 50 kW/m^2 heat flux also corresponds well with the standard time-temperature curve for the first 30 to 40 minutes of the fire resistance tests in EN 1363-1 and ISO 834 (Bregulla, 2003; Naughton *et al*., 2014; Tsantaridis *et al*., 1999, Tsantaridis and Östman, 1998).

Additional four specimens (see Table 7-1) were prepared and attached with thermocouples to measure the temperature profiles at different depths. Type K fiber glass insulated thermocouples with diameter of 1.5 mm were positioned horizontally, parallel to the isotherm (Figure 7-2). The thermocouples were connected to a datalogger and the specimens were tested without applying any load during the fire test. Thermocouple T1 was positioned at a distance of 5 mm from the exposed top surface and the subsequent thermocouples (T2 to T8) were located every 5 mm across the specimen. The tip of the thermocouples was inserted into holes which were drilled 5 mm into the specimen's surface to measure the internal temperature of the specimens. The thermocouples were also positioned alternately so that the measurement of the temperature could be uniformly measured to represent the whole depth of the specimens.

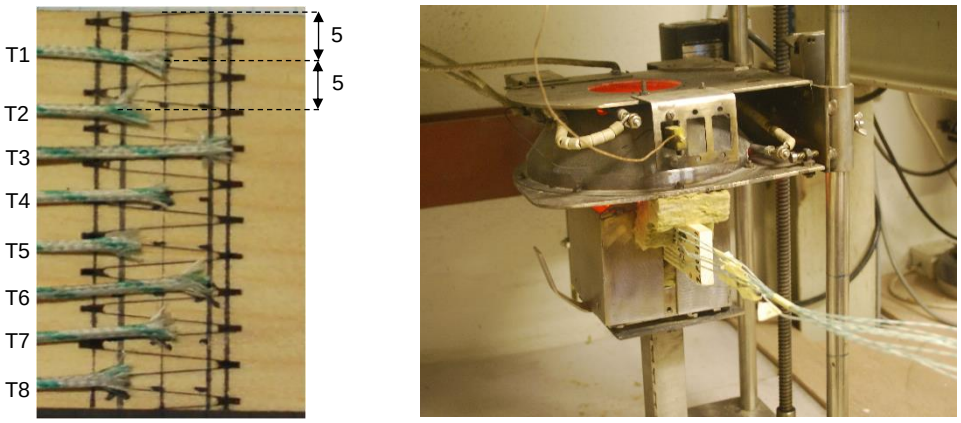

Figure 7-2: Specimens with attached thermocouples (measurements in mm)

During the bench-scale fire test, the specimens' ignition time and the time to reach failure were recorded. The residual cross-section of the tested specimens was measured after completion of the tests. One-dimensional charring rate (β) and residual tensile strength were calculated using the equations below:

One dimensional charring rate (mm/min), $\beta = \frac{t_{char}}{\text{TTF}}$ (Eq. 7-1)

Residual tensile strength (N/mm^2), $f_{t,residual} = \frac{F_{2.5}}{A_{residual}}$ (Eq. 7-2)

Key:

t_{char}	charred depth, (mm)
TTF	time to failure, (min)
$F_{2.5}$	applied load, (2.5kN)
$A_{residual}$	residual cross section (mm^2)

7.3 Results and discussion

The typical failures of the DRM and Spruce finger-jointed specimens in the bench-scale fire tests are shown in Figure 7-3. Most of the specimens showed failure along the glue lines as shown in Figure 7-3a. This failure indicates the influence of adhesives in the fire performance of the finger-jointed specimens. Other specimens exhibited fracture of fingers and a mixture of glue line and wood failure as shown in Figures 7-3b and 7-3c respectively. A few of the specimens showed failures along the slope of grain (Figure 7-3d) and near to some knots. The fracture in the wood instead of the glue lines of the finger joints indicates higher tensile strength of the joints compared to the solid wood when tested in a fire condition (Klippel and Frangi, 2017).

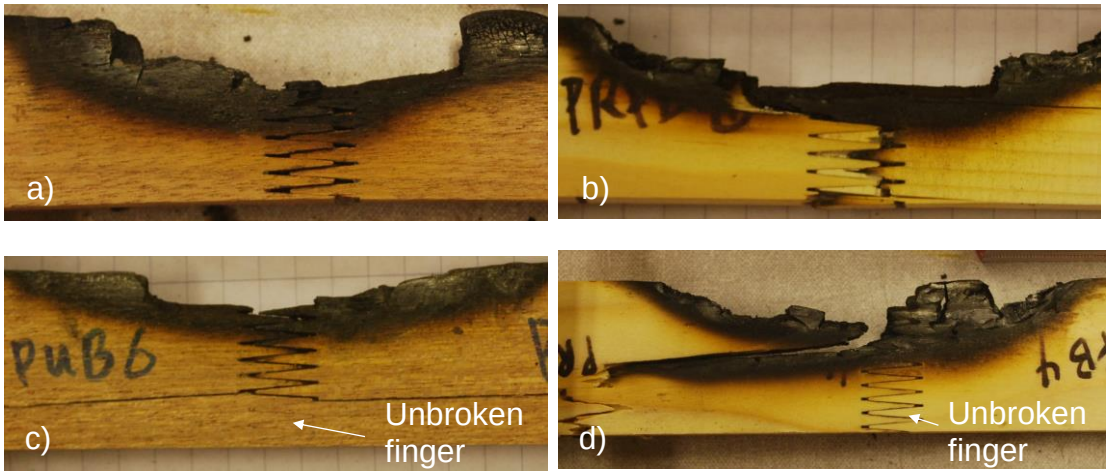

Figure 7-3: Typical failures of finger-jointed specimens a) failure along the glue lines; b) failure of the fingers; c) mixture of joint and wood failure; d) wood failure

7.3.1 Fire performance of finger joints

The fire performance of PRF finger-jointed specimens in the bench-scale fire tests was better than the finger-jointed specimens bonded with PUR as shown in Table 7-2. The average residual cross-section (A_r) of PRF finger-jointed specimens was lower than the specimens bonded with PUR adhesive. This resulted in the higher average residual strength of PRF finger-jointed specimens compared to the PUR for both DRM (33%) and Spruce (20%) specimens. The average time to failure (TTF) for PUR finger joints was also lower, with values of 57% (DRM) and 72% (Spruce) of the TTF measured for finger joints bonded with PRF adhesive. From these results, it can be concluded that the specimens finger-jointed with PRF adhesive exhibited better fire performance compared to the PUR finger joints. Figure 7-4 shows the residual tensile strength plots as a function of density for specimens finger-jointed with PRF and PUR.

Table 7-2: Fire performance of the finger-jointed specimens

Species	Adhesives		Time to failure, TTF (min)	Residual cross-section, A_r (mm^2)	Charring rate, β (mm/min)	Ignition time (min)	Residual tensile strength (N/mm^2)
Spruce	PRF	Average	7.59	258.8 (61*)	2.03	0.37	9.70
		SD	1.18	17.26	0.19	0.08	0.58
Spruce	PUR	Average	5.47	310.3 (73*)	1.99	0.38	8.10
		SD	0.98	22.21	0.26	0.16	0.60
DRM	PRF	Average	11.0	244.2 (58*)	1.61	0.48	10.3
		SD	2.31	10.11	0.37	0.19	0.41
DRM	PUR	Average	6.24	330.3 (76*)	1.50	0.47	7.72
		SD	0.89	13.65	0.09	0.14	0.31

*Ratio to the original cross-section (in percent)

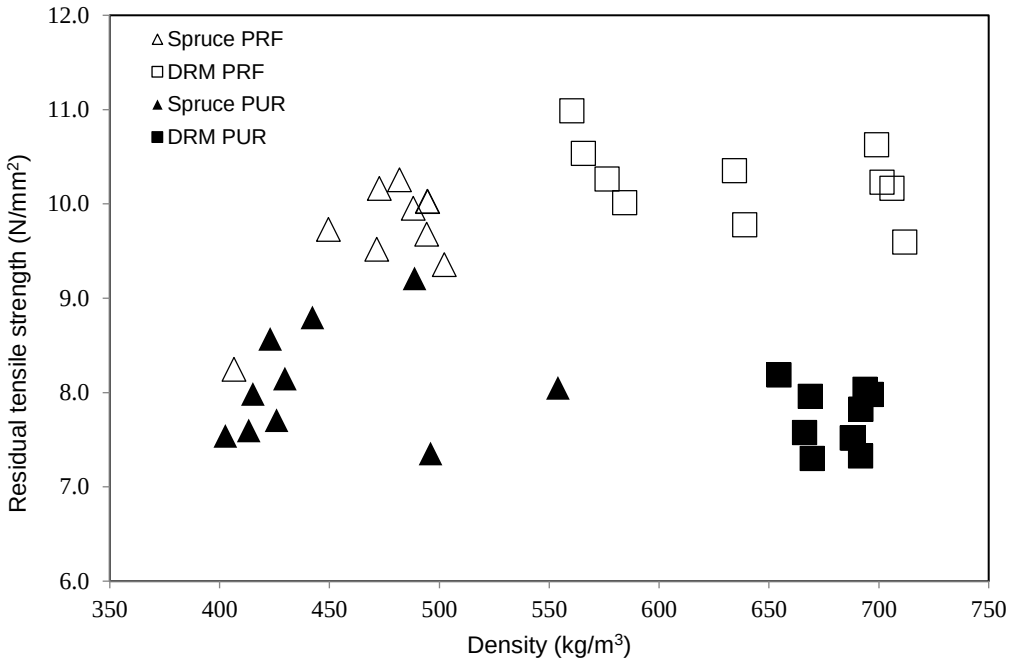

Figure 7-4: Residual tensile strength of finger-jointed specimens of DRM and Spruce as a function of density

The PUR adhesive in this study showed a worse fire performance because it may not have been fully cross-linked and might have been expected to fail viscoelastically at elevated temperature compared to the highly cross-linked PRF adhesive. Other studies also reported that PRF adhesives exhibited better fire performance compared to PUR adhesives. Studies by König *et al*. (2008) indicated that the moment resistance of glulam beams with PUR finger joints was 70 to 80% of the beams consisted of PRF finger joints when tested in fire conditions. Nevertheless, Klippel *et al*. (2014) reported that one of the PUR adhesives in their study which was specially formulated to resist higher temperature under load showed comparable performance to PRF adhesives when tested in tension at elevated temperature. They concluded that structural PRF finger joints might not always perform better in fire conditions when compared to finger joints bonded with PUR adhesives.

7.3.2 Factors affecting the charring rates

In general, DRM specimens have higher density than Spruce specimens which resulted in the higher charring rates of Spruce for both PRF and PUR finger-jointed specimens compared to the DRM (Figure 7-5). From the graph, several DRM specimens with lower density values can be seen showing similar charring rates to the Spruce specimens. A one-way analysis of variance was used to examine whether there was a significant difference between the charring rates of DRM and Spruce specimens. The results indicate a statistically significant difference at 95% confidence level for charring rate values between Spruce and DRM specimens. The graph also exhibited an increasing trend for charring rate values with the reduction in density of the specimens. Previous studies reported that wood with higher density exhibited lower charring rate values (Yang *et al*., 2009; Njankouo *et al*., 2004; Cachim and Franssen, 2010).

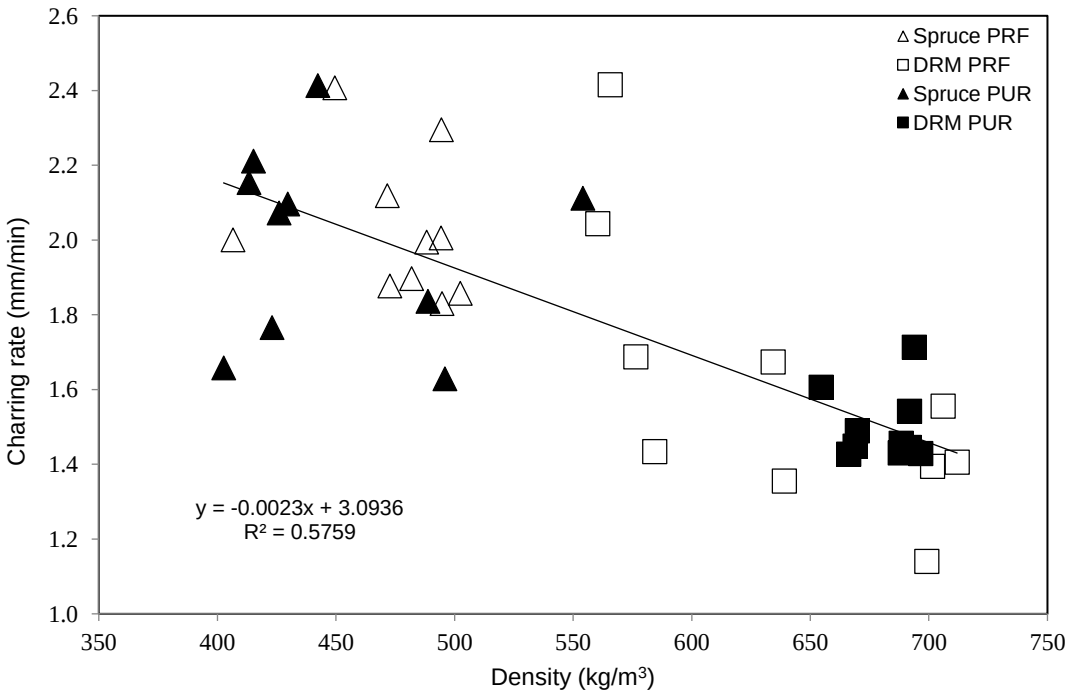

Figure 7-5: Charring rates as a function of density for finger-jointed specimens

ANOVA test results showed no significant difference between the charring rate values of specimens finger-jointed with different adhesives, namely PUR and PRF, for the same wood species. These findings indicate that the charring rate in this bench-scale fire test is not influenced by the different adhesives used to

bond the finger joints. The fact that the bonding area of the joints were small compared to the overall cross-section of the specimen explained the insignificant influence of the adhesives on the charring rate values.

The test specimens in this study exhibited higher charring rates compared to the notional and one-dimensional charring rates published in BS EN 1995-1-2:2004. The published charring rates are taken as constant with time in the simplified design methods although in reality, the charring rate is not linear (Cachim and Franssen, 2009). In practice, the charring rate was often higher initially and then decreased after the build up of a charred layer that insulates and protects the inner unburnt wood. The charring rate finally stabilises to a constant rate after a period of time. Majamaa (1991) (cited by Friquin, 2011, p.317) reported that specimens with 40 and 80 mm thickness require 10 and 30 minutes respectively for the charring to achieve a constant rate. The author concluded that specimens with different thicknesses require different time periods for the charring to achieve a constant rate. In this study, the average TTF of the specimens with nominal thickness 42 mm was between 5 to 11 minutes. It can be concluded that the measurement of charring rate was made in the early stages of fire, thus the built-up charred layer was insufficient to insulate the inner unburnt wood of the specimens, resulting in higher charring rates.

The high charring rates in this study could also be attributed to the use of constant heat flux compared to using a time-increasing heat flux (Lizhong *et al*., 2008). The bench-scale fire in this study was purposely structured to imitate the condition of secondary failure of a glulam beam in fire where the inner layer of the tension region was exposed to a sudden constant heat flux. Thus, a constant heat flux was selected rather than applying the time-increasing heat flux in the fire tests.

The size of the specimens may also influence the charring rate of the wood. In this study, the specimens were considerably smaller compared to the glulam beams in a standard fire test. Since the objective of using this bench-scale fire test was to imitate the full-scale standard fire test with a simpler and faster

method, it was necessary to use a small-sized specimen. Frangi & Fontana (2003) reported that the bottom region of beams exposed to fire on three sides showed increased charring rate when the residual cross-section reduced to a certain minimum value. They also concluded that if the residual cross-section was larger than 40 by 60 mm, the constant charring rate in the simplified calculation method of fire resistance for structural members could be used as a reference. Since the size of the specimens in the tests reported here are small, the charring rate was expected to be high and not so constant.

ANOVA test results showed a statistically significant difference between the average ignition time of DRM and Spruce specimens. From Table 7-2, the average ignition time of DRM was approximately 20% higher than Spruce specimens. White (2000) indicated that the ignition time was correlated to the density of various hardwood species. The findings correspond well with the results in this study where the higher density of DRM specimens resulted in higher ignition time while Spruce specimens with lower density ignited more easily.

7.3.3 Temperature profiles of DRM and Spruce specimens

The objective of this section was to observe the temperature increment along the depth of the specimens during fire exposure. Thus, no load was applied to the specimens during the bench-scale fire tests. Figure 7-6 shows the temperature profiles of DRM and Spruce specimens. From the graph, the temperature profiles of Spruce specimens exhibited less time to reach a charring temperature of 300°C (timber turns into char at this temperature (Brandon *et al*., 2014; Klippel *et al*., 2013)) compared to the DRM specimens. It can be concluded that the different wood species, or specifically the different material densities, influence the charring rate in this bench-scale fire test.

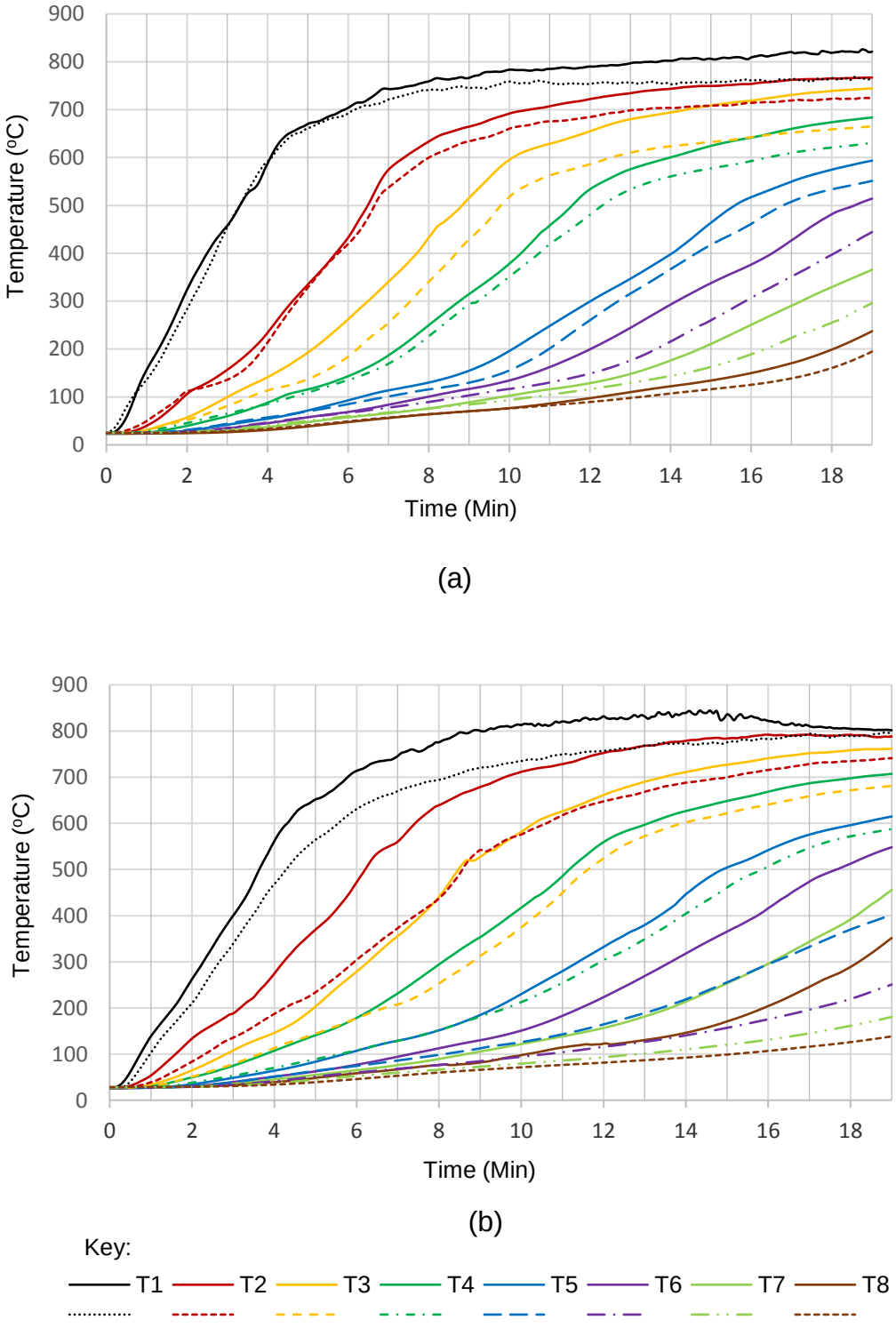

Figure 7-6: Temperature profiles of Spruce (solid lines) and DRM (dash lines) specimens finger-jointed with (a) PRF; (b) PUR

The char depths of the specimens were determined based on the positions of the thermocouples with the time taken to reach the charring temperature of 300°C (Figure 7-7). From the graph, the relationship is seen to be nonlinear indicating non-constant charring rates. It can be seen that the charring rates were higher initially and reduce after a char depth of 20 mm was reached for DRM finger-jointed specimens bonded with PRF and PUR adhesives. Meanwhile, Spruce specimens showed a reduced charring rate after char depth of 20 mm was reached for finger joints bonded with PUR adhesive. Spruce finger-jointed specimen bonded with PRF adhesive showed no trend of reduced char rate in the graph.

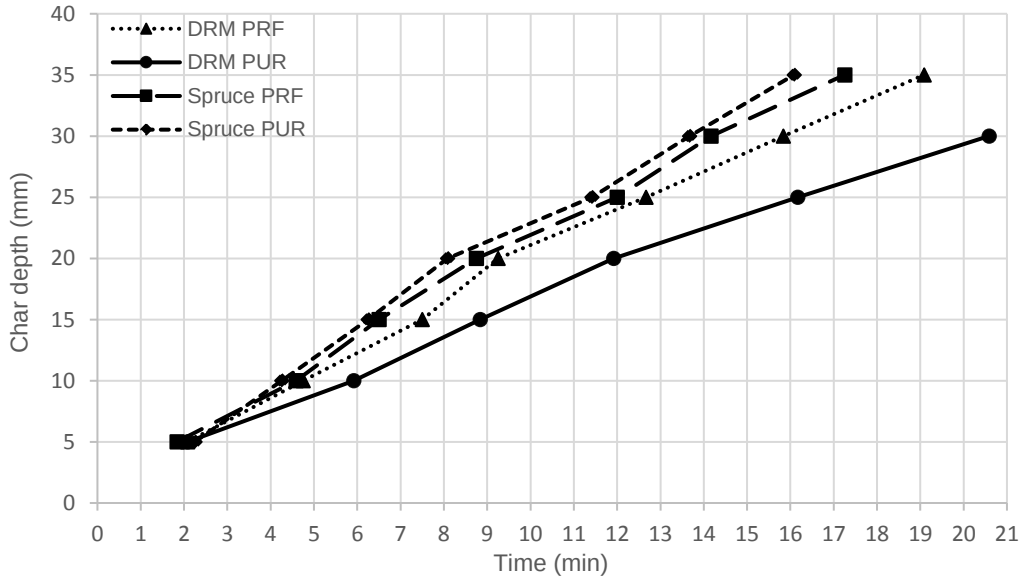

Figure 7-7: Char depth as a function of time at a temperature of 300°C

7.3.4 Influence of density on the tensile strength of finger joints tested at ambient temperature

Figure 7-8 shows the typical failures of the finger-jointed specimens tested at ambient temperature. Comparing the average tensile strength, DRM finger-jointed specimens bonded with PRF (72.8 N/mm^2) and PUR (72.9 N/mm^2) were higher than the Spruce specimens bonded with PRF (43.1 N/mm^2) and PUR (41.1 N/mm^2) adhesives. ANOVA test results indicated a statistically significant difference between the tensile strength of DRM and Spruce finger-jointed

specimens. Figure 7-9 shows the distribution of the tensile strength of the finger joints tested at ambient temperature as a function of density. From the graph, it can be concluded that there exists a positive relationship between the tensile strength and the density of the specimens.

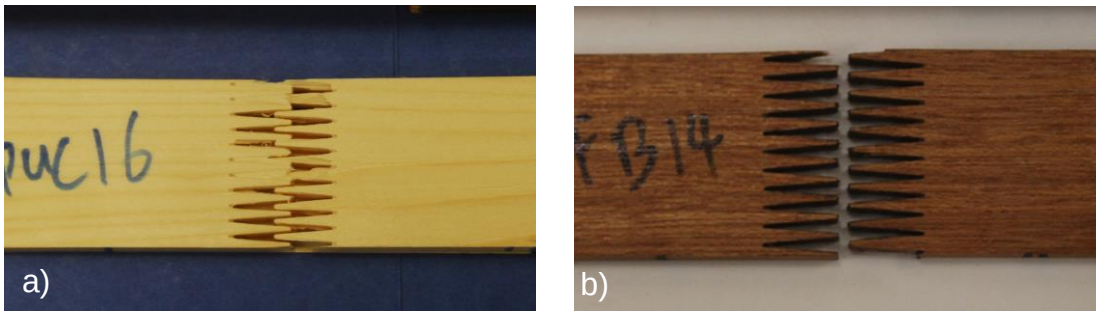

Figure 7-8: Typical tensile failures of specimens at ambient temperature
a) Spruce; b) DRM

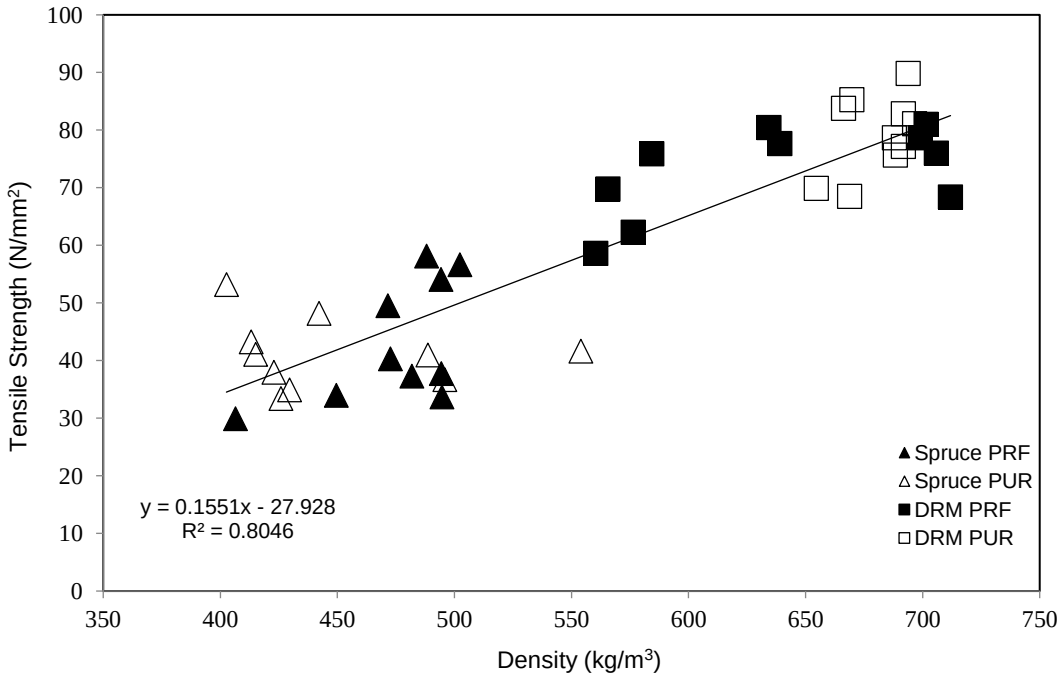

Figure 7-9: Tensile strength as a function of density for finger joints tested at ambient temperature

ANOVA test results showed no significant difference between the tensile strength of the finger joints bonded with PRF and PUR for the same species when tested at ambient temperature. Meanwhile, DRM specimens with PRF finger joints exhibited better performance than DRM specimens with PUR finger

joints in the bench-scale fire tests, indicating the influence of temperature on the tensile strength of the finger joints. Thus, the proposed bench-scale fire test in this study is suitable for evaluating and differentiating the fire performance of the finger-jointed specimens bonded with PRF and PUR when tested in a fire condition.

7.4 Summary

In this study, a bench-scale fire test was used to provide a simpler and less costly set-up with faster completion time as an alternative to the standard fire resistance tests. The finger-jointed specimens in this experiment were exposed to sudden constant heat-flux so as to imitate the secondary failure of a glulam beam in the standard full-scale fire test. Comparison made using the time to failure and residual strength results of the finger-jointed specimens indicated that the finger-jointed specimens bonded with PRF adhesive showed better fire performance compared to the PUR adhesive.

The determination of charring rate is important for accurately calculating the depth of the residual cross-sections, so that the fire design of timber structures can be optimised. In this experiment, DRM finger-jointed specimens exhibited lower charring rate than Spruce because of the higher density of the DRM wood. Overall, the charring rate results in the bench-scale fire test showed higher char rates than the published values in other studies. The influence of constant heat flux, in contrast to time-increasing heat flux, and the smaller specimen size of this study might contribute to the higher charring rates observed. As explained in Section 7.3.2, the higher charring rates were caused by the lack of an insulating charred layer which would have protected the inner layers of the unburnt wood.

The tensile strength of the DRM finger-jointed specimens tested at ambient temperature was higher than the Spruce finger-jointed specimens. For the same wood species, the finger joints bonded with PRF did not show any significant difference in tensile strength from the PUR finger-jointed specimens.

Meanwhile, results from the bench-scale fire test showed that PRF finger-joints have a higher residual tensile strength than PUR finger-joints. Thus, it can be concluded that temperature influences the tensile strength of finger-jointed specimens bonded with different types of adhesive. Furthermore, the proposed bench-scale fire test was able to evaluate the performance of finger joints under a fire condition and was able to differentiate the quality of finger-jointed specimens bonded with different adhesives. Nevertheless, this bench-scale fire test needs to be further investigated and compared to the standard full-scale fire test so that a correlation between these methods can be determined. Importantly, this correlation also needs to compare the process of secondary failure of the glulam beam in a fire test.

Chapter 8 Conclusions and future work

8.1 Conclusions

The lack of understanding of the structural performance of the components of glulam beams, including finger joints and laminations, discourages the Malaysian timber industries from venturing into the production of glulam beams for structural uses using local hardwood species. This thesis has attempted to fill this gap by generating essential technical information required to produce and test glulam beams produced from a local Malaysian species, specifically Dark Red Meranti. The findings of the experimental work are summarised below.

8.1.1 Mechanical properties of finger joints

Factors affecting the strength of the finger joints were investigated in this study. The finger-jointed DRM specimens tested in bending achieved an average joint efficiency of 77% compared to the solid DRM specimens. Higher end pressures of 12.5 and 15 N/mm^2 produced finger joints with higher bending and tensile strengths compared to the specimens finger-jointed with an end pressure of 10 N/mm^2. Different specimen widths and the orientation of finger joints (vertical and horizontal joints with similar bonding area) did not affect the bending strength of the finger-jointed specimens. The bending stiffness of the finger-jointed DRM specimens showed no significant difference from the solid specimens.

The tensile strength of the finger joints was not influenced by the bonding medium (PRF and epoxy adhesives), indicating a good bonding performance with most failures involving pulled-out wood fibres and finger fractures. The finger-jointed DRM specimens with finger length of 15 mm possessed higher tensile strength than specimens with a finger length of 10 mm. As expected, the compressive strength of the finger-jointed DRM specimens, bonded with either

PRF or epoxy adhesives, showed no significance difference from the solid specimens.

Overall, the finger-jointed DRM specimens had higher bending and compressive strengths compared to Spruce. Higher end pressures were required to produce stronger finger jointed DRM specimens but a lower end pressure was sufficient to produce strong Spruce finger joints. All these factors must be taken into consideration when attempting to produce strong structural finger joints using Malaysian hardwood.

8.1.2 Bonding strength of laminations

The shear strength of DRM specimens bonded with PRF was investigated in this study. The findings showed that higher cramping pressures of 0.8 and 0.96 N/mm^2 were able to produce specimens with good bonding performance compared to the application of a lower cramping pressure of 0.64 N/mm^2 which did not meet the minimum wood failure requirement recommended by BS EN 14080:2013. The shear strength of the glue lines exhibited a positive trend as a function of the density of DRM block shear specimens. This trend agrees well with the findings reported by other studies where shear strength of glue lines increased with an increase in wood density (Frihart and Hunt, 2010; Selbo, 1975).

The minimum requirements recommended by BS EN 14080:2013 related to wood failure percentages and shear strength (see Table 5-4) can be further improved to better suit the DRM species. A revised minimum requirement for DRM species was proposed and could be validated by increasing the number of specimens and including higher variation in the density of DRM specimens.

The shear strengths of the DRM specimens in this study were lower than the published results in other studies. The limited number of specimens tested may not have been sufficient to determine a realistic average shear strength for the DRM species. The large variation of DRM density is likely to have contributed to

the differences in the shear strength results. Furthermore, the block shear specimen configurations such as the offset cut (see Figure 5-10) may induce crack initiation in the wood and reduce the shear strength. Thus, improvement is needed in the preparation of specimens and test set-up so that the factors which introduce variation in shear strength can be controlled.

8.1.3 Full size glulam beam tests

The glulam beams in this study were manufactured in the laboratory in accordance with the minimum production requirements of the BS EN 14080:2013 standard in order to produce beams with quality equivalent to commercial production. The fully reinforced beam exhibited ductile behaviour and higher bending strength compared to the unreinforced beam. The beam with reinforcement at the finger joints exhibited early crack initiation at the edge of a CFRP sheet, resulting in the lowest bending strength of all the beams.

In general, the beams showed predominant failures at the finger joints with cracks propagating between the joints of subsequent layers. Post-failure observations indicated that the failure of the unreinforced and fully reinforced beams initiated from the failure of finger joints on the outermost tension layer. No signs of cracking or failures were observed during the tests prior to the catastrophic failure on the tension face of the beams except for the beam with reinforcement at the finger joints. The beam with reinforced finger joints displayed premature crack initiation at the edge of the CFRP sheet that subsequently delaminated the outermost tension layer as the load increased. Nevertheless, this beam still exhibited catastrophic tensile failure when the ultimate load was reached.

From the strain analysis, the neutral axis of the reinforced beam shifted towards the tension region of the beam when tested in bending. There was no significant difference in bending stiffness between the unreinforced and reinforced beams. There was also no debonding of the CFRP sheet from the surface of the wood during the bending test of the fully reinforced beam. Post-failure observation

showed debonding of the interface between the first and second layer of the CFRP and no debonding from the surface of the wood, indicating an effective transfer of load from the beam to the CFRP reinforcement during the bending test.

8.1.4 Bench-scale fire tests

A bench-scale fire test was proposed in this study to provide an alternative method which is faster, simpler and less costly compared to a full-scale standard fire test. The bench-scale fire test was set up to imitate the secondary failure of finger joints when tested under conditions similar to the full-scale standard fire test of a glulam beam. The bench-scale fire tests showed that the DRM finger-jointed specimens have a lower charring rate compared to Spruce. The specimens finger-jointed with PRF adhesive showed better fire performance than the PUR adhesive indicating the influence of temperature on the tensile strength of specimens bonded with different adhesives. It can be concluded that the bench-scale fire test was able to evaluate and differentiate the quality of finger joints bonded with different types of adhesive when tested in fire conditions.

The charring rate results in this study are higher when compared to the published values from other studies. Factors affecting the char rates such as constant heat in contrast to time-increasing heat-flux and smaller specimen size were discussed in this study. The higher charring rate also agrees well with findings from other studies which indicated that the charring rate is not linear and exhibited higher values initially before decreasing to a constant rate after the build up of a charred layer that insulates and protects the inner unburnt wood.

8.1.5 Major outcomes of the thesis

- The demonstration of standard production requirements to produce and test finger-joints, laminations and glulam beams will benefit the manufacturers of glulam beams, especially in Malaysia. The much needed technical information gathered in this study will act as a guide for further research using less-utilised tropical hardwood species for structural uses.

- Factors influencing the strength of the components of glulam beams reported in this study will significantly improve the understanding of the mechanical properties of finger joints, bonding strength of laminations and behaviour of the glulam beams in bending for specimens produced from local Malaysian hardwood, specifically Dark Red Meranti timber.

- The results from the bench-scale fire test were promising and the set-up was able to evaluate the fire performance of finger joints in secondary failure. Furthermore, the bench-scale fire test was able to differentiate the quality of finger joints produced with different types of adhesive, which will prove useful for future investigations using the various types of adhesive available in the market to produce structural finger joints.

8.2 Recommendations for future work

The less-utilised Malaysian species, especially the fast-growing plantation species, such as *Acacia mangium* and *Khaya ivorensis*, are in abundance and the small log diameter makes these species suitable for use in the production of glulam beam. Future studies should evaluate the various species from plantation forests to increase the database of hardwood species suitable for producing structural timber products, specifically glulam beams.

The mechanical properties of the finger joints and bonding strength of the DRM specimens would be made more representative by increasing the number of specimens. The testing of DRM specimens from different sources to reflect the

huge variation of density within the species will also improve the research data since density plays a significant role in influencing the mechanical properties of timber.

It would also be interesting to evaluate the shear strength of glue lines produced from wood species with higher density since denser wood was reported to be difficult to glue and may not exhibits good bonding performance (Frihart and Hunt, 2010). The modification factor k_v recommended by BS EN 14080:2013 for the calculation of the shear strength could be improved by increasing the number of block shear specimens with different sheared areas. Gaspar *et al*. (2017) reported that the factor k_v may not be correct for specimens with glue lines above a shear strength of 15 N/mm^2.

Bonding performance under different service conditions is an important indication of the structural performance of glulam beams. The standard testing requirements to determine the bonding strength of glue lines with delamination test are specified in BS EN 14080:2013. Future tests incorporating this delamination test will prove useful for determining the suitability of the glulam beams for use in different service classes, especially for high density wood which exhibits higher swelling and shrinking with changes in moisture content compared to low density wood (Frihart and Hunt, 2010).

In practice, PRF adhesive is commonly utilized in the production of finger joints and beams. Alternatively, polyurethane adhesive, melamine urea formaldehyde or emulsion polymer isocyanate adhesives could be used in future studies depending on their availability and price. Frangi *et al*. (2012) noted that melamine urea formaldehyde adhesive is becoming popular due to its low price and shorter cure time. One component polyurethane adhesive is also attracting much interest because it contains no formaldehyde and cures quickly at room temperature.

Carbon fibre reinforced polymer used as a reinforcement will enhance the performance of glulam beams. Apart from strengthening glulam beams and reducing material costs by reducing the section thickness of unreinforced

beams, CFRP can prevent surface checking of timber exposed to heat and high humidity in tropical countries such as Malaysia. Furthermore, CFRP may also be able to protect the inner wood from termite attack and may also act as an insulator to improve the glulam's fire performance. Thus, it is pertinent to investigate the bonding compatibility of CFRP with wood and to ascertain termite and moisture resistance with further tests. It would be also interesting to evaluate the behaviour of glulam beams with CFRP reinforcement when tested under fire conditions.

Further bench-scale fire tests are required to improve correlation with the standard full-scale fire test. Further fire tests using the bench-scale set-up are needed to evaluate the effect of thicker specimens, different material densities, time-increasing heat flux and test configurations on the charring rates of the solid and finger-jointed specimens. Furthermore, the secondary failure of the glulam beam under fire conditions should be further investigated using both full-scale and bench-scale fire tests.

References

Ahmad, M., Muhammed, S., Mohd Noh, M.S. and Nordin, K., 1997. The strength of finger joints in three Malaysian timbers – meranti, kempas and keruing. *Journal of Tropical Forest Products 3*, pp.158-164.

Ahmad, Y., 2013. Ductility of timber beams strengthened using fiber reinforced polymer. *Journal of Civil Engineering and Architecture*, *7*(5), pp.535-544.

Ahmad, Z., Chen, L.W., Razlan, M.A. and Noh, N.M., 2016. The effect of finger-joint profile and orientation on the strength properties of timber beam for selected Malaysian timber species. In: *Advances in Civil, Architectural, Structural and Constructional Engineering: Proceedings of the International Conference on Civil, Architectural, Structural and Constructional Engineering*. Busan, South Korea, pp.121-124.

Aicher, S., Höfflin, L. and Behrens, W., 2001. A study on tension strength of finger joints in beech wood laminations. *Otto-Graf-Journal*, 12: 169-186.

Aicher, S. and Ohnesorge, D., 2011. Shear strength of glued laminated timber made from European beech timber. *European Journal of Wood and Wood Products*, 69(1), pp.143-154.

AITC Test T103:2007. Calibration of clamping system: Bolts or screw type jacks. *Test Methods for Structural Glued Laminated Timber*. American Institute of Timber Construction.

Alamsyah, E. M., Yamada, M. and Taki, K., 2008. Bondability of tropical fast-growing tree species III: Curing behavior of resorcinol formaldehyde resin adhesive at room temperature and effects of extractives of Acacia mangium wood on bonding. *Journal of Wood Science*, 54(3), pp.208-213.

Alhayek, H. and Svecova, D., 2012. Flexural stiffness and strength of GFRP-reinforced timber beams. *Journal of Composites for Construction*, 16(3), pp.245-252.

ANSI A190.1-2012:2013. *Standard for wood products – Structural glued laminated timber*. American National Standards Institute.

Archila, H.F., Brandon, D., Ansell, M.P., Walker, P. and Ormondroyd, G.A., 2014. Evaluation of the mechanical properties of cross laminated bamboo panels by digital image correlation and finite element modelling, In: *Proceedings of the 11th World Conference on Timber Engineering (WCTE 2014)*. Quebec City, Canada, pp.8.

Ayarkwa, J., Hirashima, Y., Sasaki, Y. and Yamasaki, M., 2000. Influence of finger-joint geometry and end pressure on tensile properties of three finger-jointed Tropical African Hardwoods. *Southern African Forestry Journal*, 188, pp.37-49.

Azlan, H.M., Ahmad, Z., Ibrahim, A. and Hassan, R., 2013. Behaviour of kempas timber beam strengthened with CFRP and steel plates under bending. In: *IEEE Business Engineering and Industrial Applications Colloquium (BEIAC),* pp.483-488.

Bacher, M., 2008. Comparison of different machine strength grading principles. In: *Proceedings of the Conference in COST E53*. Delft, Netherlands, pp.183-193.

Baillères, H., Hopewell, G., Boughton, G. and Brancheriau, L., 2012. Strength and stiffness assessment technologies for improving grading effectiveness of radiata pine wood. *BioResources*, 7(1), pp.1264-1282.

Barboutis, I., 2007. Bending strength of the finger jointed chestnut wood. In: Bejo, L. (Ed.), *Proceedings of 3rd European Conference on Hardwood,*

Hardwood Research and Utilization in Europe: The Beauty of Hardwood. University of West Hungary, pp.5-11.

Barrett, D., Lam, F., Anastas, H. and Chen, Y., 2008. Comparison of machine grading methods for Canadian Hemlock. In: *Proceedings of the 10th World Conference on Timber Engineering.* Miyazaki, Japan, Vol. 2, pp.629-634.

Benham, C., Holland, C. and Enjily, V., 2003. Guide to machine strength grading of timber. BRE Digest 476, pp.12.

Boström, L., 1999. Determination of the modulus of elasticity in bending of structural timber – comparison of two methods. *European Journal of Wood and Wood Products*, 57(2), pp.145-149.

Brandon, D., Ansell, M.P., Harris, R., Walker, P. and Bregulla, J., 2014. Modelling of non-metallic timber connections at elevated temperatures. In: Aicher, S., Reinhardt H.-W. and Garrecht, H. (Eds.), *Materials and Joints in Timber Structures*. Springer Netherlands, pp.231-241.

Brandon, D., Maluk, C., Ansell, M.P., Harris, R., Walker, P., Bisby, L. and Bregulla J., 2015. Fire performance of metal-free timber connections. In: *Proceedings of the Institution of Civil Engineers: Construction Materials*, 168(4), pp.173-186.

Bregulla, J., 2003. *Investigation into the fire and racking behaviour of structural sandwich panel walls – A methodology to assess load bearing sandwich panel in fire*. PhD thesis. University of Surrey, UK.

BS 4978:2007+A1:2011. *Visual strength grading of softwood – Specification*. BSI.

BS 5756:2007+A1:2011. *Visual strength grading of hardwood – Specification*. BSI.

BS EN 301:2017. *Adhesives, phenolic and aminoplastic, for load-bearing timber structures – Classification and performance requirements*. BSI.

BS EN 302-5:2013. *Adhesives for load-bearing structures – Test methods, Part 5: Determination of maximum assembly time under referenced conditions*. BSI.

BS EN 302-6:2013. *Adhesives for load-bearing timber structures – Test methods, Part 6: Determination of the minimum pressing time under referenced conditions*. BSI.

BS EN 302-7:2013. *Adhesives for load-bearing timber structures – Test methods, Part 7: Determination of the working life under referenced conditions*. BSI.

BS EN 384:2016. *Structural timber – Determination of characteristic values of mechanical properties and density*. BSI.

BS EN 408:2010+A1:2012. *Timber structures – Structural timber and glued-laminated timber – Determination of some physical and mechanical properties*. BSI.

BS EN 1365-3:2000. *Fire resistance tests for loadbearing elements, Part 3: Beams*. BSI.

BS EN 1995-1-2:2004. *Eurocode 5, Design of timber structures, Part 1-2: General – Structural fire design*. BSI.

BS EN 13183-1:2002. *Moisture content of a piece of sawn timber – Part 1: Determination by oven dry method*. BSI.

BS EN 14080:2013. *Timber structures – Glued laminated timber and glued solid timber – Requirements*. BSI.

BS EN 14081-2:2010+A1:2012. *Timber structures – Strength graded structural timber with rectangular cross section – Part 2: Machine grading; additional requirements for initial type testing*. BSI.

BS EN 14358:2016. *Timber structures – Calculation and verification of characteristic values*. BSI.

BS EN 15416-4:2017. *Adhesives for load bearing timber structures other than phenolic and aminoplastic – Test methods – Part 4: Determination of open assembly time under referenced conditions*. BSI.

BS EN 15416-5:2017. *Adhesives for load bearing timber structures other than phenolic and aminoplastic – Test methods – Part 5: Determination of minimum pressing time under referenced conditions.* BSI.

BS EN 15425:2017. *Adhesives – One component polyurethane for load bearing timber structures – Classification and performance requirements*. BSI.

BS EN 15497:2014. *Structural finger jointed solid timber – Performance requirements and minimum production requirements*. BSI.

BS EN 16254:2013+A1:2016. *Adhesives – Emulsion polymerized isocyanate (EPI) for load-bearing timber structures – Classification and performance requirements*. BSI.

BS EN 16737:2014. *Structural timber – Visual strength grading of tropical hardwood*. BSI.

BS ISO 11003-2:2001. *Adhesives – Determination of shear behaviour of structural adhesives – Part 2: Tensile test method using thick adherends*. BSI.

BS ISO 13061-2:2013. *Physical and mechanical properties of wood – Test methods for small clear specimen, Part 2: Determination of density of physical and mechanical tests*. BSI.

Bustos, C., Beauregard, R., Mohammad, M. and Hernández, R.E., 2003a. Structural performance of finger-jointed black spruce lumber with different joint configurations. *Forest Products Journal*, 53(9), pp.72-76.

Bustos, C., Mohammad, M., Hernández, R.E. and Beauregard, R., 2003b. Effects of curing time and end-pressure on the tensile strength of finger-jointed black spruce lumber. *Forest Products Journal*, 53(11/12), pp.85-89.

Bustos, C., Hernández, R.E., Beauregard, R. and Mohammad, M., 2004. Influence of machining parameters on the structural performance of finger-joined black spruce. *Wood Fiber Science*, 36(3), pp.359-367.

Bustos, C., Hernández, R.E., Beauregard, R. and Mohammad, M., 2011. Effects of end-pressure on the finger-joint quality of black spruce lumber: A microscopic analysis. *Maderas. Ciencia y tecnología*, 13(3), pp.319-328.

Cachim, P.B. and Franssen, J.M., 2009. Comparison between the charring rate model and the conductive model of Eurocode 5. *Fire and Materials*, 33(3), pp.129-143.

Cachim, P.B. and Franssen, J.M., 2010. Assessment of Eurocode 5 charring rate calculation methods. *Fire Technology*, 46(1), pp.169-181.

Canadian Wood Council, 2010. *Case study: The Richmond Olympic Oval* [Online]. Available from: http://cwc.ca/wp-content/uploads/publications-casestudy-RichmondOval_hi-res.pdf [Accessed 11 March 2018].

Chai, K.F., 1994. *Effects of timber grade arrangement and finger joint placement on glued laminated beams*. BEng thesis. Universiti Malaya, Malaysia.

Choo, K.T., Gan, K.S. and Lim, S.C., 1998. Timber Notes – Light Hardwoods I. FRIM Timber Technology Bulletin No. 9. Forest Research Institute Malaysia, pp.8.

Chu, Y.P., Ho, K.S., Midon, M.S. and Malik, A.R.A., 1997. *Timber Design Handbook*. Forest Research Institute Malaysia, pp.288.

Craft, S.T., Desjardins R., Richardson L.R., 2008. Development of small-scale evaluation methods for wood adhesives at elevated temperatures. In: *Proceedings of the 10th World Conference on Timber Engineering (WCTE 2008)*. Miyazaki, Japan, 2, pp.583-590.

De Luca, V. and Marano, C., 2012. Prestressed glulam timbers reinforced with steel bars. *Construction and Building Materials*, 30, pp.206-217.

Dinwoodie, J.M., 1981. *Timber, its nature and behavior*. Van Nostrand Reinhold Co. Ltd., pp.190.

Echavarría, C., Jiménez, L. and Ochoa, J.C., 2012. Bamboo-reinforced glulam beams: An alternative to fiberglass-reinforced glulam beams. Dyna, 174, pp.24-30.

Falk, R.H. and Hernandez, R., 1995. Performance of glued-laminated timber beams of European manufacture. *Forest Products Journal*, 45(7/8), pp.27-34.

Falk, R.H., Solli, K.H. and Aasheim, E., 1992. The performance of glued laminated beams manufactured from machine stress graded Norwegian spruce. The Norwegian Institute of Wood Technology, Report no.77. Oslo, Norway, pp.60, ISBN 82-7120-029-1, ISSN 0546-3637.

Farreyre, A. and Journot, J.B., 2005. *Timber trussed arch for long span*. Master thesis. Chalmers University of Technology, Sweden, pp.119.

Frangi, A. and Fontana, M., 2003. Charring rates and temperature profiles of wood sections. *Fire and Materials*, 27, pp.91-102.

Frangi, A., Bertocchi, M., Clauß, S. and Niemz, P., 2012. Mechanical behaviour of finger joints at elevated temperatures. *Wood Science and Technology*, 46(5), pp.793-812.

Frihart, C.R. and Hunt, C.G., 2010. Chapter 10: Adhesives with wood materials - Bond formation and performance. In: *Wood Handbook – Wood as an Engineering Material.* General Technical Report, FPL-GTR-190. Madison, WI: United States Department of Agriculture, Forest Service, Forest Products Laboratory, pp.10-1 to 10-24.

Friquin, K.L., 2011. Material properties and external factors influencing the charring rate of solid wood and glue-laminated timber. *Fire and Materials*. 35(5), pp.303-327.

Garbett, J.F., 2008. A critical analysis of the Leonardo da Vinci bridge in Ås, Norway. In: *Proceedings of Bridge Engineering 2 Conference*. University of Bath, UK, pp.10.

Gaspar, F., Cruz, H., Gomes, A., and Nunes, L., 2010. Production of glued laminated timber with copper azole treated maritime pine. *European Journal of Wood and Wood Products*, 68(2), pp.207-218.

Gaspar, F., Cruz, H. and Gomes, A., 2017. Evaluation of glue line shear strength of laminated timber structures using block and core type specimens. *European Journal of Wood and Wood Products*, pp.1-13.

Glišović, I., Stevanović, B. and Todorović, M., 2016. Flexural reinforcement of glulam beams with CFRP plates. *Materials and Structures*, 49(7), pp.2841-2855.

Green, D.W., Winandy, J.E. and Kretschmann, D.E., 1999. Chapter 4: Mechanical properties of wood. In: *Wood Handbook – Wood as an Engineering Material*. General Technical Report, FPL-GTR-113. Madison, WI: United States

Department of Agriculture, Forest Service, Forest Products Laboratory, pp.4-1 to 4-45.

Guan, Z.W., Rodd, P.D. and Pope, D.J., 2005. Study of glulam beams pre-stressed with pultruded GRP. *Computers and Structures*, 83(28), pp.2476-2487.

Habipi, B. and Ajdinaj, D., 2015. Wood finger-joint strength as function of finger length and slope positioning of tips. *International Journal of Engineering and Applied Sciences (IJEAS)*, 2(12), pp.128-132.

Hafizah, M.A., Zakiah, A. and Azmi, I., 2014. Characteristics of bonded-in steel and carbon-fibre-reinforced polymer (CFRP) plates into timber. *Journal of Tropical Forest Science*, 26(2), pp.178-187.

Haiman, M. and Baljkas, B., 2000. New glulam timber structures in Croatia. In: *6th World Conference on Timber Engineering (WCTE 2000)*. Canada, pp.9.

Hamid, N.H.A., Ahmad, M., Suratman, M.N. and Abu, F., 2016. Bending strength of finger jointed Kelat wood (*Syzygium* spp.) as affected by finger length and orientation. In: *Advanced Materials Research*. Trans Tech Publications, Switzerland, 1134, pp.138-142.

Hassan, R., Ghazali, N. and Zamli, A.O.A., 2015. Bending strength performance of selected timber species with different GFRP strips pattern, In: *InCIEC 2014*. Springer, Singapore, pp.1129-1139.

Hernández, R.E. and Almeida, G., 2003. Effects of wood density and interlocked grain on the shear strength of three Amazonian tropical hardwoods. *Wood and Fiber Science*, 35(2), pp.154-166.

Holtman, D.F., 1929. *Wood Construction: Principles-Practice-Details*. McGraw-Hill. New York.

How, S.S., Sik, H.S. and Anwar, U.M.K., 2016. An overview of manufacturing process of glued-laminated timber. FRIM Timber Technology Bulletin No. 63. Forest Research Institute Malaysia, pp.8.

Issa, C.A. and Kmeid, Z., 2005. Advanced wood engineering: Glulam beams. *Construction and Building Materials*, 19(2), pp.99-106.

JAS Notification No. 1152:2007. *Japanese Agricultural Standard for Glued Laminated Timber*. Ministry of Agriculture, Forestry and Fisheries.

Jeong, G.Y., Zink-Sharp, A. and Hindman, D.P., 2009. Tensile properties of earlywood and latewood from loblolly pine (*pinus taeda*) using digital image correlation. *Wood and Fiber Science*, 41(1), pp.51-63.

Jokerst, R.W., 1981. Finger-jointed wood products. Research Paper FPL 382. United States Department of Agriculture, Forest Service, Forest Products Laboratory, Madison, WI, pp.24.

Jumaat, M.Z., Rahim, A.H.A., Othman, J. and Razali, F.M., 2006. Timber engineering research and education in Malaysia. In: *Proceedings of the 9th World Conference on Timber Engineering (WCTE 2006)*. Portland, United States, pp.2494-2497.

Khaidzir, M.O.M and Wahab, M.J.A, 2011. Mechanical properties. In: Lim, S.C., Gan, K.S. and Tan, Y.E. (Eds.), *Properties of Acacia mangium Planted in Peninsular Malaysia*. ITTO Project on Improving Utilization and Value Adding of Plantation Timbers from Sustainable Sources in Malaysia. Forest Research Institute Malaysia, pp.23-45.

Kilmer, W.R., Blankenhorn, P.R., Labosky, P. and Janowiak, J.J, 1998. Laminating creosote-treated hardwoods. *Wood and Fiber Science*, 30(2), pp.175-184.

Kishan Kumar, V.S., Upreti, N.K. and Khanduri, A.K., 2010. Effect of finger tip area on the compression strength of finger jointed sections. *Journal of the Indian Academy of Wood Science*, 7(1-2), pp.25-29.

Klippel, M., Clauß, S. and Frangi, A., 2014. Experimental analysis on small-scale finger-jointed specimens at elevated temperatures. *European Journal of Wood and Wood Products*, 72(4), pp.535-545.

Klippel, M. and Frangi, A., 2017. Fire safety of glued-laminated timber beams in bending. *Journal of Structural Engineering*, 143(7):04017052.

Klippel, M., Frangi, A. and Hugi, E., 2013. Experimental analysis of the behavior of finger-jointed timber members. *Journal of Structural Engineering*, 140(3), pp.12.

Klippel, M., Frangi, A. and Hugi, E., 2014. Experimental analysis on small-scale finger-jointed specimens at elevated temperatures. *European Journal of Wood and Wood Products*, 72(4), pp.536-545.

Knorz, M., Schmidt, M., Torno, S. and van de Kuilen, J.W., 2014. Structural bonding of ash (*Fraxinus excelsior* L.): resistance to delamination and performance in shearing tests. *European Journal of Wood and Wood Products*. 72(3), pp.297-309.

Knowles, C.D., Stamey, J.D. and Dougal, E.F., 2006. The effect of specific gravity and growth rate on bending strength of finger-jointed Southern Pine. *Wood and Fiber Science*, 38(3), pp.379-389.

Kok, W.K., 2000. *Mengkaji sifat-sifat kekuatan tanggam jari untuk spesis kayu bintangor dan keledang*. BEng thesis. Universiti Sains Malaysia.

König, J., Norén, J. and Sterley, M., 2008. Effect of adhesives on finger joint performance in fire. In: *CIB-W18 Meeting 41*. August 25-28, Saint Andrews, Canada.

Krishnapillay, D.B. and Varmola, M., 2002. Case study of the tropical forest plantations in Malaysia. Forest Plantations Thematic Papers. Working Paper FP/23, Food and Agriculture Organization of the United Nations (FAO).

Lava, P., Cooreman, S., Coppieters, S., De Strycker, M. and Debryune, D., 2009. Assessment of measuring errors in DIC using deformation fields generated by plastic FEA. *Optics and Lasers Engineering*, 47(7-8), pp.747-753.

Lehringer, C. and Gabriel, J., 2014. Review of recent research activities on one-component PUR-adhesives for engineered wood products. In: Aicher S., Reinhardt, H.-W. and Garrecht, H. (Eds.), *Materials and Joints in Timber Structures*. RILEM Bookseries 9, Springer, pp.405-420, ISBN 978-94-007-781-5 (eBook).

Lim, S.C., Gan, K.S. and Choo, K.T., 2003. The characteristics, properties and uses of plantation timbers – rubberwood and *Acacia mangium.* FRIM Timber Technology Bulletin No. 26. Forest Research Institute Malaysia, pp.11.

Lim, S.C., Gan, K.S. and Tan, Y.E., 2011. Properties of *Acacia mangium* planted in Peninsular Malaysia. ITTO Project on Improving Utilization and Value Adding of Plantation Timbers from Sustainable Sources in Malaysia. Forest Research Institute Malaysia.

Lizhong, Y., Yupeng, Z., Yafei, W. and Zaifu, G., 2008. Predicting charring rate of woods exposed to time-increasing and constant heat fluxes. *Journal of Analytical and Applied Pyrolysis*, 81(1), pp.1-6.

Madsen, B., 1992. *Structural behavior of timber*. Timber Engineering Ltd., pp.405.

Malaysian Timber Council, 2016. MTC-PJC to build Malaysia's longest glulam bridge. *Timber Malaysia*, 22(3), pp.3.

Malaysian Timber Council, 2018. *Wood Wizard Version 1.1* [Online]. Available from: http://mtc.com.my/wizards/mtc_tud/items/report(103).php [Accessed 11 March 2018].

Malaysian Timber Industry Board, 2009. *The Malaysian grading rules for sawn hardwood timber.* Ministry of Primary Industries, Malaysia.

Malaysian Timber Industry Board, 2016. *Performance of the Malaysian timber trade* [Online]. Available from: http://www.mtc.com.my/resources-TradeInfo-2016.php [Accessed 11 March 2018].

Mansur, A., Suhaimi, M., Mohd Salleh, M.N. and Kamarulzaman, N., 1997. The strength of finger joints in three Malaysian timbers – meranti, kempas and keruing. *Journal of Tropical Forest Products*, 3, pp.158-164.

Martin, Z.A., Stith, J.K. and Tingley, D.A., 2000. Commercialization of FRP reinforced glulam beam technology. In: *Proceedings of the 6th World Conference on Timber Engineering (WCTE 2000)*. Whistler, Canada, pp.5.

Martin, Z.A. & Tingley, D.A., 2000. Fire resistance of FRP reinforced glulam beams. In: *Proceedings of the 6th World Conference on Timber Engineering (WCTE 2000)*. Whistler Resort, Canada, pp.8.

Micelli, F., Scialpi, V. and La Tegola, A., 2005. Flexural reinforcement of glulam timber beams and joints with carbon fiber-reinforced polymer rods. *Journal of Composites for Construction*, 9(4), pp.337-347.

Mohamad, W.W., Razlan, M. A., and Ahmad, Z., 2011. Bending strength properties of glued laminated timber from selected Malaysian hardwood timber. *International Journal of Civil & Environmental Engineering*, 11(4), pp.7-12.

Moody, R.C., Hernandez, R. and Liu, J.Y., 1999. Chapter 11: Glued structural members. In: *Wood Handbook – Wood as an Engineering Material*. General

Technical Report, FPL-GTR-113. Madison, WI: United States Department of Agriculture, Forest Service, Forest Products Laboratory, pp.11-1 to 11-24.

MS 544:2001. *Code of Practice for Structural Use of Timber - Part 2: Permissible Stress Design of Solid Timber*. Department of Standard Malaysia.

MS 758:2001. *Glued laminated timber – Performance requirements and minimum production requirements*. Department of Standard Malaysia.

Naughton, A., Fan, M. and Bregulla, J., 2014. Fire resistance characterisation of hemp fibre reinforced polyester composites for use in the construction industry. *Composites Part B: Engineering*, 60, pp.546-554.

Njankouo, J.M., Dotreppe, J.C. and Franssen, J.M., 2004. Experimental study of the charring rate of tropical hardwoods. *Fire and Materials*, 28(1), pp.15-24.

Ohnesorge, D., Richter, K. and Becker, G., 2010. Influence of wood properties and bonding parameters on bond durability of European Beech (*Fagus sylvatica* L.) glulams. *Annals of Forest Science*, 67(6), pp.601.

Ong, C.B., 2015. Glue-laminated timber (Glulam), In: Ansell, M.P. (Ed), *Wood Composites*. Woodhead Publishing, pp.123-140.

Ong, C.B. and Ting, K.B., 2011. Finger-jointing and lamination properties for non-structural purposes. In: Lim, S.C., Gan, K.S. and Tan, Y.E. (Eds.), *Properties of Acacia mangium Planted in Peninsular Malaysia*. ITTO Project on Improving Utilization and Value Adding of Plantation Timbers from Sustainable Sources in Malaysia. Forest Research Institute Malaysia, pp.87-99.

Özçifçi, A. and Yapıcı, F., 2007. Structural performance of the finger-jointed strength of some wood species with different joint configurations. *Construction and Building Materials*, 22(7), pp.1543-1550.

Özçifçi, A. and Yapici, F., 2008. Effects of machining method and grain orientation on the bonding strength of some wood species. *Journal of Materials Processing Technology*, 202, pp.353-358.

Pop, O. Ispas, M., Reynaud, P. and Dubois, F., 2013. Study of mechanical behavior of finger joints using the optical full-field method. *Pro Ligno*, 9(4), pp.568-575.

Rao, S., Gong, M., Chui, Y.H. and Mohammad, M., 2012. Effect of geometric parameters of finger joint profile on ultimate tensile strength of single finger-joined boards. *Wood and Fiber Science*, 44(3), pp.263-270.

Riberholt, H., 2007. Performance of old glulam structures in Europe. Rapport, BYG.DTU R-177. Danmarks Tekniske Universitet, pp.18, ISBN 9788778772527.

Ridley-Ellis, D., 2017. *Grading machines and their speeds* [Online]. Available from: http://blogs.napier.ac.uk/cwst/grading-machines-speeds/ [Accessed 18 April 2018].

Ridley-Ellis, D., Stapel, P. and Bano, V., 2016. Strength grading of sawn timber in Europe: an explanation for engineers and researchers. *European Journal of Wood and Wood Products,* 74, pp.291-306.

Roseley, A.S.M., 2013. *Time- and temperature-dependent properties of structural timber adhesives used for on-site bonding*. PhD thesis. University of Bath, UK.

Selbo, M.L., 1975. Adhesive bonding of wood. Technical Bulletin No. 1512. United States Department of Agriculture, pp.124.

Serrano, E., Gustafsson, P.J., & Larsen, H.J., 2001. Modeling of finger-joint failure in glued-laminated timber beams. *Journal of Structural Engineering*, 127(8), pp.914-921.

Singh, A.P., Anderson, C.R., Warnes, J.M. and Matsumara, J., 2002. The effect of planing on the microscopic structure of *Pinus radiata* wood cells in relation to penetration of PVA glue. *Holz als Roh- und Werkstoff,* 60, pp.333-341.

Smedley, D., Tiew, J., Roseley, A., Ahmad, Z. and Ansell, M.P., 2012. Innovative timber exhibition hall in Johor, Malaysia, constructed from indigenous hardwood using bonded-in moment-resisting connections. In: *Proceedings of the World Conference on Timber Engineering (WCTE 2012)*. Auckland, New Zealand, Vol. 1, pp.502-503, ISBN 978-1-62276-305-4.

St-Pierre, B., Beauregard, R., Mohammad, M., and Bustos, C., 2005. Effect of moisture content and temperature on tension strength of fingerjointed black spruce lumber. *Forest Products Journal*, 55(12), pp.9-16.

Steiger, R., Gehri, E. and Richter, K., 2010. Quality control of glulam: shear testing of bondlines. *European Journal of Wood and Wood Products*, 68, pp.243-256.

Tajaddini, A., 2015. *Investigation of moment redistribution in FRP-strengthened continuous RC beams and slabs*. PhD thesis. University of Bath, UK.

Tan, Y.E. and Chu, Y.P., 1990. Design and construction of a glue-laminated foot-bridge. FRIM Technical Information No. 22. Forest Research Institute Malaysia, pp.4.

Tan, Y.E. and Hse, C.Y., 1998. Finger-jointed meranti tembaga (Shorea leprosura) for structural use. *Adhesive Technology and Bonded Tropical Wood Products*. Taiwan Forestry Research Institute, pp.464-472.

Tan, Y.E., Jumaat, M.Z. and Chai, K.F., 2002. Flexural behaviour of visually strength graded glued-laminated meranti beam. In: *Proceedings of 7th World Conference on Timber Engineering (WCTE 2002)*. Shah Alam, Malaysia, Vol. 1, pp.214-221.

Tan, Y.E., Lim, N.P.T, Lim, S.C., Josue, J. and Maniam, T., 2010. Wood properties of and utilization opportunities for selected plantation-grown species in Malaysia. In: *Proceedings of the Seminar and Workshop on Improved Utilization of Tropical Plantation Timbers*. Kuala Lumpur, Malaysia, pp.46-60, ISBN 978-967-5221-49-1.

Tan, Y.E. and Ong, C.B., 2007. Advantages of wood lamination for modern applications. FRIM Timber Technology Bulletin No. 42. Forest Research Institute Malaysia, pp.4.

Tran, V.D., Oudjene, M. and Méausoone, P.J., 2014. FE analysis and geometrical optimization of timber beech finger-joint under bending test. *International Journal of Adhesion & Adhesives*, 52, pp.40-47.

Tsantaridis, L.D. and Östman, B.A.-L., 1998. Charring of protected wood studs. *Fire and Materials*, 22, pp.55-60.

Tsantaridis, L.D., Östman, B.A.-L. and König, J., 1999. Short communication: Fire protection of wood by different gypsum plasterboards. *Fire and Materials*, 23, pp.45-48.

Vick, C.B., 1999. Chapter 9: Adhesive bonding of wood materials. In: *Wood as an Engineering Material*. General Technical Report, FPL-GTR-113. Madison, WI: United States Department of Agriculture, Forest Service, Forest Products Laboratory, pp.463.

Vrazel, M. and Sellers, T., 2004. The effects of species, adhesive type, and cure temperature on the strength and durability of a structural finger-joint. *Forest Products Journal*, 54(3), pp.66-75.

Wahab, M.J.A., Azmi, J.K., & How, S.S., 2016. Wood properties and bonding shear strength of hardwood glulam after fire exposure. In: *InCIEC 2015*. Springer Singapore, pp.747-757.

White, R.H., 2000. Fire performance of hardwood species, In: *Presentation at the XXI IUFRO World Congress*, August 7-12, Kuala Lumpur, Malaysia.

Wilson, T.R.C., 1939. The glued laminated wooden arch. Technical Bulletin No. 691. United States Department of Agriculture, Washington D.C., pp.123.

Wong, T.M., 2002. *A Dictionary of Malaysian Timbers*. Malaysian Forest Records No. 30, 2nd Ed. Forest Research Institute Malaysia.

Yang, T.H., Wang, S.Y., Tsai, M.J. and Lin, C.Y., 2009. The charring depth and charring rate of glued laminated timber after a standard fire exposure test. *Building and Environment*. 44(2), pp.231-236.

Yeboah, D., Taylor, S., McPolin, D. and Gilfillan, R., 2013. Pull-out behaviour of axially loaded Basalt Fibre Reinforced Polymer (BFRP) rods bonded perpendicular to the grain of glulam elements. *Construction and Building Materials*, 38, pp.962-969.

Zaini, A.R., 2010. Forest plantation programme in Malaysia – the way forward. In: *Proceedings of the Seminar and Workshop on Improved Utilization of Tropical Plantation Timbers*. Kuala Lumpur, Malaysia, pp.23-29, ISBN 978-967-5221-49-1.

Zink, A.G., Davidson, R.W. and Hanna, R.B., 1995. Strain measurement in wood using a digital image correlation technique. *Wood and Fiber Science*, 27(4), pp.346-359.

Appendix A

Table A-1: Bending properties of solid DRM specimens ($Solid_{drm}$)

No.	MC (%)	Density (kg/m^3)	MOR (N/mm^2)	MOE (N/mm^2)
1	11.5	540	86.6	14400
2	11.6	496	84.2	15800
3	11.4	533	91.4	14600
4	11.5	508	89.3	16000
5	11.6	649	98.3	17500
6	12.0	651	99.8	19000
7	11.4	609	101.3	15300
8	11.1	598	106.9	16700
9	11.6	493	83.1	14600
10	11.4	572	89.7	15200
Average	11.5	565	93.1	15900
SD	0.2	60	8.03	1450

Table A-2: Bending properties of solid Spruce specimens ($Solid_{spruce}$)

No.	MC (%)	Density (kg/m^3)	MOR (N/mm^2)	MOE (N/mm^2)
1	12.3	581	101.8	23200
2	12.2	429	51.1	12400
3	12.2	485	81.7	19900
4	12.3	597	99.6	19800
5	12.5	451	58.6	11600
6	12.1	449	84.2	17400
7	12.8	514	82.5	13500
8	12.4	585	105.6	23000
9	12.4	476	83.9	15200
10	12.6	428	72.5	14900
11	12.9	483	82.5	15700
12	12.3	468	78.2	17100
Average	12.4	495	81.8	17000
SD	0.3	61	16.2	3860

Table A-3: Bending properties of DRM vertical finger-jointed PRF specimens with recommended end pressure, 12.5 N/mm^2 ($FJ_{drm,prf,v,R}$)

No.	MC (%)	Density (kg/m^3)	MOR (N/mm^2)	MOE (N/mm^2)	Joint efficiency (%)
1	12.0	521	63.9	11200	69
2	12.2	649	85.2	17400	92
3	12.1	679	69.8	17200	75
4	12.2	550	69.9	14500	75
5	12.2	654	68.9	13500	74
6	12.4	649	76.9	19200	83
7	12.3	576	70.4	16700	76
8	12.2	569	68.7	14400	74
9	11.8	480	79.6	15300	86
10	12.0	662	66.6	15600	72
Average	12.1	599	71.9	15500	77
SD	0.2	69	6.50	2270	7

Table A-4: Bending properties of DRM vertical finger-jointed epoxy specimens with recommended end pressure, 12.5 N/mm^2 ($FJ_{drm,epoxy,v,R}$)

No.	MC (%)	Density (kg/m^3)	MOR (N/mm^2)	MOE (N/mm^2)	Joint efficiency (%)
1	12.0	522	44.4	16900	48
2	12.3	415	47.1	11000	51
3	12.3	550	64.1	15600	69
4	12.4	410	56.8	12600	61
5	12.2	399	48.9	11200	53
6	12.2	399	30.9	10800	33
7	12.4	416	48.9	12100	53
8	11.9	528	55.1	17200	59
9	11.9	533	70.6	18300	76
10	12.3	517	58.6	17900	63
11	12.1	418	62.5	13600	67
12	12.4	539	60.3	20300	65
Average	12.2	470	54.0	14800	58
SD	0.2	65	10.6	3310	11

Table A-5: Bending properties of Spruce vertical finger-jointed PRF specimens with recommended end pressure, 12.5 N/mm^2 ($FJ_{spruce,prf,v,R}$)

No.	MC (%)	Density (kg/m^3)	MOR (N/mm^2)	MOE (N/mm^2)	Joint efficiency (%)
1	12.5	499	69.9	19900	85
2	12.5	471	42.9	12500	52
3	12.7	513	46.6	12100	57
4	12.6	450	53.4	17500	65
5	12.6	469	48.7	15300	60
6	12.5	438	39.0	14700	48
7	12.6	452	54.6	16100	67
8	12.5	526	61.3	20500	75
9	12.3	540	66.2	20100	81
10	12.2	460	45.4	16300	55
11	12.1	507	48.5	15400	59
12	12.4	567	61.3	14100	75
13	11.2	668	50.2	15300	61
Average	12.4	505	52.9	16100	65
SD	0.4	62	9.31	2730	11

Table A-6: Bending properties of DRM vertical finger-jointed PRF specimens (increased width) with recommended end pressure, 12.5 N/mm^2 ($FJ_{drm,prf,wv,R}$)

No.	MC (%)	Density (kg/m^3)	MOR (N/mm^2)	MOE (N/mm^2)	Joint efficiency (%)
1	12.1	513	60.7	13600	65
2	12.4	652	83.5	15900	90
3	12.4	708	72.8	20200	78
4	12.4	586	72.7	13500	78
5	12.6	617	63.9	13100	69
6	12.2	632	82.3	16900	88
7	12.3	560	65.1	15600	70
8	12.1	567	64.6	13400	69
9	12.0	494	63.2	13300	68
10	12.0	685	67.2	14900	72
Average	12.3	601	69.6	15000	75
SD	0.2	70	8.02	2240	9

Table A-7: Bending properties of DRM horizontal finger-jointed PRF specimens with recommended end pressure, 12.5 N/mm^2 ($FJ_{drm,prf,h,R}$)

No.	MC (%)	Density (kg/m^3)	MOR (N/mm^2)	MOE (N/mm^2)	Joint efficiency (%)
1	11.9	586	54.7	11500	59
2	11.9	525	64.4	13600	69
3	12.0	524	76.6	14000	82
4	12.0	563	76.9	14700	83
5	12.1	554	71.3	13800	77
6	11.8	571	55.4	12200	60
7	12.0	703	81.9	13900	88
8	12.4	666	84.7	15200	91
9	12.5	719	54.0	15300	58
10	12.7	645	57.6	14900	62
Average	12.1	606	67.8	13900	73
SD	0.3	72	11.9	1250	13

Table A-8: Bending properties of DRM vertical finger-jointed PRF specimens with lower end pressure, 10.0 N/mm^2 ($FJ_{drm,prf,v,L}$)

No.	MC (%)	Density (kg/m^3)	MOR (N/mm^2)	MOE (N/mm^2)	Joint efficiency (%)
1	12.7	561	56.6	13100	61
2	12.4	597	59.7	19700	64
3	12.6	653	51.5	16600	55
4	12.5	607	67.5	20300	73
5	12.4	505	60.5	15100	65
6	12.7	563	49.6	13700	53
7	12.5	505	53.9	14300	58
8	12.6	679	60.0	19400	65
9	12.6	664	63.7	17400	68
10	12.4	527	64.9	17200	70
11	12.4	594	70.6	22500	76
12	12.7	549	54.7	15100	59
Average	12.5	584	59.4	17000	64
SD	0.1	60	6.46	2930	7

Table A-9: Bending properties of DRM vertical finger-jointed PRF specimens with higher end pressure, 15.0 N/mm^2 ($FJ_{drm,prf,v,H}$)

No.	MC (%)	Density (kg/m^3)	MOR (N/mm^2)	MOE (N/mm^2)	Joint efficiency (%)
1	12.4	642	71.7	18500	77
2	12.4	642	60.1	18400	65
3	12.9	738	56.1	18700	60
4	12.8	625	62.7	20600	67
5	12.5	583	69.2	17900	74
6	12.2	598	67.2	18600	72
7	13.0	729	59.1	20000	63
8	13.0	654	59.5	20500	64
9	12.5	660	85.5	22900	92
10	12.8	720	52.3	23600	56
11	12.8	638	74.3	23500	80
12	12.5	646	66.8	21400	72
Average	12.7	656	65.4	20400	70
SD	0.3	49	9.09	2070	10

Table A-10: Tensile strength parallel to grain of DRM finger-jointed PRF specimens with recommended end pressure, 12.5 N/mm^2 ($FJ_{T,prf,R}$)

No.	MC (%)	Density (kg/m^3)	Tensile Strength (N/mm^2)	Failure modes
1	12.1	635	57.1	Glue lines with fibres
2	12.0	632	40.1	Glue lines with fibres
3	12.0	766	46.1	Glue lines with fibres
4	12.5	832	55.1	Glue lines with fibres
5	12.1	645	48.7	Glue lines with fibres
6	12.2	609	52.8	Slip at grips
7	12.4	589	56.1	Slip at grips
8	12.0	606	35.9	Glue lines with fibres
9	11.7	690	53.7	Glue lines with fibres
10	12.1	643	53.5	Glue lines with fibres
Average	12.0	651	49.9	
SD	0.4	72	7.16	

Table A-11: Tensile strength parallel to grain of DRM finger-jointed epoxy specimens with recommended end pressure, 12.5 N/mm^2 ($FJ_{T,epoxy,R}$)

No.	MC (%)	Density (kg/m^3)	Tensile Strength (N/mm^2)	Failure modes
1	11.7	618	54.4	Slip at grips
2	11.5	634	52.1	Glue lines with fibres
3	11.4	567	41.5	Glue lines with fibres
4	12.2	627	61.4	Slip at grips
5	12.5	634	63.7	Slip at grips
6	11.7	496	42.2	Glue lines with fibres
7	11.3	601	27.9	Wood fracture
8	11.3	584	27.5	Wood and finger fractures
9	11.5	424	43.9	Wood split and glues line with fibres
10	11.5	392	28.8	Slip at grips
Average	11.7	545	44.3	
SD	0.3	97	13.5	

Table A-12: Tensile strength parallel to grain of DRM finger-jointed PRF specimens with lower end pressure, 10.0 N/mm^2 ($FJ_{T,prf,L}$)

No.	MC (%)	Density (kg/m^3)	Tensile Strength (N/mm^2)	Failure modes
1	11.4	510	50.8	Glue lines with fibres and finger fracture
2	11.4	670	43.3	Glue lines with fibres
3	11.7	544	37.7	Glue lines with fibres
4	11.3	596	43.9	Glue lines with fibres
5	11.4	660	47.2	Glue lines with fibres
6	11.9	514	38.6	Glue lines with fibres and finger fracture
7	12.4	552	39.4	Glue lines with fibres
8	11.9	612	55.7	Glue lines with fibres
9	11.8	438	13.2	Slip at grips
10	11.7	421	23.4	Wood split and glue lines with fibres
Average	11.8	538	39.3	
SD	0.4	91	21.8	

Table A-13: Tensile strength parallel to grain of DRM finger-jointed PRF specimens with higher end pressure, 15.0 N/mm^2 ($FJ_{T,prf,H}$)

No.	MC (%)	Density (kg/m^3)	Tensile Strength (N/mm^2)
1	12.3	650	58.9
2	11.8	639	44.7
3	12.2	606	55.9
4	11.9	606	44.5
5	11.9	654	31.8
6	12.1	660	56.9
7	12.7	687	55.4
8	12.3	667	54.3
9	11.7	670	53.1
10	11.7	642	60.9
Average	12.1	642	52.2
SD	0.3	29	8.85

*All specimens showed failure in glue lines with wood fibres attached

Table A-14: Tensile strength parallel to grain of DRM finger-jointed PRF specimens with recommended end pressure, 12.5 N/mm^2 (finger length 15 mm) ($FJ15_{T,prf,R}$)

No.	MC (%)	Density (kg/m^3)	Tensile Strength (N/mm^2)	Failure modes
1	13.3	707	68.4	Glue lines with fibres
2	13.5	701	75.9	Wood split and glue lines with fibres
3	13.9	692	78.6	Wood split and glue line swith fibres
4	13.9	695	80.9	Glue lines with fibres
5	14.3	632	77.6	Glue lines with fibres
6	14.4	627	80.4	Glue lines with fibres
7	14.9	576	75.9	Glue lines with fibres
8	14.5	569	62.3	Glue lines with fibres
9	14.2	554	58.6	Wood split and glue lines with fibres
10	14.4	559	69.7	Glue lines with fibres
Average	14.1	631	72.8	
SD	0.5	64	7.77	

Table A-15: Compressive strength parallel to grain of solid DRM specimens ($Solid_{C,drm}$)

No.	MC (%)	Density (kg/m^3)	Compressive Strength (N/mm^2)	Failure modes
1	12.2	571	52.1	Central region
2	11.5	534	50.2	Near edge
3	12.3	636	54.8	Central region
4	11.7	545	50.1	Near edge
5	12.4	619	58.7	Near edge
6	12.1	605	60.1	Near edge
7	12.2	649	58.2	Central region
8	12.0	538	49.6	Central region
9	12.0	568	52.6	Near edge
10	12.1	540	49.6	Near edge
11	12.2	657	60.8	Near edge
12	11.8	640	53.0	Near edge
Average	12.0	592	54.2	
SD	0.3	48	4.24	

Table A-16: Compressive strength parallel to grain of solid Spruce specimens ($Solid_{C,spruce}$)

No.	MC (%)	Density (kg/m^3)	Compressive Strength (N/mm^2)	Failure modes
1	12.7	449	41.5	Near knots
2	12.0	555	54.4	Central region
3	11.9	566	55.5	Central region
4	12.3	433	41.0	Near edge
5	11.9	423	37.2	Central region
6	11.8	411	37.9	Near knots
7	12.4	553	46.0	Near knots
8	12.8	587	48.0	Central region
9	12.3	525	44.1	Central region
10	12.2	544	51.5	Central region
11	12.2	481	47.2	Central region
Average	12.2	502	45.9	
SD	0.3	64	6.24	

Table A-17: Compressive strength parallel to grain of DRM finger-jointed PRF specimens with recommended end pressure, 12.5 N/mm^2 ($FJ_{C,drm,prf}$)

No.	MC (%)	Density (kg/m^3)	Compressive Strength (N/mm^2)	Failure modes
1	11.6	502	44.4	At finger tips
2	12.3	648	46.3	At finger tips
3	11.7	617	56.5	At finger tips
4	11.9	530	45.5	At finger tips
5	11.9	612	56.5	At finger tips and central region
6	11.6	571	54.0	At finger tips
7	11.4	667	48.4	At finger tips
8	11.9	627	58.1	At finger tips and central region
9	12.0	691	57.5	At finger tips
10	11.8	541	48.8	At finger tips
11	11.8	603	57.8	At finger tips
12	11.5	655	49.1	At finger tips
Average	11.8	621	51.9	
SD	0.3	72	5.30	

Table A-18: Compressive strength parallel to grain of DRM finger-jointed epoxy specimens with recommended end pressure, 12.5 N/mm^2 ($FJ_{C,drm,epoxy}$)

No.	MC (%)	Density (kg/m^3)	Compressive Strength (N/mm^2)	Failure modes
1	12.6	656	57.2	Central region
2	12.3	633	57.8	At finger tips
3	11.8	566	55.6	At finger tips
4	11.5	628	55.3	Near edge
5	12.4	513	47.9	At finger tips
6	12.3	523	47.7	At finger tips
7	12.7	733	53.7	At finger tips
8	12.7	652	59.3	Near edge
9	12.4	624	54.7	Near edge
10	12.8	747	50.9	At finger tips
11	11.8	658	55.5	Central region
12	12.1	578	56.9	Central region
13	12.4	607	57.7	At finger tips
Average	12.3	629	54.6	
SD	0.4	60	3.69	

Table A-19: Compressive strength parallel to grain of Spruce finger-jointed PRF specimens with recommended end pressure, 12.5 N/mm^2 ($FJ_{C,spruce,prf}$)

No.	MC (%)	Density (kg/m^3)	Compressive Strength (N/mm^2)
1	11.8	487	36.3
2	12.3	444	39.3
3	12.4	460	31.7
4	11.9	480	41.7
5	12.6	574	42.4
6	12.0	527	42.9
7	12.2	558	51.3
8	12.0	459	41.4
9	11.8	550	42.3
10	12.5	470	35.7
Average	12.1	500	40.5
SD	0.3	43	5.30

*All specimens showed failure at finger tips

List of publications

Journal paper:

Ong, C.B., Chang, W.S., Ansell, M.P., Brandon, D., Sterley, M. and Walker, P., 2018. Bench-scale fire tests of Dark Red Meranti and Spruce finger joints in tension. *Construction and Building Materials*, *168*, pp.257-265.

Book chapter:

Ong, C.B., 2015. Glue-laminated timber (Glulam). In: Ansell, M.P. (Ed), *Wood Composites*. Woodhead Publishing, pp.123-140.

Conference paper:

Ong, C.B., Chang, W.S., Brandon, D., Sterley, M., Ansell, M.P. and Walker, P., 2016. Fire performance of hardwood finger joints. In: *World Conference on Timber Engineering (WCTE 2016)*. Vienna, Austria, 22-25 August.

Ong, C.B., M., Ansell, Chang, W.S. and Walker, P., 2018. Bending properties of finger-jointed Malaysian Dark Red Meranti. [Submitted]. In: *Timber 2018*. Wood Technology Society, Institute for Materials, Minerals and Mining (IOM3). London, UK, 26-27 June 2018.